Investigating the Effects of Simian Retrovirus (SRV) Infection on the Autophagic Pathway, Apoptotic Pathway and m6A RNA Methylation in Jurkat Cells

Thesis submitted in accordance with the requirements of the University of Liverpool for the degree of Doctor in Philosophy

by Jingting Zhu

Primary Supervisor: Dr. Rong Rong

Co-supervisors: Dr. Qibo Zhang and Prof. Zhi-Liang Lu

Biological Sciences

Institute of Infection & Global Health

Faculty of Health & Life Sciences

University of Liverpool

UK

November 2018

Contents

Declaration

I hereby declare that the work presented within this Ph.D. thesis was carried out by me for the degree of Doctor of Philosophy in Biological Sciences and that it has not been submitted in any form for any other degree or qualification. Where the others' work was used, the sources of information have been detailed clearly in the thesis.

Jingting Zhu

Acknowledgments

I would like to express my gratitude to my supervisors Dr. Rong Rong, Dr. Qibo Zhang and Prof. Zhi-Liang Lu for all of their guidance and support throughout the past 4 years. Thank you sincerely for giving me the opportunity to undertake this journey in science. I am not sure whether I could have held on without your unquestionable help. I would also like to thank Xi'an Jiaotong-Liverpool University (XJTLU) and the University of Liverpool for providing me with the research funding and Ph.D. Scholarship, which allowed me to pursue my Ph.D. study.

I would like to thank all colleagues and staffs in the Department of Biological Science at XJLTU for giving me the help with any questions I might have had. In particular, I would like to thank Dr. Jia Meng for giving me scientific guidance and suggestions on Bioinformatics issues. I am grateful for the help of Dr. Jian Liu and Dr. Meng Huee Lee for their kindness and scientific guidance on experimental techniques. I would also like to thank Dr. Ferdinand Kappes for providing me with the plasmids used for lentiviral transduction, as well as his scientific guidance throughout the experimental stages.

I would like to thank all technicians in the Department of Biological Science at XJLTU for their time and friendly help. Thanks Miss. Qiaoli Feng, Mr. Zhongkai Huang, Mr. Ziwen Xie, Mr. Deyi Lu, Mrs. Yan Zhang and Mrs. Sijing Meng. I would also like to thank the lab manager, Mrs. Jie Jiang, for keeping the lab perfectly organized and providing me with an enjoyable place to work in.

I would like to thank all Ph.D. candidates in the lab for their company and help. It has been wonderful and I am grateful to having studied and worked with you in the lab. It made me happy to have scientific and nonscientific discussions with you all. I am grateful for the help of Zhen Wei for his time and help on the bioinformatics analysis sections in this Thesis.

Last but not least, I want to thank my family and friends for their continued emotional and financial support through everything in the past 4 years.

Abbreviations

Abbreviation	Full name
ALKBH5	AlkB homolog 5
Apaf-1	Apoptotic peptidase activating factor-1
ATG	Autophagy-related genes
BH	Bcl-2 homology
BSA	Bovine serum albumin
CARD	Caspase recruitment domain
CCR5	C-C chemokine receptor type 5
CDS	Coding DNA sequence
cFLIP	Cellular FLICE-like inhibitor protein
Co-IP	Co-immunoprecipitation
CPE	Cytopathic effect
CQ	Chloroquine
CVB3	Coxsackievirus B3
CVCR4	C-X-C chemokine receptor type 4
DD	Death domain
DED	Death effector domain
DENV	Dengue virus
DISC	Death-inducing signal complex
DMEM	Dulbecco's modified Eagle's medium
DMSO	Dimethyl sulfoxide
DNA	Deoxyribonucleic acid
Dox	Doxycycline
EBV	Epstein-Barr virus
EDTA	Ethylene diamine tetraacetic acid

eIF3	Eukaryotic initiation factor 3
ER	Endoplasmic reticulum
f6A	*N6*-formyladenosine
FADD	Fas-associated death domain
Fas	Fas receptor
FasL	Fas ligand
FLV	Feline leukemia virus
FMDV	Food-and-mouth disease virus
FTO	Obesity associated protein
GO	Gene ontology
HCV	Hepatitis C virus
HIV	Human immunosuppressive virus
hm6A	*N6*-hydroxymethyladenosine
HSV-1	Herpes simplex virus type 1
IAV	Influenza virus
iDISC	Intracellular death inducing signaling complex
IFN	Interferon
IP	Immunoprecipitation
JEV	Japanese encephalitis virus
KEGG	Kyoto Encyclopedia of Genes and Genomes
KIAA1429	Vir-like m6A methyltransferase associated
KSHV	Kaposi's Sarcoma herpesvirus
LC3	Microtubule-associated proteins 1A/1B, light chain 3
LIR	LC3-interacting region
LTR	Long terminal repeat
m1A	*N1*-methyladenosine

M2	matrix protein 2
m5C	C5-methyl cytosine
m6A	*N6*-methyladenosine
$m6A_m$	*N6*,2'-O-dimethyladenosine
MeRIP-seq	Methylated RNA immunoprecipiation sequencing
METTL	Methyltransferase-like
MHC-II	Major histocompatibility complex class II
MHV-68	Murine γ-herpesvirus 68
miR-30	microRNA-30
MOI	Multiplicity of infection
MOMP	Mitochondrial outer membrane permeabilization
MP1	Matrix protein 1
M-PMV	Mason-Pfizer monkey virus
mRNA	Messerger ribonucleic acid
mTOR	Mammalian target of rapamycin
NBR1	Neighbor of BRCA1 gene 1
NDP52	Nuclear dot protein 52 kDa
Nef	Negative regulatory factor
NPRC	National primate research center
NXF1	Nuclear RNA export factor 1
ORF	Open reading frames
P bodies	Processing bodies
PAGE	Polyacrylamide gel electrophoresis
PAMP	Pathogen-associated molecular pattern
PARP	Poly (ADP-Ribose) Polymerase
PAR-CLIP	Photoactivatable ribonucleoside-enhanced cross-linking and immunoprecipitation

PBS	Phosphate buffered saline
PCD	Programmed cell death
PCR	Polymerase chain reaction
pDC	Plasmacytoid dendritic cells
PE	Phosphatidylethanolamine
PI3K	Class III phosphatidylinositol 3-OH kinase
PPT	Polypurine tract
PRR	Pattern recognition receptor
PVDF	Polyvinylidene difluoride
RBM15	RNA-binding motif protein 15
RBM15B	RNA-binding motif protein 15B
RF	Retroperitoneal fibromatosis
RNA	Ribonucleic acid
RNA-seq	RNA-sequencing
rRNA	Ribosomal ribonucleic acid
RSV	Respiratory syncytial virus
SAIDS	Simian immunosuppressive syndrome
SAM	S-adenosyl-methionine
SDS	Sodium dodecyl sulfate
SF	Subcutaneous fibrosarcomas
SFV	Simian foamy virus
shRNA	Short hairpin RNA
SIV	Simian immunosuppressive virus
SLR	Sequestosome 1/p62-like Receptor
SPF	Specific pathogen-free
SRSF	Serine- and arginine-rich splicing factor

SRV	Simian retrovirus
STLV	Simian T-lymphotropic virus
SU	Surface protein
SV40	Simian virus 40
Tat	Transactivator
$TCID_{50}$	50% Tissue Culture Infective Dose
TLR	Toll-like receptor
TMV	Tobacco mosaic virus
TNFR	Tumor necrosis factor receptor
TRAIL	TNF-related apoptosis-inducing ligand
tRNA	Transfer ribonucleic acid
UBA	Ubiquitin-binding association
Ubl	Ubiquitin-like
ULK1/2	Unc-51-like kinase
UTR	Untranslated region
UV	Ultraviolet
vBCL-2	Viral Bcl-2 homologue
Vps	Vacuolar protein sorting
VSV	Vesicular stomatitis virus
WTAP	Wilms tumor 1-associating protein
YTHDC	YTH domain containing
YTHDF	YTH domain family
ZIKV	Zika virus

List of Figures

Abstract

Simian type D retrovirus (SRV) is an etiological agent for the fatal simian acquired immunodeficiency syndrome (SAIDS), which mainly infects Asian macaques and leads to varying degrees of immunosuppression. Until now, little was known about the underlying pathogenic mechanisms of SRV infection. Especially, the effects of SRV infection on T lymphocytes, the major host cells of SRV, are still largely unclear. Apoptosis and autophagy are two important evolutionarily conserved host immune defense pathways against viral invasion and mediate viral pathogenesis. In addition, in the last decade, a growing number of studies has revealed the emerging roles of m6A RNA modification in regulating the viral infection and virus-host cell interactions. Therefore, the aims of this thesis are to investigate the effects of SRV infection on the autophagic pathway, apoptotic pathway and m6A RNA modification in Jurkat T lymphocytes (Jurkat cells). The capacities of SRV infection and replication in Jurkat cells were also assessed. The results showed that both SRV-4 and SRV-8, the major SRV subtypes circulated in the macaque breeding colonies in China, were able to infect and replicate in Jurkat cells. In addition, both SRV-4 and SRV-8 infection have been shown to induce autophagy and apoptosis in Jurkat cells. The results demonstrated that SRV-4/SRV-8 infection was able to enhance the formation of autophagosome as well as to increase the completed autophagic flux in Jurkat cells. Moreover, the levels of activated caspase-3 and caspase-8 and apoptosis were significantly increased in Jurkat cells by SRV-4/SRV-8 infection. In addition, the SRV-8 infection-induced autophagy was shown to inhibit SRV replication and promote apoptosis in Jurkat cells. Inhibition of

autophagy by knockdown of Beclin1 in SRV-8-infected Jurkat cells was shown to significantly increase the amount of SRV genome released in the culture medium, as well as to significantly decrease the levels of caspase-3/-8 activation and inhibit apoptosis. Interestingly, further investigations on the interaction between LC3 and procaspase-8 in SRV-8-infected Jurkat cells suggested that the autophagosomes was, at least partially, involve in the process of caspase-8 activation. In addition, the results in this thesis also showed that SRV-8 viral RNAs in the infected Jurkat cells contain six distinct m6A peaks. Moreover, SRV-8 infection was shown to decrease the global m6A level in Jurkat cells, as well as to reprogramme the Jurkat cellular m6A epitranscriptome. Interestingly, depletion of ALKBH5, an m6A “eraser”, or YTHDF1, an m6A “reader”, in the infected Jurkat cells was demonstrated to significantly decrease SRV-8 replication, suggesting the regulatory roles of m6A modification and the components of the cellular m6A machinery in SRV replication. The results in this thesis have revealed for the first time the effects of SRV infection on the autophagic and apoptotic pathways as well as on the m6A RNA methylation in Jurkat cells, which have the potential to provide novel insights for the development of new antiviral therapies.

Chapter 1

Introduction

1.1 Overview

Simian retroviruses (SRVs) are a group of genetically closely related viruses that belong to the genus of type-D *Beta-retrovirus*, within the subfamily of *Orthoretrovirinae* and the family of *Retroviridae* [1]. SRV commonly infects wild and captive Asian monkeys of the genus *Macaca* worldwide [2, 3]. The prototype of SRV, Mason-Pfizer monkey virus (M-PMV, now known as SRV-3), was first isolated in 1970 from the spontaneous mammary carcinoma tissue of a rhesus macaque [4, 5]. Both exogenous and endogenous SRVs have been identified in nonhuman primates; however, there are no diseases caused by the endogenous SRV. To date, nine exogenous subtypes of SRV have been identified from both captive and feral monkeys [6, 7]. The exogenous SRV was indicated as an etiologic agent of the fatal simian immunosuppressive syndrome (SAIDS) in several macaque species that display the similar clinical features to the human acquired immune deficiency syndrome (AIDS) [8-10]. Based on the phylogenetic analysis, SRV is classified into the branch of *Beta-retrovirus* with a simple genome that is different from the lentiviruses, such as simian immunosuppressive virus (SIV) and human immunosuppressive virus (HIV) which could also cause the immunosuppressive disease in monkey and human, respectively (Fig. 1.1) [11].

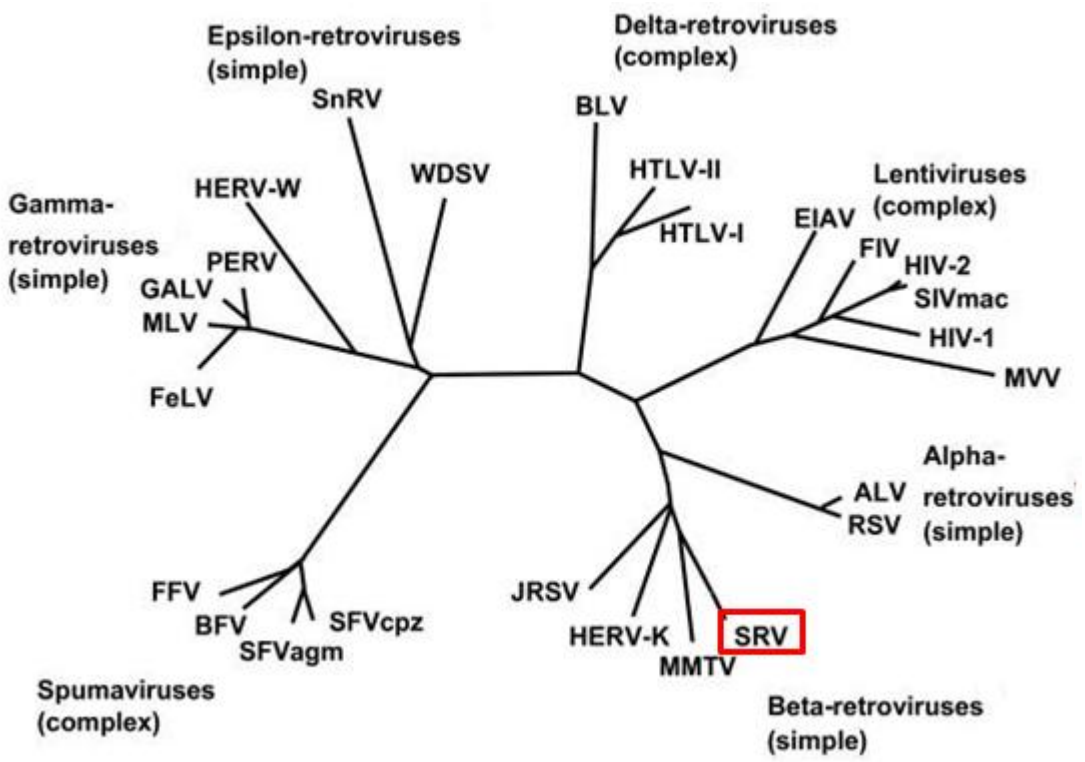

Figure 1.1 Phylogenetic relationships between SRV and other retroviruses. Retroviruses can be classified as those that have complex genomes or simple genomes. SRV is highlighted in a red rectangle and belongs to the genus of *Beta-retroviruses* with a simple genome. This figure is adapted from Weiss, 2006. The discovery of endogenous retroviruses. *Retrovirology*, 2006. **3**: p. 67. [11]

SRV infection can lead to broad pathological and clinical features in the infected monkeys, ranging from no clinical manifestations to overt diseases (e.g. diarrhea and anemia) and the fatal SAIDS [12, 13]. In particular, it has been shown that SRV infection can cause varying degrees of immunosuppressive diseases by modulating the host immune system, such as decreasing the production of serum immunoglobulin and inducing the depletion of lymphocytes [9, 14-16]. However, the underlying pathogenic mechanisms of SRV-induced modulation of host immune responses are still unclear. Autophagy and apoptosis are two evolutionarily conserved pathways that take part in the host immune defense responses against viral infections [17-20]. Autophagy is a

lysosomal degradative process to digest intracellular unwanted or dysfunctional components for recycling. Thus, it was recognized as an important process to maintain cellular homeostasis under stressful conditions including the viral invasion [21, 22]. Besides autophagy, apoptosis as a type of programmed cell death (PCD) is also an important immune defense process that leads to irreversible cell death and responsible for many pathogen-associated diseases [23]. Indeed, a growing number of studies has demonstrated that the autophagic and/or apoptotic responses were initiated in various virus-infected cells which in turn affected viral replication and pathogenesis [19, 20, 24-31]. However, some viruses have developed strategies to modulate these two pathways for escaping the immune defense and promoting the viral infection and replication [24, 32-37]. In addition, numerous studies have shown that the crosstalk between the autophagic and apoptotic pathways also play an important role in regulating viral infection and pathogenesis [38-40]. Giving these connections, it would be necessary and interesting to investigate the effects of SRV infection on the autophagic and apoptotic pathways, as well as to examine the interactions between the two pathways in SRV-infected cells.

Ribonucleic acid (RNA) modifications play important roles in RNA post-transcriptional regulation to affect the metabolism and function of the modified RNAs. Among the known RNA modifications, m6A modification is the most prevalent messenger RNA (mRNA) modification that has been discovered in a broad range of eukaryotes including plants, yeast, mice and human, as well as in bacteria and a variety of viruses

[41-47]. As a dynamic process, m6A modification is regulated by the cellular m6A machinery, which consists of the m6A “writers”, m6A “erasers” and m6A “readers”. The “writers” and “erasers” can mediate the methylation and demethylation of m6A, respectively, while the “readers” can directly bind to the specific m6A sites on mRNA and play a key role to execute the functions of m6A modification, such as to affect mRNA stability, splicing, structure and translation [48-51]. Although m6A RNA modification has been identified in the 1970s, its function on various biological processes and human diseases such as stem cell differentiation and tumor development, haven’t been shown until recently [52-55]. In addition, results of the recent studies have also revealed the emerging regulatory roles of m6A modification and the cellular m6A machinery in viral infection [45, 46, 56, 57].

In the following sections, the biological and pathological features of SRV, the molecular regulation of apoptosis, autophagy and m6A RNA modification, the complex interplay among apoptotic pathway, autophagic pathway and viral infection, as well as the roles of m6A in viral infection will be discussed.

1.2 Background of simian retrovirus (SRV)

1.2.1 Characterization of SRV

SRV is an enveloped retrovirus which has a positive sense (+) and single-stranded (ss) RNA genome. Figure 1.2 shows the general schematic diagram of the retroviral structure. The diameter of the extracellular retroviral virion ranges from 80-100 nm, which means that the virus could only be observed with an electron microscope. All retroviruses are composed of a flexible lipid envelope and a capsid that is surrounded by the envelope. The surface of the viral envelope is covered by the viral *env* gene-encoded glycoproteins, which consist of the transmembrane glycoprotein (TM) and the surface glycoprotein (SU). The glycoproteins play important roles in the binding of virus to the host cellular receptors as well as the fusion of viral envelope with the cellular plasma membrane. The retroviral capsid consists of several structural proteins, including matrix protein (MA), capsid protein (CA) and nucleocapsid (NC), and several functional proteins, including integrase (IN), reverse transcriptase (RT) and protease (PR). The capsid functions as a protective protein shell to enclose the viral genome and separate it from the external environment. The retroviral genome contains two identical linear (+)ssRNA as a dimer. The diameter of the extracellular SRV virion is about 125 nm, with 6-8 nm short protuberances distributed on the envelope surface [6]. And the mature SRV virion has an icosahedral capsid that encloses an inner ribonucleoprotein core, which contains the dimer of the two copies of the linear (+)ssRNA genomes.

SRV genome is about 8.1 kb in length that contains four long open reading frames (ORFs) and one short ORF (Fig. 1.3). Each long ORF encodes one gene and the four genes are organized in the order of *5'-gag-prt-pol-env-3'* flanked by the 5'-R-U5 region and the U3-R-3' region [58, 59]. Moreover, the genome contains a cap at the 5' end and a poly(A)-tail at the 3' end. The genome of all retroviruses contains three essential genes: *gag, pol* and *env.* The *gag* gene encodes the core structural proteins, which are essential for the assembly of immature virus-like particles within the host cells [60]. The *pol* gene encodes some functional enzymes, including the endonuclease, reverse transcriptase and integrase [59]. The *env* gene encodes the viral surface glycoproteins, which can mediate the binding of the virus to the host cell receptor and the fusion of the viral envelope with the cellular plasma membrane. [59]. In addition to the three major genes, SRV genome also contains the *prt* gene which encodes the protease. During the maturation of infectious virions, the protease is able to cleave the precursor Gag protein, yielding the structural polypeptides such as P4, P10, P12, P14, P24 and P27 [61]. In addition, a primer-binding site (PBS) at the 5' end of the SRV genome can bind to the transfer RNA (tRNA) and initiate the reverse transcription of the viral genome. And the polypurine tract (PPT) at the 3' end can serve as the primer for the plus-strand viral DNA synthesis during the reverse transcription.

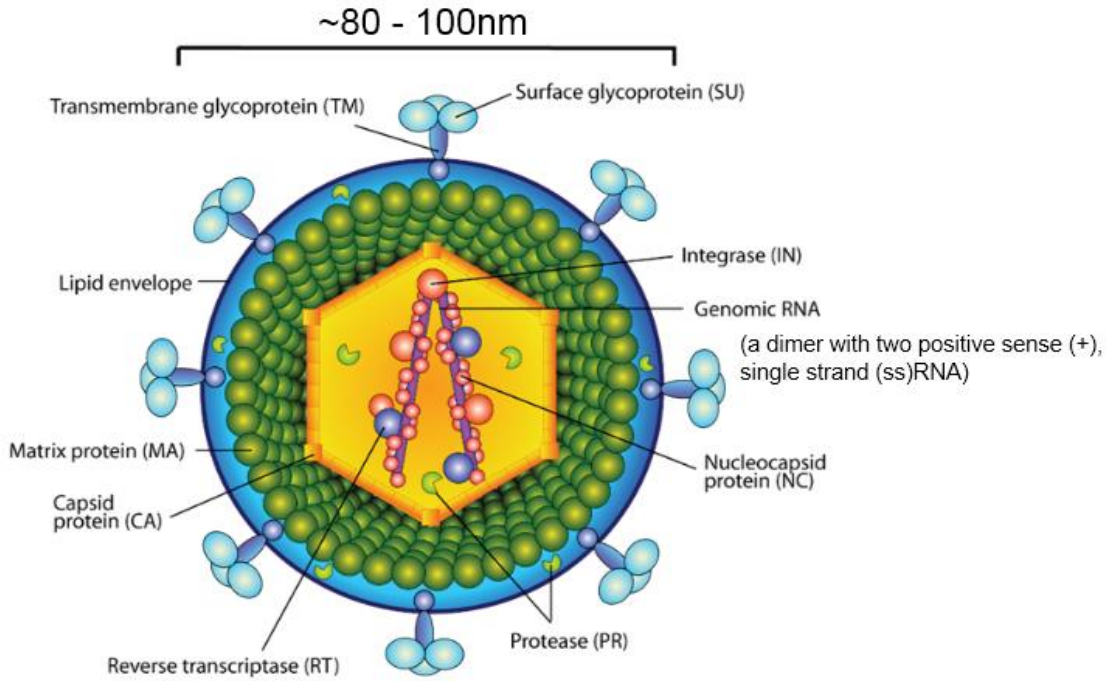

Figure 1.2 A schematic diagram of the retroviral structure. The retroviral virion has a lipid envelope of about 80-100 nm in diameter. The envelope encloses a capsid that consists of matrix protein (MA), capsid protein (CA), integrase (IN), reverse transcriptase (RT), protease (PR), nucleocapsid protein (NC) and the RNA genome. The retroviral genome is an RNA dimer consisting of two identical positive sense (+) single-stranded (ss) RNA. The figure is adapted from Gifford, 2013. Retroviral virion structure. *figshare.* doi:10.6084/m9.figshare.807677.v1

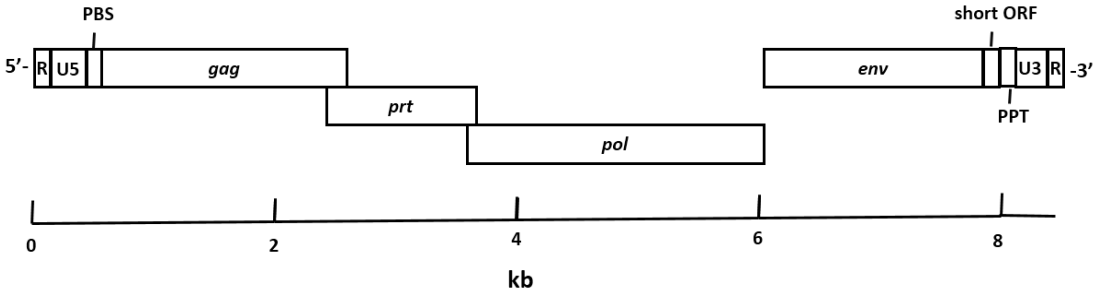

Figure 1.3 Genomic organization of SRV. The SRV genome contains four genes in the order of 5'-*gag*-*prt*-*pol*-*env*-3'. The *prt* gene is partially overlapped with the *gag* gene and the *pol* gene. The scale bar was shown on the bottom to present the position and approximate length of each gene. R: repeat sequence. U5: unique sequence at the 5' end of genome. U3: unique sequence at the 3' end of genome. PBS: primer binding site. PPT: polypurine tract.

The replication of SRV undergoes the following steps: the attachment and entrance to the host cells, reverse transcription of the genomic RNA into the proviral DNA, integration of the proviral DNA into the host genome, transcription of the proviral DNA and genome replication, translation and post-translational modifications, and assembly and release of the progeny virions. The attachment of SRV virions is mediated by the interaction between the surface glycoprotein (SU) of the viral envelope and the specific receptor on the host cell surface followed by the fusion of the viral envelope with the cellular plasma membrane, leading to the release of viral capsid into the cytoplasm. Previous studies have demonstrated that ASCT2, a neutral amino acid transporter, might be the cellular surface receptor for SRV [62-64]. The carboxyl-terminal region (termed region C) in the extracellular loop 2 of ASCT2 plays an essential role in the interaction with SRV [65]. Moreover, ASCT2 has been shown to be widely distributed in various tissues in Japanese macaque including, but not limited to, the lung, thymus, lymph nodes, spleen and stomach [63]. Once the viral capsid enters the cytoplasm, the genomic RNA is reverse transcribed into a double-stranded DNA, known as the proviral DNA, by using $tRNA^{Lys}$ as the primer [59]. Different from the viral genome, a copy of the proviral DNA has two identical sequences at each terminus, known as the long terminal repeat (LTR) that consists of a U3-R-U5 sequence. The LTR contains the important sequences that are essential for the integration of the proviral DNA into the host genome as well as the expression of the viral genes [59, 66]. After the reverse transcription, the proviral DNA is transported to the nucleus and randomly inserted into the host genome by the action of integrase. After the

integration is completed, the viral genes will be expressed through the host RNA polymerase II-mediated transcription. The proviral LTR functions as an enhancer and promoter to regulate the viral gene transcription. Some of the transcription products will function as mRNAs for translation into the regulatory and structural proteins; others will become the RNA genome of progeny virions. With the increasing number of genomic RNAs and viral proteins in the infected cells, the assembly of progeny virions occurs. For SRV, the immature core is assembled in the cytoplasm before being transferred to the plasma membrane in regions where the envelope proteins have accumulated. The envelope is then acquired by budding of the core from the plasma membrane.

To date, nine exogenous subtypes of SRV have been identified from the captive and feral non-human primates, named from SRV-1 to SRV-8 and SRV-Tsukuba (SRV-T). The genomes of SRV-1 through SRV-5 and SRV-8 have been completely sequenced [7, 58, 59, 67-71]; while the genomes of SRV-T, SRV-6 and SRV-7 have been only partially sequenced [72-74]. SRV-1 and SRV-2 were both isolated in the 1980s from the rhesus macaques at the California National Primate Research Center (NPRC) and the pig-tailed macaques at the Washington NPRC respectively [75, 76]. SRV-3 is the first SRV subtype isolated from a rhesus monkey in 1970 at Mason research Institute in the USA and was originally recognized as a Mason-Pfizer monkey virus [5]. In 1984, SRV-4 was isolated from a cynomolgus macaque at the California NPRC [77]. In 2015, SRV-5 was discovered in the rhesus macaques imported from China at the Oregon NPRC [78].

SRV-6 and SRV-7 were isolated from the wild-caught Hanuman langurs and wild rhesus macaques, respectively, in India [72, 79]. SRV-T was isolated from the cynomolgus macaques at the Tsukuba Primate Center in Japan [73]. And recently, a new SRV subtype, named SRV-8, was discovered in the USA and China from Cambodian-origin cynomolgus macaques [7]. According to the complete genome comparison and phylogenetic analysis, SRV-8 was indicated to be serologically and phylogenetically closer to SRV-4 than other SRV subtypes.

1.2.2 Pathology and pathogenesis of SRV

SRV can cause a broad spectrum of clinical and pathological manifestations in the infected monkeys, ranging from no clinical signs to overt diseases (e.g. fever and diarrhea) and the fatal SAIDS [12, 13]. SRV was recognized as the etiological agent of SAIDS, which presents a disease spectrum varying from lymphadenopathy to hematologic abnormalities and severe immune deficiencies [9, 12, 80, 81]. Common clinical manifestations of SRV-infected monkeys include weight loss, anemia, lymphopenia, neutropenia, diarrhea and lymphadenopathy [80, 82, 83]. Moreover, lesions of the gastrointestinal tract are also commonly detected in SRV-infected monkeys, including enteritis and villous blunting [80, 82, 84]. Additionally, SRV infection has been shown to be associated with several neoplastic diseases, including subcutaneous fibrosarcomas (SF), retroperitoneal fibromatosis (RF) and B cell lymphomas [85-88]. There was evidence indicating that the development of

lymphomas and fibromatosis in the infected monkeys were due to the co-infection of herpesviruses secondary to SRV-induced immunodeficiency. The development of lymphomas was due to the co-infection of the Epstein-Barr-like herpesvirus (EBV), whereas the gammaherpesvirus was identified as the etiologic agent for SRV-induced fibromatosis. [87, 89].

Histopathologic changes are also consistently found in lymphoid tissues of SRV-infected monkeys. Early stages of SRV infection are commonly characterized by lymphoid hyperplasia in lymph nodes and other non-lymphoid tissues such as kidney and bone marrow [80, 82, 90], while the late stages are usually accompanied by varying degrees of lymphoid depletion, including the loss of both B and T lymphocytes [16, 90]. Additionally, SRV infection has been shown to decrease serum immunoglobulin production, reduce mitogen-induced proliferative responses by peripheral mononuclear cells, induce functional deficiencies in polymorphonuclear cells, and down-regulate the major histocompatibility complex class II (MHC-II) antigen expression [9, 14, 15]. Moreover, hematologic abnormalities, such as anemia and neutropenia, are also the prominent characteristics of SRV infection [81, 82, 91]. However, the mechanisms responsible for the pathological changes and hematologic abnormalities are not well understood.

SRV has been detected in various tissues and organs of the infected monkeys, such as digestive tract, salivary glands, nervous system, as well as lymph nodes, spleen, and

thymus by using *in situ* hybridization, immunohistochemical staining, electron microscopy or polymerase chain reaction (PCR) [63, 84, 92-94]. Moreover, previous studies have also indicated the broad cellular tropism of SRV in both lymphoid and non-lymphoid cells, including but not limited to B lymphocytes, T lymphocytes, macrophages, lung fibroblasts, and epithelial cells of the gastrointestinal tract and mouth [16, 92, 95, 96]. More viruses have been detected in CD4+ T cells than CD8+ T cells, suggesting that CD4+ T cells might be the major host cells of SRV [16]. Additionally, SRV virions have been commonly detected in various body fluids, including the saliva, urine, blood and breast milk [13, 83, 97]. The natural transmission of SRV commonly occurs horizontally, through the direct contact of the normal and the infected monkeys with SRV shed in body fluids [13, 98]. The maternal transmission has also been demonstrated in the females that are infected with SRV during pregnancy [99].

Development of neutralizing antibodies is the major host immune response to SRV infection. In the infected monkeys, antibody titers and viremia display an inverse correlation. The infected animals with high neutralizing titers exhibit less severe diseases and histologic lesions, while the viremic animals usually have undetectable or low antibody titers [12, 82, 91, 100]. Generally, during viral invasion, the innate and adaptive immunities and inflammatory responses will be activated in hosts through the actions of cytokines and growth factors. However, little is currently known regarding the effects of SRV infection on the expression of cytokines and cell surface

markers.

Due to the close phylogenetic relationship between non-human primates and human beings, Asian macaques of the genus *Macaca* are commonly used as the animal model for biomedical studies [3]. There are three major simian viruses that can naturally harbor in Asian macaques, including SRV, simian foamy virus (SFV) and simian T-lymphotropic virus (STLV) [101, 102]. Among them, SRV infects large percentages of Asian macaques and is able to establish persistent infection, which might lead to immunosuppression and malignant diseases in the infected hosts [3, 10]. Therefore, studies on the immune-modulating effects of SRV infection will help us to better understand the retrovirus-host interactions and the retrovirus-induced immunosuppression [6].

1.3 The apoptotic pathway, autophagic pathway and viral infection

1.3.1 Molecular mechanism of the apoptotic pathway

Apoptosis, also named PCD, is an evolutionarily conserved process used by organisms to eliminate unwanted cells [103]. In 1972, the term 'apoptosis' was first proposed to describe the natural cell death that maintains tissues homeostasis by mediating the balance between cell death and proliferation [103]. This self-destruction process was also identified as the cellular response to a variety of stimuli, such as DNA damage and viral invasion [104]. Apoptosis is characterized by various morphological changes, including nuclear fragmentation, chromatin condensation, cell rounding and shrinkage, and the formation of apoptotic bodies which are then recognized and ingested by neighboring phagocytic cells [105-107].

Apoptosis is a complex but highly regulated process that can be triggered by two major apoptotic pathways: the intrinsic (or mitochondrial) pathway and the extrinsic (or death receptor) pathway (Fig. 1.4) [23]. The intrinsic and extrinsic pathways are initiated and mediated by two energy-dependent caspase cascades [108]. Caspases are a group of proteins that belong to the family of cysteine protease and are highly conserved among mammals. Normally, caspases exist as the inactive precursors, known as procaspases, which are activated by the proteolytic cleavage during the process of apoptosis [109, 110]. Depending on their functions in the apoptotic pathway, caspases are classified into two categories: the upstream initiators and the downstream executioners [111]. The initiator caspases contain either the caspase

recruitment domain (CARD) or the death effector domain (DED) which could interact with other apoptotic signaling proteins containing the same domains through homophilic interactions, triggering the activation of the initiator caspases [112, 113]. Caspase-8 and caspase-9 are two important initiator caspases involved in the extrinsic and intrinsic pathway respectively. Executioner caspases such as caspase-3, -6 and -7, also known as effector caspases, are activated by the proteolytic cleavage mediated by the activated initiator caspases. The activated effector caspases will then selectively cleave a range of structural proteins as well as DNA repair related proteins, such as actin and Poly (ADP-Ribose) Polymerase (PARP), thereby leading to the apoptotic cell death.

The intrinsic, or mitochondrial, apoptotic pathway is usually activated in response to the intracellular stress, such as hypoxia, extensive DNA damage and defective cell cycle. The process of the intrinsic apoptotic pathway was shown in Figure 1.4a. The mitochondrial outer membrane permeabilization (MOMP) caused by the intracellular stress is an essential step to initiate the intrinsic pathway. MOMP leads to the release of caspase activators, such as cytochrome c, from mitochondria to cytoplasm [114]. The released cytochrome c binds to the apoptotic peptidase activating factor-1 (Apaf-1) to facilitate the formation of an apoptosome. In the presence of deoxyadenosine triphosphate (dATP), the CARD domain of Apaf-1 can bind to procaspase-9 and recruit it into apoptosome, leading to the oligomerization and autoactivation of procaspase-9 [115-118]. The activated caspase-9 is then turned to proteolytically cleave and

activate the effector procaspase-3, leading to apoptosis.

The pro- and anti-apoptotic proteins in the Bcl-2 family are essential to control the permeabilization of mitochondrial outer membranes [119, 120]. Members of the Bcl-2 family contain one or more Bcl-2 homology (BH) domains, including BH1, BH2, BH3, and BH4. Some of the pro-apoptotic proteins, such as Bax and Bak, contain three BH domains (BH1-3); while other pro-apoptotic proteins, such as Bad and Bid, are BH-3 only proteins. All anti-apoptotic Bcl-2 family proteins, such as Bcl-2 and Bcl-xL, contain all four BH domains [121]. Under stressful conditions, the pro-apoptotic proteins can aggregate and form the homo-oligomers on the mitochondrial membrane, creating pores and leading to the release of cytochrome C. On the other hand, the anti-apoptotic proteins can bind to and inhibit the function of pro-apoptotic proteins, resulting in the inhibition of apoptosis. Therefore, the equilibrium between the pro- and anti-apoptotic proteins plays a key role to mediate the intrinsic apoptotic pathway, and the imbalance of Bcl-2 family proteins could induce MOMP followed by the activation of caspase-9 and apoptosis [122, 123].

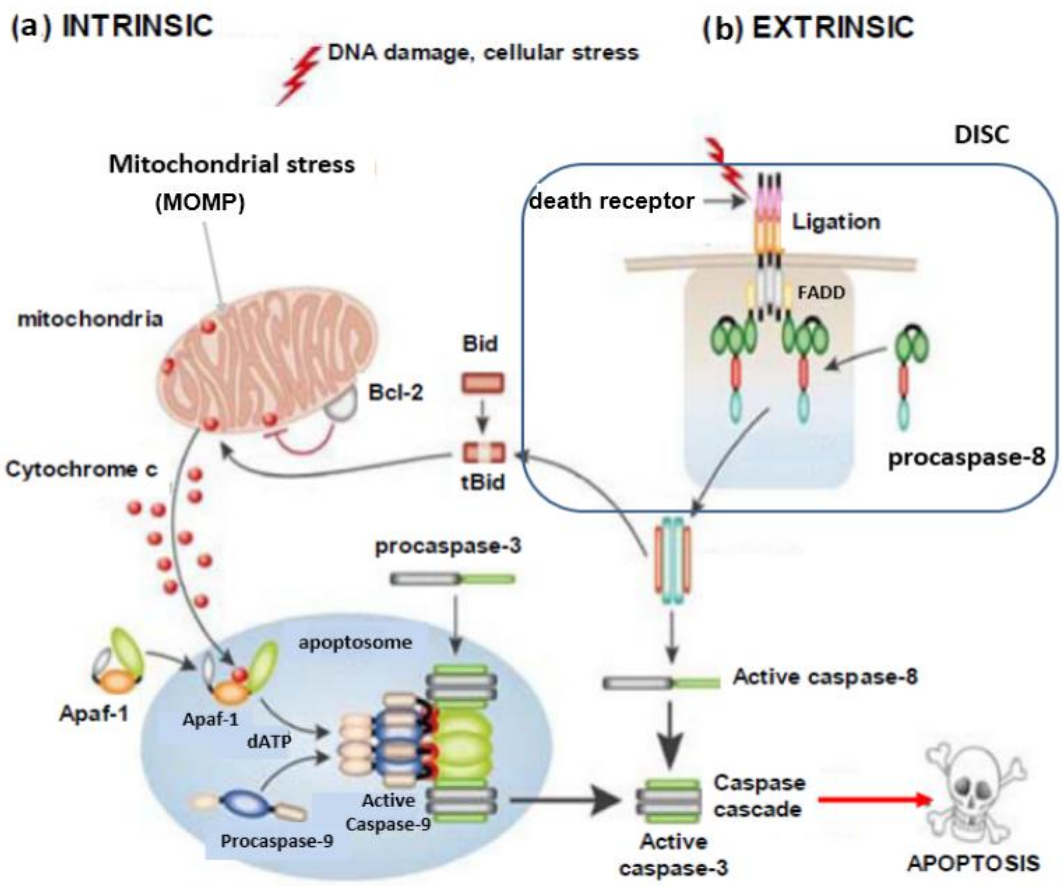

Figure 1.4 Overview of the intrinsic and extrinsic apoptotic pathway. The schematic representation of the (a) intrinsic and (b) extrinsic apoptotic pathways. The figure is adapted from MacFarlane *et al.,* 2004. Apoptosis and disease: a life or death decision. *Conference and Workshop on Apoptosis and Disease*, 5(7): p. 674-678. [124]

The extrinsic apoptotic pathway is initiated through the binding of ligands with the respective cell surface death receptors classified in the subclass of the tumor necrosis factor receptor (TNFR) superfamily [125]. The death receptor is structurally characterized by an extracellular ligand-binding region, a membrane-spanning region, and an intracellular death domain (DD) motif, which is essential for the transduction of apoptotic signals [126, 127]. Currently, the well-characterized death receptors and the corresponding ligands include TNF receptor 1 (TNFR1) and TNF-α, Fas receptor (Fas)

and Fas ligand (FasL), TNF-related apoptosis-inducing ligand (TRAIL) receptor 1 (TRAIL-R1, also known as DR4) and TRAIL, and TRAIL-R2 (also known as DR5) and TRAIL [127-131].

The binding of ligands and their respective death receptors induces the formation of the death-inducing signal complex (DISC), which is a multiprotein complex composed of the death receptor, Fas-associated death domain (FADD) and procaspase-8 (Fig. 1.4b). Upon the binding of ligands, the intracellular death domain of the death receptor binds to FADD, which in turn recruits the inactivated procaspase-8 via dimerization of the DED [132, 133]. At this point, the DISC is formed, leading to the oligomerization and autoactivation of procaspase-8 through self-cleavage [134]. The activated caspase-8 is then released from the DISC and activates the effector procaspase-3 by proteolytic cleavage, leading to apoptosis. Notably, for the intrinsic and extrinsic pathways, the activated caspase-9 and caspase-8 is able to activate the same effector caspases, such as procaspase-3. However, caspase-8 can not only activate procaspase-3 but also cleave Bid which is a member of the Bcl-2 family that is involved in the intrinsic pathway. The resulting 15 kDa truncated Bid (tBid) C-terminal fragment is then transfered to the mitochondria and induces MOMP by cooperating with Bak and Bax [135, 136]. This mechanism connects the extrinsic and intrinsic apoptotic pathways, leading to the amplification of apoptotic signals and the efficient execution of apoptosis.

1.3.2 Molecular mechanism of the autophagic pathway

Autophagy is an evolutionarily conserved and highly regulated intracellular digestion process to disassemble dysfunctional or unnecessary components for recycling. Thus, the autophagic degradation plays an important role in maintaining cell homeostasis by replenishing the cells with building blocks, such as fatty acids and amino acids, for anabolic processes [21, 22, 137]. There are three major types of autophagy, known as macroautophagy, microautophagy and chaperone-mediated autophagy [138]. Macroautophagy, often simply referred to as autophagy, accompanies a dynamic process of autophagosome formation followed by the lysosome-mediated degradation [139]. Microautophagy is characterized as the direct engulfment of the targets for degradation by lysosome [140]. Differently, chaperone-mediated autophagy is a highly selective degradation pathway, which specifically recognizes and digests the proteins containing the KFERQ sequence [141]. The hsc70 complex in the chaperone can recognize and interact with the target proteins to form the substrate/chaperone complex, which in turn translocates to the lysosome for degradation [141]. Among the three types of autophagy, macroautophagy, hereafter referred to as autophagy, is the predominant form of the autophagic pathway and has been mostly investigated in recent years.

Autophagy-related genes (*atg*) play critical roles to regulate the autophagic pathway. The first *atg* gene was discovered in the nutrient-deprived yeast through genetic screening [142]. Currently, more than 30 *atg* genes have been identified in yeast, and

some of them were further defined as the core *atg* genes, which are highly conserved from yeast to humans and essential for the formation of autophagosome [143, 144]. The core *atg* genes can be further divided into three functional groups: (1) the class III phosphatidylinositol 3-OH kinase (PI3K) complex, including vacuolar protein sorting (Vps)15, Vps34 and Atg6 (Beclin1 in mammals); (2) Atg9 and the related functional system, including Atg1, Atg9, Atg2 and Atg18; and (3) two ubiquitin-like (Ubl) conjugating systems, including the Atg12-Atg5-Atg16 complex and the Atg8 (microtubule-associated proteins 1A/1B-light chain 3 (referred as LC3) in mammals) conjugation system [143, 145].

The autophagic process occurs in a stepwise manner comprising steps of induction, phagophore nucleation, phagophore elongation and autophagosome maturation, and eventually autophagosome-lysosome fusion and cargo degradation (Fig. 1.5) [146]. In normal growth conditions, autophagy is maintained at low basal levels; therefore, an efficient mechanism to mediate the initiation of autophagy is important for cells to adapt to different stresses. Generally, the induction of autophagy is regulated by the mammalian target of rapamycin (mTOR), which normally blocks the autophagic pathway by binding and phosphorylating the unc-51-like kinase 1/2 (ULK1/2)-Atg13-FIP200 complex. Under stressful conditions, such as starvation, mTOR is suppressed and thus results in the dephosphorylation and activation of the ULK1/2-Atg13-FIP200 complex, which in turn initiates the autophagic process [147, 148]. The formation and nucleation of the phagophore, a pre-autophagosomal structure, is regulated by the

class III PI3K complex consisting of Vps34, Vps15 and Beclin1 [149]. The activity of this kinase complex is mediated by a series of negative and positive regulators, such as Bcl-2 and Atg14L respectively. Notably, Beclin1, the mammalian homologues of Atg6, interacts with Vps34 in the class III PI3K complex and plays a critical role in the induction of autophagosome formation [150]. Although Beclin 1 does not have any enzymatic activity, it acts as an essential platform to recruit the regulators to mediate the activation of class III PI3K complex [151, 152].

Expansion of the phagophore is mediated by two Ubl-conjugation systems. One is the Atg12-Atg5-Atg16 conjugation system. Atg12, a Ubl protein, is activated by Atg7 and Atg10 (E1- and E2-like enzyme, respectively) followed by conjugation with Atg5. The Atg12-Atg5 complex then interacts with Atg16, forming the Atg12-Atg5-Atg16 complex, which mainly attaches to the outer side of phagophore and initiates the LC3 conjugation system [153, 154]. LC3 is firstly cleaved by Atg4, a cysteine protease, to expose the glycine residue and form the soluble LC3-I that locates in the cytoplasm [155]. LC3-I is then converted to a lipid-conjugated form, LC3-II, by conjugating with phosphatidylethanolamine (PE) under the help of Atg7 and Atg3 [156, 157]. Under the stable cellular state, LC3 normally exists as the soluble form dispersed throughout the cytoplasm; however, upon the induction of autophagy, the majority of LC3-I is converted to LC3-II that tightly binds to both the outer and inner membranes of phagophores [158-160]. Therefore, the level of LC3-II, as well as the conversion of LC3-I to LC3-II are widely used to evaluate the autophagic flux [161, 162]. After the

completion of autophagosome formation, the Atg12-Atg5-Atg16 complex is released back to the cytosol for recycling usage [163, 164]. Meanwhile, LC3-II in the outer membrane of autophagosome is cleaved from PE by Atg4 and released back to the cytosol for recycling; however, LC3-II in the inner membrane is retained and degraded after the fusion of autophagosome with lysosome [159, 165]. Notably, LC3 has been identified to play a role not only in the phagophore elongation but also in the cargo-selection for the autophagic degradation [166-168]. LC3 can interact with the WXXL motif in the LC3-interaction region (LIR) of the adaptor molecules, such as p62/SQSTM1 and neighbor of BRCA1 gene 1 (NBR1), and recruit them into autophagosome [168-171]. p62/SQSTM1 and NBR1 are ubiquitin-binding proteins, which contain the ubiquitin-binding association (UBA) domain that can selectively bind to the ubiquitinated cargos and recruit them into autophagosome, resulting in the degradation of ubiquitinated proteins by autophagy [172-174].

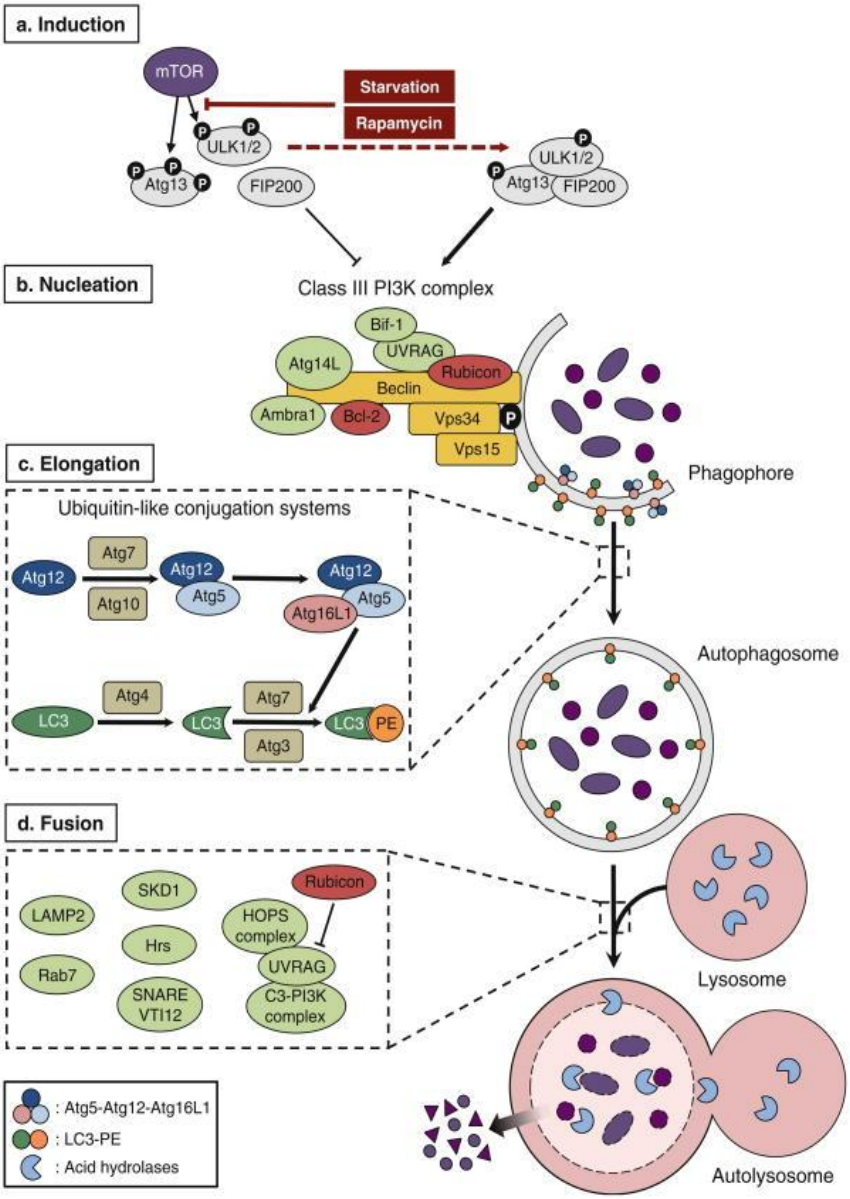

Figure 1.5 Overview of the autophagic pathway. The autophagic pathway can be divided into different phases: induction, nucleation, elongation, lysosomal fusion and cargo degradation. Inhibition of mTOR results in the activation of ULK1/2-Atg13-FIP200 complex, which is essential for the induction of phagophore nucleation. The class III PI3K complex, including Vps15, Vps34 and Beclin1 in mammals (*yellow*), plays a critical role to mediate the nucleation of phagophore. The activity of this complex is regulated by negative (*red*) and positive (*green*) regulators that associate with Beclin1. The elongation of phagophore is mediated by two ubiquitin-like conjugation systems, including the Atg12-Atg5-Atg16 complex and the LC3 conjugation system. The completed autophagosome then fuses with lysosomes to form autolysosome by the action of various negative (*red*) and positive (*green*) regulators. Finally, the cargos in the inner vesicle of autolysosome are degraded by lysosomal acid hydrolases and released to the cytosol for recycling. The figure is adapted from Kim et al., 2010. When autophagy meets viruses: a double-edged sword with functions in defense and offense. *Semin Immunopathol*, 32(4): p. 323-41. [175]

Autophagosome has a spherical structure with double membranes. Several organelles have been identified as the sources of the autophagosomal membrane, including Golgi complex, mitochondria and the endoplasmic reticulum (ER) [176-178]. Different from other endomembrane trafficking systems, which normally generate the membrane by budding from the surface of the donor organelles; the assembly of autophagosomal membrane is achieved by the addition of new membranes. However, the mechanism of how the additional membranes are delivered is still largely unknown. Atg9 and Atg27 are the only known integral membrane proteins that have been demonstrated to facilitate the growing of autophagosomal membrane [179]. Atg9 functions as a carrier of the lipid bilayer, together with Atg27 and Atg23, circulating between the donor membrane and the growing autophagosomal membrane to support the addition of the new membrane [180-182].

The completed autophagosome then fuses with the lysosome to form autolysosome, with the help of small GTPase Rab7 and the lysosomal membrane protein LAMP-2 [183, 184]. After the formation of autolysosome, the degradation of cargos in the inner vesicle is conducted and mediated by a series of lysosomal acid hydrolases, such as cathepsins B, D and L [185, 186]. The resulting degraded molecules, mainly amino acids and fatty acids are released back to the cytosol for recycling.

1.3.3 Crosstalk between the apoptotic and autophagic pathways

Apoptosis and autophagy are two important cellular processes that usually

interconnect with each other to determine cell fate between death and survival [187, 188]. Generally, following the activation of the caspase cascade, apoptosis leads to the irreversible cell death. Whereas autophagy is commonly recognized as a cytoprotective process to mediate cellular homeostasis that allows cells to survive. Under some conditions, autophagy is believed to avert the induction of apoptosis and promote cell survival. However, under other conditions, autophagy may lead to cell death either by directly inducing apoptosis or being independent of apoptosis. The crosstalk between apoptosis and autophagy is complex and mainly regulated by the proteins with dual roles in these two pathways [189, 190].

Autophagy has been shown to inhibit apoptosis. One of the examples is mitophagy, which is defined as the degradation process of mitochondria by autophagy [191]. During the intrinsic apoptosis, the occurrence of MOMP leads to the inhibition of PTEN-induced putative kinase 1 (PINK1) proteolysis. PINK1 then accumulates at the outer membrane of mitochondria and recruits the E3 ubiquitin ligase, Parkinson's disease protein (Parkin), which in turn ubiquitylates the substrates at the surface of mitochondria, thus targeting the damaged mitochondria for autophagic degradation [191, 192]. Therefore, mitophagy can remove the damaged and apoptosis injured mitochondria to delay or block the onset of the intrinsic apoptosis [188]. In addition, Atg5 has been shown to directly interact with FADD to inhibit the extrinsic apoptosis without affecting the autophagic pathway [193]. Moreover, autophagy can also inhibit apoptosis by selectively degrade the specific pro-apoptotic proteins, such as caspase-

8 [194-196]. In this process, the targeted proteins are ubiquitinated followed by interacting with selective autophagy receptors, such as p62/SQSTM1, to be recruited into autophagosomes for degradation.

Autophagy has also been shown to induce apoptosis via several mechanisms. Atg12 was shown to directly interact with anti-apoptotic Bcl-2 family proteins, such as Mcl-1 and Bcl-2, to inhibit their functions thus induce the intrinsic apoptosis [197]. Moreover, Atg5 and Atg4 can be cleaved by calpain and caspase-3 respectively; and the cleaved Atg5 and Atg4 then translocate to the mitochondria and interact with anti-apoptotic proteins to trigger MOMP, thereby switching autophagy to apoptosis [198-200]. In addition to the role that autophagic proteins play in apoptosis, the autophagosome has recently been identified to regulate apoptosis. Autophagosomal membranes can serve as a platform for assembly of the death signaling complex, which is known as the intracellular death-inducing signaling complex (iDISC) that can lead to the activation of caspase-8 independent of death ligands/receptors [201]. Several studies have shown that the intracellular persistent ER stress or proteotoxicity stress can induce the assembly of iDISC on the autophagosomal membrane, leading to apoptosis [202-205]. Under the stressful conditions, procaspase-8 can be polyubiquitinated at K63 by TRIM13, a RING-E3 ubiquitin ligase [206]. The polyubiquitinated procaspase-8 then translocates to autophagosomal membranes, where it interacts with LC3 and p62/SQSTM1, resulting in its oligomerization and activation. LC3 and p62/SQSTM1 are two important markers of the autophagosome that also play important roles in the

process of recruiting the ubiquitinated procaspase-8 to the autophagosome. In addition, Atg5 and FADD have also been shown to take part in the formation of iDISC. The C-terminal region of Atg5 interacts with the death domain of FADD, which might act as the adaptor protein to associate with procaspase-8 and recruit it to the expanding autophagosomal membrane [207]. In the cases of iDISC-mediated apoptosis, knockdown of either Atg5, FADD, LC3 or p62/SQSTM1 was demonstrated to significantly reduce the activation of caspase-8 and apoptosis; while overexpression of p62/SQSTM1 was shown to promote the aggregation and activation of caspase-8 on the autophagosome [201, 203, 205, 207, 208]. Notably, different from the autophagic degradation of activated caspase-8, the iDISC-mediated intracellular activation of procaspase-8 occurs on the expanding autophagosomal membrane and does not depend on the entire process of the autophagic flux.

Similar to the regulatory roles of autophagic proteins in the apoptosis pathway, components of the apoptotic pathway have also been shown to regulate the autophagic pathway [187-189]. One example is that the anti-apoptotic proteins, Bcl-2 and Bcl-xL, can bind to the BH3 domain of Beclin1 to inhibit the Beclin1-dependent autophagy [209-211]. However, the phosphorylation of Bcl-2 can dissociate it from Beclin1, leading to the initiation of autophagy [212]. Furthermore, several studies have shown that the caspases, such as caspase-3 and caspase-8, were able to cleave and inactive some essential autophagic proteins, including Beclin1 [213, 214], Atg3 [215] and the positive regulator in Beclin1 regulated autophagy (AMBRA1) [216]. The

cleaved autophagic proteins could significantly inhibit autophagy. Interestingly, the cleaved Beclin1, which loses the BH3 domain, could not only inhibit the autophagic pathway but also translocate to the mitochondria to mediate MOMP and induce the intrinsic apoptosis [213].

Crosstalk between apoptosis and autophagy also plays important roles in regulating viral infection and determining the fate of the infected cell. A growing number of studies has shown that the viral infection-induced autophagy was able to either inhibit or promote the apoptotic pathway in the infected cells [25, 38, 40, 217-220]. The human T cell leukemia virus (HTLV) transactivator (Tax)-induced autophagy has been shown to inhibit apoptosis and promote cell proliferation of the Tax-immortalized T cells [217]. Moreover, hepatitis C virus (HCV) infection could induce mitophagy, which selectively degrades the damaged mitochondria, to inhibit the intrinsic apoptosis in the infected cells thus leading to the persistent viral infection and replication [219]. Similarly, a recent study has demonstrated that the respiratory syncytial virus (RSV) infection-induced autophagy significantly enhanced viral replication by inhibiting the apoptotic pathway in the infected Hep2 cells [40]. However, in some cases, the autophagic process has been shown to promote the apoptotic cell death in the infected cells. Matrix protein 2 (M2) of the influenza virus (IAV) has been demonstrated to block the degradation of autophagosome in the infected cells, and the accumulated autophagosomes were shown to significantly increase the apoptotic death of IAV-infected cells [25, 218]. Interestingly, studies have demonstrated that during HIV

infection, the apoptotic cell death of uninfected bystander CD4+ T cells was induced by autophagy [38, 220-222]. The increased autophagic flux in the uninfected CD4+ T cells was due to the binding of HIV envelope glycoprotein (Env) in the infected cell surface to the C-X-C chemokine receptor type 4 (CXCR4) or C-C chemokine receptor type 5 (CCR5) in the uninfected cells. However, the underlying mechanism of the autophagy-mediated apoptosis in the uninfected bystander CD4+ T cells was still unclear.

Although the crosstalk between apoptosis and autophagy are complex and diverse under different scenarios, their interactions have been demonstrated to play important roles in stressful conditions, such as cancer development, viral invasion as well as other human diseases (e.g. Alzheimer's disease) [223-226]. For viral infection, investigation of these interactions could certainly help us to better understand the virus-host interactions and provide the new insights for the development of novel antiviral therapies.

1.3.4 Roles of autophagy in viral infection

Autophagy is an evolutionarily conserved host defense response that plays essential roles in innate and adaptive immunity against viral infection [17, 18]. However, a growing number of studies has demonstrated that some viruses can suppress the autophagic pathway to escape the immune defense, while other viruses can enhance and hijack this pathway for their own benefits, including fostering the viral replication

[24, 32-34]. Therefore, depending on the types of viruses and host cells, autophagy can act as either the anti-viral or pro-viral process.

As a fundamentally important cellular degradative process, autophagy is able to directly eliminate the intracellular pathogens. Autophagosome can selectively recruit the cytoplasmic virions and viral components for the lysosomal degradation, in the process termed xenophagy [227, 228]. One example is that herpes simplex virus type 1 (HSV-1) virions could be degraded by xenophagy [229, 230]. However, the ICP34.5 protein of HSV-1 has been shown to interact with Beclin1 and inhibit the Beclin1-mediated autophagy in the infected neurons [231]. The major autophagic adaptors to target and recruit pathogens into the autophagosome are classified as Sequestosome 1/p62-like Receptors (SLRs), including p62/SQSTM1, NBR1 and nuclear dot protein 52 kDa (NDP52) [232]. SLRs were shown to interact with the capsid of Sindbis virus for the autophagic degradation [233]. Moreover, the previous study with HIV-1 has shown that HIV-1 infection-induced autophagy was able to selectively degrade HIV Tat protein and thus restrict viral replication in CD4+ T lymphocytes [234].

Autophagy also takes part in the innate immunity by delivering the intracellular pathogen-associated molecular patterns (PAMPs), such as viral nucleic acids, to endosomal pattern recognition receptors (PRRs) for interferon (IFN) production [235, 236]. Toll-like receptors (TLRs) are the best-characterized group of PRRs to recognize viral PAMPs, such as ssRNA (TLR7/8), dsRNA (TLR3) and CpG DNA (TLR9) [237]. Upon

activation, the signaling transduction from TLRs leads to the expression of type I IFN, which in turn mediates the expression of IFN-regulated genes and leads to immune responses [238]. Autophagy has been demonstrated to play a key role in the process of delivering viral nucleic acids to TLRs, and thus promote the TLR-mediated IFN secretion and innate immunity [239-241]. Generally, autophagosome can package and deliver viral replication intermediates into the endosomes, where TLR signaling is triggered as an antiviral innate immune response [242]. One example is that the production of INF-α in vesicular stomatitis virus (VSV)-infected plasmacytoid dendritic cells (pDCs) depends on the autophagic delivery of viral intermediates to TLR7 [240].

Autophagy is not only involved in the innate immunity but also plays a critical role in the adaptive immunity by delivering the intracellular antigens onto the major histocompatibility complex (MHC)-I and MHC-II molecules for presentation [243-245]. Upon viral infection, MHC molecules on the cell surface can present the fragments of viral antigens, which are generated by distinct proteolytic mechanisms, to stimulate T cells and initiate the adaptive immunity [246]. Studies with HSV-1 and EBV have suggested that autophagosome could efficiently and constitutively deliver cytoplasmic viral components for the lysosomal degradation and the subsequent presentation of viral antigens onto MHC molecules [247, 248]. Moreover, the fusion of influenza matrix protein 1 (MP1) to LC3, which results in the increased recruitment of MP1 to autophagosomes, was shown to significantly enhance the MHC-II presentation for CD4+ T cell activation [249].

As an important part of the host defense system, autophagy has been identified to suppress the replication and pathogenicity of various viruses, such as Sindbis virus, VSV, tobacco mosaic virus (TMV) and Japanese encephalitis virus (JEV) [250-253]. However, several studies have shown that some viruses have developed a serial of strategies to exploit the autophagic pathway to benefit their replications [24, 254, 255]. In general, viruses could interfere with the autophagic pathway at two stages of autophagosome biogenesis: one is the formation of autophagosome and the other is the fusion of autophagosome with lysosome [256-258].

Some DNA viruses, especially HSVs mainly inhibit the formation of autophagosome to escape the autophagic degradation of the viral components. Other HSVs, such as Kaposi's Sarcoma herpesvirus (KSHV) and murine γ-herpesvirus 68 (MHV-68), encode the viral Bcl-2 homologue (known as vBcl-2) to interact with Beclin1, thereby inhibiting the biogenesis of autophagosome [37, 259, 260]. In addition, several HSVs encode the homologs of cellular FLICE-like inhibitor protein (cFLIP), known as vFLIPs, to inhibit the elongation of autophagosome [261]. vFLIP is able to interact with Atg3 to reduce the affinity between Atg3 and LC3, thereby inhibiting the function of LC3.

In contrast to DNA viruses that mainly inhibit the formation of autophagosome, RNA viruses generally interfere with the autophagic pathway by inhibiting the maturation of autophagosome or blocking the fusion of autophagosome with lysosomes. Accordingly, the accumulated autophagosomal membrane was often acted as a

scaffold to support the viral replication or promote the maturation of viral particles [34, 262]. Poliovirus, a member of the *Picornaviridae* family, is the first virus that was identified to induce the accumulation of autophagosome in the infected cells [263]. Poliovirus proteins 3A and 2BC induce the lipidation of LC3 and thus promote the formation of autophagosome, which provides the membrane-associated 'factories' to enhance the viral replication [26, 264]. Other picornaviruses, such as coxsackievirus B3 (CVB3) and food-and-mouth disease virus (FMDV), also lead to the accumulation of LC3-positive vesicles in the infected cells to support the viral replication [265-267]. Similarly, the pro-replication role of autophagy has been also discovered in flavivirus infection, such as HCV and dengue virus (DENV) [268-271].

Utilization of the autophagic flux to facilitate viral replication and propagation has been shown not only by the RNA viruses that replicate in the cytosol, but also by the RNA viruses that replicate in the nucleus. The well-characterized examples are IAV and HIV. The IAV M2 protein has been identified as an essential and sufficient factor to block the degradation of autophagosome in the infected cells [25]. Meanwhile, M2 could interact with LC3 through the LIR, leading to the redistribution of LC3-conjugated autophagosomal membranes to the budding sites of IAV, thereby promoting the assembly and budding of IAV from the infected cells [272, 273]. HIV infection has been shown to inhibit or induce autophagy in different scenarios, and the different effects appear to be host cell type specific [220, 221, 274-277]. In HIV-infected macrophages, HIV negative regulatory factor (Nef) acts as an anti-autophagic maturation factor

through the interactions with Beclin1 [278-280]. HIV seems to benefit from the autophagic inhibition, by preventing the autophagic degradation of viral components, such as transactivator (Tat) and Gag precursor, which are essential for HIV replication [280]. Moreover, the accumulated autophagosomal membranes in the infected macrophages may serve as a platform to facilitate the processing of Gag precursor into the core structural proteins, thereby increasing viral replication [280]. However, different from the HIV infection of macrophage, HIV displayed diverse abilities in modulating autophagy in the infected CD4+ T lymphocytes. Two independent researches showed that HIV-1 infection was able to inhibit the autophagic pathway in CD4+ T cells and MOLT-4 T lymphocytes by reducing the levels of LC3-II and Beclin1 [222, 281]. On the contrary, another research has shown that autophagy was enhanced in HIV-1-infected CD4+ T cells and Jurkat T lymphocytes [29]. Moreover, HIV-1 was shown to increase the levels of LC3, Beclin1, ULK1, Atg5 and Atg12 in the infected Jurkat T lymphocytes; and the inhibition of autophagy by 3-Methyladenine treatment or Beclin1 silencing was shown to reduce viral replication. Indeed, the interaction between HIV and autophagy in T cells is still not fully understood and needs further investigations.

As discussed above, there is certainly a complex interaction between the autophagic pathway and viral infection and the nature of interaction might depend on the types of viruses and host cells. Collectively, autophagy is recognized as a part of innate and adaptive immunity against the viral invasion; however, certain viruses have developed

a variety of strategies to inhibit autophagy or utilize the autophagic machinery to benefit their infection and replication. Therefore, autophagy is a 'double-edged sword' in viral infection and pathogenesis that acts as both anti-viral and pro-viral pathways.

1.4 *N6*-methyladenosine (m6A) RNA modification and viral infection

1.4.1 m6A and the cellular m6A machinery

RNA plays a crucial role in a wide range of cellular processes, such as in the epigenetic regulation of gene expression. Similar to DNA and protein modifications, RNA undergoes more than 150 post-transcriptional chemical modifications and this number continues to grow [282, 283]. Majority of these RNA modifications have been detected in transfer RNA (tRNA) and ribosomal RNA (rRNA), which can directly affect the processes of translation by changing their structures and functions [284]. In addition, it has also been shown that mRNA carries various modifications, such as *C5*-methylcytosine (m5C), m6A and *N1*-methyladenosine (m1A), which could affect mRNA metabolisms and functions [285-288]. So far, m6A is recognized as the most prevalent internal modification on eukaryotic mRNA, which is characterized as the replacement of the hydrogen by a methyl group on the *N6*-nitrogen in adenosine (Fig. 1.6).

In the 1960s, m6A modification was first discovered in rRNA and tRNA from mammalian cells [289, 290]. With the development of technology on mRNA

purification in the 1970s, studies have revealed that m6A was also widely distributed in the mature mRNA, with about half methylated bases are m6A-modified in the mRNA of mammalian cells [291-293]. Recent studies have also shown that there are 3 to 5, 1.4 to 2 and ~3 m6A sites on per transcript from mammalian cells, *Arabidopsis* and IAV, respectively [41, 294-296]. Furthermore, m6A has been discovered in RNAs of a broad range of eukaryotes, such as yeast, plants, *Drosophila*, human and mice, as well as in bacteria and a variety of viruses [41-47]. Considering the high conservation of m6A in different species and the high abundance of m6A in mRNA, it is not surprising that m6A modification plays an essential role in a wide range of biological processes [297-299].

Transcriptome-wide mapping of m6A had been lacking until the development of a new method in 2012, named the methylated RNA immunoprecipitation sequencing (MeRIP-seq) [41, 294]. Briefly, in this technology, poly(A)-tailed RNAs were extracted and purified from cells and fragmented into approximately 100 nucleotides (nt) lengths oligonucleotides (as input control). m6A-containing fragments were then pulled down by the m6A-specific antibody. The immunoprecipitated product (IP sample) and the input sample were then converted into the cDNA library, followed by being subjected to next-generation sequencing and mapped onto the relevant mRNA transcripts through bioinformatics methods. m6A peaks were determined by comparing the number of reads in the input and IP samples. The MeRIP-seq-based studies revealed that the occurrence of m6A modification is around 1 in 2000 bases in

human cellular transcripts, and the m6A sites were enriched in the 3' untranslated region (UTR) and the region adjacent to the stop codon [41, 294]. Additionally, a degenerate consensus motif for m6A was determined as 'DR(m6A)CH', where D represents A, G or U; R represents A or G, and H represents A, C or U [300, 301].

m6A is a dynamic reversible RNA modification process controlled by the cellular m6A machinery, including methyltransferases or "writers", demethylases or "erasers", and the m6A-specific binding proteins or "readers" (Fig. 1.6). In mammalian cells, the m6A "writers" is a large methyltransferase complex consisting of multisubunits. To date, only a few subunits have been determined, including methyltransferase-like 3 (METTL3), METTL14, Wilms tumor 1-associating protein (WTAP), RNA-binding motif protein 15 (RBM15), RBM15B, and Vir-like m6A methyltransferase associated (KIAA1429) [302-307]. Among these "writers", the complex of METTL3-METTL14-WTAP has been mostly well studied [308]. METTL3 and METTL14 are two methyltransferases that contain the S-adenosyl-methionine (SAM)-dependent methyltransferase domain to mediate the m6A methylation in mRNA. METTL14 displays 43% protein sequence identity with METTL3 and heterodimerizes with METTL3 through extensive hydrogen bonds [304]. However, only METTL3 has the catalytic activity, but METTL14 serves as an RNA-binding platform and plays a role in substrate recognition [309, 310]. Although METTL14 is catalytically inactive, its heterodimerization with METTL3 is essential for the activation of m6A methyltransferase complex [310]. At the steady state of cells, METTL3 and METTL14

are commonly localized in the nucleus, where the majority of m6A modification occurs; however, under some cellular stressful conditions, such as viral infection, METTL3 and METTL14 were detected in the cytoplasm [288, 311-314]. The other subunits of the methyltransferase, such as WTAP, RBM15, KIAA1429 and RBM15B, are recognized as the regulators to interact with the METTL3-METTL14 complex and function on the selective methylation of adenosine [305-307]. WTAP acts as a scaffold protein to mediate the translocation of the METTL3-METTL14 complex to the nuclear speckles, where the majority of m6A modification occurs [304, 306, 307]. In addition, WTAP has also been proposed to regulate the recruitment of target mRNA to the m6A methyltransferase complex [306]. Interestingly, the WTAP-independent m6A RNA modifications mainly occur at the 5’ cap of transcripts; whereas the WTAP-dependent m6A modifications primarily occur at the internal positions of the transcripts [307]. In addition, one study has revealed that knockdown of WTAP, METTL3 and METTL14 in HeLa cells resulted in the loss of around 50%, 30% and 40% global m6A sites in the cellular transcripts, respectively [304, 307]. Moreover, knockdown of KIAA1429 in human A549 cells could lead to a ~4-fold depletion of the global m6A level [307].

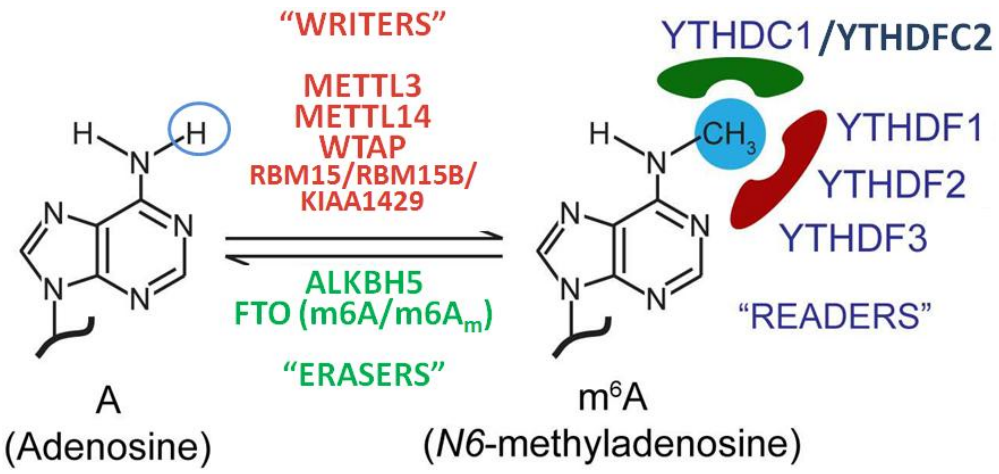

Figure 1.6 The cellular m6A machinery. m6A modification is a process to replace the hydrogen on the *N6*-nitrogen in adenosine of RNA by a methyl group. It is a dynamic reversible process that is governed by a cellular m6A machinery, including the m6A-specific "writers" and "erasers". Cellular m6A "writers" is a huge methyltransferase complex consists of two methyltransferases, METTL3 and METTL14, and other noncatalytic regulators, such as WTAP, RBM15, RBM15B and KIAA1429. M6A demethylases, FTO and ALKBH5, are the "erasers" to reverse the m6A modification by removing the methyl group. FTO has been recently proposed to preferentially demethylate $m6A_m$ than m6A, whereas ALKBH5 only targets m6A. A group of m6A-specific binding proteins is recognized as the "readers", including the cytoplasmic YTHDF1, YTHDF2, YTHDF3, and the nuclear YTHDC1, YTHDC2, to mediate the specific functions of m6A on mRNA. Figure is adapted from Gokhale, N.S. and S.M. Horner, RNA modifications go viral. 2017. 13(3): p. e1006188. [56]

To date, two m6A "erasers" have been identified, including fat mass and obesity-associated protein (FTO) and AlkB homolog 5 (ALKBH5), which are both markedly enriched in the nuclear speckles [315]. FTO was originally shown to strongly correlate with obesity, then it was identified as the first demethylase of m6A [316, 317]. In the presence of α-ketoglutarate and Fe(II), FTO oxidizes m6A into *N6*-hydroxymethyladenosine (hm6A) followed by further conversion of hm6A into another oxidized product, *N6*-formyladenosine (f6A) [318]. Both hm6A and f6A can be subjected to further demethylation into A. Studies have shown that overexpression of

FTO significantly decreased the global level of m6A in cellular RNAs, with ~18% reduction in HeLa cells; whereas knockdown of FTO greatly increased m6A levels by 42% and 23% in 293FT cells and HeLa cells respectively [294, 316]. However, recent studies reported that FTO only targets a specific subset of m6A-containing mRNA, with preference to demethylate *N6*,2'-O-dimethyladenosine ($m6A_m$) rather than m6A *in vivo* [319, 320]. Different from m6A, $m6A_m$ modification mostly occurs on the first few nucleotides at the 5' end of mRNA [321, 322]. Nevertheless, it is still unknown how FTO selectively targets the specific $m6A_m$ and m6A sites on mRNA. The other demethylase, ALKBH5, is an FTO homologue belonging to the AlkB family that only targets the m6A sites [323]. In HeLa cells, overexpression of ALKBH5 decreased the level of global m6A by ~29%, while knockdown of ALKBH5 increased the level of m6A by ~9% [323]. ALKBH5 was demonstrated to mediate the assembly of mRNA processing factors and affect nuclear RNA export through the demethylation activity [323]. ALKBH5 was also shown to play essential roles on the spermatogenesis in mice through the regulation of correct splicing of the 3'UTR of transcripts [323, 324].

Functions of m6A are determined by the m6A-specific binding proteins, known as the m6A "readers". Members of the YT521-B homology (YTH) domain family, including YTHDF1, YTHDF2 and YTHDF3 in the cytoplasm and YTHDC1, YTHDC2 in the nucleus, have been mostly studied as the major m6A "readers" that specifically interact with m6A sites through a hydrophobic pocket [48, 325-328]. YTHDF1 has been demonstrated to promote protein synthesis by interacting with translation initiation

factors, such as eukaryotic initiation factor 3 (eIF3) [326]. In contrast, YTHDF2 was able to induce the degradation of target mRNA by translocating them from the translation pool to mRNA decay sites, such as processing bodies (P bodies) [48, 329, 330]. YTHDF2-mediated degradation of m6A-containing mRNA was carried out by the CCR4-NOT complex and the DCP1/2 in P bodies [48, 331]. YTHDF3 has been shown to directly bind with YTHDF1 and/or YTHDF2 to facilitate their functions [332, 333]. In the nucleus, YTHDC1 was able to interact with the nuclear RNA export factor 1 (NXF1) and the serine- and arginine-rich splicing factor 3 or 10 (SRSF3 or SRSF10) to regulate the nuclear export and splicing of m6A-containing mRNA, respectively [49, 334, 335]. YTHDC2 mediates either degradation or translation of m6A-containing mRNA and plays an important role in mammalian spermatogenesis by mediating successful meiotic division of germ cells [333, 336, 337].

1.4.2 The emerging roles of m6A on viral infection

M6A modification has been shown to widely affect mRNA stability [48, 333], splicing [49, 338, 339], structure [51, 340] and translation [50, 326, 333, 341, 342]. Therefore, it is not surprising that m6A plays a critical role to regulate many fundamental biological processes and human diseases [297, 311, 343, 344]. To date, the dynamic change of m6A modification has been demonstrated to be involved in a broad range of biological processes, such as stem cell differentiation [54, 55, 345, 346], yeast sporulation [42], circadian rhythm [347, 348], plant development [47, 349, 350],

spermatogenesis and oogenesis [323, 333, 351-353], response to heat shock [341, 342], response to DNA damage [354], and tumor development and progression [355-359]. In addition, some studies have revealed that m6A was also distributed on several virus species and m6A modification was able to affect viral replication and the virus-host cell interactions [45, 46, 56, 57, 360-362].

m6A modification has been detected in the genome of RNA viruses as well as the transcripts of DNA and RNA viruses. Indeed, in the past few decade years, studies have demonstrated that m6A was detected in the viral genome of several viruses in the *Flaviviridae* family, such as Zika virus (ZIKV) and HCV [312, 313]; in the viral genome and viral mRNA transcripts of IAV [296, 363, 364]; in the viral mRNA transcripts of several DNA viruses, such as SV40, Adenovirus-2 and KSHV [365-369]; as well as in the viral genome and viral mRNA transcripts of several retroviruses, such as HIV-1, RSV and feline leukemia virus (FLV) [361, 370-374]. However, there is no such research to investigate the m6A modification of simian retrovirus, including SRV.

Early research on m6A in viral infection has proposed that this modification was able to regulate viral RNA splicing [375-377]. For example, the inhibition of m6A modification has been shown to reduce the splicing of RSV envelope mRNA [375]. With the recent development of MeRIP-seq technology and the discovery of the cellular m6A machinery, by modulating the levels of m6A-specific “readers”, “writers” and “erasers” in the host cells, recent studies have found the important roles of m6A on

viral infection [45, 46, 56, 57, 362, 368]. HIV is one of the most well-studied viruses to clarify that m6A modification and the m6A machinery are important regulators in the viral infection. Studies have mapped the distribution of m6A sites on the genome and viral transcripts of HIV in the infected HeLa cells, 293T cells and CD4+ T cells [361, 370, 371, 378]. Interestingly, the number and distribution of m6A sites on HIV genome were varied in different cell lines, suggesting that the dynamic process of m6A modification might depend on the types of the host cell. Two studies further revealed the pro-viral functions of m6A in HIV replication, showing that knockdown of ALKBH5 increased viral replication while knockdown of METTL3 and/or METTL14 had the opposite effect [361, 370]. Additionally, multiple YTHDF1-3 protein binding sites have been detected on the HIV genome, suggesting that these “readers” bind to m6A and mediate the processing and/or metabolism of the methylated viral RNAs. Indeed, studies have proposed that in the early stage of HIV replication cycle, YTHDF1-3 bind to m6A-methylated HIV RNA genome to inhibit HIV infection primarily by suppressing reverse transcription; whereas in the stage of viral gene expression, YTHDF1-3 bind to m6A-methylated viral transcripts to promote HIV replication by enhancing viral protein production, such as Gag protein [360, 361, 371, 378, 379]. Taken together, the previous results strongly suggest that m6A and its cellular machinery are involved in the regulation of viral gene expression in different steps of the viral replication cycle.

Besides the effect of m6A on viral replication in host cells, viral infection is able to induce a wide range of changes in the host transcriptome, including the m6A

epitranscriptome. Studies have demonstrated that host cellular m6A epitranscriptome was reprogrammed during the viral infection, such as during KSHV, HIV and ZIKV infection [313, 367, 370]. Based on the MeRIP-seq data, the analysis of the m6A motifs showed that the viral infection was able to switch the preferred consensus m6A motifs in the host cells, suggesting that viral infection might affect the substrate specificity of the m6A regulators [313, 371]. For instance, HIV infection of Jurkat cells and primary CD4+ cells slightly decreased the frequency of the consensus GGACU motif within the m6A peaks, whereas the frequency of the consensus RRACH motif was slightly increased [371]. In addition, the results of the gene ontology (GO) enrichment analysis have shown that viral infection was able to change the distribution of m6A sites in host cellular transcripts; and the redistribution of m6A sites mainly occurred in the transcripts related to the immune responses and viral replication [313, 370]. For example, one study indicated that 56 cellular gene transcripts were methylated by m6A after HIV infection of human MT4 cells, and 19 out of the 56 methylated transcripts are associated with immune-related pathways and HIV replication [370]. Moreover, ZIKV infection could change the distribution of m6A sites in the host cellular transcripts, with a decrease in the 3'UTR and a concomitant increase in the 5'UTR, implying the potential function of the redistributed m6A on mRNA splicing and translation [313].

In summary, the dynamic reversible m6A modification is the most abundant mRNA modification in eukaryotic organisms and plays important roles in a broad range of

biological processes. In the past few years, studies have revealed the emerging roles of m6A on viral infection. By using the sequencing-based technologies, the m6A-modified RNA has been widely found in various viruses and proposed to affect different stages of the viral replication. Additionally, viral infection was able to alter the cellular m6A epitranscriptome, which in turn might affect viral and cellular gene expression. Therefore, understanding the effect of viral infection on m6A RNA methylation in host cells, as well as investigating the functions of m6A on viral infection might provide new insights into how viral infection is regulated and offer new potential targets for antiviral therapies.

1.5 Aims

The aims of the thesis are to investigate the effects of SRV infection on the autophagic pathway, apoptotic pathway and m6A RNA methylation in Jurkat T lymphocytes. Firstly, in order to understand the SRV infection of Jurkat cells, the infectivity and replication capacity of SRV on Jurkat cells was examined. Then, the effects of SRV infection on the levels of apoptosis and autophagy in Jurkat cells were investigated. Moreover, the potential regulatory roles of autophagy on SRV replication and apoptosis in the infected Jurkat cells were examined; and the possible mechanism by which autophagy-regulated apoptosis was further investigated. In addition, in this thesis, the presence of m6A modification in SRV viral RNAs and the effects of SRV infection on the m6A RNA methylation as well as m6A epitranscriptomes of Jurkat cells were examined. Lastly, the potential influences of cellular m6A machinery on SRV replication in the infected Jurkat cells was explored.

Chapter 2

Materials and Methods

2.1 Introduction

This chapter introduces the materials and laboratory methods used in the research presented within the thesis. The materials that were obtained from external sources and any work that was not conducted by me were acknowledged.

2.2 Cell culture

Jurkat cell line (human T lymphocytes) and HEK293T cell line (human embryonic kidney cells) were kindly provided by Prof. Zhi-Liang Lu, Xi'an Jiaotong-Liverpool University, China. Raji cell line (human B lymphocytes) was obtained from the Chinese Academy of Sciences (CAS) Cell Bank, Shanghai. Jurkat cells and Raji cells were grown in Roswell Park Memorial Institute (RPMI) 1640 medium (Hyclone) supplemented with 5% (v/v) and 10% (v/v) fetal bovine serum (FBS; Gibco, Waltham, USA), respectively. HEK293T cells were grown in Dulbecco's Modified Eagle's Medium (DMEM; Hyclone) supplemented with 10% (v/v) FBS. All medium was additionally supplemented with 100 U/mL penicillin and 100 µg/mL streptomycin. All cells were cultured at 37°C in a humidified 5% (v/v) CO_2 incubator.

Jurkat cells and Raji cells were routinely cultured in 25 cm^3 cell culture flasks (T25; Corning) and passaged at 1:5 dilutions every 3 days by directly remove cell suspension and add the same volume of fresh complete culture medium back to the flask. To remove cell debris, every two weeks, cells were centrifuged at 900 revolutions per minute (rpm) for 3 minutes; cell debris in suspension was removed, the cell pellet was

suspended in the complete culture medium and transferred back into T25 flasks for routine culture.

HEK293T cells were routinely cultured in 75 cm^3 cell culture flasks (T75; Corning) and passaged at 1:10 dilutions every 3 days. Briefly, the adherent cells were washed twice with 5 mL Mg^{2+} and Ca^{2+} free phosphate buffered saline (PBS; Hyclone) followed by 1 mL Trypsin- ethylenedinitrilotetraacetic acid (EDTA) solution (#T4049, Sigma, St Louis, USA) treatment for 3 minutes in a 37°C incubator. 5 mL complete culture medium was then added into the flasks to stop trypsin reaction. Cells were collected by centrifuging at 300 x g for 3 minutes followed by suspended in the complete culture medium. 1/10 volume of the cell suspension was transferred back into the T75 flask and cultured in 10 mL complete culture medium. For all cell lines, cell number was measured by CASY Cell Counter and Analyzer (CASY Model TT; Germany) according to the manufacturer's instruction.

2.3 Virus stock preparation and viral infection

SRV-4 virus strain, SRV4/TEX/2009/V1 (GenBank accession number: FJ971077.1); and SRV-8 virus strain, SRV8/SUZ/2012 (GenBank accession number: KU605777) were kindly provided by VRLcn Ltd. (Suzhou, China). SRV-4 was firstly identified from cynomolgus monkeys in California at the USA in 1984. The strain of SRV4/TEX/2009/V1 was isolated from cynomolgus monkeys (*Macaca fascicularis*) which were imported from China to the USA in 2008 [67]. SRV-8 is a novel subtype of SRV that was recently

identified from cynomolgus monkeys (*Macaca fascicularis*) in USA and China. The strain of SRV8/SUZ/2012 was isolated from a juvenile cynomolgus monkey (2-3 years old) in a breeding colony in China [7].

Both SRV-4 and SRV-8 were propagated in Raji cells and stored in the cell freezing medium containing 90% (v/v) complete culture medium and 10% (v/v) dimethyl sulfoxide (DMSO; #D2650, Sigma, St Louis, USA), and stored in liquid nitrogen until use. As a susceptible cell line for SRV infection, Raji cells have been widely used to isolate SRV from the infected animals, and the infected Raji cells have been commonly used to produce the infectious SRV particles for *in vitro* study [73, 74, 380]. Therefore, in this study, SRV-4/SRV-8-infected Raji cells were used to produce the infectious SRV-4/SRV-8 particles. 2 X 10^6 Raji cells were co-cultured with 1 X 10^6 SRV-4- or SRV-8-infected Raji cells in the complete culture medium. Cytopathic effect (CPE) in the infected cells was monitored daily under the optical microscope (ECLIPSE-TS100; Nikon, Japan). The virus-containing medium will be harvested when more than 70% of the cells displayed CPE (on around day 7 to day 10 postinfection). The infected Raji cells were pelleted by centrifugation at 1500 rpm for 3 minutes, the virus-containing supernatant was filtered through the Nalgene™ Rapid-Flow™ 0.45 μm filter (#168-0045; Thermo Fisher Scientific, Waltham, USA), aliquoted and stored at -80°C until use. SRV genome copy number in the harvested supernatant was examined by using realtime PCR analysis (Section 2.4). In parallel, the supernatant of uninfected Raji cells was collected and served as the negative control for SRV-4/SRV-8 infection of Jurkat

cells.

For SRV infection of Jurkat cells, 2 X 10^5 Jurkat cells were cultured in 1 mL complete culture medium for 3 hours followed by incubated with known amounts (3 X 10^8 genome copies) of SRV-4 or SRV-8 for 18 hours at 37°C. Equal amounts of Jurkat cells were incubated with the supernatant of uninfected Raji cells and served as the control uninfected cells. After incubation, the cells were centrifuged to remove the free virus, washed three times with PBS, resuspended and maintained in the complete culture medium for the indicated time. Successful infection was determined by the appearance of cytopathic effect in the cultured cells on day 8 to day 10 postinfection.

2.4 Reverse transcription and realtime PCR

The copy number of SRV RNA genome in the culture medium was examined by using reverse transcription followed by realtime PCR analysis. Viral RNA genome was isolated from 140 μL culture medium by using the viral RNA extraction kit (#DP316-R; TIANGEN, China) according to the manufacturer's protocol. The isolated RNA was treated with RQ1 RNase-Free DNase (#M6101; Promega, Madison, USA) and reversed transcribed into cDNA by using the Reverse Transcriptase M-MLV (RNase H-) kit (#2641; TaKaRa, China) according to the manufacturer's protocol. The synthesized cDNA was then used as the template for realtime PCR analysis. The standard SRV plasmid, which includes a conserved sequence for all SRV subtypes, was used to generate the standard curve for SRV RNA genome quantification by using realtime PCR analysis.

To examine the SRV-LTR level in the infected Jurkat cells, the cellular genome was extracted by using the TIANamp Genomic DNA kit (#DP304; TaKaRa, China), and 100 ng of the cellular genome was used as the template for realtime PCR analysis. GAPDH was used as an internal control to quantify the relative level of SRV-LTR. For the detection of SRV RNA genome and SRV-LTR, realtime PCR was performed by using the Premix Ex Taq (Probe qPCR) kit (#RR390A; TaKaRa, China). The standard SRV plasmid, SRV genome primers and probe, as well as GAPDH primers and probe were kindly provided by VRLcn Ltd. (Suzhou, China) [381]. For SRV-LTR, the forward primer was 5'-AAAAGGGTGACCTGTCCG-3', the reverse primer was 5'-GACACAAGARATGGAGACAAG-3' and the Taq-Man probe was 5'-FAM-AAGATGGCGYACTTCCTGSTTCTTCT-TAMRA-3'.

To examine the mRNA levels of death receptors and ligands in Jurkat cells, at the indicated time, total RNA was isolated with TRI Reagent® (#T9424; Sigma, St Louis, USA) followed by RNase-free DNase treatment and cDNA synthesis as described above. GAPDH was used as an internal control and the relative level of the indicated mRNA was calculated by normalizing the Ct values to those of GAPDH to yield $2^{-\Delta\Delta Ct}$ values. Realtime PCR was performed by using the SYBR Premix Ex Taq (Tli RNase H Plus) kit (#RR420; TaKaRa, China). Primers were used as follows: Fas forward 5'-TGAAGGACATGGCTTAGAAGTG-3' and reverse 5'-GGTGCAAGGGTCACAGTGTT-3'; FasL forward 5'-TGCCTCTGGAATGGGAAGAC-3' and reverse 5'-TGCAAGATTGACCCCGGAAG-3'; TRAIL forward 5'-CGACTGCCTGGCTGACTTAC-3' and reverse 5'-GATCACGATCAGCACGCAGG-3'; DR5 forward 5'-AAGGTGGCTAAAGCTGAGGC-3' and

reverse 5’-GCTTGGCAAGTCTCTCTCCC-3’;

For validation of MeRIP experiment, 5 ng of input controls and m6A IP samples were reverse transcribed into cDNA followed by realtime PCR analysis to examine the levels of JunB with m6A, Dicer1 with m6A and Dicer1 without m6A. Fold increase of each indicated sequence was obtained by calculating the $2^{-\Delta Ct}$ value of m6A IP sample relative to the input control. Realtime PCR was performed by using the SYBR Premix Ex Taq (Tli RNase H Plus) kit (#RR420; TaKaRa, China). Primers were used as follows: JunB with m^6A forward 5’- GAACGCCTGATTGTCCCCAA-3’ and reverse 5’-AAAAGTACTGTCCCGGGGGT-3’; Dicer1 with m^6A forward 5’-GCTGCACATCAAGGTGCTAA-3’ and reverse 5’- GCAACGTTCTGCAGTTCACA-3’; Dicer1 without m^6A forward 5’-AACGAAGGCAGTGCTACCC-3’ and reverse 5’-GGCTGATCAGGTCTGGGATAAC-3’.

Realtime PCR reaction programs were set as follows: 95°C for 30 seconds (1 cycle), 95°C for 5 seconds and 55°C (for Fas, FasL, TRAIL, GAPDH, Dicer1 with m^6A and JUNB with m^6A) or 59°C (for DR5) or 60°C (for SRV-LTR) or 62°C (for Dicer1 without m^6A) for 30 seconds (45 cycles). All realtime PCR reactions were performed in the 7500 Fast Real-Time PCR System (Applied Biosystems).

2.5 Immunofluorescence staining

Cells were seeded on 0.01% poly-L-lysine (#P4832; Sigma, St Louis, USA) –coated

Nunc™ Lab-Tek™ Chamber Slide (#177380PK; Thermo Fisher Scientific, Waltham, USA), and fixed in 4% paraformaldehyde diluted in PBS for 15 minutes at room temperature. After washed with PBS twice, the cells were permeabilized with pre-cold pure methanol for 20 minutes at -20°C. Then washed with PBS twice, cells were blocked with 5% Bovine Serum Albumin (BSA; Sigma, St Louis, USA)/ 0.3% (v/v) Triton X-100 in PBS for 1 hour at room temperature. Cells were then stained with the indicated primary antibody (diluted in antibody dilution buffer: 1% BSA/ 0.3% (v/v) Triton X-100 in PBS) overnight at 4°C. After incubation, cells were washed with PBS three times with 5 minutes incubation during each time. Cells were then incubated with the fluorescence-conjugated secondary antibody (diluted in antibody dilution buffer) for 2 hours at room temperature in the dark. After rinse three times in PBS for 5 minutes each time, cells were incubated with Hoechst (1:5000 dilution in PBS; #H1399, Thermo Fisher Scientific, Waltham, USA) for 10 minutes at room temperature. After two washes with PBS, the cells were mounted with ProLong™ Gold Antifade Mountant (#P36934; Thermo Fisher Scientific, Waltham, USA) and imaged with a ZEISS LSM 880 Confocal Laser Scanning Microscope. For double immunofluorescence staining, two primary antibodies or two secondary antibodies were mixed, respectively, to stain the cells. The primary antibodies used in immunofluorescence staining are: rabbit monoclonal anti-LC3B antibody (1:200 dilution; #3836, Cell Signaling Technology, USA), rabbit polyclonal anti-SQSTM1/p62 antibody (1:500 dilution; #ab91526, Abcam, Cambridge, UK) and mouse monoclonal anti-human caspase-8 antibody (1:60 dilution; #746109, R&D Systems, USA). The secondary antibodies are FITC-conjugated swine

anti-rabbit antibody (1:30 dilution; #F020502, DAKO, Japan) and Alexa Fluor® 555-conjugated goat anti-mouse antibody (1:1000 dilution; #A21424, Invitrogen, Shanghai, China).

2.6 Cell lysate preparation and western blot analysis

At the indicated time, cells were collected, washed twice with cold PBS and lysed with Laemmli Sample Buffer (24 mM Tris-HCl at pH 6.8, 0.8% sodium dodecyl sulfate (SDS), 2% (v/v) beta-mercaptoethanol and 20% (v/v) glycerol) supplemented with EDTA-free complete™ protease inhibitor cocktail (#04693116001; Roche, Basel, Switzerland) by incubating on ice for 10 minutes. Nuclear contents in the cell lysate were sheared by sonication (Q700, Qsonica, USA) with 6 amplitudes for two times, 6 seconds each time. Lysates were then boiled at 100°C for 10 minutes, allowed to cool down and stored at -80°C until use.

Equal amounts of protein were separated by SDS-polyacrylamide gel electrophoresis (SDS-PAGE) in 10% or 12% Tris-Glycine gel, which was run at 120 voltages for 90 minutes in running buffer (25 mM Tris, 192 mM glycine and 0.1% SDS). Separated proteins in the gel were then transferred onto 0.2 μm polyvinylidene difluoride (PVDF) membranes (Millipore, USA) by being run at 100 voltages for 60 minutes in transfer buffer (25 mM Tris, 192 mM glycine, 0.03% SDS and 20% (v/v) methanol). SDS-PAGE and membrane transfer were both achieved by using the Mini-PROTEAN® Tetra System (Bio-rad, Hercules, USA). PVDF membranes were then blocked with blocking buffer (5%

(w/v) skimmed milk in PBS-T (PBS containing 0.1% (v/v) Tween-20) for 1 hour at room temperature. The membranes were then incubated with the specific primary antibody (1:1000 dilution in blocking buffer) overnight at 4°C. After three times PBS-T washing for totally 30 minutes, membranes were incubated with the IRDye® goat anti-rabbit IgG (H + L) (#926-32211; LI-COR, Lincoln, USA) or IRDye® donkey anti-mouse IgG (H + L) (#926-68072 ; LI-COR, Lincoln, USA) secondary antibody (1:10000 dilution in blocking buffer) for 1 hour at room temperature in the dark. After rinse three times in PBS-T for 10 minutes each time, the membranes were visualized under the infrared by using the Odyssey® infrared imaging system (LI-COR, Lincoln, USA). The band intensities were measured and analyzed using the Odyssey® application software (version 3.0).

Primary antibodies used in western blot analysis are: rabbit monoclonal anti-LC3B antibody (1:1000 dilution; #3836, Cell Signaling Technology, USA); rabbit monoclonal anti-cleaved caspase 3 antibody (1:1000 dilution; #9664, Cell Signaling Technology, USA); rabbit monoclonal anti-cleaved caspase 8 antibody (1:1000 dilution; #9496, Cell Signaling Technology, USA); rabbit polyclonal anti-cleaved caspase 9 antibody (1:1000 dilution; #9496, Cell Signaling Technology, USA); rabbit monoclonal anti-Beclin1 antibody (1:1000 dilution; #3495, Cell Signaling Technology, USA); mouse monoclonal anti-caspase 8 antibody (1:500 dilution; #66093-1-Ig, Proteintech Group, USA); rabbit polyclonal anti-METTL3 antibody (1:1000 dilution; #15073-1-AP, Proteintech Group, USA); rabbit polyclonal anti-METTL14 antibody (1:1000 dilution; #HPA038002, Sigma,

St Louis, USA); mouse monoclonal anti-WTAP antibody (1:1000 dilution; #60188-1-Ig, Proteintech Group, USA); rabbit polyclonal anti-ALKBH5 antibody (1:1000 dilution; #HPA007196, Sigma, St Louis, USA); mouse monoclonal anti-FTO antibody (1:1000 dilution; #ab92821, Abcam, Cambridge, UK); rabbit polyclonal anti-YTHDF1 antibody (1:1000 dilution; #17479-1-AP, Proteintech Group, USA); rabbit polyclonal anti-YTHDF2 antibody (1:1000 dilution; #24744-1-AP, Proteintech Group, USA); rabbit polyclonal anti-YTHDF3 antibody (1:200 dilution; #ab103328, Abcam, Cambridge, UK) and mouse monoclonal anti-β-actin antibody (1:2000 dilution; #3700, Cell Signaling Technology, USA)

2.7 Flow cytometry analysis

Apoptosis in Jurkat cells was measured by using the Annexin V-PE/7-AAD staining assay with flow cytometry. At the indicated time, the cells were collected, washed twice with cold PBS and stained by using the PE Annexin V Apoptosis Detection Kit I (#559763; BD Biosciences, San Diego, USA) according to the manufacturer's instruction. Briefly, 1 X 10^5 cells were suspended in 100 µL of the 1X binding buffer and transferred into a 5 mL culture tube. The cells were then incubated with 5 µL of PE-conjugated Annexin V and 5 µL of 7-Amino-Actinomycin D (7-AAD) for 15 minutes at room temperature in the dark. After incubation, 400 µL of the 1X binding buffer was added into each tube. The apoptotic cells were then detected by using the FACSCalibur flow cytometry (BD Biosciences, San Diego, USA) and the collected data was analyzed by using the Cell Quest Pro software (BD Biosciences, San Diego, USA). Cells were gated into four groups:

Annexin V^-/7-AAD^- cells in the left lower quadrant represent viable cells, Annexin V^+/7-AAD^- cells in the right lower quadrant represent early apoptotic cells, Annexin V^-/7-AAD^+ cells in the left upper quadrant represent necrotic cells and Annexin V^+/7-AAD^+ cells in the right upper quadrant represent late apoptotic cells.

For the Annexin V single staining, 1 X 10^5 cells were stained with 5 µL of APC-conjugated Annexin V (#550474; BD Biosciences, San Diego, USA) for 15 minutes at room temperature in the dark. The detailed procedure and detection method of single staining were the same as described above.

2.8 Restriction enzyme digestion, agarose gel electrophoresis, DNA ligation, and competent cell transformation

Restriction enzyme digestion was conducted by incubating 1 µg DNA with 1 unit of the appropriate enzyme (New England Biolabs, Ipswich, USA) in a 50 µL reaction system using the suitable reaction buffer which provides the maximum enzymatic activity. Digestion was performed at 37°C for 1~2 hours. The digested DNA was purified by using QIAquick® PCR Purification Kit (Qiagen, Crawley, UK) or separated by agarose gel electrophoresis followed by recovering the target DNA from the gel by using QIAquick® Gel Extraction Kit (Qiagen, Crawley, UK).

The appropriate concentration of agarose gel was prepared by dissolving agarose powder (Sigma, St Louis, USA) in TAE buffer (Thermo Fisher Scientific, Waltham, USA)

supplemented with 1X Gelred (Biosharp, Hefei, China). Electrophoresis was conducted at 120 voltages for 60~90 minutes, and the separated DNA samples were visualized under ultraviolet (UV) light using Gel Doc™ XR+ imager (Bio-rad, Hercules, USA).

Ligation of the linearized vector and insert DNA was conducted by using the Quick Ligation™ Kit (#M2200S; New England Biolabs, Ipswich, USA) according to the manufacturer's protocol. Briefly, 50 ng of vector DNA (250 ng of vector DNA in the lentiviral system) was mixed with the insert DNA at a 3:1 molar ratio of vector : insert (5:1 molar ratio was used in the lentiviral system). The mixture of vector and insert DNA was incubated with 1 unit of Quick Ligase in a 20 µL reaction system containing 1X Quick Ligase Reaction Buffer for 10 minutes at room temperature followed by chilled on ice until transformation.

The entire DNA ligation product was then transformed into competent cells. TOP10 competent cells (or Stbl3 cells for the lentiviral system) were thawed on ice followed by incubation with the DNA ligation product on ice for 30 minutes. The competent cells were then heat shocked in 42°C water bath for 90 seconds, and quickly placed back on ice for 3 minutes. To recover the transformed bacteria, 1 mL Luria broth (LB) medium (without antibiotic) was used to incubate the bacteria at 37°C for 1 hour with 160 rpm shaking. The bacterial suspension was then plated onto a 10 cm LB agar plate containing the appropriate antibiotic (100 µg /mL of ampicillin or 50 µg/mL of kanamycin). These plates were face-down incubated at 37°C overnight. Single colonies

were picked and amplified in LB medium with the appropriate antibiotic, and the extracted plasmids were applied to sequencing. The single colony, which contains the correct recombinant plasmid, was amplified in LB medium supplemented with the appropriate antibiotic. Bacteria amplification was conducted at 37°C for 14-16 hours with 220 rpm shaking. Plasmid DNAs were then extracted by using QIAprep® Spin Miniprep Kit (for 6 mL bacterial suspension) or QIAprep® Plasmid *Plus* Maxi Kit (for 120 mL bacterial suspension) (Qiagen, Crawley, UK) according to the manufacturer's instructions. The concentration of eluted plasmid DNA was measured by using a NanoDrop spectrophotometer 2000 (Thermo Fisher Scientific, Waltham, USA). The bacterial glycerol stocks were prepared by thoroughly mixing bacterial suspension with the equal volume of sterile 50% (v/v) glycerol (Sigma, St Louis, USA), and stored at -80°C.

2.9 Short hairpin RNA design and lentiviral vector construction

The Dharmacon™ TRIPZ™ lentiviral short hairpin RNA (shRNA) vector (Dharmacon, UK) used in this study contains a unique microRNA-30 (miR-30) -based short hairpin cassette, which has been shown to facilitate knockdown efficiency [382-384]. Sequence of the miR-30 -based short hairpin cassette is 5'-AAGGTATATTGCTGTTGACAGTGAGCG (5' basal stem) - 22 nucleotides sense sequence - TAGTGAAGCCACAGATGTA (miR-30 loop)- 22 nucleotides antisense sequence - TGCCTACTGCCTCGG (3' basal stem)-3'. The 22 nucleotides sense/antisense sequences are gene-specific sequences that could guide the intracellular RNA-induced silencing

complex (RISC) to degrade the target mRNA. The gene-specific 22 nucleotides sense sequence for Beclin1 is 5'-TCCCGTGGAATGGAATGAGATT-3'; for ALKBH5 is 5'-AGCTGCAAGTTCCAGTTCAAGC-3'; for YTHDF1 is 5'-ACCCGAAAGAGTTTGAGTGGAA-3' and for YTHDF3 is 5'-AGATAAGTGGAAGGGCAAATTT-3'. A non-silencing sequence of 5'-ATCTCGCTTGGGCGAGAGTAAG-3', which might not target any mRNAs, was designed and used as the non-silencing control. All short hairpin cassette sequences were synthesized by the company (GENEWIZ, Suzhou, China) and cloned into Dharmacon™ TRIPZ™ lentiviral shRNA vector. The recombinant lentiviral shRNA vectors were introduced into Jurkat cells by using the lentiviral system (Section 2.10).

2.10 Transfection and lentiviral transduction

HEK293T cells were used to produce lentiviral particles. 5 X 10^5 HEK293T cells were cultured in 6 cm^2 dishes (Corning) with 5 mL complete culture medium without penicillin/streptomycin for 20 hours prior to transfection. The cells were then transfected with 4 µg of Dharmacon™ TRIPZ™ lentiviral shRNA vector that contains the gene-specific shRNA sequence (lentiviral shRNA vector), 3 µg of pSPAX2 (lentiviral packaging vector) and 1 µg of pMD2.G (lentiviral envelope vector) using 24 µL of Fugene® 6 Transfection Reagent (#E2691; Promega, Madison, USA**)** and Opti-MEM®I Reduced-Serum Medium (#31985062; Invitrogen, Shanghai, China) according to the manufacturer's instructions. At 63 hours post-transfection, the supernatant containing lentiviral particles was harvested by centrifuging at 500 x g for 5 minutes followed by filtered through a 0.45 µm membrane to remove the remaining cell debris. Lentiviral

particles in the filtered supernatant were directly used to infect Jurkat cells or stored at -80°C. The Dharmacon™ TRIPZ™ lentiviral shRNA vector, pSPAX2, and pMD2.G vectors were kindly provided by Dr. Ferdinand Kappes, Xi'an Jiaotong-Liverpool University, China.

Jurkat cells were transduced with the packaged lentiviral particles by using the spinoculation. Spinoculation, also called centrifugal inoculation, is a transduction method that has been widely used to increase the efficiency of *in vitro* viral infection as well as lentiviral transduction of suspension cells [385-387]. 2 X 10^5 Jurkat cells were suspended in 1 mL complete culture medium in a 15 mL centrifuge tube. 4 mL lentiviral particles-containing medium was added into Jurkat cell suspension with the presence of polybrene (#H9268; Sigma, St Louis, USA) at the final concentration of 8 μg/mL. The virus-cell mixture was gently mixed and incubated for 15 minutes at room temperature, following by centrifuging at 800 x g for 30 minutes at 32°C. The supernatant was removed, and the cell pellet was resuspended and cultured in 3 mL complete culture medium. On day 2 postinfection, the transduced Jurkat cells were selected with 4 μg/mL of puromycin dihydrochloride hyclate (#A610593; Sangon Biotech, China) in the complete culture medium for 7 days. After puromycin selection, the survived stable Jurkat cell lines were maintained in the complete culture medium containing 1 μg/mL of puromycin. The Dharmacon™ TRIPZ™ lentiviral shRNA vector contains a Tet-On system, which is induced by doxycycline (Dox). To induce the expression of shRNA in the stable Jurkat cells, 1 μg/mL of doxycycline hyclate (#ST039A; Beyotime, China) was

used to treat the cells for the indicated time.

2.11 Co-immunoprecipitation assay

On day 10 postinfection, 1 X 10^7 uninfected or SRV-8-infected Jurkat cells were collected, washed twice with cold PBS and lysed with 700 µL of lysis buffer (20 mM Tris-HCl at pH 7.6, 150 mM NaCl, 1% (v/v) NP-40 and 10% (v/v) glycerol supplemented with EDTA-free complete™ protease inhibitor cocktail) by incubating at 4°C for 30 minutes with continuous up-and-down rotation. Meanwhile, the recombinant protein A beads (#IPA300; Repligen, USA) were blocked with 2 mg/mL of BSA in 1 mL of lysis buffer at 4°C for 30 minutes with continuous rotation. The lysed cells were then centrifuged at 14,000 x g for 15 minutes at 4°C to remove cell debris, and the cell lysates in the supernatant were collected and pre-cleared with 30 µL of the blocked recombinant protein A beads by incubating at 4°C for 30 minutes with continuous rotation. After incubation, the beads were removed by centrifugation and the protein concentration in the supernatant was measured by using the bicinchoninic acid (BCA) Assay Kit (#P0010; Beyotime, Shanghai, China) according to the manufacturer's instruction.

For LC3 protein immunoprecipitation, 880 µg of cell lysate was diluted in 330 µL of cold lysis buffer and incubated with 10 µL (~4.8 µg) of rabbit monoclonal anti-LC3B antibody (#3868; Cell Signaling Technology, USA) overnight at 4°C with continuous rotation. The equal amount of cell lysate was incubated with 4.8 µg of rabbit IgG

antibody (#3900; Cell Signaling Technology, USA), which was served as the isotype control. After incubation, 50 μL of the BSA blocked beads were added into each sample followed by incubating at 4°C for 2 hours with continuous rotation. The beads were then washed three times with 1 mL of cold lysis buffer. After the final washing, the immunocomplexes were dissociated from the beads by dissolving in 20 μL of 2 X Laemmli Sample Buffer and boiling for 10 minutes at 95°C. The immunocomplexes were then collected by centrifuging at 14,000 x g for 1 minute and stored at -80°C before western blot analysis (Section 2.6).

2.12 MTT colorimetric assay

The 3-(4,5-dimethylthiazol-2-yl)-2,5-diphenyltetrazolium bromide (MTT) colorimetric assay was used for analyzing cell viability. After the indicated treatment, 100 μL of 5 mg/mL MTT solution (dissolved in PBS; #M2818, Sigma, St Louis, USA) was added into 1 mL cell suspension in a 24-well plate. After 4 hours incubation at 37°C and 5% CO_2, the cells were collected by centrifuging at 10,000 x g for 1 minute, the supernatant was removed, and the cell pellet was dissolved in 500 μL of DMSO. The absorbance at 570nm was read on a microplate reader (Biotek, Canada).

2.13 Immuno-Northern blot analysis

On day 10 postinfection, total RNA was extracted from uninfected and SRV-8-infected Jurkat cells with TRI Reagent® (#T9424; Sigma, St Louis, USA). RNA concentration was measured by using the Qubit™ RNA BR Assay Kit (#Q10210; Invitrogen, Shanghai,

China) in a Qubit™ 3 Fluorometer (#Q33216; Invitrogen, USA) according to the manufacturer's instruction. 10 μg of RNA was mixed with the equal volume of RNA loading buffer (#9168; Takara, China) and denatured by incubating at 70°C for 10 minutes, followed by quickly chilled on ice. The RNA was then separated using the formaldehyde gel electrophoresis. The formaldehyde denatured gel was prepared by dissolving 0.5 g of agarose, 1.5 mL of 37% (v/v) formaldehyde and 5 mL of 10X MOPS (0.2 M MOPS, pH7.0, 1 mM EDTA and 50 mM sodium acetate) in 50 mL diethylpyrocarbonate (DEPC)-treated water. Electrophoresis was conducted in 1X MOPS at 100 voltages for 60 minutes, and the separated RNA samples were stained with SYBR® Green II RNA Gel Stain (#S7564; Thermo Fisher Scientific, Waltham, USA) and visualized under UV light using Gel Doc™ XR+ imager (Bio-rad, Hercules, USA). RNA was then transferred overnight to a positively charged nylon membrane (#FFN10; Beyotime, China) in 20X SSC buffer (#B548110; Sangon Biotech, China). After transfer, RNA was crosslinked to the membrane by baking in a vacuum oven for 2 hours at 80°C.

The membrane was blocked in 5% (w/v) skimmed milk in 0.1% (v/v) PBS-T for 1 hour at room temperature and then incubated with the rabbit polyclonal anti-m6A primary antibody (1:1000 dilution in 0.1% (v/v) PBS-T; #202 003, Synaptic Systems, Germany) for 1 hour at room temperature. Subsequent steps for m6A immunoblotting were performed according to the protocol of western blot analysis in Section 2.6.

2.14 MeRIP-seq

High throughput transcriptome-wide mapping of m6A in Jurkat cells was carried out by using the MeRIP-seq technique according to the published protocol with minor modifications [388]. Briefly, on day 10 postinfection, total RNA was extracted from uninfected and SRV-8-infected Jurkat cells by using the TRI Reagent® (#T9424; Sigma, St Louis, USA), following by mRNA purification using the PolyATtract® mRNA Isolation System III Kit (#Z5300; Promega, Madison, USA) according to the manufacturer's instruction. The purified mRNA was then concentrated by ethanol precipitation to the final concentration of 1 μg/uL and fragmented by incubating with the fragmentation buffer (100 mM $ZnCl_2$ and 100 mM Tris-HCl at pH 7.0) at 94°C for 3 minutes. The fragmentation was stopped by adding EDTA into the reaction mixture to the final concentration of 0.05M. The fragmented mRNA was then purified by ethanol precipitation, dissolved in RNase-free water (#9012; TaKaRa, China) and stored at -80°C until use. Partial of the fragmented mRNA was used as the input control in MeRIP-seq. Successful mRNA fragmentation with the size around 100 nucleotides was validated by running agarose electrophoresis.

Before m6A immunoprecipitation, the recombinant protein A beads (IPA300; Repligen, USA) were blocked with 0.5 mg/mL BSA in 1mL immunoprecipitation (IP) buffer (10 mM Tris-HCl at pH 7.4, 150 mM NaCl and 1% (v/v) Igepal CA-630 (#I8896; Sigma, St Louis, USA)) for 1 hour at 4°C with continuous up-and-down rotation. 100 μL of the blocked beads were then incubated with 10 μg of rabbit polyclonal anti-m^6A antibody (#202 003; Synaptic Systems, Germany) in 300 μL of cold PBS for 3 hours at 4°C with

continuous rotation. After incubation, the m6A antibody-conjugated beads were washed three times with cold PBS followed by washing with the IP buffer once. To isolate the m6A-containing mRNA, 120 µg of the purified fragmented mRNA was incubated with the m6A antibody-conjugated beads in 300 µL of IP buffer supplemented with 6 µL of RNasin Plus RNase inhibitor (#N2611; Promega, Madison, USA) for 2 hours at 4°C with continuous rotation. The beads were then washed six times with 1mL IP buffer. After final washing, the immunoprecipitated mRNA was dissociated from the beads by incubating with the elution buffer (100 µL IP buffer supplemented with 6.67 mM of m^6A sodium salt (#M2780; Sigma, St Louis, USA)) for 1 hour at 4°C with continuous rotation. The eluate was then collected after incubation, and the second round of elution was performed. The eluates from two-round elution were pooled together and purified by ethanol precipitation without using glycogen.

The input control and the purified eluate (also named the m6A IP sample) were used for RNA-sequencing (RNA-seq) library preparation. RNA concentration of each sample was measured by using the Agilent RNA 6000 Pico Kit (#5067-1513; Agilent, USA) on an Agilent 2100 Bioanalyzer. 20 ng of each sample was used to prepare the cDNA library by using the TruSeq® RNA Sample Preparation v2 kit (#15026495; Illumina, USA) according to the manufacturer's instruction with two modifications. First, starting from the step of Elute-Prime-Fragment by heating the samples at 80°C for 2 minutes instead of 94°C for 8 minutes, which allows samples annealing to random primers for the synthesis of first strand cDNA but avoids further fragmentation. Second, during the

clean-up step of Adapter Ligation, a DNA : bead ratio of 1:3 instead of 1:1 was applied to preserve the short fragments. The synthesized cDNA libraries were then sequenced on the HiSeq X10 platform (Illumina, San Diego, USA) using the paired-end 2 X 150 bp sequencing module. All RNA-seqs were performed by Suzhou Institute of Systems Medicine Chinese Academy of Medical Sciences in China.

2.15 MeRIP-seq data analysis

Reads of the Input/IP samples were aligned to the human genome (hg19) using HISAT2 (version 2.0.0) with default settings. The reads were aligned to SRV-8 genome (GenBank accession number: NC_031326.1) using Bowtie (version 1.2.2) under setting -k 2. Following this, m6A peak calling and the differential m6A methylation analysis were conducted in R (version 3.4.4) using the exomePeak package (version 1.9.1), which is a software specifically used for MeRIP-seq data analysis [389, 390]. The downstream bioinformatics analysis was performed in R. All MeRIP-seq data analysis was conducted by Zhen Wei, a Ph.D. student in Dr. Jia Meng group at Xi'an Jiaotong-Liverpool University, China.

2.16 Statistical analysis

All experiments were repeated independently for at least three times. All data were analyzed and graphed by using the GraphPad Prism 6.0 (GraphPad Software, San Diego, USA). All data were presented as the mean value ± the standard deviation. Significant differences between two group of data were analyzed using the unpaired Student's *t*-test. Wherever indicated, *p* values are as follows: $*p < 0.05$, $**p < 0.01$, $***p < 0.001$.

Chapter 3

Understanding SRV infection in Jurkat T lymphocytes

3.1 Outline

SRVs are a group of genetically closely related retroviruses that mainly infect Asian macaques, which are predominantly used in biomedical research. Importantly, SRV is the etiological agent of the simian acquired immune deficiency syndrome (SAIDS) that can lead to severe immunosuppressive diseases and cause high mortality. In the late stages of SRV infection, varying degrees of T lymphocyte-depletion was detected in the infected macaques. However, the pathogenetic mechanisms underlying SRV infection, as well as the specific effects of SRV infection on T lymphocytes are not well understood. In order to investigate the pathogenicity of SRV infection in immune cells, in this chapter, we first assessed the SRV infectivity and replication capacity in Jurkat T lymphocytes (Jurkat cells). The appearance of cytopathic effect (CPE) and the formation of syncytium in SRV-inoculated Jurkat cells was examined by using the optical microscope. In addition, the specific primers and probe for SRV proviral 3'LTR were designed to monitor SRV infectivity by detecting the amount of SRV provirus in the infected Jurkat cells through realtime PCR analysis. Moreover, SRV replication capacity in the infected Jurkat cells was monitored by measuring the copy number of viral genomes released in the culture medium through realtime PCR analysis. The viral infectivity and replication capacity were studied in two SRV subtypes, SRV-4 and SRV-8, which are currently circulated in the macaque breeding colonies in China.

3.2 Introduction

SRV has a broad tropism that was found in several lymphoid and non-lymphoid organs and tissues of the infected monkeys including lymph nodes, thymuses, salivary glands, spleens, neural system and digestive tract [63, 84, 92-94]. Additionally, SRV also exhibits broad cellular tropisms both *in vivo* and *in vitro*. Previous studies have shown that in the infected macaques, SRV was detected in T inducer/helper/cytotoxic/suppressor lymphocytes, B lymphocytes, neutrophils, macrophages and mucosal epithelial cells [16, 95, 96]. Moreover, SRV has also been demonstrated to be able to *in vitro*-infect a variety of monkey cells, including B-lymphoblastoid cell line (B-LCL) [15], hematopoietic progenitor cells (CD34+) [391] and lung fibroblasts [16]; as well as some human cells, including Raji cells (human B cell line), TE671 cells (human rhabdomyosarcoma cell line), HEK293T cells (human embryonic kidney cell line), and CEM-SS, MT-4, Hut78, H9 and SupT-1 cells (human T cell lines) [63, 68, 74]. The infectivity of SRV in human cell lines might be due to the close phylogenetic relationship between non-human primates and human species. Moreover, a recent study has shown that the receptor of SRV in human cells is ASCT2, which shows 100% identity in region C with that of the ASCT2 from cynomolgus and Japanese macaque cells; and the region C of ASCT2 has been shown to play the key roles for SRV to attach to and enter the host cells [62, 63, 65].

As the etiological agent for immunosuppressive diseases, the main targets of SRV are lymphoid tissues and lymphocytes. In the early stages of SRV infection, lymphoid

hyperplasia were commonly observed in spleen, lymph nodes, and other non-lymphoid tissues such as the salivary gland and brain of the infected monkeys [82, 92, 391]; while in the late stages, varying degrees of lymphoid depletion including the loss of both B and T lymphocytes were commonly detected [16, 90]. All the above discoveries suggested the effect of SRV infection in lymphocytes of host animals. However, the specific effects of SRV on T lymphocytes and the underlying mechanisms, as well as the roles of these effects on the pathogenesis of SRV are still largely unknown. Therefore, in this study, Jurkat cells were used as the cell model to investigate the interactions between SRV and T lymphocytes. Jurkat cells have been widely used in previous studies for the *in vitro* investigation of HIV infection and pathogenesis [29, 392, 393].

SRV-8 is a novel SRV subtype which was discovered in China and the USA from Cambodian-origin cynomolgus monkeys [7]. Phylogenetic analysis showed that SRV-8 is more closely related to SRV-4 than any other SRV subtypes. Moreover, the results of western blot analysis have also demonstrated the strong serological cross-reactivity of the SRV-4 antigen reacting with SRV-8 [7]. However, different from SRV-8, which has been only isolated in cynomolgus monkeys, SRV-4 has been detected in both cynomolgus monkeys and Japanese macaques [63, 67, 73]. Moreover, SRV-8 and SRV-4 appear to have different pathological effects on their natural hosts. SRV-8 infection was shown to cause no or little harm to cynomolgus macaques, with no common manifestations of SRV infection, such as neutropenia, anemia and body weight loss [3,

7]. However, varying degrees of histiocytic and lymphoplasmacytic inflammation were commonly detected in SRV-4-infected animals [394]. And the PRI-172 strain of SRV-4 has been shown to induce the lethal acute thrombocytopenia in the infected Japanese macaques [63, 395]. The different clinical features of SRV-4 and SRV-8 infections suggested that these two subtypes might have different pathogenic mechanisms. Therefore, in this thesis, SRV-4 and SRV-8 were used to infect Jurkat cells, and the effects of the two subtypes on the host cells were compared and contrasted.

The common detection method of SRV is the serological testing by using western blot analysis, immunofluorescence assay and enzyme-linked immune sorbent assay, which can detect the reacting SRV antibodies in the samples of infected animals [74, 396-398]. However, the additional virion-detection is necessary in addition to the serological testing as some SRV-infected animals fail to make the detectable antibody or exhibit a long interval between infection and seroconversion [3, 399]. Currently, virion-detection has been largely replaced by PCR and realtime PCR technologies, which are able to rapidly detect SRV proviral DNA and viral genomic RNA in tissues or cells for the fast and precise screening of SRV infection [391, 400-402]. Different from the serological testing methods, which might have cross-reactivity among different SRV subtypes, the PCR technology can distinguish different subtypes of SRV by using the subtype-specific primers [403, 404]. Importantly, realtime PCR method has high sensitivity and specificity that can precisely detect and quantify the number of viral particles. Thus, in this chapter, two realtime PCR-based methods were used to

evaluate the infectivity and replication capacity of SRV-4 and SRV-8 in Jurkat cells: one is to examine the amount of SRV proviral DNA in the infected Jurkat cells, aiming to evaluate the infectivity of SRV; the other is to measure the copy number of SRV viral genomic RNA released in the culture medium of the infected Jurkat cells, aiming to investigate the replication capacity of SRV.

3.3 Results

3.3.1 SRV-4 and SRV-8 are able to infect Jurkat cells

CPE, which is characterized as the swelling of the infected cells, has been detected in SRV-infected human Raji, Hut78 and H9 cells, and was recognized as an important marker of the successful SRV infection [73, 74, 398]. Moreover, the formation of syncytium is another feature of CPE that has been discovered in SRV-infected Raji cells [73, 74]. Syncytium is a multinucleated cell that is produced by the fusion of the plasma membranes of adjacent cells. During viral invasion, syncytium formation allows the virus to spread from infected cells to uninfected cells. Therefore, in order to investigate the infectivity of SRV on Jurkat cells, the appearance of CPE and the formation of syncytium in SRV-4/SRV-8-inoculated Jurkat cells were examined. A total of 2 X 10^5 Jurkat cells were inoculated with 3 X 10^8 genome copies of SRV-4 or SRV-8 for 18 hours, followed by washing three times with PBS to remove the free viruses. The cells were then incubated in the complete culture medium for the indicated time. The results showed that on day 10 post-inoculation, both SRV-4- and SRV-8-inoculated Jurkat cells displayed obvious CPE, which was presented as the enlarged cell size when compared with the uninfected cells (Fig. 3.1). Moreover, some syncytia were also detected in SRV-4/SRV-8-inoculated Jurkat cells after nuclear staining by Hoechst, whereas no syncytium was observed in the uninoculated cells (Fig. 3.1). The findings suggest that SRV might be able to infect Jurkat cells *in vitro*.

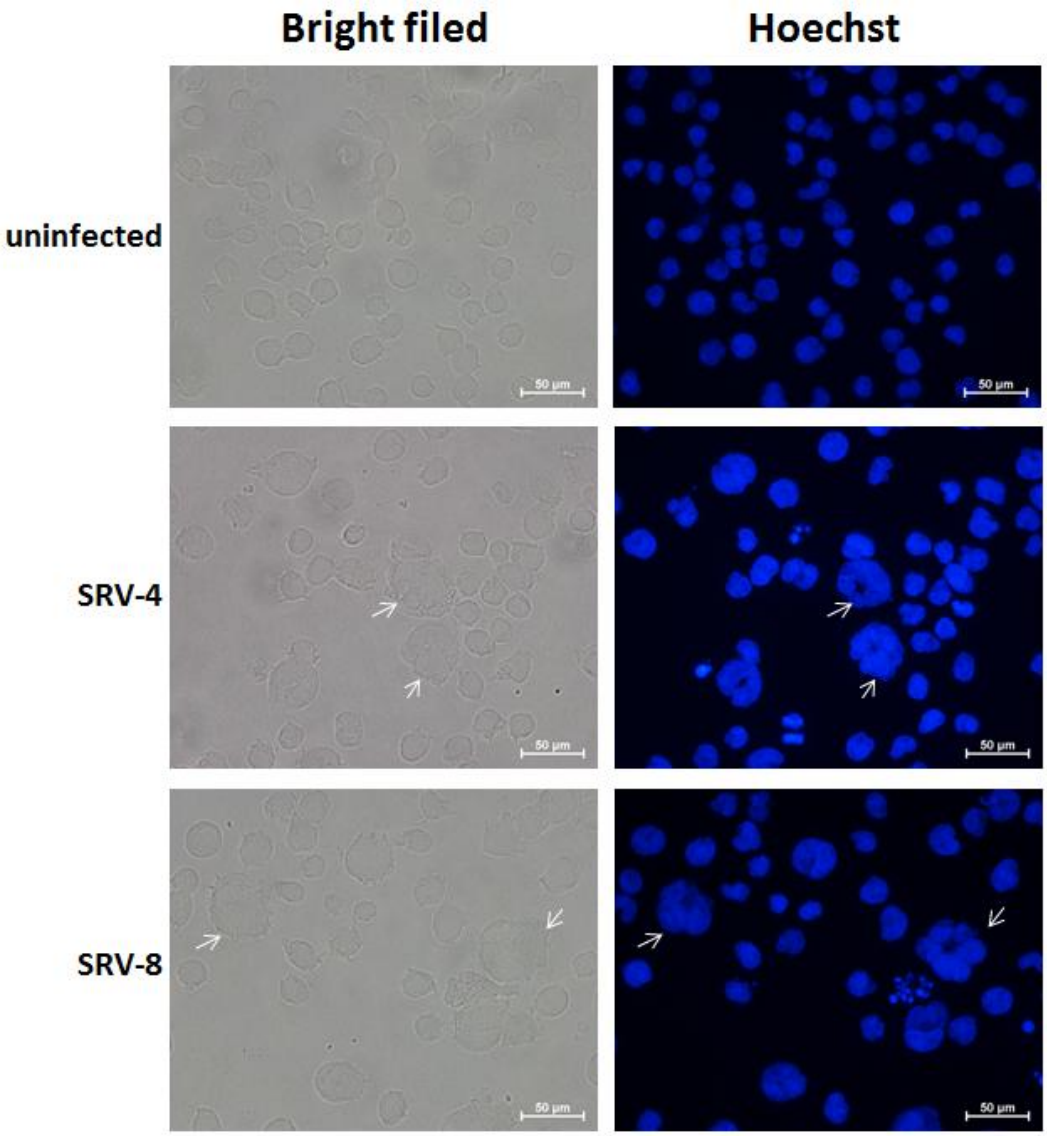

Figure 3.1 SRV-4/SRV-8-inoculation led to the cytopathic effect and the formation of syncytium in Jurkat cells. On day 10 post-inoculation, uninoculated and SRV-4/SRV-8-inoculated Jurkat cells were observed using an optical microscope. Nuclei were visualized by Hoechst staining (blue). Arrows indicate the syncytia of the inoculated cells. Scale bar: 50 µM.

In order to confirm the appearance of CPE and formation of syncytium in the inoculated cells were caused by SRV infection, the extent of SRV infection was investigated by monitoring SRV proviral DNA level in the inoculated cells. Synthesis of proviral DNA in host cells is an important characteristic of the successful retroviral

infection, and the LTRs in the proviral DNA contain crucial sequences that are essential for the synthesis, integration and expression of viral DNA. Therefore, the amount of SRV proviral DNA was determined by measuring the level of SRV-LTR in the inoculated cells using realtime PCR assay.

The primers and probe that could target both SRV-4-LTR and SRV-8-LTR sequences were designed and used in realtime PCR assay. Different from the SRV viral genome, SRV proviral DNA contains the identical LTR sequences at each terminus, which consists of three regions in the orders of 5'-U3-R-U5-3' (Fig. 3.2a). Therefore, in order to design the primers and probe that could specifically target the SRV-LTR sequence, the forward and reverse primer should be located in the U3 and U5 region respectively. As shown in Figure 3.2b, the SRV-4 and SRV-8 3'LTR sequences alignment result showed that SRV-8-LTR sequence shares 76.7% identity with the sequence of SRV-4-LTR. In the U3 region, there is a GC (G: Guanine; C: Cytosine) rich sequence that might lead to a secondary structure and need a high annealing temperature during the PCR process, thus is unsuitable for primer. Therefore, the forward primer was designed to locate in the polypurine tract (PPT) and U3 region (Fig. 3.2b). For the reverse primer, there is a 'CCCG' and 'GGGC' pattern at the end of the U5 region that might lead to self-complementary and decrease the efficiency of primer. Therefore, the reverse primer was designed on the other highly conserved sequence within the U5 region. However, for the sequence of reverse primer, the nucleotide at the position of 276 is Thymine (T) for SRV-4 but is Cytosine (C) for SRV-8. Thus, for a better fitting for both

SRV-4 and SRV-8, this nucleotide was replaced by the degenerate base of 'R' in the reverse primer. The Primer-BLAST result from the National Center of Biotechnology Information (NCBI) database demonstrated the specificity of the primers for the sequence of SRV-3'LTR. In addition, in the region between the forward and reverse primers, the highest conserved sequence was chosen as the target of the probe. Moreover, for a better fitting of both SRV-4 and SRV-8 subtypes, the nucleotide at the position of 90 was replaced by the degenerate base of 'S'. The probe is labeled by a fluorescent reporter, FAM, at the 5' end, and a quencher of fluorescence, TAMRA, at the 3' end.

Since the amplification efficiency is an important factor that could affect the accurate interpretation of realtime PCR data, it was then decided to examine the amplification efficiencies of SRV-LTR and the internal control, GAPDH, by using the designed primers and probes. Calibration curves were generated for the SRV-LTR and GAPDH realtime PCR reactions using 10-fold serial dilutions of SRV-4/SRV-8-inoculated Jurkat cellular genome (Fig. 3.3). The results showed that for both SRV-4- and SRV-8-inoculated Jurkat cells, the cycle threshold (Ct) values of SRV-LTR and the $-\log_{10}$ dilutions of cellular genome displayed a strong linear correlation, with the correlation coefficients (R^2) greater than 0.99. Moreover, the calibration curves of SRV-LTR and GAPDH were nearly in parallel with similar slopes, suggesting that these two targets have the equivalent amplification efficiencies in realtime PCR. The above findings suggest that SRV-LTR has a high amplification efficiency in realtime PCR by using the designed primers and probe,

and GAPDH could be used as the internal control to quantify SRV-LTR in realtime PCR.

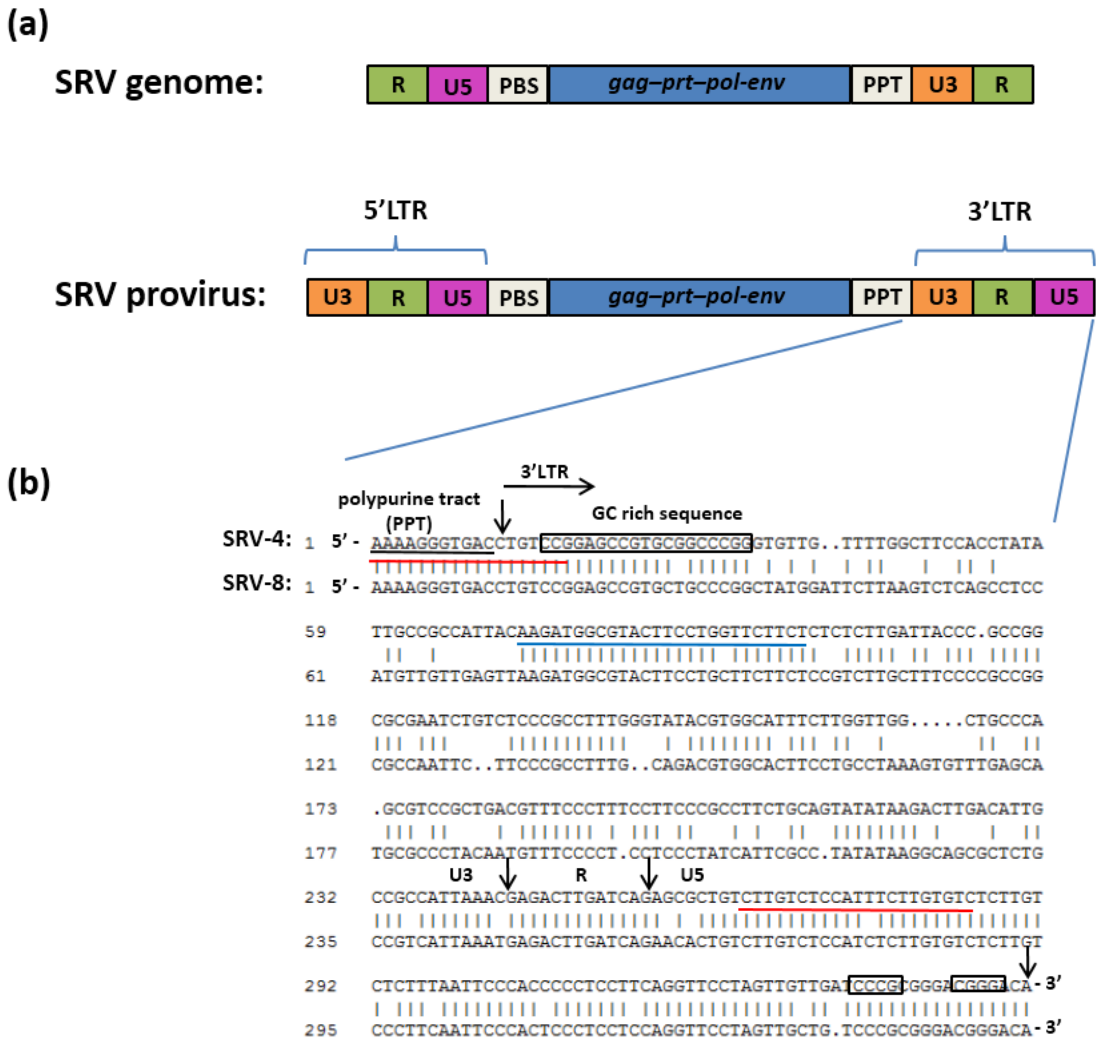

Figure 3.2 Sequences alignment of SRV-4 3'LTR and SRV-8 3'LTR. (a) The schematic maps of SRV genome and SRV provirus. R: repeat sequence. U5: unique sequence at the 5' end of genome. U3: unique sequence at the 3' end of genome. PBS: primer binding site. PPT: polypurine tract. (b) Nucleotide sequences alignment of SRV-4 3'LTR and SRV-8 3'LTR. The regions of U3, R and U5 were labeled and separated by four vertical arrows. The sequence underlined in black belongs to the polypurine tract (PPT). The sequences underlined in red and blue are the targets of primers and probe respectively for both SRV-4-LTR and SRV-8-LTR. The black boxes circled the GC rich sequence in the U3 region and the 'CCCG' and 'GGGC' pattern in the U5 region.

(a)

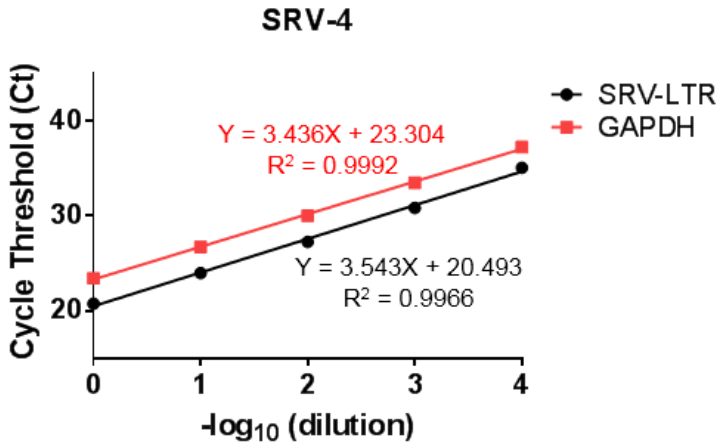

(b)

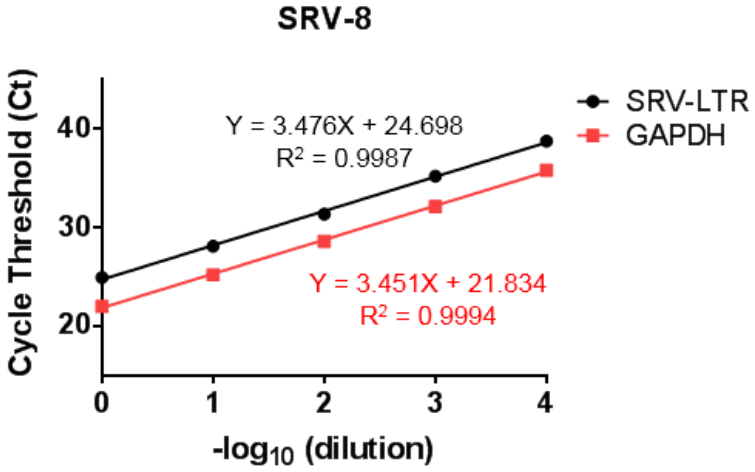

Figure 3.3 SRV-LTR and GAPDH have equivalent amplification efficiencies in realtime PCR. Jurkat cells were inoculated with (a) SRV-4 or (b) SRV-8. On day 8 post-inoculation, the cellular genome was extracted, 10-fold serial diluted and analyzed by realtime PCR for SRV-LTR and GAPDH. The calibration curves were generated by linear regression analysis of the Ct values *versus* -$\log_{10}$ dilutions of the cellular genome. Data from one experiment was analyzed and plotted. The equations represent the linear relationship between Ct values (y) and -$\log_{10}$ dilutions of the cellular genome (x) in the indicated sample. The correlation coefficients (R^2) are shown for each calibration curve.

In order to examine the level of SRV-LTR, Jurkat cells were inoculated with SRV-4/SRV-8 and the cellular DNA was harvested every two days from day 2 to day 14 post-inoculation. The level of SRV-LTR in the cellular DNA was then quantified by realtime

PCR assay using GAPDH as the internal control. For data analysis, the ΔCt value (ΔCt=Ct of SRV-LTR – Ct of GAPDH) of each sample was calculated and normalized to the ΔCt value of the sample on day 2 post-inoculation, generating the value of ΔΔCt (ΔΔCt=ΔCt of each sample –ΔCt of the sample on day 2). The 2^(-ΔΔCt) value of each sample was calculated and used to represent the relative fold change of SRV-LTR. As shown in Figure 3.4, the results showed that for both SRV-4- and SRV-8-inoculated Jurkat cells, the level of SRV-LTR was increased from day 6 to day 10 post-inoculation and then dramatically decreased on day 12 and day 14 post-inoculation (Fig. 3.4). The results suggest that SRV was able to infect Jurkat cells and the infection reached a maximum level on day 10 post-inoculation. Moreover, the decreased SRV-LTR level on day 12 and day 14 post-inoculation implies the elimination of SRV proviral DNA in the inoculated Jurkat cells. Interestingly, although the relative fold change patterns of SRV-LTR are similar in SRV-4- and SRV-8-inoculated cells, the SRV-8-inoculated cells displayed a significant lower SRV-LTR level when compared with that in the SRV-4-inoculated cells on day 8, day 10 and day 14 postinfection (Fig. 3.4). The finding suggests that compared with SRV-4, SRV-8 might have less infectivity in Jurkat cells.

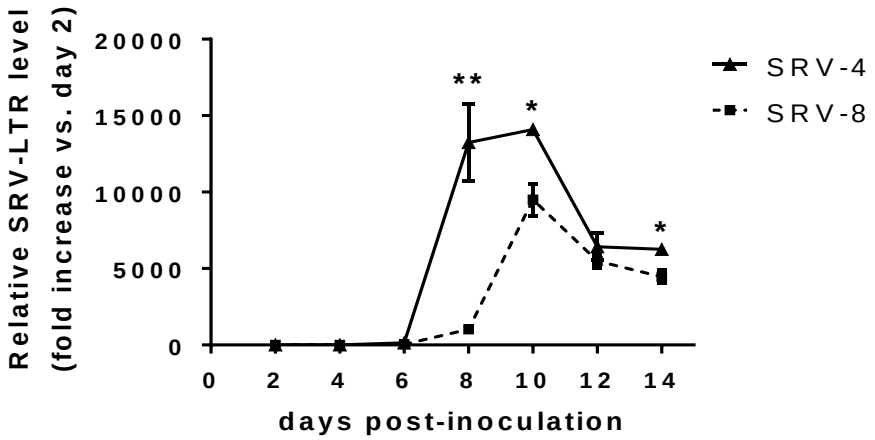

Figure 3.4 SRV-LTR level was increased in SRV-4/SRV-8-inoculated Jurkat cells. Jurkat cells were inoculated with SRV-4/SRV-8. From day 2 to day 14 post-inoculation, the cellular DNA was harvested every two days and analyzed by realtime PCR for SRV-LTR. GAPDH was used as the internal control. The relative level of SRV-LTR at each time point was normalized to the data on day 2, presenting as the relative fold change at the y-axis. SRV-LTR was not detected in all uninoculated Jurkat cells. Data from three independent experiments were quantified and the mean fold over the data on day 2 is presented. Error bars represent the standard deviation. The data was statistically analyzed using the unpaired Student's *t*-test. *$p<0.05$(*) and $p<0.01$(**)* represent significant differences between SRV-4- and SRV-8-inoculated Jurkat cells.

3.3.2 SRV-4 and SRV-8 are able to replicate in the infected Jurkat cells

The previous results in Section 3.3.1 have demonstrated that SRV could infect Jurkat cells, our next question is whether SRV could replicate in the infected cells. Therefore, the SRV virions released in the culture medium of SRV-4/SRV-8-infected cells were measured by monitoring the viral genome copy number through realtime PCR assay.

Due to the lack of suitable internal control gene in the culture medium, the absolute copy number of viral genome was quantified based on the standard curve. The standard SRV plasmids, which contain the conserved sequence for all SRV subtypes, were applied in realtime PCR to generate the standard curve. Serial 10-fold dilutions

of the standard SRV plasmids from 8.5 X 10^8 copies/reaction to 85 copies/reaction were detected. As shown in Figure 3.5, the Ct values and $\log_{10}$ copy numbers of the standard SRV plasmids displayed a strong linear correlation (R^2=0.9996), suggesting the high amplification efficiency of the standard SRV plasmid in the realtime PCR reaction programme.

In order to examine the SRV virions released in the culture medium, the culture medium of uninfected or SRV-4/SRV-8-infected Jurkat cells were harvested every two days from day 2 to day 14 postinfection. The viral RNA in the culture medium was extracted by using the TIANamp Viral RNA extraction kit (#DP315-R, TIANGEN), treated with RNase-free DNase and reverse transcribed into the complementary DNA (cDNA). SRV viral genome in the cDNA was measured using realtime PCR assay and the absolute copy number was calculated according to the standard curve. As shown in Figure 3.6, for both SRV-4- and SRV-8-infected Jurkat cells, the copy number of SRV genome was increased from day 2 to day 12 postinfection, suggesting that SRV was able to replicate in Jurkat cells. Notably, the genome copy number was slightly decreased in SRV-8-infected cells on day 14 postinfection, whereas it was still increased in SRV-4-infected cells. Moreover, at all examined time points, the average copy number of SRV genomes in SRV-8-infected Jurkat cells were slightly higher than that of in the SRV-4-infected cells. Although there are no significant differences, the results implying that SRV-8 might have a higher replication capacity in the infected Jurkat cells.

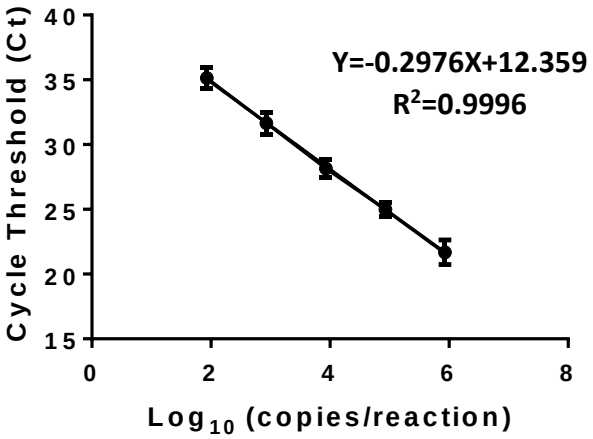

Figure 3.5 The Standard Curve for SRV genome quantification by realtime PCR. The standard curve was generated by linear regression analysis of the Ct values *versus* $\log_{10}$ copy numbers of the standard SRV plasmids (85 to 8.5 X 10^8 copies/reaction). Data from three independent experiments were analyzed and plotted. Error bars represent the standard deviation. The equation: Y=-0.2976X + 12.359 represents the linear relationship between Ct value (y) and $\log_{10}$ copy number of standard SRV plasmids per reaction (x). The correlation coefficient (R^2) is shown.

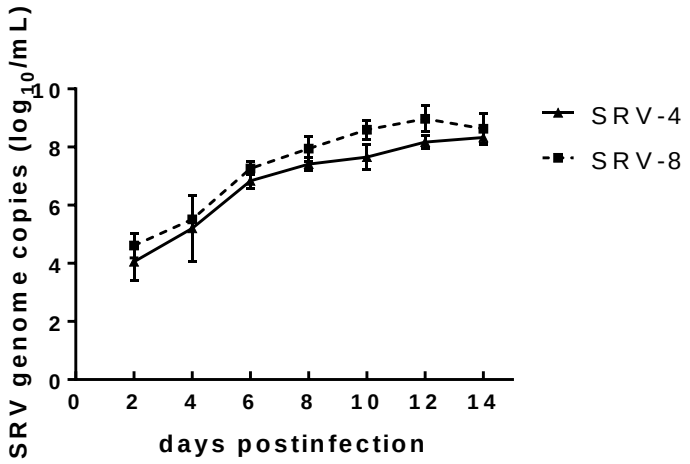

Figure 3.6 SRV-4/SRV-8 genome copies were increased in the culture medium of infected Jurkat cells. Jurkat cells were infected with SRV-4/SRV-8. From day 2 to day 14 postinfection, viral genome in the culture medium of SRV-4/SRV-8-infected Jurkat cells was measured every two days by realtime PCR assay. The copy number of SRV genome was calculated based on the standard curve. SRV genome was not detected in all uninfected Jurkat cells. Data from three independent experiments were quantified and the mean $\log_{10}$ copy number per milliliter ($\log_{10}$/mL) is presented. Error bars represent the standard deviation.

3.4 Discussion

In this chapter, the infectivity and replication capacity of SRV-4 and SRV-8 on Jurkat cells were investigated. The results have shown that SRV-4 or SRV-8 inoculation on Jurkat cells could induce the formation of syncytium, which is an important marker of the cytopathic effect. Moreover, the increased SRV-LTR level in SRV-4/SRV-8-inoculated Jurkat cells has further suggested that SRV was able to infect Jurkat cells and the infection reached the maximum level on day 10 post-inoculation. In addition, the results have shown that the amount of SRV genome was gradually increased in the culture medium of SRV-4/SRV-8-infected cells, suggesting that SRV was able to replicate in the infected Jurkat cells. Interestingly, SRV-8-infected Jurkat cells were shown to produce a relatively lower level of SRV-LTR, but replicate and release more SRV virions when compared with the SRV-4-infected cells. However, the mechanisms behind the different infectivity and replication capacity of SRV-4 and SRV-8 are still unknown.

Previous studies have demonstrated that several SRV subtypes, such as SRV-1, SRV-2 and SRV-6, could *in vitro*-infect human B and T lymphocytes, including Raji (B cells), and H9, Hut78, K-562, MT-4, CEM-SS and SupT-1 (T cells) [16, 68, 74]. Moreover, the characteristic syncytium formation was commonly detected in SRV-infected Raji cells [73, 74]. Consistent with the previous results, the findings in this chapter have shown that SRV-4 and SRV-8 were able to *in vitro*-infect Jurkat T lymphocytes as well as induce the formation of syncytium. The level of SRV-LTR in SRV-4/SRV-8-infected Jurkat cells

was gradually increased from day 6 to day 10 postinfection followed by dramatical reduction on day 12 and day 14 postinfection. Interestingly, a recent study has also demonstrated that the number of SRV-4 proviral DNA in blood samples of the infected Japanese macaques was gradually increased until 23 days post-inoculation and then dramatically decreased [63]. The reduction of proviral DNA occurred at different days postinfection might due to the different experimental conditions: one is *in vivo* whereas the other is *in vitro* experiment. Moreover, the underlying mechanisms of the proviral DNA reduction in the SRV-4/SRV-8-infected cells are still unclear. In addition, previous studies have also demonstrated the replication capacity of SRV in several human B and T lymphocytes, such as Raji and MT-4 cells, and the non-lymphocytes such as HEK293T cells [68, 402]. Consistently, an increased amount of SRV genome has been detected in the culture medium of the infected Jurkat cells, implying the replication capacity of SRV-4 and SRV-8 on Jurkat cells.

Comparing with SRV-8, SRV-4-infected Jurkat cells displayed a relative higher SRV-LTR level within 14 days infection period, implying that SRV-4 might have a higher infectivity on Jurkat cells. The differences might be due to the diversity of envelope (Env) proteins of SRV-4 and SRV-8. A number of researches have demonstrated that the variation of Env proteins in retroviruses could change the cell tropisms of virus as well as influence the viral pathogenesis both *in vivo* and *in vitro* [405-409]. The retroviral Env protein contains the viral *env* gene-encoded glycoproteins (gp), which play important roles in viral attachment and entry of the host cells. Although the

sequence identity of the gp70 and gp20 domain in Env protein of SRV-8 and SRV-4 are 68.24% and 91.15% respectively, which is the highest among all subtypes, a conserved amino acid substitution from alanine to threonine has been detected in the immunosuppressive peptide sequence within the Env protein of SRV-8 [7]. The immunosuppressive peptide sequence is highly conserved among several retroviruses and might affect the transformation and proliferation of lymphocytes [59, 410, 411]. However, the effects of the Env proteins variation on the infectivity of SRV-4 and SRV-8 are still unclear and needed to be investigated in further studies. In addition, the result in this chapter has also suggested that SRV-8 might have a stronger replication capacity in Jurkat cells than SRV-4. However, the strategy of SRV-8 to enhance their replication in the infected cells is not clear at present.

In this chapter, the copy number of SRV genome was examined to estimate the number of SRV virions released by the infected Jurkat cells. However, in most of the cases, the copy number of viral genome is larger than the number of infectious viral particles. Because the viral genome extracted from the culture medium includes not only the genome from infectious particles but also from the noninfectious particles or the free-RNA genome. Therefore, although the SRV genome copy number was gradually increased in the culture medium of the infected Jurkat cells, the replication capacity of the infected Jurkat cells on infectious SRV particles still remains to be investigated in further studies. In this study, a large amount of SRV with high genome copies was used to infect Jurkat cells (3 X 10^8 genome copies per 2 X 10^5 cells); however, the

number of infectious SRV is unclear. In the previous study, SRV was used to infect rhesus bone marrow CD34+ hematopoietic progenitor cells with an estimated multiplicity of infection (MOI, represents the ratio of infectious particles to infection targets) number of 0.1 to 1 [391]. In further experiments, the infectivity assays such as the plaque assay and the 50% Tissue Culture Infective Dose ($TCID_{50}$) assay can be conducted to estimate the titer of SRV.

Taken together, the results in this chapter mark the first time showing that SRV-4 and SRV-8 were able to *in vitro*-infect and replicate in Jurkat cells. The results could give an insight for the understanding of SRV infection on human T lymphocytes, and provide a basis for the further investigation on the interactions between SRV and T cells.

Chapter 4

Investigation of the effects of SRV infection on the autophagic and apoptotic pathways in Jurkat T lymphocytes

4.1 Outline

SRV infection can affect the host immune system, including the decrease of serum immunoglobulin production and the dysfunction of polymorphonuclear cells. Moreover, lymphocyte depletion and immunosuppression were also commonly found in SRV-infected macaques. However, until now, the underlying pathogenetic mechanisms of SRV are still unclear. Indeed, little is known about the effects of SRV infection on T lymphocytes, which is the major cellular target of SRV infection. Autophagy and apoptosis are two important evolutionarily conserved pathways that are involved in immune responses to regulate the virus-host cell interactions, as well as mediate the viral pathogenesis. In order to understand the interactions between SRV and T lymphocytes, in this chapter, the effects of SRV infection on autophagic and apoptotic pathways in Jurkat T lymphocytes were investigated. Furthermore, the potential regulatory roles of autophagy on SRV replication and apoptotic cell death were investigated in the infected Jurkat T lymphocytes.

4.2 Introduction

Autophagy is an evolutionarily conserved degradative process to mediate cellular homeostasis under a variety of stressful conditions including viral invasion. A growing number of studies has shown that the autophagic pathway is modulated in various virus-infected cells that might, in turn, affect viral replication and pathogenesis [24-29]. It is not surprising that, for different types of viruses and host cells, autophagy can play either anti-viral or pro-viral roles in viral infection and pathogenesis [18, 257, 258]. For instance, autophagosome is able to recruit and deliver viral particles to lysosome for degradation, which directly limits viral replication [233, 240]. In addition, autophagy also takes part in the activation of adaptive immune responses, especially by presenting pathogen antigens to immune receptors [240, 412, 413]. However, as the successful intracellular parasites, a number of viruses has developed different defensive strategies to escape or even utilize the autophagic pathway for their own benefits [25, 231, 414]. For different types of viruses and host cells, the autophagic pathway can be blocked or induced at different stages. For example, in HIV-1-infected macrophages, the HIV-1 Nef protein can interact with Beclin1 to disrupt its function and inhibit autophagic flux, thus preventing the degradation of viral particles [415]. However, HIV-1 and HIV-2 infection in CD4+ T cells and Jurkat cells have been shown to induce the formation of autophagosome by increasing the levels of LC3 and Beclin1 in the infected cells [416]. Moreover, the enhanced autophagosome formation has been shown to promote HIV replication since the inhibition of autophagy by Beclin1 knockdown significantly decreased HIV replication. Other viruses, such as poliovirus

and HCV, can block the fusion of autophagosome to lysosome and utilize the autophagosome for the intracellular transportation of viral particles to enhance viral replication [26, 268]. Due to the important roles of autophagy in immune responses against viral infection and the close interactions between autophagy and viral replication, it is necessary to investigate the potential interactions between SRV infection and the autophagic pathway in Jurkat cells.

Besides autophagy, apoptosis is another important immune defense mechanism that is closely associated with viral infection and responsible for many pathogen-associated diseases [19, 20, 30, 31, 417]. Apoptosis is PCD program that responses to a variety of cellular stresses, such as viral invasion, leading to irreversible cell death [23]. For different types of viruses and host cells, it has been shown that either the intrinsic or extrinsic apoptotic pathway or both of them could be induced in the infected cells [31, 36, 418, 419]. Moreover, the viral infection-induced apoptosis could act as an anti-viral or pro-viral mechanism in viral pathogenesis. As a form of cell death, apoptosis is able to inhibit viral replication and transmission by directly eliminating the infected cells [24, 420]. On the other hand, some viruses are able to employ apoptosis to break down the infected cells, which leads to release and disseminate progeny viruses [35, 36, 421, 422]. In this regard, it is necessary for the virus to delay or block the apoptotic pathway in order to increase progeny production and establish successful viral infection [417, 423, 424]. Indeed, as the successful intracellular parasites, viruses have developed different strategies to inhibit the premature apoptosis in the infected cells [35, 425-

427], by inhibiting both intrinsic [36] and extrinsic [31] pathways. However, the effects of SRV infection on the apoptotic pathway in host cells are still unknown. Since the depletion of lymphocytes has been reported in SRV-infected macaques [16, 90], it is necessary to investigate whether SRV infection of Jurkat cells can lead to the apoptotic cell death, which might contribute to the T lymphocytes depletion and immunosuppressive disease in SRV-infected macaques.

Over the last decade, numerous studies have indicated the complex crosstalk between autophagic and apoptotic pathways [189, 190, 428]. The interconnections between these two pathways have been shown to play important roles in regulating cell fate in response to different cellular stresses, including viral invasion [38, 190, 429-431]. Although the autophagic pathway is commonly recognized as a cytoprotective process that facilitates cellular homeostasis and suppresses cell death, persistent or excessive autophagy has been shown to promote apoptotic cell death or itself constitutes an alternative cell death (named autophagic cell death) [187, 432-434]. Similarly, the apoptotic pathway has also been demonstrated to regulate autophagy in the cells [213, 214, 428, 435, 436]. Although the complete molecular mechanisms of the interconnections between the autophagic and apoptotic pathways are still unclear, several important proteins and their functions on the connections of autophagy and apoptosis have been identified [437-440]. One example is Beclin1, which is a key molecule involved in the autophagosome formation. Besides its role in autophagy, Beclin1 has been also shown to interact with several Bcl-2 family members in the

apoptotic pathway; thus it plays double roles in regulating both autophagic and apoptotic pathways [441, 442]. Moreover, recent studies have shown that the autophagosomal membrane was able to serve as a platform for the formation of iDISC, which could recruit and mediate the activation of caspase-8 and thus promote apoptosis [201, 203, 204].

It is not surprising that the crosstalk between autophagy and apoptosis is also widely associated with viral infection and pathogenesis [38, 39]. Indeed, depending on the types of viruses and host cells, the virus-induced autophagy has been shown to either block or promote apoptosis in the infected cells [38, 40, 416].

4.3 Results

4.3.1 SRV-4/SRV-8 infection enhances the autophagic flux in Jurkat cells

The formation of autophagosome is one of the main characteristics of autophagic process. During the process of autophagy, cytosolic LC3-I is conjugated to PE to form LC3-II, which is incorporated into the autophagosomal membrane and could be detected as the LC3 puncta in the cellular cytoplasm by using immunofluorescent labeling [443]. Since LC3 is the only known protein that could specifically interact with autophagosomes but not with other intracellular vesicular structures, the amount of LC3 puncta is commonly correlated with the number of autophagosomes [158, 444].

In order to investigate whether SRV infection affects the autophagic pathway in Jurkat cells, the number of autophagosomes was measured in the uninfected and SRV-4/SRV-8-infected Jurkat cells by immunofluorescence staining assay with anti-LC3 antibody. This antibody is able to detect both endogenous LC3-I and LC3-II with stronger reactivity to LC3-II. The results indicated that compared with the uninfected cells, SRV-4/SRV-8-infected Jurkat cells displayed an increased number of LC3 puncta on day 10 postinfection (Fig. 4.1a). The quantitative data showed that the average number of LC3 puncta was 3~4 per SRV4/SRV8-infected cell, whereas less than 2 LC3 puncta per cell were observed in the uninfected cells (Fig. 4.1b). This finding suggests that SRV-4/SRV-8 infection was able to increase the formation of autophagosome in Jurkat cells.

To further examine the effect of SRV-4/SRV-8 infection on the autophagic flux, the conversion of LC3-I to LC3-II in the uninfected and SRV-4/SRV-8-infected Jurkat cells was examined by western blot analysis. Since the lipidation of LC3-I to form LC3-II is an essential step for autophagosome formation, the conversion of LC3-I to LC3-II was widely used to evaluate the autophagic activity [162]. Our data showed that compared with the uninfected cells, the LC3-II level was increased in SRV-4/SRV-8-infected Jurkat cells on day 8 and then decreased to the basal level on day 10 and day 12 postinfection (Fig. 4.2a). Meanwhile, the LC3-I level was significantly decreased in SRV-4/SRV-8-infected cells on day 10 and day 12 postinfection, especially for the SRV-8-infected cells (Fig. 4.2a). Thus, as shown in Figure 4.2b, the ratios of LC3-II/LC3-I on day 10 and day 12 postinfection were significantly increased to about 2-fold to 4-fold in the infected

cells, when compared to that in the uninfected cells.

Because the autophagosome accumulation and the increase of LC3-II/LC3-I ratio could result from either the increase of autophagosome formation or decrease of autophagosome degradation, in order to further investigate the status of autophagic flux under SRV infection, chloroquine (CQ) was used to treat the cells during SRV infection. Chloroquine is a lysosomotropic agent that can inhibit autophagosome degradation by blocking the fusion of autophagosome and lysosome. If SRV infection could activate the completed autophagic flux, the CQ treatment should lead to an additive increase of LC3-II when compared with the untreated cells. However, if SRV infection could block the degradation of autophagosome, no further increase of LC3-II should be observed in response to CQ treatment. On day 8 postinfection, the uninfected and SRV-4/SRV-8-infected Jurkat cells were treated with 15 μM CQ for 48 hours. The results indicated that CQ treatment significantly increased the LC3-II level in the uninfected as well as the SRV-4/SRV-8-infected Jurkat cells when compared with the untreated cells (Fig. 4.3a). The quantitative data showed that CQ treatment brought around a 10-fold and an 11-fold increase of LC3-II in SRV-4- and SRV-8-infected Jurkat cells respectively, but only led to a 6-fold increase in the uninfected Jurkat cells (Fig. 4.3b). Taken together, the above results indicated that SRV-4/SRV-8 infection was able to enhance the completed autophagic flux in Jurkat cells.

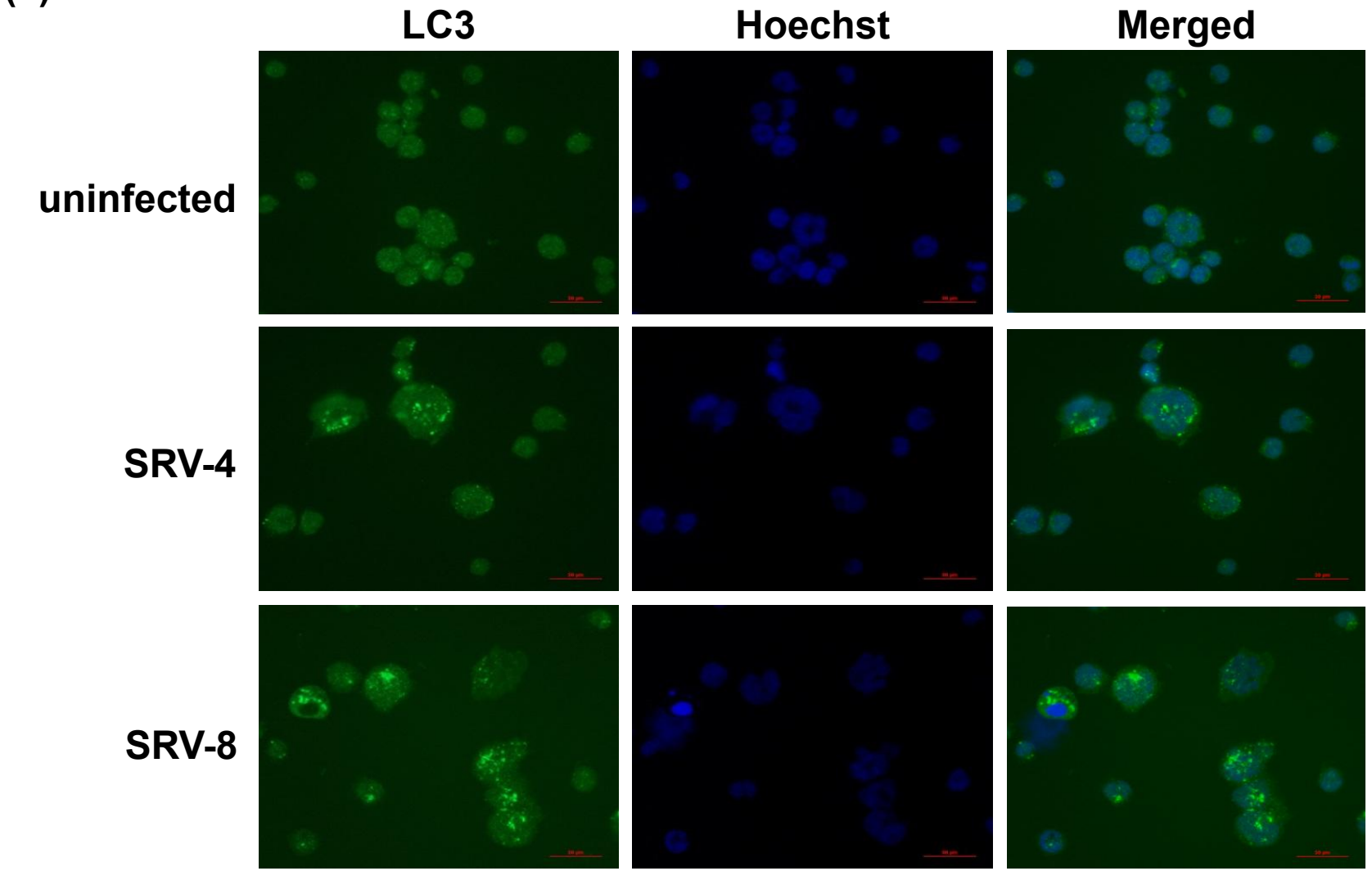
(a)
LC3
Hoechst
Merged
uninfected
SRV-4
SRV-8

(b)

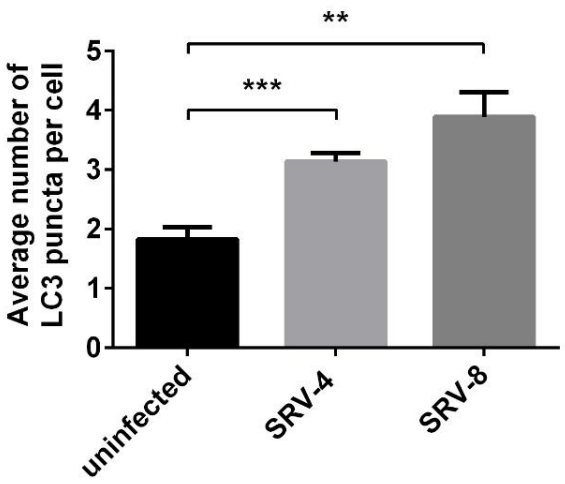

Figure 4.1 LC3 puncta were increased in SRV-4/SRV-8-infected Jurkat cells. On day 10 postinfection, the uninfected and SRV-4/SRV-8-infected Jurkat cells were stained with anti-LC3 antibody (green) to reveal autophagosomes. Nuclei were visualized by Hoechst staining (blue). Scale bar: 50 μM. (a) One of the three independent experiments is shown. (b) The average number of LC3 puncta per cell in the uninfected and SRV-4/SRV-8-infected Jurkat cells. A minimum number of 100 cells for each condition were analyzed by Image J. Error bars represent the standard deviation of the mean data. The data was statistically analyzed using the unpaired Student's *t*-test. *p<0.01(**)* and *p<0.001 (***)* represent significant differences compared with the uninfected control.

(a)

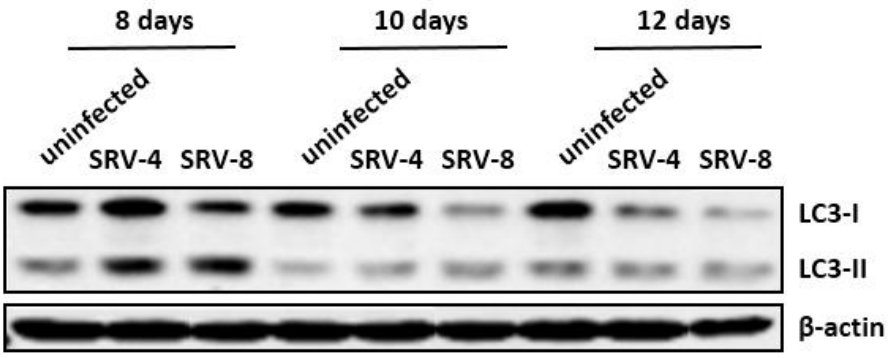

(b)

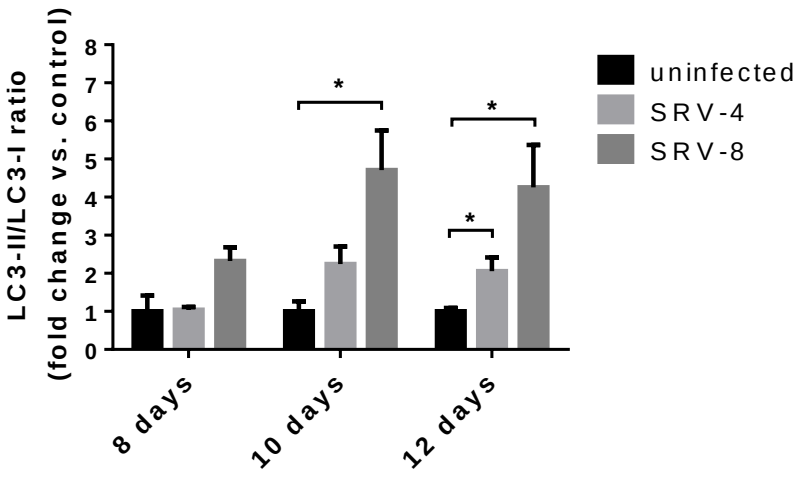

Figure 4.2 The conversion of LC3-I to LC3-II was increased in SRV-4/SRV-8-infected Jurkat cells. Jurkat cells were infected with SRV-4/SRV-8. On day 8, day 10 and day 12 postinfection, lysates of the uninfected and infected cells were analyzed by western blot for LC3. (a) Representative blots are shown. (b) The mean folds of LC3-II/LC3-I ratios relative to an uninfected control under each condition were quantified (using β-actin as a loading control) from three independent experiments. Error bars represent the standard deviation. The data was statistically analyzed using the unpaired Student's *t*-test. *p<0.05(*)* represents significant differences compared with the uninfected control.

(a)

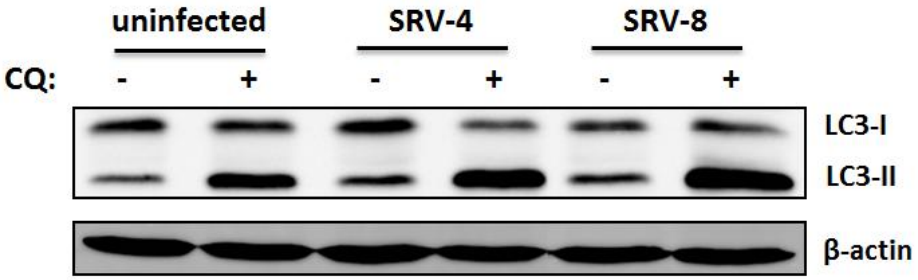

(b)

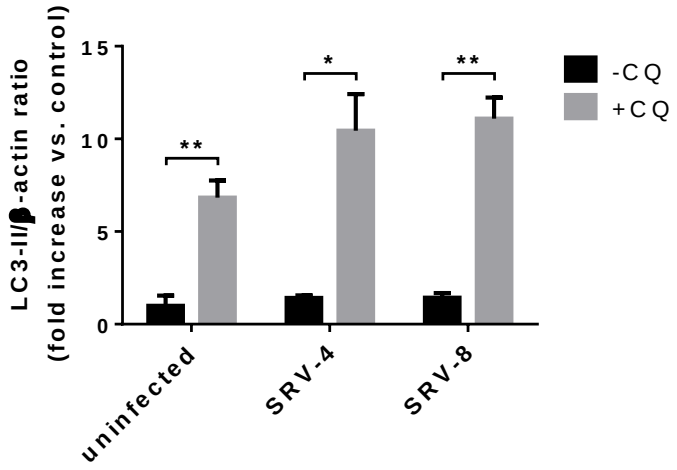

Figure 4.3 Chloroquine treatment increased the level of LC3-II in SRV-4/SRV-8-infected Jurkat cells. On day 8 postinfection, the uninfected and SRV-4/SRV-8-infected Jurkat cells were treated with 15 µM chloroquine (CQ) for 48 hours. Cell lysates were analyzed by western blot for LC3. (a) Representative blots are shown. (b) The mean folds of LC3-II/β-actin ratios relative to an uninfected control without CQ treatment were quantified from three independent experiments. Error bars represent the standard deviation. The data was statistically analyzed using the unpaired Student's *t*-test. *p<0.05(*), p<0.01(**)* and *p<0.001 (***)* represent significant differences compared with the indicated sample.

4.3.2 SRV-4/SRV-8 infection induces apoptosis in Jurkat cells

In order to investigate whether SRV infection is able to affect the apoptotic pathway in Jurkat cells, apoptosis of the SRV-4/SRV-8-infected cells was measured by the Annexin V-PE/7-AAD double staining using flow cytometric analysis. Annexin V can detect phosphatidylserine (PS), which is a marker for the early apoptosis. PS is normally found in the intracellular leaflet of plasma membrane in healthy cells but it will translocate to the external leaflet, where it could be detected by Annexin V, during the early apoptosis [445]. 7-AAD is a fluorescent dye that can stain DNA in the nucleus when the cellular membrane integrity lost, which occurs in the late stage of apoptosis [446]. Thus, the cells of Annexin V^+/7-AAD^- are in the early stage of apoptosis, the cells of Annexin V^+/7-AAD^+ are in the late stage of apoptosis, and the percentage of Annexin V^+ cells (including both Annexin V^+/7-AAD^- and Annexin V^+/7-AAD^+ cells) is commonly used to represent the overall level of apoptosis.

The uninfected and SRV-4/SRV-8-infected Jurkat cells were analyzed on a flow cytometer on day 8, day 10 and day 12 postinfection. The results indicated that for SRV-4-infected Jurkat cells, the percentages of Annexin V^+/7-AAD^- cells and Annexin V^+/7-AAD^+ cells were increased on day 10 and day 12 postinfection when compared to the uninfected cells (Fig. 4.4a). The quantitative data showed that for the SRV-4-infected cells, the percentage of Annexin V^+ cells was increased from 14.29% on day 8, 19.78% on day 10 to 24.75% on day 12 postinfection (Fig. 4.4b). For SRV-8-infected Jurkat cells, the percentage of Annexin V^+ cells were gradually increased from 24.8%

on day 8, 32% on day 10 to 34.6% on day 12 postinfection, and all of them were significantly higher than that in the uninfected cells (Fig. 4.4b). However, no noticeable changes of the Annexin V^+ cells percentage were observed in the uninfected cells on day 8, day 10 and day 12 postinfection. The above findings suggest that SRV-4/SRV-8 infection might induce apoptosis in Jurkat cells. In addition, the result also showed that the percentage of Annexin V^+ cells in the SRV-8-infected cells was significantly higher than that in the SRV-4-infected cells on day 8 and day 10 postinfection.

Since apoptosis is a highly regulated process that is mainly initiated and mediated by the apoptotic caspase cascades, the effect of SRV-4/SRV-8 infection on the apoptotic caspase cascades in Jurkat cells was then investigated. As the activated/cleaved caspase-3 is a major executioner caspase involved in the apoptotic caspase cascades, the level of cleaved caspase-3 was measured in the uninfected and SRV-4/SRV-8-infected Jurkat cells on day 8, day 10 and day 12 postinfection by western blot analysis. As shown in Figure 4.5a, the cleaved caspase-3 level was gradually increased in SRV-4/SRV-8-infected Jurkat cells from day 8 to day 12 postinfection, whereas no noticeable changes were observed in the uninfected cells. The quantitative data showed that the cleaved caspase-3 level in SRV-4 infected cells was increased about a 1.1-fold on day 8, a 1.7-fold on day 10 and a 2.9-fold on day 12 postinfection respectively when compared with the uninfected cells (Fig. 4.5b). Meanwhile, SRV-8 infection brought about a 2.3-fold, a 3.4-fold and a 3.6-fold increase on day 8, day 10 and day 12 postinfection respectively, and the cleaved caspase-3 levels in the infected

(a)

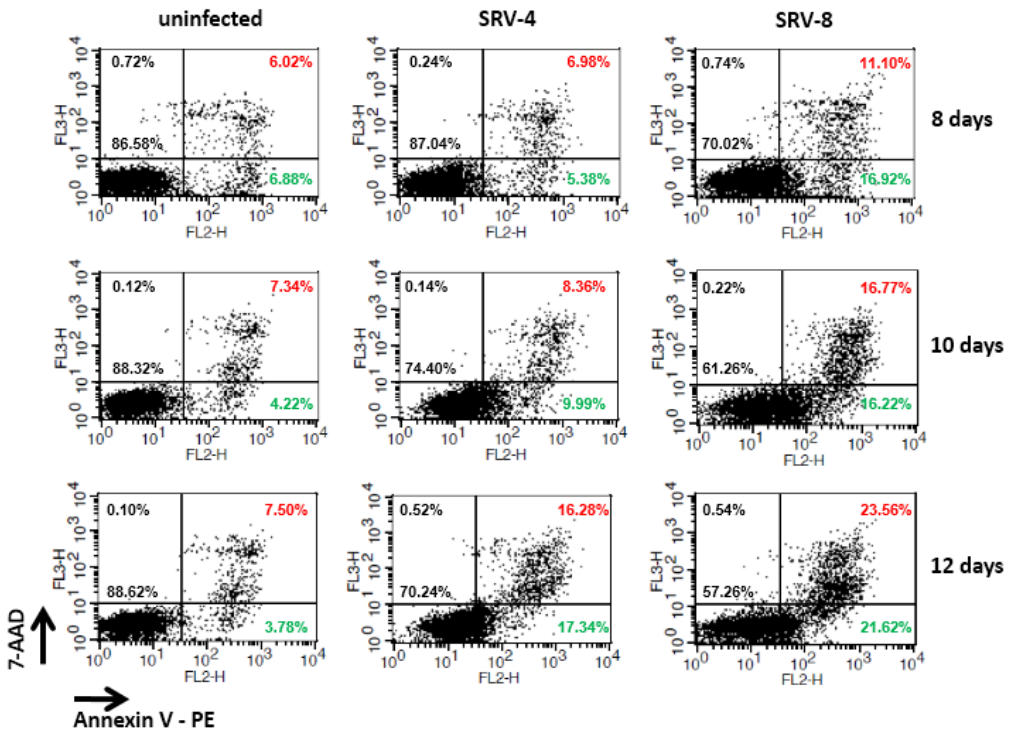

(b)

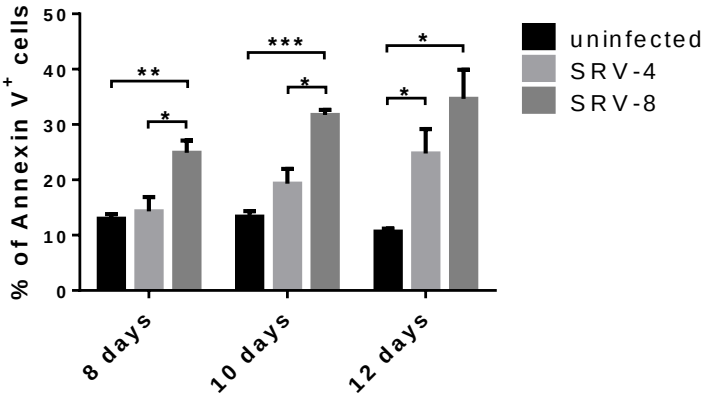

Figure 4.4 Apoptosis was increased in SRV-4/SRV-8-infected Jurkat cells. Jurkat cells were infected with SRV-4/SRV-8. On day 8, day 10 and day 12 postinfection, the level of apoptosis was analyzed on a flow cytometer using Annexin V-PE/7-AAD staining assay. (a) In each individual experiment, 10000 cells were examined and analyzed for each sample under the indicated condition. Representative graphs are shown. The percentage of the cells in each quadrant was labeled in the graphs. (b) The percentage of Annexin V^+ cells, including both Annexin V^+/7-AAD^- cells and Annexin V^+/7-AAD^+ cells, in each sample was quantified from three independent experiments. Error bars represent the standard deviation. The data was statistically analyzed using the unpaired Student's *t*-test. *p<0.05(*), p<0.01(**)* and *p<0.001 (***)* represent significant differences compared with the indicated sample.

cells were all significantly higher than that in the uninfected cells (Fig. 4.5b). The findings confirm that SRV infection was able to induce apoptosis in Jurkat cells and the enhanced activation of caspase-3 might responsible for the increased apoptosis in the infected cells.

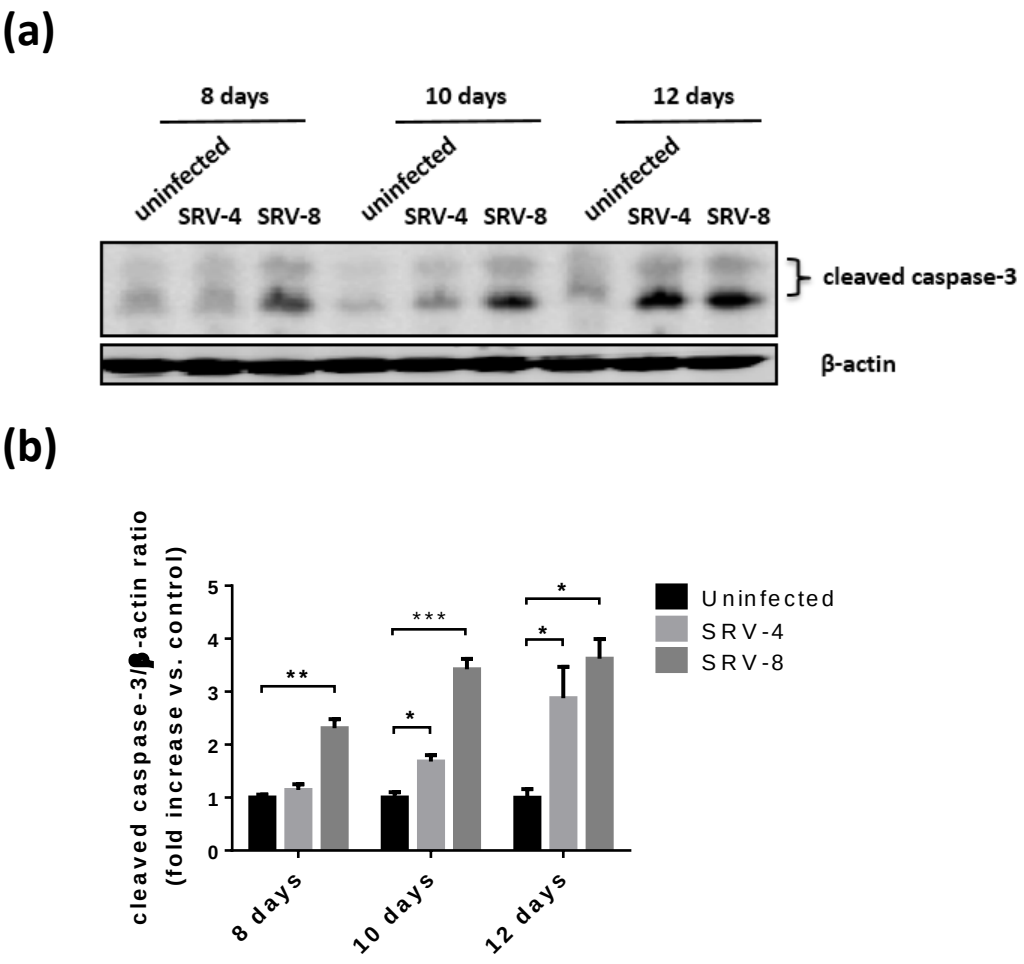

Figure 4.5 The cleaved caspase-3 level was increased in SRV-4/SRV-8-infected Jurkat cells. Jurkat cells were infected with SRV-4/SRV-8. On day 8, day 10 and day 12 postinfection, lysates of the uninfected and infected cells were analyzed by western blot for cleaved caspase-3. (a) Representative blots are shown. (b) The mean folds of cleaved caspase-3/β-actin ratios relative to an uninfected control under each condition were quantified from three independent experiments. Error bars represent the standard deviation. The data was statistically analyzed using the unpaired Student's *t*-test. *p<0.05(*), p<0.01(**)* and *p<0.001 (***)* represent significant differences compared with the uninfected control.

Since the activation of caspase-3 could result from both intrinsic and extrinsic apoptotic pathway, it was then decided to investigate which of these two pathways contribute to the SRV-induced caspase-3 activation and apoptosis in the infected Jurkat cells. Caspase-9 and caspase-8 are the major initiator caspases of the intrinsic and the extrinsic apoptotic pathway respectively. Therefore, the levels of activated/cleaved caspase-8 and activated/cleaved caspase-9 in the uninfected and SRV-4/SRV-8-infected Jurkat cells were measured by western blot analysis. The results indicated that the cleaved caspase-8 level was gradually increased in SRV-4/SRV-8-infected Jurkat cells from day 8 to day 12 postinfection, and there was a significantly increased on day 12 when compared to that in the uninfected cells (Fig. 4.6). Notably, the increasing tendency of the percentages of Annexin V^+ cells and the levels of cleaved caspase-3 and cleaved caspase-8 were consistent in SRV-4- or SRV-8-infected Jurkat cells from day 8 to day 12 postinfection, suggesting that SRV-4/SRV-8 infection-induced apoptosis in Jurkat cells might be attributed to the activation of caspase-8 and caspase-3 (Fig. 4.4, Fig. 4.5 and Fig. 4.6). However, SRV-4/SRV-8 infection did not change the level of cleaved caspase-9 in Jurkat cells from day 8 to day 12 postinfection (Fig. 4.7). In order to validate the quality of anti-cleaved caspase-9 antibody, whole cell lysate from the Jurkat cells treated with 25 μM etoposide was used as a positive control in western blot analysis. Etoposide is a topoisomerase II enzyme inhibitor that causes errors in DNA synthesis and leads to caspase-9 activation [447, 448]. The result showed that there was a distinct cleaved caspase-9 band for the positive control but only the fade bands for all of the uninfected and SRV-4/SRV-8-infected samples, and there were

no noticeable differences between the uninfected and SRV-4/SRV-8-infected cells (Fig. 4.7).

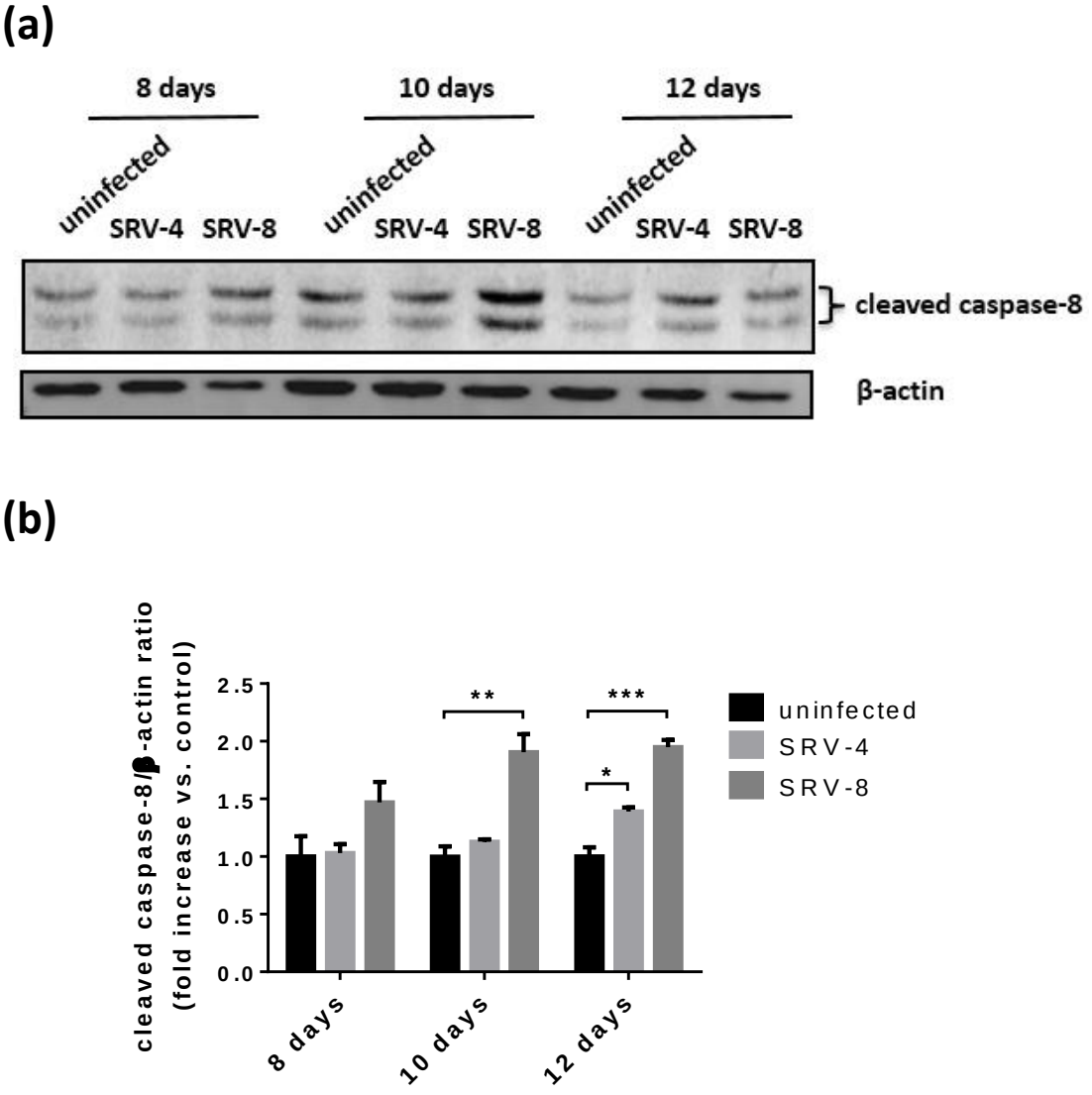

Figure 4.6 The cleaved caspase-8 level was increased in SRV-4/SRV-8-infected Jurkat cells. Jurkat cells were infected with SRV-4/SRV-8. On day 8, day 10 and day 12 postinfection, lysates of the uninfected and infected cells were analyzed by western blot for cleaved caspase-8. (a) Representative blots are shown. (b) The mean folds of cleaved caspase-8/β-actin ratio relative to an uninfected control under each condition were quantified from three independent experiments. Error bars represent the standard deviation. The data was statistically analyzed using the unpaired Student's *t*-test. *p<0.01(**)* and *p<0.001 (***)* represent significant differences compared with the uninfected control.

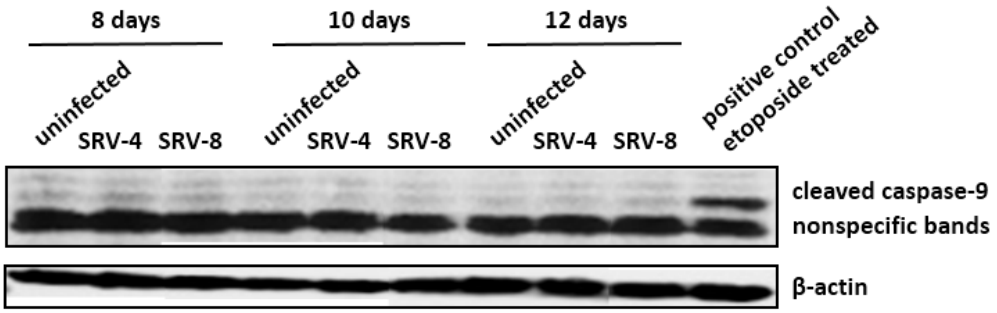

Figure 4.7 The cleaved caspase-9 level did not change in SRV-4/SRV-8-infected Jurkat cells. Jurkat cells were infected with SRV-4/SRV-8. On day 8, day 10 and day 12 postinfection, lysates of the uninfected and infected cells were analyzed by western blot for cleaved caspase-9. Whole cell lysate of the Jurkat cells treated with 25 μM etoposide for 5 hours was used as a positive control. Representative blots are shown from three independent experiments. β-actin was used as a loading control.

The extrinsic apoptotic pathway could be initiated by the binding of death ligands to the interrelated receptors to form the death-inducing signaling complex (DISC), which leads to the activation of caspase-8 (Section 1.3.1). In order to investigate whether the death receptors and their ligands are involved in the activation of caspase-8 in SRV-infected Jurkat cells, the mRNA expression levels of two pairs of important death receptors and their ligands, Fas/FasL and DR5/TRAIL, were analyzed by using realtime PCR method. The results indicated that compared with the uninfected cells, the mRNA levels of Fas, DR5 and TRAIL did not change in SRV-4/SRV-8-infected Jurkat cells on day 10 postinfection, which was the time point that caspase-8, caspase-3 and apoptosis were activated in the infected cells (Fig. 4.8). Interestingly, the mRNA level of FasL was significantly decreased to 16% and 28% in SRV-4- and SRV-8-infected Jurkat cell respectively when compared to that in the uninfected cells. Collectively, the findings suggest that SRV infection might not increase the expression of death

receptors/ligands in Jurkat cells and the activation of caspase-8 in the infected cells might be death receptors/ligands independent.

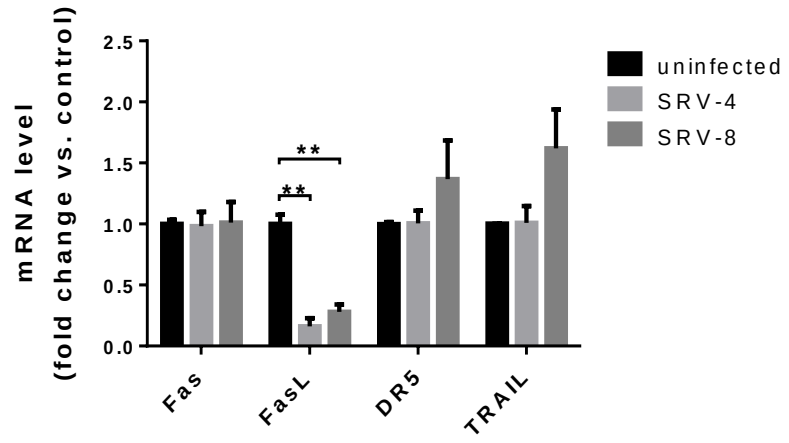

Figure 4.8 The mRNA levels of Fas, FasL, DR5 and TRAIL did not increase in SRV-4/SRV-8-infected Jurkat cells. Jurkat cells were infected with SRV-4/SRV-8. On day 10 postinfection, mRNA levels of Fas, FasL, DR5 and TRAIL in the uninfected and infected cells were analyzed by realtime PCR. The mean folds of the indicated mRNA relative to an uninfected control under each condition were quantified (using GAPDH as an internal control) from three independent experiments. Error bars represent the standard deviation. The data was statistically analyzed using the unpaired Student's *t*-test. *p<0.01(**)* and *p<0.001 (***)* represent significant differences compared with the indicated sample.

Taken together, the above results indicated that both SRV-4 and SRV-8 infection was able to induce apoptosis, as well as increase the levels of cleaved caspase-3 and cleaved caspase-8 in Jurkat cells. However, the level of cleaved caspase-9 did not increase in SRV-4/SRV-8-infected Jurkat cells when compared to that in the uninfected cells. Moreover, the transcripts levels of Fas/FasL and DR5/TRAIL did not significantly increase in SRV-4/SRV-8-infected Jurkat cells, suggesting that the activation of caspase-8 in the infected cells might be death receptors/ligands-independent.

The above results in Section 4.3.1 and Section 4.3.2 have shown that both SRV-4 and SRV-8 infection was able to induce the autophagic and apoptotic pathways in Jurkat cells. However, compared with SRV-4, SRV-8 infection was shown to induce more obvious impacts on the two pathways in Jurkat cells. Therefore, SRV-8 was used to further investigate the potential regulatory roles of SRV-induced autophagy on viral replication and apoptosis in Jurkat cells.

4.3.3 SRV-8 infection-induced autophagy inhibits viral replication in Jurkat cells

The above results suggested that SRV was able to induce the completed autophagic flux in the infected Jurkat cells (Section 4.3.1). To elucidate the effect of SRV-induced autophagy on viral replication, the autophagic pathway was inhibited in Jurkat cells by decreasing the expression of an important autophagy-related gene (atg), BECN1 (encodes the protein named Beclin1), by using the RNA interference (RNAi) technique. A doxycycline (Dox)-inducible short hairpin RNA (shRNA) vector that targets the BECN1 was constructed and transduced into Jurkat cells by using lentiviral transduction method, generating the doxycycline-inducible shBeclin1 stable Jurkat cell line. Additionally, the doxycycline-inducible scramble stable Jurkat cell line, which was transduced by the non-silencing shRNA that has no effects on the expression of any gene, was constructed and used as the non-silencing control. Only in the presence of doxycycline in the culture medium, the specific doxycycline-inducible shRNA within the transduced stable Jurkat cells will be expressed to silence the target gene

expression.

To examine the knockdown efficiency of the shBeclin1 construct in Jurkat cells, Beclin1 protein levels in the scramble and shBeclin1 Jurkat cells with or without doxycycline treatment were measured by using western blot assay. As shown in Figure 4.9a, compared with the doxycycline uninduced group, induction of shBeclin1 expression with 1 μg/mL doxycycline for 3 days significantly decreased Beclin1 protein expression in the shBeclin1 Jurkat cells; whereas the protein level of Beclin1 did not change in the doxycycline-induced scramble Jurkat cells. The quantitative data indicated that when the shBeclin1 Jurkat cells were induced with the doxycycline, the expression of Beclin1 protein was significantly reduced to about 25% of that expressed in the uninduced cells (Fig. 4.9b). In addition, the effect of Beclin1 knockdown on cell viability in Jurkat cells was examined using the MTT colorimetric assay. The results showed that the doxycycline-induced Beclin1 knockdown could lead to a ~9% decrease of cell viability in shBeclin1 Jurkat cells; however, the change is not statistically significant (Fig. 4.9c). Moreover, doxycycline induction did not change the cell viability in scramble Jurkat cells, suggesting that the doxycycline treatment might be not toxic to Jurkat cells.

In order to examine SRV replication in the Beclin1 knockdown Jurkat cells, scramble and shBeclin1 Jurkat cells were infected with SRV-8 for 6 days followed by 1 μg/mL doxycycline induction for 3 days. Viral RNA genomes in the culture medium of SRV-8 infected cells with or without doxycycline induction were harvested and quantified by

(a)

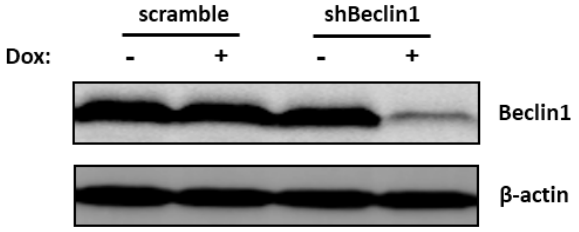

(b)

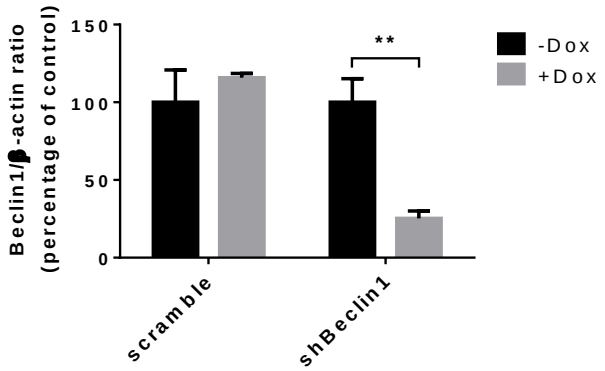

(c)

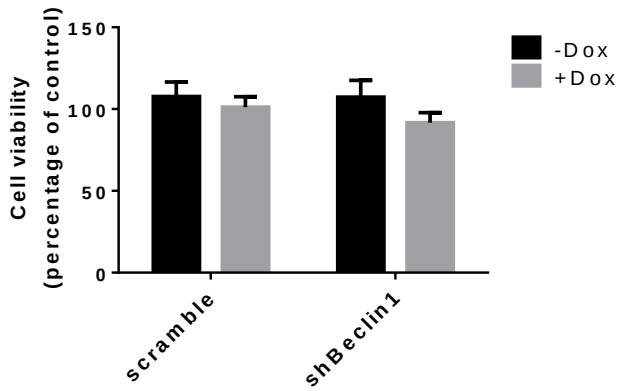

Figure 4.9 The Beclin1 protein expression level was reduced in the shBeclin1 Jurkat cells by doxycycline induction. Scramble and shBeclin1 Jurkat cells were induced with 1 μg/mL doxycycline for 3 days. (a&b) The protein level of Beclin1 was examined by western blot assay. (a) Representative blots are shown. (b) Data from three independent experiments were quantified and expressed as the mean percentage of the uninduced control. (c) Cell viability was examined by MTT colorimetric assay. Data from three independent experiments were quantified and expressed as the mean percentage of the uninduced control. Error bars represent the standard deviation. The data was statistically analyzed using the unpaired Student's *t*-test. *p<0.001 (***)* represents a significant difference compared with the uninduced control.

using realtime PCR method. The results showed that doxycycline induction significantly increased the copy number of released viral genome in the culture medium of shBeclin1 Jurkat cells; whereas it has no effect on the scramble Jurkat cells (Fig. 4.10). The results indicated that the inhibition of autophagy by Beclin1 knockdown was able to enhance SRV replication in the infected Jurkat cells and thus increase the number of released viral particles, suggesting that SRV infection-induced autophagy in Jurkat cells might inhibit SRV replication.

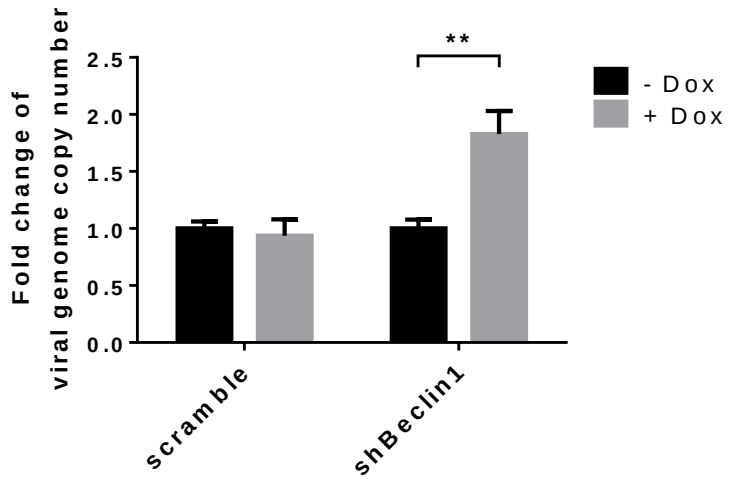

Figure 4.10 Knockdown of Beclin1 enhanced SRV-8 replication in Jurkat cells. Scramble and shBeclin1 Jurkat cells were infected with SRV-8 for 6 days followed by 1 µg/mL doxycycline induction for 3 days. Viral RNA genomes in 140 µL culture medium were extracted and the copy number was measured using realtime PCR assay. Data from five independent experiments were quantified and the mean fold relative to the uninduced control is presented. Error bars represent the standard deviation. The data was statistically analyzed using the unpaired Student's *t*-test. *p<0.01 (**)* represents a significant difference compared with the uninduced control.

4.3.4 SRV-8 infection-induced autophagy promotes apoptosis in Jurkat cells

A growing number of studies has indicated the complex interplay between autophagic and apoptotic pathways in host cells during viral infection [189, 190, 449, 450]. In order to investigate the effect of SRV infection-induced autophagy on apoptosis in Jurkat cells, the level of apoptosis in the infected Beclin1 knockdown cells was examined by Annexin V assay using flow cytometric analysis. Scramble and shBeclin1 Jurkat cells were infected with SRV-8 for 5 days followed by 1 μg/mL doxycycline treatment for 3 days prior to the Annexin V assay. As shown in Figure 4.11a, the M1 gate was set to indicate the cell population that was defined as the Annexin V^+ cells. The results showed that compared with the uninfected cells, the percentage of Annexin V^+ cells were significantly increased in both SRV-8-infected scramble and shBeclin1 Jurkat cells without doxycycline induction (Fig. 4.11b). This finding was consistent with the above result in Figure 4.4, suggesting that SRV infection was able to induce apoptosis in Jurkat cells. Interestingly, doxycycline-induced Beclin1 knockdown in the infected shBeclin1 Jurkat cells was showed to significantly decrease the percentage of Annexin V^+ cells from 65.6% to 50.8% (Fig. 4.11b). However, doxycycline induction did not affect the apoptosis level in the infected scramble cells. The results suggest that the inhibition of autophagy by Beclin1 knockdown was able to reduce SRV infection-induced apoptosis in Jurkat cells.

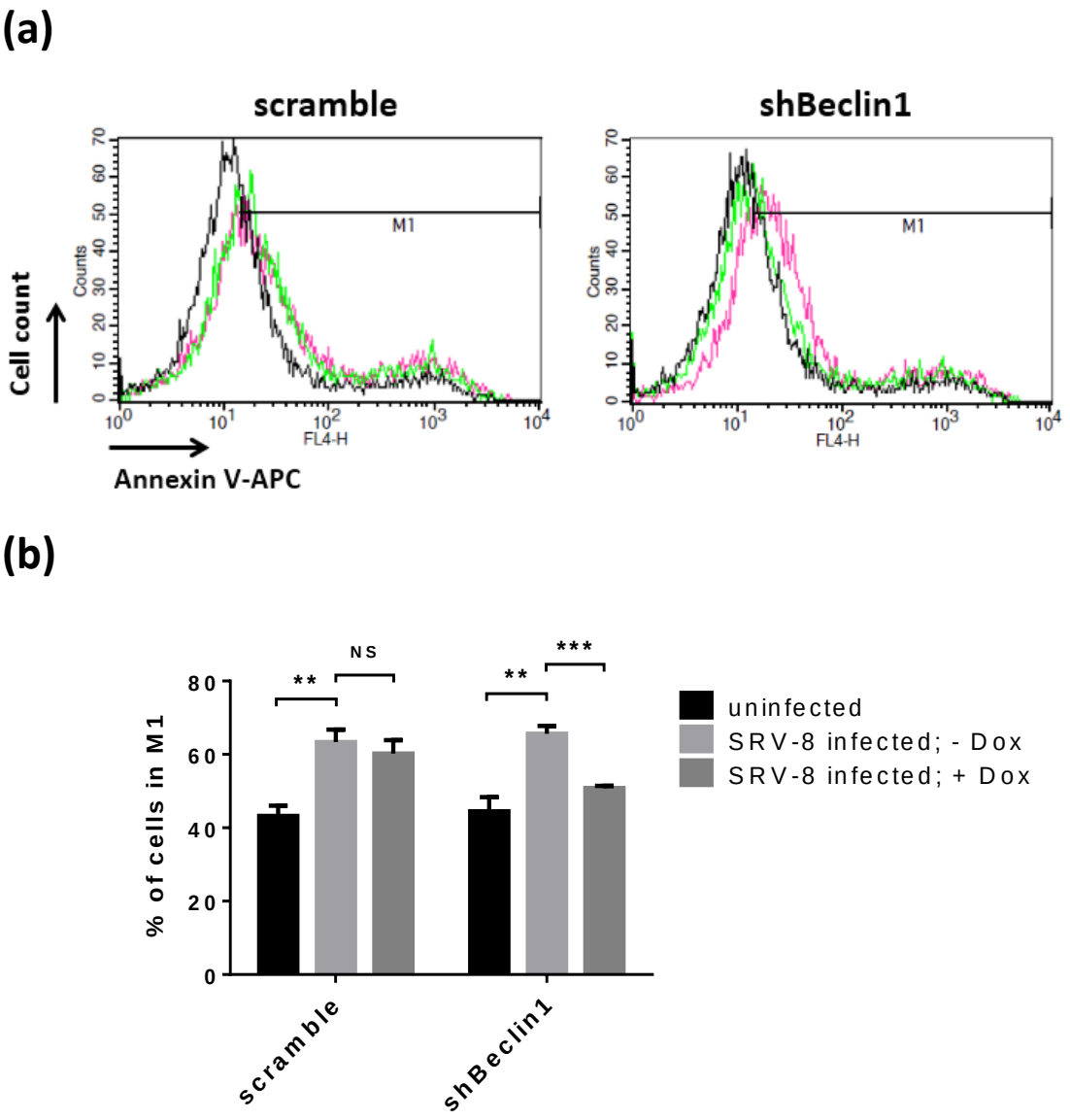

Figure 4.11 Knockdown of Beclin1 decreased SRV-8-induced apoptosis in Jurkat cells. Scramble and shBeclin1 Jurkat cells were infected with SRV-8 for 5 days followed by 1 µg/mL doxycycline induction for 3 days. The level of apoptosis was examined by Annexin V assay using flow cytometric analysis. In each individual experiment, 10000 cells were examined and analyzed for each sample under the indicated condition. (a) Representative graphs are shown. Graphs were plotted with the Annexin V-APC fluorescence intensity (x-axis) against cell count (y-axis). M1 gates were set to mark the cell population that used to observe fluorescence shift across the x-axis. Each graph includes the data of uninfected cells without doxycycline induction (black), SRV-8-infected cells without doxycycline induction (red) and SRV-8-infected cells with doxycycline induction (green). (b) The percentage of cells in M1 gate was quantified from five independent experiments and the mean value is presented. Error bars represent the standard deviation. The data was statistically analyzed using the unpaired Student's *t*-test. NS represents non-signification, *p<0.01 (**) and p<0.001 (***)* represent significant differences compared with the indicated sample.

Since caspase-8 and caspase-3 were both activated during SRV-4/SRV-8 infection of Jurkat cells (Section 4.3.2), the effect of autophagy inhibition by Beclin1 knockdown on the caspase-8/-3 activation in the infected cells was then examined. Scramble and shBeclin1 Jurkat cells were infected with SRV-8 for 5 days followed by 1 μg/mL doxycycline treatment for 3 days. The whole cellular proteins were harvested and used to examine the levels of Beclin1, LC3 and cleaved caspase-8/-3 by western blot analysis. The results indicated that doxycycline induction could significantly decrease the levels of Beclin1 as well as the ratios of LC3-II/LC3-I in the infected shBeclin1 Jurkat cells, implying that Beclin1 knockdown was able to inhibit the autophagic pathway (Fig. 4.12). Additionally, SRV-8 infection was shown to increase the levels of cleaved caspase-8/-3 in both scramble and shBeclin1 Jurkat cells without doxycycline induction; the finding is consistent with the previous results (Fig. 4.12a, Fig. 4.5 and Fig. 4.6). Interestingly, the results showed that doxycycline-induced Beclin1 knockdown in the infected shBeclin1 Jurkat cells significantly decreased the levels of both cleaved caspase-8 and cleaved caspase-3 when compared to that in the uninduced cells (Fig. 4.12b and Fig. 4.12c). Nevertheless, no noticeable differences were observed for the levels of Beclin1, LC3-II/LC3-I and cleaved caspase-8/-3 in the infected scramble Jurkat cells with or without doxycycline induction. Collectively, the findings suggest that the inhibition of autophagy by Beclin1 knockdown was able to rescue the activation of caspase-8/-3 and apoptosis in SRV-infected Jurkat cells.

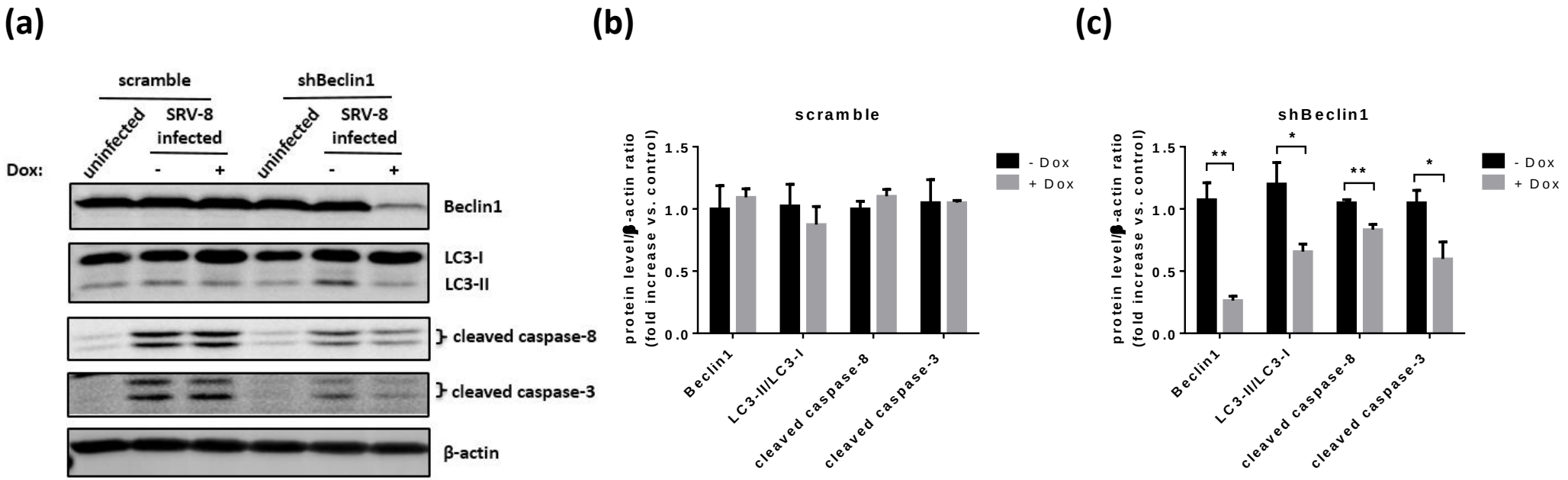

Figure 4.12 Knockdown of Beclin1 decreased the levels of LC3-II/LC3-I, cleaved caspase-8 and cleaved caspase-3 in SRV-8-infected Jurkat cells. Scramble and shBeclin1 Jurkat cells were infected with SRV-8 for 5 days followed by 1 μg/mL doxycycline induction for 3 days. The levels of Beclin1, LC3-II/LC3-I, cleaved caspase-8 and cleaved caspase-3 were examined by western blot analysis. (a) Representative graphs are shown. (b&c) Data from four independent experiments were quantified and the mean folds relative to the infected (b) scramble or (c) shBeclin1 cells without doxycycline induction for the level of indicated protein are presented. Error bars represent the standard deviation. The data was statistically analyzed using the unpaired Student's *t*-test. *p<0.05(*), p<0.01(**)* and *p<0.001 (***)* represent significant differences compared with the indicated sample.

In order to further elucidate the interplay between autophagic and apoptotic signaling pathways in Jurkat cells during SRV infection, we used a pharmacological inhibitor of autophagy, chloroquine (CQ), to suppress the autophagic pathway in the infected Jurkat cells. Different from Beclin1 knockdown that inhibits the formation of autophagosome, CQ treatment cannot affect the initiation of autophagy but inhibits the degradation of autophagosome by blocking the fusion of autophagosome to lysosome. 15 μM CQ was used to treat the uninfected and SRV-8-infected Jurkat cells on day 8 postinfection for 48 hours and the level of apoptosis was examined by Annexin V-PE and 7-AAD double staining assay using flow cytometric analysis. In contrast with the previous results, different from Beclin1 knockdown in the SRV-8-infected cells, the inhibition of autophagosome degradation by CQ treatment significantly increased the accumulation of Annexin V^+ cells (Fig. 4.13). In the presence of CQ, the percentage of Annexin V^+ cells were increased from 14.97% to 21.09% in the infected Jurkat cells (Fig. 4.13b). However, CQ treatment has no significant effect on the apoptosis level of uninfected Jurkat cells.

In order to confirm the effect of CQ treatment on the apoptotic pathway in SRV-8 infected Jurkat cells, the levels of cleaved caspase-8/-3 in the infected cells with or without CQ treatment were examined by western blot analysis. As shown in Figure 4.14, for both uninfected and SRV-8-infected cells, the level of LC3-II in CQ treated groups were dramatically increased when compared with that in the untreated groups, indicating the degradation of autophagosome was inhibited. Moreover, for the SRV-8-

(a)

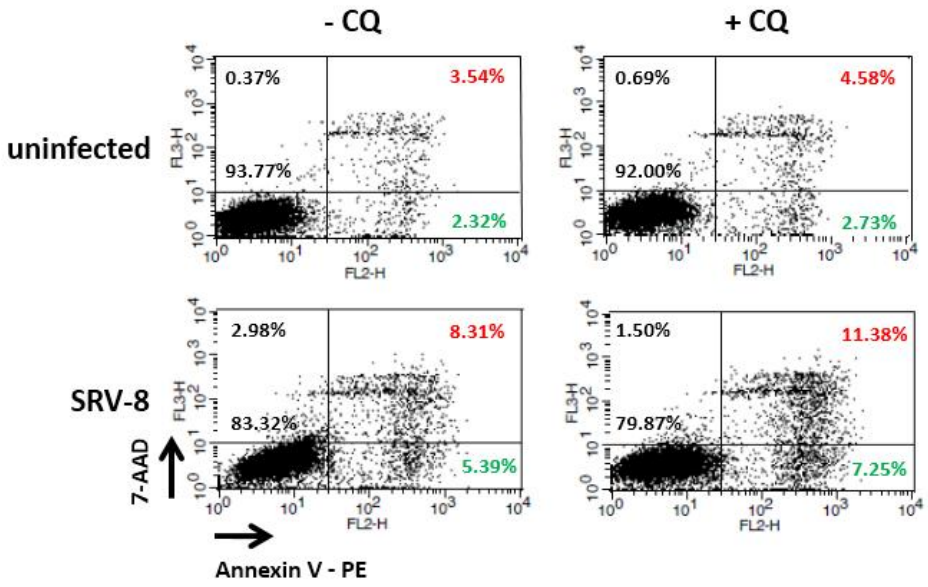

(b)

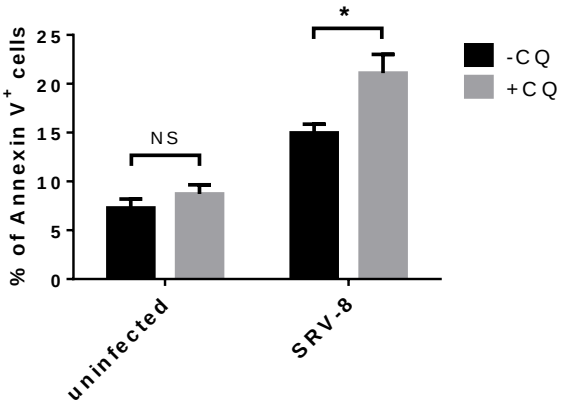

Figure 4.13 Chloroquine treatment increased apoptosis in SRV-8-infected Jurkat cells. Uninfected and SRV-8-infected Jurkat cells on day 8 postinfection were treated with 15 µM chloroquine (CQ) for 48 hours. The level of apoptosis was examined by Annexin V-PE/7-AAD staining assay using flow cytometry. (a) In each individual experiment, 10000 cells were examined and analyzed for each sample under the indicated condition. Representative graphs are shown. The percentage of the cells in each quadrant was labeled in the graph. (b) The percentage of Annexin V^+ cells of each sample was quantified from three independent experiments. Error bars represent the standard deviation. The data was statistically analyzed using the unpaired Student's *t*-test. NS represents non-signification, *p<0.05(*)* represents a significant difference compared with the chloroquine untreated control.

infected Jurkat cells, CQ treatment significantly increased the cleavage of both caspase-8 and caspase-3 when compared with the untreated cells. Under SRV infection, the presence of CQ led to a 1.8-fold and a 1.7-fold increase in the level of cleaved caspase-8 and cleaved caspase-3 respectively (Fig. 4.14b). However, CQ treatment did not change the levels of cleaved caspase-8/-3 in the uninfected cells.

The above results indicated that the inhibition of autophagosome formation by Beclin1 knockdown was able to suppress apoptosis in SRV-8-infected Jurkat cells, suggesting that the SRV-induced autophagy might promote apoptosis in the infected cells. However, the inhibition of autophagosome degradation by chloroquine treatment was shown to enhance apoptosis in the infected cells. Collectively, the findings suggest that the amount of autophagosome formation is positively correlated with the degree of apoptosis in SRV-infected Jurkat cells.

(a)

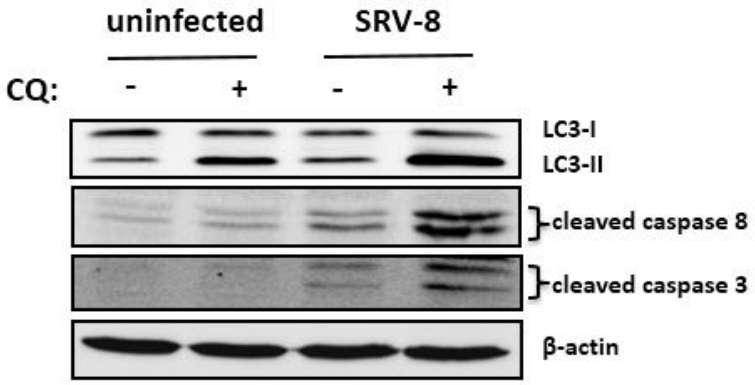

(b)

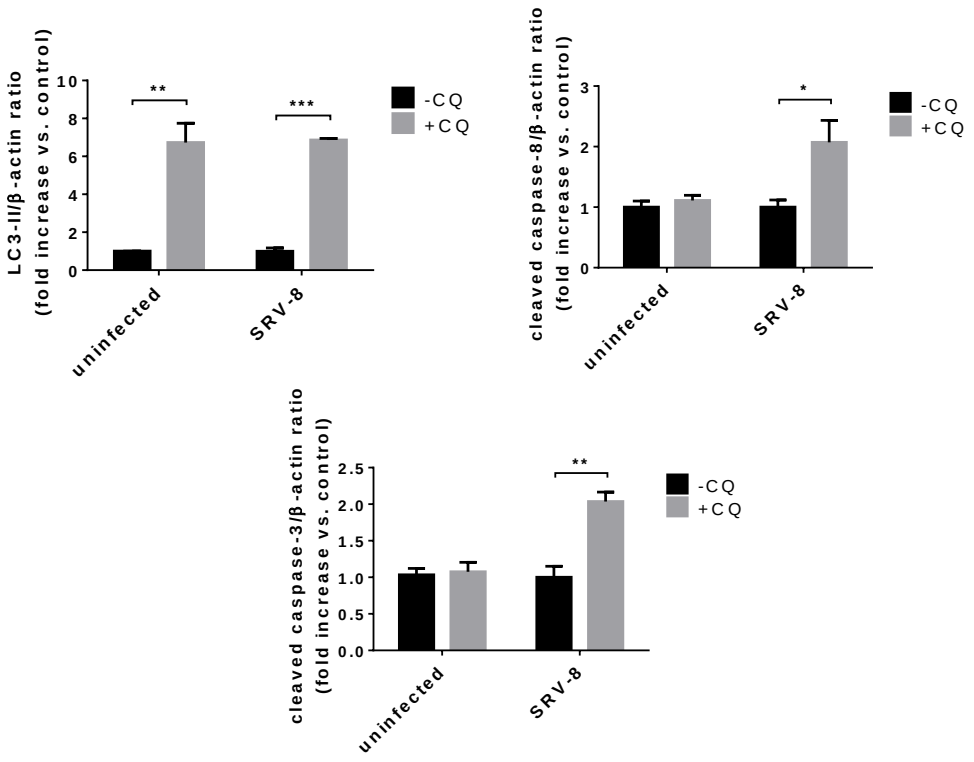

Figure 4.14 Chloroquine treatment increased the levels of cleaved caspase-8 and cleaved caspase-3 in SRV-8-infected Jurkat cells. Uninfected and SRV-8-infected Jurkat cells on day 8 postinfection were treated with 15 µM chloroquine (CQ) for 48 hours. The levels of LC3, cleaved caspase-8 and cleaved caspase-3 were examined using western blot analysis. (a) Representative blots are shown. (b) Data from five independent experiments were quantified and the mean fold relative to the chloroquine untreated group is presented. Error bars represent the standard deviation. The data was statistically analyzed using the unpaired Student's *t*-test. *p<0.05 (*), p<0.01 (**)* and *p<0.001 (***)* represent significant differences compared with the chloroquine untreated control.

4.3.5 Procaspase-8 locates on autophagosome and interacts with LC3 and p62/SQSTM1 in SRV-8-infected Jurkat cells

Recent studies have demonstrated that the autophagosomal membrane is able to act as a scaffold for the formation of iDISC to induce the oligomerization and auto-cleavage of procaspase-8, which initiates the caspase-8/-3 cascade and apoptosis [201, 203, 204]. Our previous results have shown that SRV infection was able to induce the activation of caspase-8 in Jurkat cells, and this might be independent of death receptors/ligands (Section 4.3.2). Moreover, the results in Section 4.3.4 suggested that there might be a potential correlation between the number of autophagosomes and the level of cleaved caspase-8/-3 and apoptosis in SRV-8-infected Jurkat cells. Therefore, it is necessary to investigate whether the formation of autophagosome in SRV-8-infected Jurkat cells is able to recruit and mediate the activation of procaspase-8, which leads to apoptosis in the infected cells.

As discussed above (Section 1.3.2), the autophagic protein LC3 and p62/SQSTM1 are two important markers of autophagosome in mammalian cells. Moreover, previous studies have demonstrated that LC3 and p62/SQSTM1 are involved in the formation of iDISC to promote the aggregation and self-processing of procaspase-8 [201, 203]. Thus, in order to investigate the interaction between autophagosome and procaspase-8 in SRV-8-infected Jurkat cells, the co-localization of procaspase-8 with LC3 and p62/SQSTM1 was examined by using the double immunostaining assay. As shown in Figure 4.15, several endogenous procaspase-8 puncta were detected in SRV-8 infected Jurkat cells on day 10 postinfection, and a portion of them was co-localized with LC3

puncta. Moreover, a portion of the endogenous procaspase-8 was also co-localized with p62/SQSTM1 in the SRV-8-infected Jurkat cells (Fig. 4.16). These results suggest the potential interaction between autophagosome and procaspase-8 in SRV-8-infected Jurkat cells.

To further confirm the interaction between procaspase-8 and LC3, the co-immunoprecipitation (co-IP) assay was conducted with uninfected and SRV-8-infected Jurkat cells. On day 10 postinfection, the cell lysates were incubated with anti-LC3 antibodies and precipitated using agarose beads. The level of co-immunoprecipitated procaspase-8 was then examined by using western blot analysis. As shown in Figure 4.17, the co-immunoprecipitated procaspase-8 was detected in both uninfected and SRV-8-infected Jurkat cells. However, a significantly higher level of procaspase-8 was detected in SRV-8-infected cells when compared to the uninfected cells (Fig. 4.17b). In addition, neither LC3 nor procaspase-8 was detected in the IgG control samples. The finding suggested that the interaction between LC3 and procaspase-8 was significantly enhanced in the Jurkat cells with SRV-8 infection.

Collectively, the results in this chapter led us to propose a model in which the enhanced formation of autophagosomes in the SRV-8-infected Jurkat cells were able to recruit procaspase-8 for its activation, leading to the apoptotic cell death; and p62/SQSTM1 and LC3 might be involved in the recruitment of procaspase-8 (Fig. 4.18).

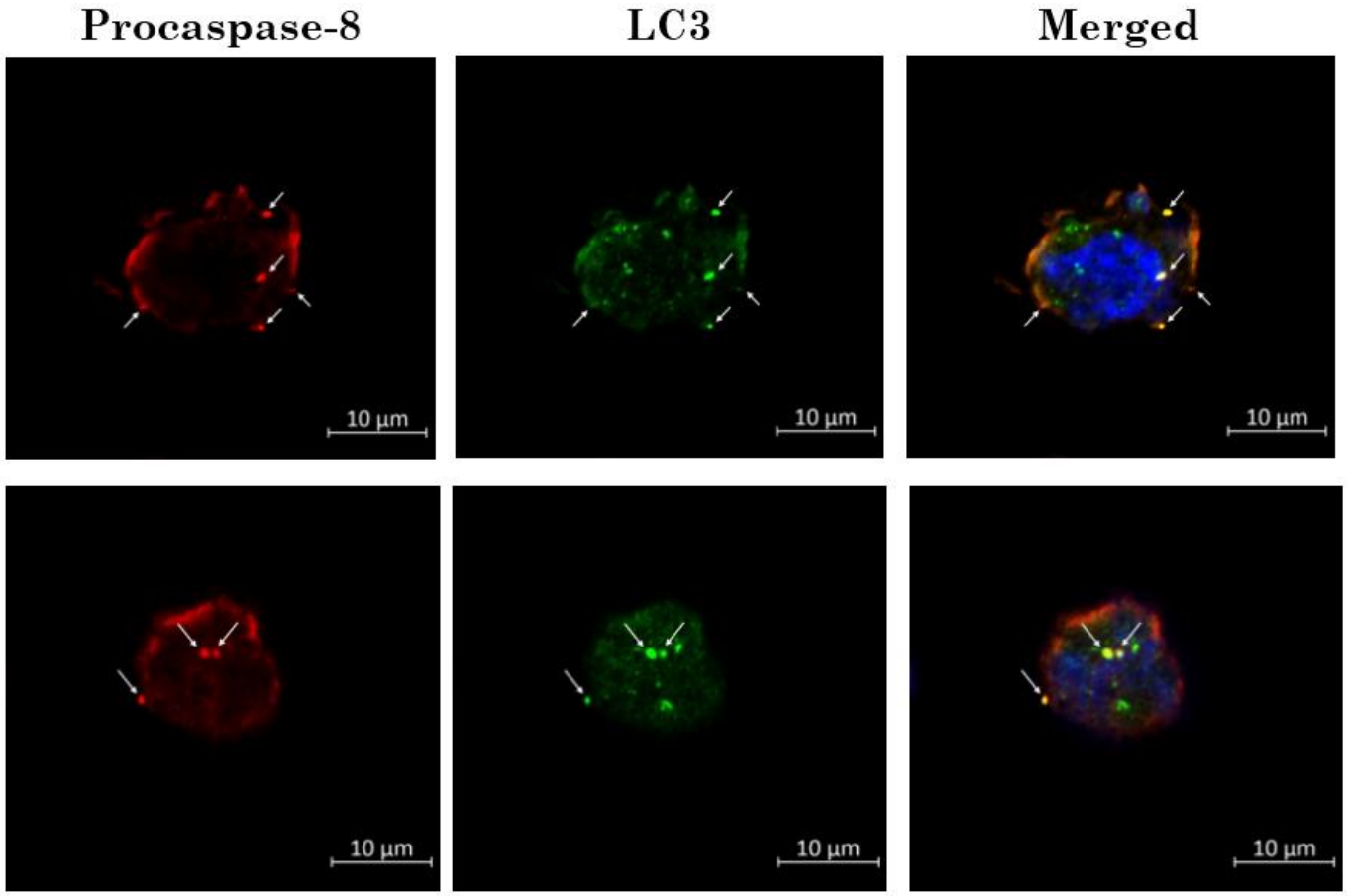

Figure 4.15 Procaspase-8 co-localized with LC3 in SRV-8-infected Jurkat cells. On day 10 postinfection, SRV-8-infected Jurkat cells were double stained with anti-procaspase-8 and anti-LC3 antibodies followed by labeling with fluorescence dye-conjugated secondary antibodies. Red, anti-procaspase-8; green, anti-LC3; the white arrows indicate yellow puncta that represent co-localization. Nuclei were visualized by Hoechst staining (blue). Scale bar: 10 µM.

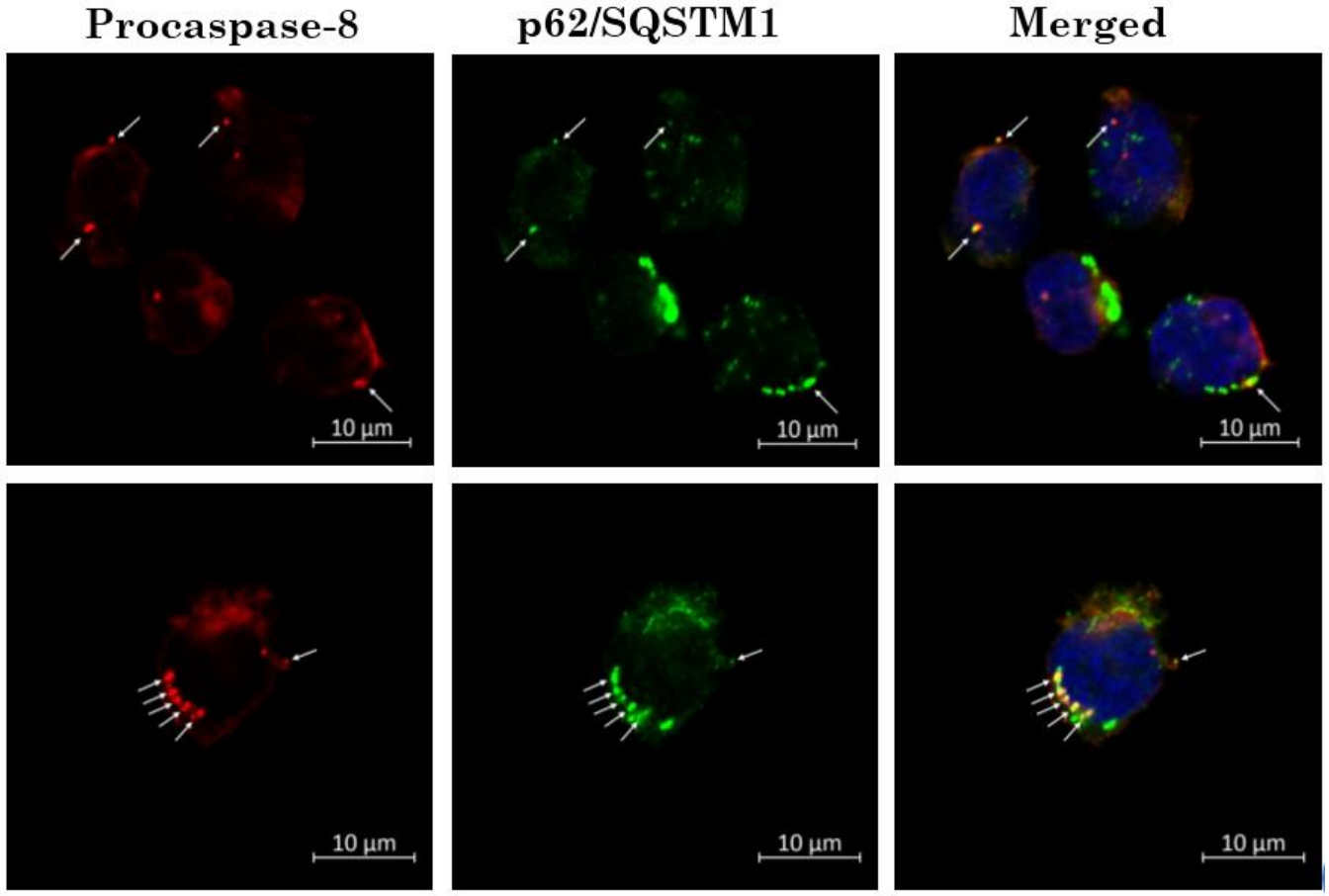

Figure 4.16 Procaspase-8 co-localized with p62/SQSTM1 in SRV-8-infected Jurkat cells. On day 10 postinfection, SRV-8-infected Jurkat cells were double stained with anti-procaspase-8 and anti-p62/SQSTM1 antibodies followed by labeling with fluorescence dye-conjugated secondary antibodies. Red, anti-procaspase-8; green, anti-p62/SQSTM1; the white arrows indicate yellow puncta that represent co-localization. Nuclei were visualized by Hoechst staining (blue). Scale bar: 10 µM.

(a)

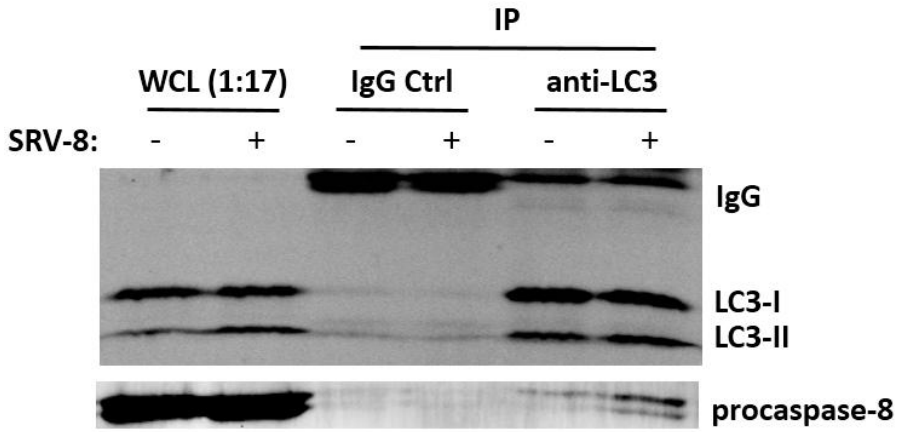

(b)

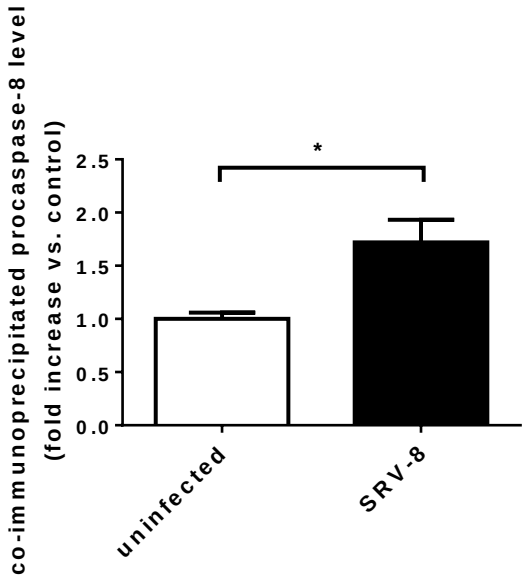

Figure 4.17 Co-immunoprecipitation assay displayed the interaction between procaspase-8 and LC3 in SRV-8-infected Jurkat cells. On day 10 postinfection, cell lysates of uninfected and SRV-8-infected Jurkat cells were subjected to immunoprecipitation with anti-LC3 antibodies or the control rabbit IgG. The levels of LC3 and procaspase-8 in the whole cell lysates (WCL) and the immunoprecipitated (IP) samples were examined using western blot analysis. IgG light chain was served as a loading control of IP samples. (a) Representative blots are shown. (b) Data from four independent experiments were quantified and the mean fold relative to the uninfected cells for the level of co-immunoprecipitated procaspase-8 is presented. Error bar represents the standard deviation. The data was statistically analyzed using the unpaired Student's *t*-test. *$p<0.05$(*)* represents a significant difference compared with the uninfected control.

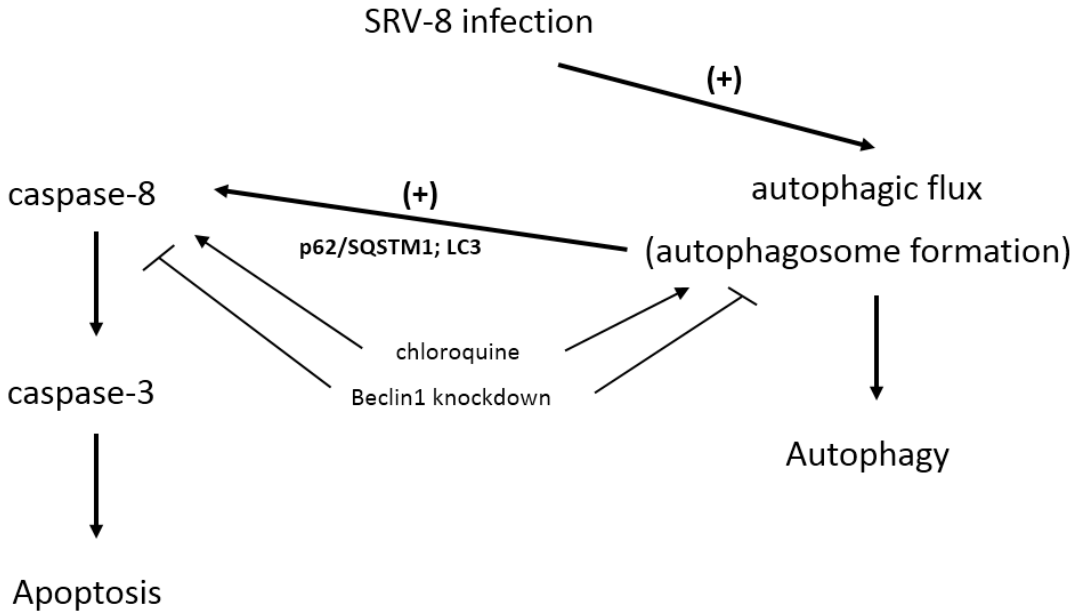

Figure 4.18 A model for SRV-8 infection-induced autophagy and apoptosis in Jurkat cells. Autophagic flux is triggered after SRV-8 infection on Jurkat cells. The enhanced formation of autophagosome is proposed to congregate procaspase-8 for its activation, which might be mediated by p62/SQSTM1 and LC3. (+): enhancement; →: stimulatory; ⊣: inhibitory.

4.4 Discussion

In this chapter, the effects of SRV infection on the autophagic pathway and apoptotic pathway in Jurkat T lymphocytes were investigated. The results demonstrated that SRV-4 and SRV-8 infection were able to induce the formation of autophagosome and enhance the completed autophagic flux in Jurkat cells. Additionally, SRV-4 and SRV-8 infection could significantly increase the levels of activated caspase-3/-8 and apoptosis in Jurkat cells. However, inhibition of autophagy by knockdown of Beclin1 in the SRV-8-infected cells significantly increased the amount of SRV genome released in the culture medium, suggesting that the autophagy induced by SRV-8 infection

might inhibit SRV replication in Jurkat cells. Moreover, Beclin1 knockdown in SRV-8-infected Jurkat cells was also shown to significantly suppress the activation of caspase-3/-8 and inhibit apoptosis, which suggests that autophagy was able to enhance apoptosis by activation of the caspase-8 pathway in SRV-infected Jurkat cells. Interestingly, further investigation on the interaction between LC3 and procaspase-8 in SRV-8-infected Jurkat cells indicated that the autophagosomes might, at least partially, be involved in the process of caspase-8 activation.

Autophagy is an evolutionarily conserved host defense response that plays essential roles in innate and adaptive immunity against viral infection [17, 18]. Moreover, as the important cellular degradative process to digest cytoplasmic unwanted components, the autophagic process has been also shown to directly eliminate the intracellular pathogens and act as a cellular intrinsic defense mechanism to inhibit viral replication [24, 229, 233, 251, 420, 451]. However, some viruses have been shown to suppress the autophagic pathway for their own benefits, such as escaping the host immune defenses and promoting viral replication [24, 32-34]. For examples, viral proteins of some retroviruses, such as Nef protein of HIV and Tax protein of HTLV, can block the fusion of autophagosome with lysosome in the host cells to prevent the degradation of viral particles, therefore increasing viral replication [415, 452, 453]. In this chapter, SRV-4/SRV-8 infection was shown to induce the formation of autophagosome and increase the conversion of LC3-I to LC3-II in Jurkat cells. Furthermore, in the presence of chloroquine, the level of LC3-II was significantly increased in the infected cells,

suggesting that the completed autophagic flux was enhanced by SRV infection of Jurkat cells. Interestingly, the inhibition of autophagy by Beclin1 knockdown was able to significantly increase the number of SRV virions released in the culture medium. All these results indicated that the SRV infection-induced completed autophagic flux in Jurkat cells might function as the pathogen defense mechanism to restrict SRV replication. However, the underlying mechanisms of how SRV viruses interfere with the autophagic pathway in Jurkat cells, and how the autophagy inhibit SRV replication in the infected cells need further investigations.

As an etiologic agent for immunosuppressive disease, SRV infection was identified to induce a series of immune responses in the host, including the reduced mitogen-induced T cell proliferation [9] and the depletion of both B and T lymphocytes [16, 90]. Although a number of studies have shown the pathologic and clinical features of SRV infection in macaques, there were only limited reports describing the underlying pathologic mechanisms at the molecular level. Thus, the mechanisms of SRV-induced depletion of T lymphocytes are still unclear. The previous animal study has indicated that the apoptotic cell death was detected in the brain tissues of SRV-infected rhesus monkeys [454]. In this chapter, our results also indicated that apoptosis might be responsible for the death of Jurkat T lymphocytes by SRV infection. Some researches on HIV, a human retrovirus that leads to immunosuppression, have also demonstrated that HIV could induce apoptosis in CD4+ T cells as well as in Jurkat cells [30, 393, 455]. Moreover, the HIV-induced apoptosis of the immune cells might be responsible for

the damage of the immune system in hosts [456]. Since SRV is the etiologic agent of SAIDS, which is commonly accompanied by the depletion of lymphocytes in the infected monkeys; it is possible that the SRV infection-induced apoptosis of T cells might contribute to the progression of SAIDS. Numbers of studies have shown that depending on the viral strain and the types of host cells, HIV is likely to induce the extrinsic or/and the intrinsic apoptotic pathways in the host cells [457-459], and the induction of the extrinsic pathway might be through the regulation of the expression of death receptors/ligands in the infected cells, such as Fas [460], FasL [461], TRAIL and DR5 [462, 463]. However, our results indicated that for SRV-4/SRV-8 infection of Jurkat cells, the activation of caspase-8 was predominated compared to caspase-9, suggesting that the extrinsic but not the intrinsic apoptotic pathway might play the key role to mediate SRV-induced apoptosis in Jurkat cells. Nevertheless, as the main upstream inducers of caspase-8 in the extrinsic apoptotic pathway, the mRNA expression levels of Fas/FasL and TRAIL/DR5 were not increased in SRV-4/SRV-8-infected Jurkat cells. However, further studies are still necessary to examine the protein levels of death receptors/ligands as well as the binding affinity between death receptors and ligands in SRV-infected Jurkat cells. Additionally, the results in this chapter also showed that compared to SRV-4, SRV-8 infection was able to induce a higher degree of apoptotic cell death with the stronger activation of caspase-3/-8 in Jurkat cells. However, the underlying mechanisms that lead to the different degrees of apoptosis are still unclear and needed to be further investigated in the future study.

Numbers of studies have demonstrated that the virus-induced autophagy was able to either promote or inhibit the apoptotic pathway in the infected cells [25, 38, 40, 218-220]. The RSV infection-induced autophagy was shown to inhibit apoptosis in the infected Hep2 cells, whereas the underlying mechanism remains unknown [40]. And HCV was demonstrated to induce mitophagy in the infected cells, leading to the selective degradation of damaged mitochondria and therefore inhibiting the intrinsic apoptotic pathway [219]. However, the matrix protein 2 (M2) of IAV has been demonstrated to induce apoptosis by accumulating the autophagosomes in the infected host cells, whereas the detail mechanisms remain unclear [25, 218]. And the Env protein of HIV can bind to the CXCR4 or CCR5 receptors in the bystander uninfected CD4+ T cells and induce autophagy, which in turn lead to the apoptotic cell death [38, 220-222]. In this chapter, SRV-8 infection-induced autophagy was shown to promote apoptosis in Jurkat cells. The results showed that the inhibition of autophagosome formation by Beclin1 knockdown could significantly decrease the levels of activated caspase-3/-8 and prevent apoptosis in SRV-8-infected Jurkat cells. Moreover, the inhibition of autophagosome degradation by chloroquine treatment significantly increased the levels of activated caspase-3/-8 and enhanced apoptosis in the infected cells. Collectively, these results implied an interplay between the amount of autophagosomes and the apoptosis induced by SRV infection in Jurkat cells.

Several studies have proposed that the autophagosomal membrane can provide a platform for the formation of iDISC to mediate the activation of caspase-8 and initiate

the apoptotic cascade [201, 203, 205, 208]. Interestingly, in this study, the reduction of autophagosome by Beclin1 knockdown was able to significantly decrease the activation of caspase-3/-8 and inhibited apoptosis, while the accumulation of autophagosome by chloroquine treatment has the opposite results, suggesting that the formation of iDISC might be the mechanism of SRV infection-induced caspase-8 activation and apoptosis in Jurkat cells.

So far, several proteins have been identified as the components of iDISC, including LC3, p62/SQSTM1, Atg5 and FADD. Besides being the important regulators for autophagosomal membrane elongation, LC3 and p62/SQSTM1 on iDISC have been shown that play the important role to promote the recruitment and activation of procaspase-8 [201, 203, 208]. p62/SQSTM1 was demonstrated that can bind to the poly-ubiquitinated procaspase-8 at the DISC, as well as at the iDISC to enhance the oligomerization and activation of procaspase-8, leading to apoptosis [203, 464]. Consistent with the previous studies, in this chapter, procaspase-8 was showed to co-localize with LC3 and p62/SQSTM1 in the SRV-8-infected Jurkat cells, suggesting the potential roles of LC3 and p62/SQSTM1 on the activation of caspase-8. Moreover, the co-immunoprecipitation assay has further confirmed the increased interaction between procaspase-8 and LC3 in Jurkat cells by SRV-8 infection. In addition, previous studies have also shown that FADD can directly interact with Atg5 and serve as an adapter protein to link procaspase-8 to the expanding autophagosomal membrane [39, 201, 439, 465]. Whether FADD and Atg5 are involved in the formation of iDISC,

together with LC3 and p62/SQSTM1 to mediate the SRV-induced activation of caspase 8 in Jurkat cells remains to be elucidated in further study.

Taken together, the results within the chapter indicated that SRV infection could induce both autophagic and apoptotic pathways in Jurkat cells, and the SRV-induced autophagy might function as the pathogen defense response to inhibit SRV replication and induce cell death through apoptosis. Moreover, a possible model by which SRV-induced autophagy enhances apoptosis was proposed, suggesting that the infection-enhanced autophagosome formation might congregate procaspase-8 for its activation, which then induce the downstream caspase cascade and lead to the autophagy-dependent apoptosis in Jurkat cells. This study firstly provides insights into the interactions among SRV infection, autophagy and apoptosis in Jurkat cells and discoveries a novel antiviral strategy to against SRV infection by activation of autophagy.

Chapter 5

Investigation of the dynamics of viral and cellular m6A RNA methylation during SRV-8 infection of Jurkat T lymphocytes

5.1 Outline

m6A is the most prevalent mRNA modification in eukaryotic organisms that can affect a broad range of biological processes by regulating mRNA metabolism. As a dynamic reversible process, m6A modification is regulated by the cellular m6A machinery, which includes the m6A “writers”, “erasers” and “readers”. Although m6A modification in viral RNAs has been discovered in the 1970s, the precise location of m6A on viral RNAs and the diverse roles of m6A in regulating viral replication haven’t been identified until recently [45, 46]. However, the roles of m6A in SRV infection are still unknown. Therefore, in this chapter, the effects of SRV-8 infection on the m6A RNA modification in Jurkat cells were investigated. The global m6A level in the infected Jurkat cells was examined by using the immune-northern blot analysis. Furthermore, the potential m6A sites on SRV-8 viral RNAs and the effects of SRV-8 infection on the Jurkat cellular m6A epitranscriptome were investigated by using the MeRIP-seq technique. Finally, the potential role of m6A in regulating SRV-8 replication was also examined by silencing the m6A “erasers”, ALKBH5, or the m6A “readers”, YTHDF1/YTHDF3, in the infected Jurkat cells.

5.2 Introduction

RNA modifications have been shown to play crucial roles in RNA post-transcriptional regulation, affecting the function, metabolism and localization of RNA. Among the known RNA modifications, m6A is the most prevalent mRNA modification in eukaryotic organisms [41, 294]. m6A modification is characterized as the addition of a methyl group to the *N6* position of the adenosine in RNA. Although m6A modification was discovered during the 1970s, the recently developed high throughput transcriptome-wide MeRIP-seq technique restored scientific interest in the field of m6A research and revealed the important regulatory roles of m6A modification on a broad range of biological processes and human diseases [52, 53, 298, 299, 466]. Notably, a growing number of studies have shown the existence of m6A modification in some viral genomes and transcripts; moreover, several studies have proposed the unique roles of m6A modification in regulating viral replication cycle and mediating virus and host cells interactions [45, 46, 56, 57, 362, 368].

The cellular m6A machinery, which regulates the dynamics of m6A modification, consists of three groups of regulators: methyltransferases or “writers”, demethylases or “erasers”, and m6A-specific binding proteins or “readers”. m6A modification is catalyzed by a large methyltransferase complex consisting of two catalytic subunits METTL3 and METTL14, along with several regulators, including WTAP, RBM15, KIAA1429, RBM15B and subunits that have not yet been identified [302-307]. Demethylation of m6A is catalyzed by two demethylases, FTO and ALKBH5 [316, 323].

FTO was recently reported to mainly target the $m6A_m$ rather than m6A in mRNA, whereas ALKBH5 is the m6A-specific demethylase [320]. The impact of m6A on the metabolism of mRNA is determined by m6A "readers" that belong to the YTH domain-containing family, which can recognize and directly interact with m6A sites through the hydrophobic pocket [48, 325-328]. m6A "readers" include the cytoplasmic YTHDF1, YTHDF2 and YTHDF3, which have been shown to regulate the stability and translation of m6A-containing mRNA; and the nuclear YTHDC1 and YTHDC2, which have been proposed to regulate the splicing and nuclear export of m6A-containing mRNA [326, 329, 331, 332, 334-337]. The reversibility of m6A modification highlights the dynamic roles of m6A in regulating the methylated mRNA metabolism. Indeed, m6A "writers", "erasers" and "readers" might work together to determine the fate and functions of m6A modification under different cellular conditions [56, 330, 344, 466, 467].

In the 1970s, studies have reported the discovery of m6A modification in the transcripts of several viruses, such as SV40, IAV, RSV and adenovirus [296, 373, 468, 469]. However, the roles of m6A modification in viral infection remained unclear until the recent development of MeRIP-seq technique. With the advancement of this transcriptome-wide m6A mapping technique, a growing number of studies has shown the distribution of m6A sites on viral RNAs as well as the important functions of m6A on viral replication cycle, suggesting the significance of m6A modification in regulating viral infection. Indeed, m6A has been detected in the transcripts and genomes of various RNA viruses, such as HIV, IAV, ZIKA and HCV; as well as the transcripts of some

DNA viruses, such as KSHV and SV40 [312, 313, 360, 361, 364, 365, 369, 371, 468]. Moreover, studies have also identified the specific YTHDF1-3 protein binding sites on viral RNAs by using photoactivatable ribonucleoside-enhanced crosslinking and immunoprecipitation (PAR-CLIP) method [361, 371]. Interestingly, in the case of HIV, three independent studies have reported the various amount of m6A sites at the different locations of the HIV genome [361, 370, 371]. Kennedy et al. found all of the m6A sites were located at the 3' UTR of the HIV genome [361], whereas the other two studies discovered that a larger number of m6A sites were present throughout the whole HIV genome [370, 371]. Although the reason for the different results is unclear, it might be due to the different viral strains and host cell types, suggesting the diversity of m6A modification in viral RNAs.

More recently, investigating the effects of m6A modification on viral infection is becoming an emerging field, which could help us to better understand the interactions between viruses and host cells. The main approach to investigate the functions of m6A during the viral infection is to modify the m6A level by perturbing the expression of m6A "writers", "erasers" or "readers". Previous studies have demonstrated the pro-viral function of m6A in HIV infection, as silencing of m6A "writers" and "erasers" could significantly reduce and increase the HIV replication, respectively [370, 371]. Furthermore, by depleting or overexpressing the YTHDF1/YTHDF2/YTHDF3 proteins in the host cells, studies have shown that YTHDF1-3 might inhibit HIV genome reverse-transcribed into provirus but enhance HIV proteins expression [361, 371, 378].

However, the underlying mechanisms behind the regulatory roles of YTHDF1-3 in HIV replication remain unclear. In addition, depletion of METTL3 expression in IAV-infected A549 cells has been shown to significantly decrease IAV replication by reducing the viral protein expression, suggesting the pro-viral functions of m6A on IAV replication [364]. Also, the overexpression of YTHDF2 has been reported to increase the levels of IAV proteins and promote the production of infectious virions; whereas overexpression of YTHDF1 and YTHDF3 have no effects on IAV replication [364]. In contrast to HIV and IAV, m6A has been shown to have anti-viral roles in ZIKV and HCV replication, as depletion of m6A "writers" and "erasers" was able to increase and decrease the viral replication, respectively [312, 313]. The above findings highlight that m6A modification is possibly involved in the regulation of viral replication and the functions of m6A might be varied among different types of viruses and host cells.

Effects of viral infection on host cellular proteome and transcriptome have been widely reported [470-472]. Interestingly, previous studies have also demonstrated that viral infection was able to change the m6A epitranscriptome of host cells [45, 56, 57, 313, 367, 370, 371]. ZIKV infection has been shown to change the distribution of m6A sites on the host cellular transcripts, with the decreased level of m6A at the 3'UTR and the concomitant increase of m6A at the 5'UTR [313]. Moreover, the preferred motif of m6A modification was changed from "GACUG" to "GAACCU" in the transcripts of host cells under ZIKV infection, implying that the substrate of m6A "writers" and "erasers" might be changed upon viral infection. Interestingly, the gene ontology (GO)

enrichment analysis has revealed that the host transcripts with altered m6A were related to immune responses and viral replication, suggesting that m6A might be involved in the modulation of host immune defense responses during ZIKV infection. Similarly, previous studies have also demonstrated that HIV infection was able to affect m6A modification of certain cellular genes with functions clustering in the cellular pathways related to immune responses and viral infection [370, 371]. Although the underlying mechanisms behind the virus-induced alteration of host cellular m6A epitranscriptome remain unclear, the above studies have suggested the importance of m6A modification in regulating virus-host interactions.

In summary, as an important post-transcriptional modification of RNA, m6A modification has been widely detected in a variety of viral RNAs. However, the functions of m6A in viral life cycles and the effects of viral infection on the viral and host cellular m6A epitranscriptomes remain largely unknown. In addition, the effects of SRV infection on m6A modification in the host cells have not yet been investigated. In this chapter, the topology of m6A modification in viral and host cellular RNAs during SRV-8 infection of Jurkat cells was explored by using the MeRIP-seq technology. Moreover, the effects of m6A modification on SRV-8 replication in Jurkat cells were investigated.

5.3 Results

5.3.1 SRV-8 infection reduces m6A RNA methylation in Jurkat cells

In order to investigate the effect of SRV-8 infection on m6A RNA methylation in Jurkat cells, the expression of the m6A regulators in the uninfected and SRV-8-infected Jurkat cells were examined by western blot. Results indicated that the protein levels of m6A "writers": METTL3, METTL14 and WTAP; m6A "erasers": ALKBH5 and FTO; and m6A "readers": YTHDF1, YTHDF2 and YTHDF3 did not change in SRV-8-infected Jurkat cells on day 10 postinfection, when compared to the uninfected cells (Fig. 5.1). However, it is worth being noticing that m6A modification of RNA is a dynamic process that might be influenced by the protein levels, location and structure of m6A regulators [304, 306, 308]. Therefore, although the protein levels of m6A regulators remained unchanged in the uninfected and SRV-8-infected Jurkat cells, it cannot be ruled out that SRV-8 infection had no effect on m6A epitranscriptome of Jurkat cells.

In order to investigate the effects of SRV-8 infection on the overall m6A level in Jurkat cells, the abundance of m6A in the total RNA was examined by using the immuno-Northern blot analysis on day 10 postinfection, when the viruses are active in replication (Fig. 3.4 and Fig. 3.6). As shown in Figure 5.2a, a reduced m6A abundance was detected in the infected Jurkat cells when compared with that in the uninfected cells. Moreover, a dramatic decrease was observed in the RNA with relatively small sizes (less than the size of 18S rRNA). The quantitative data from two independent experiments showed that SRV-8 infection led to a ~40% reduction of m6A in the total

RNA of Jurkat cells (Fig. 5.2b). However, further experiments are needed to obtain the statistical results.

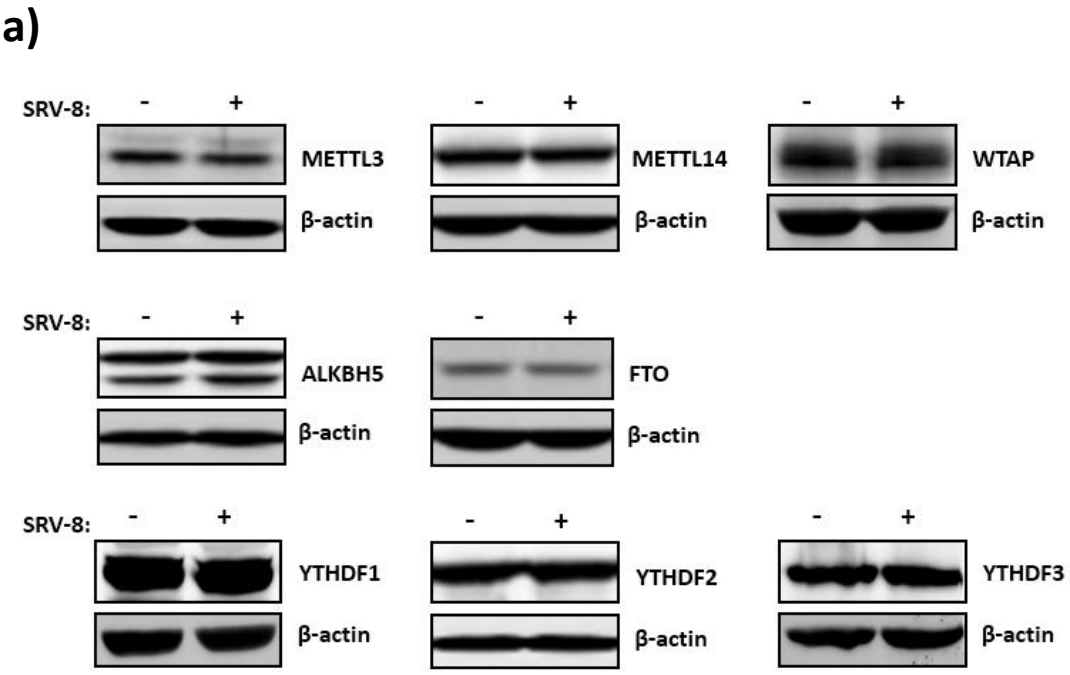

Figure 5.1 Levels of m6A "writers", "erasers" and "readers" proteins did not change in Jurkat cells by SRV-8 infection. Jurkat cells were infected with SRV-8. On day 10 postinfection, lysates of the uninfected and infected cells were analyzed by western blot for METTL3, METTL14, WTAP, ALKBH5, FTO, YTHDF1, YTHDF2 and YTHDF3. (a) Representative blots are shown. (b) The mean folds of indicated protein/β-actin ratio relative to an uninfected control were quantified from three independent experiments. Error bars represent the standard deviation.

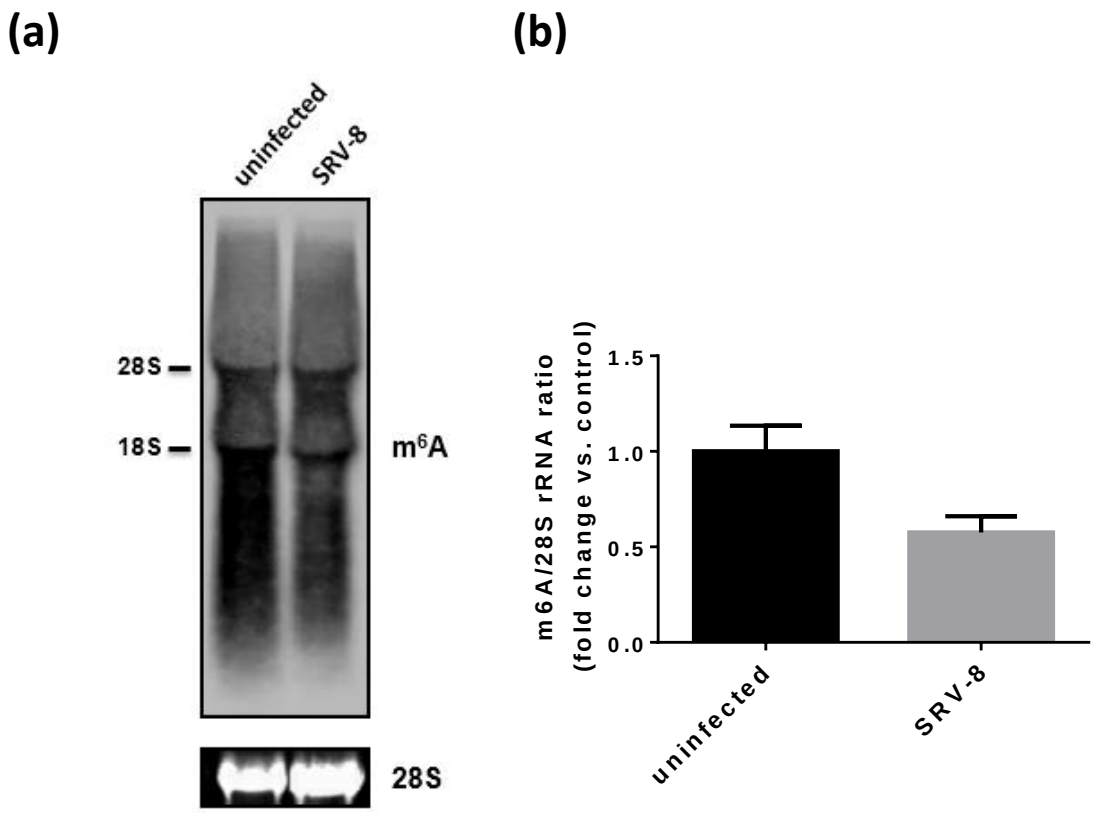

Figure 5.2 The overall m6A level was decreased in SRV-8-infected Jurkat cells. Jurkat cells were infected with SRV-8. On day 10 postinfection, total RNA of the uninfected and infected cells was analyzed by immuno-northern blot for m6A. The SYBR® Green II stained 28S rRNA was used as a loading control. (a) Representative blots are shown. (b) The mean fold of m6A/28S rRNA ratio relative to an uninfected control was quantified from two independent experiments. Error bar represents the standard deviation.

5.3.2 SRV-8 viral RNAs contain m6A sites

In order to explore the presence of m6A modification in SRV viral RNAs and the effects of SRV infection on the viral and host cellular m6A epitranscriptome, the topology of m6A RNA methylomes of the uninfected and SRV-8-infected Jurkat cells were examined by using the high throughput MeRIP-seq technology. MeRIP-seq technology is based on m6A antibody-mediated enrichment of the methylated RNA fragments

followed by massive parallel sequencing, which allows to determine the transcriptome-wide localization and the abundance of m6A in both viral RNAs and host cellular transcripts. To validate the efficiency of MeRIP, the levels of RNA transcripts JunB with m6A, Dicer1 with m6A and Dicer1 without m6A in the input controls and IP samples were measured using realtime PCR prior to cDNA library construction. Previous studies have demonstrated that the RNA sequence of JunB with m6A and Dicer1 with m6A contain the conserved m6A peaks with high confidence in the RNAs from some human and mouse cell lines and tissues, including 293T cells, HepG2 cells, human brain tissues, as well as mouse brain and liver tissues [41, 294]. Whereas, no m6A peak was detected in the RNA sequence of Dicer1 without m6A [367]. As shown in Figure 5.3, the RNA sequence levels of JunB with m6A and Dicer1 with m6A were increased about 10-fold to 20-fold in IP samples when compared with the input controls, suggesting that the m6A-containing RNA fragments were successfully selected in the process of MeRIP. Whereas, the RNA sequence level of Dicer1 without m6A was slightly decreased or had no change in IP samples when compared with the input controls, implying that the m6A-lacking RNA fragments were washed out, or at least did not be selected during m6A RNA immunoprecipitation (Fig. 5.3).

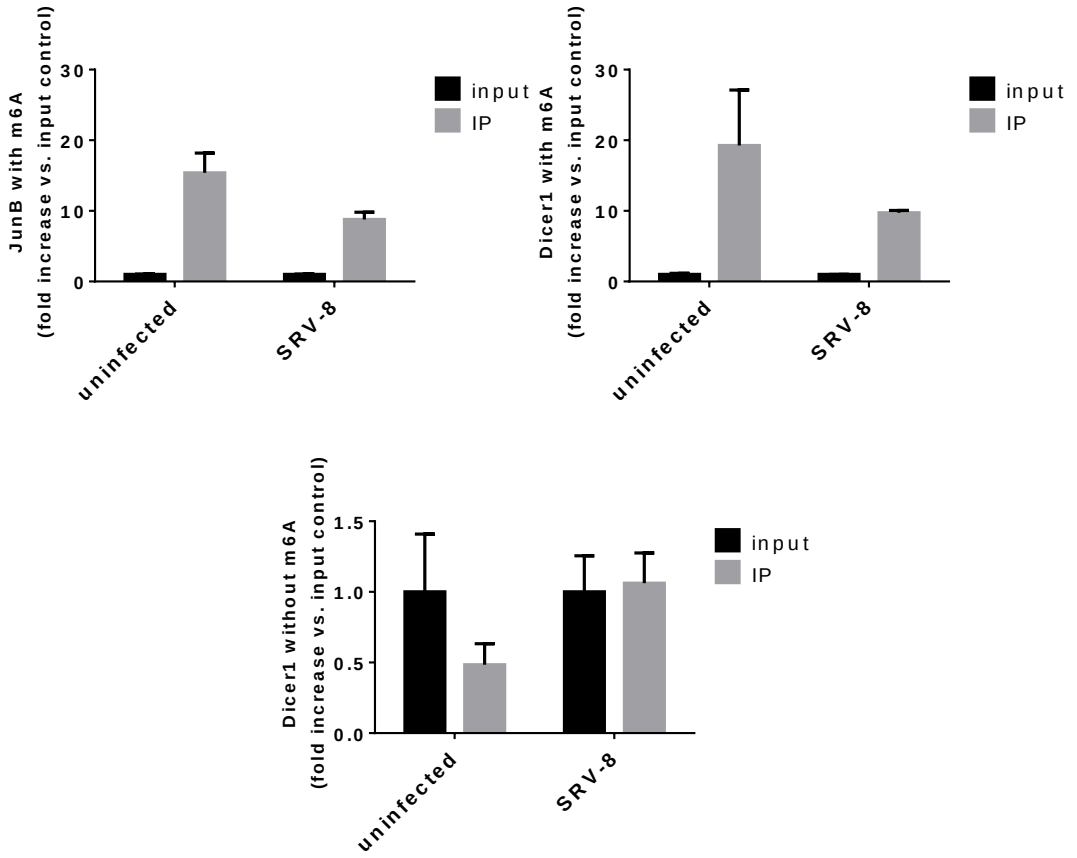

Figure 5.3 Validation of the efficiency of MeRIP using realtime PCR. On day 10 postinfection, mRNA of the uninfected and SRV-8-infected Jurkat cells was selected and subjected to MeRIP. After MeRIP, 5 ng of input controls and IP samples were reverse transcribed into cDNA followed by realtime PCR analysis to detect the RNA sequence levels of JunB with m6A, Dicer1 with m6A and Dicer1 without m6A. The mean folds of IP samples relative to an input control under each condition were quantified from two independent experiments. Error bars represent the standard deviation.

In order to investigate the presence and localization of m6A peaks on SRV-8 viral RNAs, MeRIP-seq data from SRV-8-infected Jurkat cells on day 10 postinfection was analyzed by using bioinformatics methods. Results from two individual experiments showed that there were six consistent m6A peaks mapped onto SRV-8 genome (Fig. 5.4 and

Table 5.1). The log_{10} p values for all identified m6A peaks were less than -25, suggesting the statistical significance of these peaks (Table 5.1). Peak 1, Peak 2 and Peak 3 were located in the *gag* gene, whereas Peak 4 was mapped in the *prt* gene. However, a partial sequence of Peak 3 and Peak 4 were located in the overlapped region between the *gag* and *prt* gene. Peak 5 and Peak 6 were two predominant m6A peaks located in the *env* gene, with a 2.01-fold and a 2-fold enrichment respectively (Table 5.1). However, no m6A peak was identified in the *pol* gene, the 5'UTR region, or the 3'UTR region. These findings define for the first time the topology of m6A methylomes of SRV-8 viral RNAs, suggesting the potential role of m6A modification it might play during SRV replication in host cells.

Table 5.1 Nucleotide locations of the six m6A peaks identified in SRV-8 viral RNAs by MeRIP-seq

m6A Peak Number	chromStart (nt)	chromEnd (nt)	Gene Name	Log_{10} p	Fold Enrichment
1	1027	1418	*gag*	-54.9	1.25
2	1866	1927	*gag*	-27.6	1.17
3	2256	2467	*gag*	-297	1.54
4	2283	2520	*prt*	-282	1.68
5	5881	6270	*env*	-1110	2.01
6	7253	7582	*env*	-1890	2

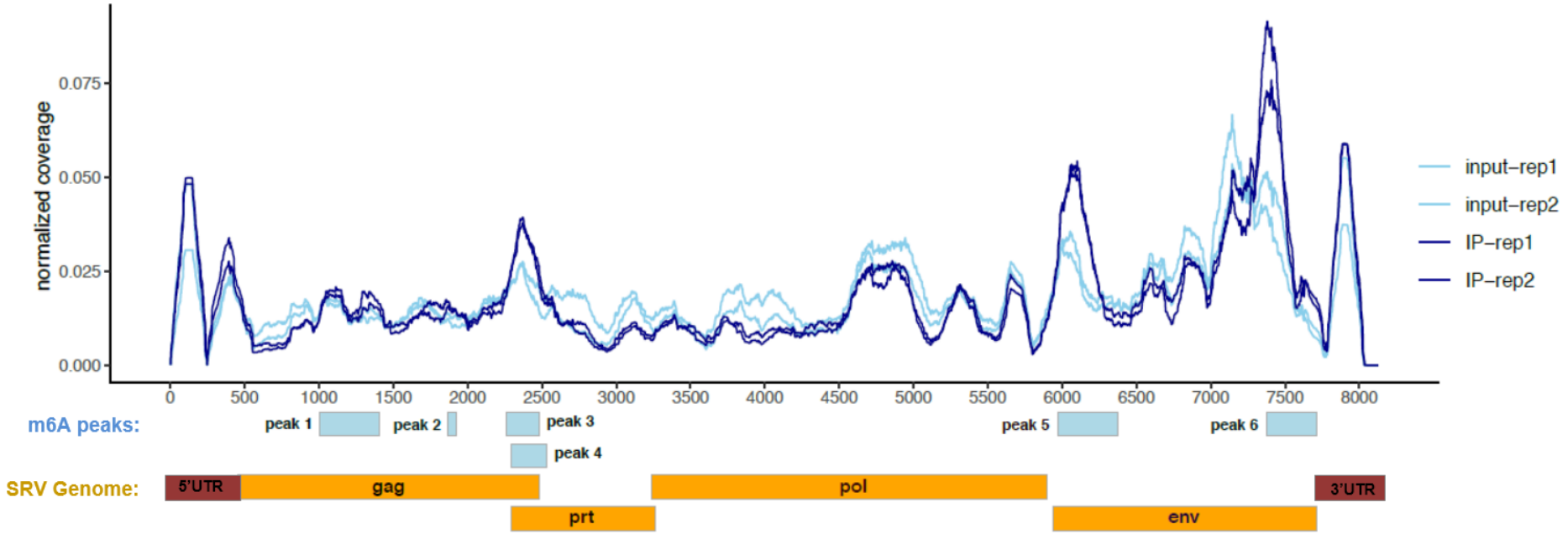

Figure 5.4 SRV-8 viral RNAs contain six m6A peaks. On day 10 postinfection, m6A-containing RNA fragments from SRV-8-infected Jurkat cells were selected and sequenced by MeRIP-seq. The reads from input controls and IP samples were mapped onto the SRV-8 RNA genome to identify m6A peaks. The normalized reads coverage (y-axis) was calculated by normalizing the reads number mapped at each site to the total reads number mapped onto the SRV-8 RNA genome. Input controls were shown with light blue lines, IP samples were shown with dark blue lines, and the 'rep1' and 'rep2' represent biological replicate 1 and 2 respectively. Below the x-axis, the blue boxes indicate the m6A peaks identified by the exomePeak analysis. The schematic map of SRV genome was shown on the bottom to align the m6A peaks with the coding sequences of SRV.

5.3.3 SRV-8 infection affects cellular m6A epitranscriptome in Jurkat cells

A growing number of studies have demonstrated that viral infection was able to induce broad changes in the cellular m6A epitranscriptome [56, 312, 313, 367, 370]. In order to investigate the effects of SRV-8 infection on m6A epitranscriptome of Jurkat cells, the abundance and distribution of m6A peaks on the cellular transcripts from uninfected and SRV-8-infected Jurkat cells were examined. As shown in Figure 5.5, the m6A peaks were enriched in the 5'UTR and around the stop codon of the methylated transcripts from both uninfected and SRV-8-infected Jurkat cells. Our results are consistent with the previous studies that reported the m6A peaks were preferentially found in the regions adjacent to the stop codon [41, 294], suggesting the high confidence of the MeRIP-seq data generated in this study. The cluster of m6A peaks mapped onto the 5'UTR of cellular transcripts might be $m6A_m$ rather than m6A (Fig. 5.5), since the m6A antibody and bioinformatics analysis developed currently could not distinguish $m6A_m$ from m6A. It has been reported that $m6A_m$ is most likely found at the beginning of mRNA in the region of 5'UTR [300, 320]. Previous studies also supported our prediction that the enriched peaks in the 5'UTR of cellular transcripts were the potential $m6A_m$ peaks [313, 367, 467]. In addition, our results showed that the abundance of m6A peak was decreased in the 5'UTR whereas slightly increased in the coding DNA sequence (CDS) region of the cellular transcripts during SRV-8 infection (Fig. 5.5), suggesting that SRV-8 infection could affect the m6A epitranscriptome in Jurkat cells.

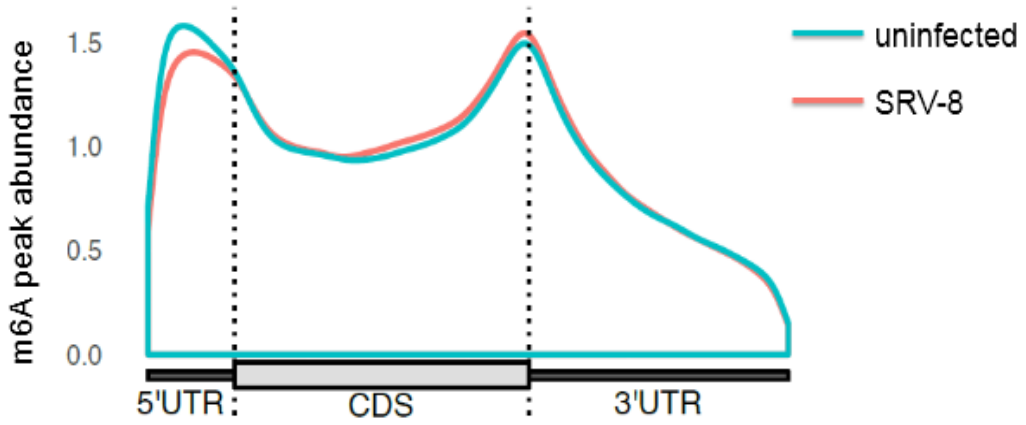

Figure 5.5 The abundance and distribution of m6A peaks on the transcripts of uninfected and SRV-8-infected Jurkat cells. On day 10 postinfection, m6A-containing mRNA fragments of uninfected and SRV-8-infected Jurkat cells were selected and sequenced using MeRIP-seq, followed by analyzed and plotted by the Guitar software package. The chart shows the abundance (y-axis) and the distribution (x-axis) of m6 peaks in the 5'UTR, coding DNA sequence (CDS) and 3'UTR regions of the cellular transcripts.

We next analyzed the differential m6A methylation in the uninfected and SRV-8-infected Jurkat cells. Our results showed that 4908 (22%) hypomethylated and 210 (1%) hypermethylated m6A peaks were identified in SRV-8-infected Jurkat cells when compared with the uninfected cells (false discovery rate [FDR] < 0.05); whereas the levels of majority of m6A peaks (77%) were not changed in Jurkat cells with SRV-8 infection (Fig. 5.6a). Consistent with the results discussed earlier (in Fig. 5.5), this result also suggests that SRV-8 infection might change the m6A epitranscriptome in Jurkat cells by triggering more m6A hypomethylation than hypermethylation. Additionally, the top enriched biological processes and pathways associated with the hypomethylated/hypermethylated genes were identified by GO enrichment analysis and Kyoto Encyclopedia of Genes and Genomes (KEGG)-pathway enrichment analysis methods (Fig. 5.6b &c). The hypomethylated/hypermethylated genes were

characterized as the genes that contain at least one hypomethylated or hypermethylated m6A peaks. Results showed that the top enriched biological processes with hypo-methylated genes were broadly related to mitochondrial functions, RNA polymerase functions, mRNA 3'-end procession and cell growth (Fig. 5.6b). Furthermore, the KEGG-pathway enrichment analysis identified that the hypomethylated genes were mainly related to the pathways of glycosaminoglycan biosynthesis, AMPK signaling pathway, and ribosome biogenesis. Meanwhile, the small number of hypermethylated genes were also identified that related to immune responses such as interferon-gamma response and innate immune response (Fig. 5.6c). Besides, the hypermethylated genes were also highly related to the insulin signaling pathways and insulin resistance responses. These findings suggest that the differential m6A methylation in SRV-8-infected Jurkat cells might be involved in a range of host cellular pathways, including the immune-related pathways, to affect the interactions between viruses and host cells.

5.3.4 The cellular m6A machinery regulates SRV-8 replication in Jurkat cells

The above results have shown that SRV-8 viral RNAs contain multiple m6A peaks (Section 5.3.2), and SRV-8 infection was able to affect the Jurkat cellular m6A epitranscriptome (Section 5.3.3). In order to investigate whether the cellular m6A machinery is involved in regulating SRV replication in Jurkat cells, the expression of m6A-specific demethylase ALKBH5 was reduced in Jurkat cells using RNAi technique. ALKBH5 was chosen as the target because it has a relatively higher expression level in

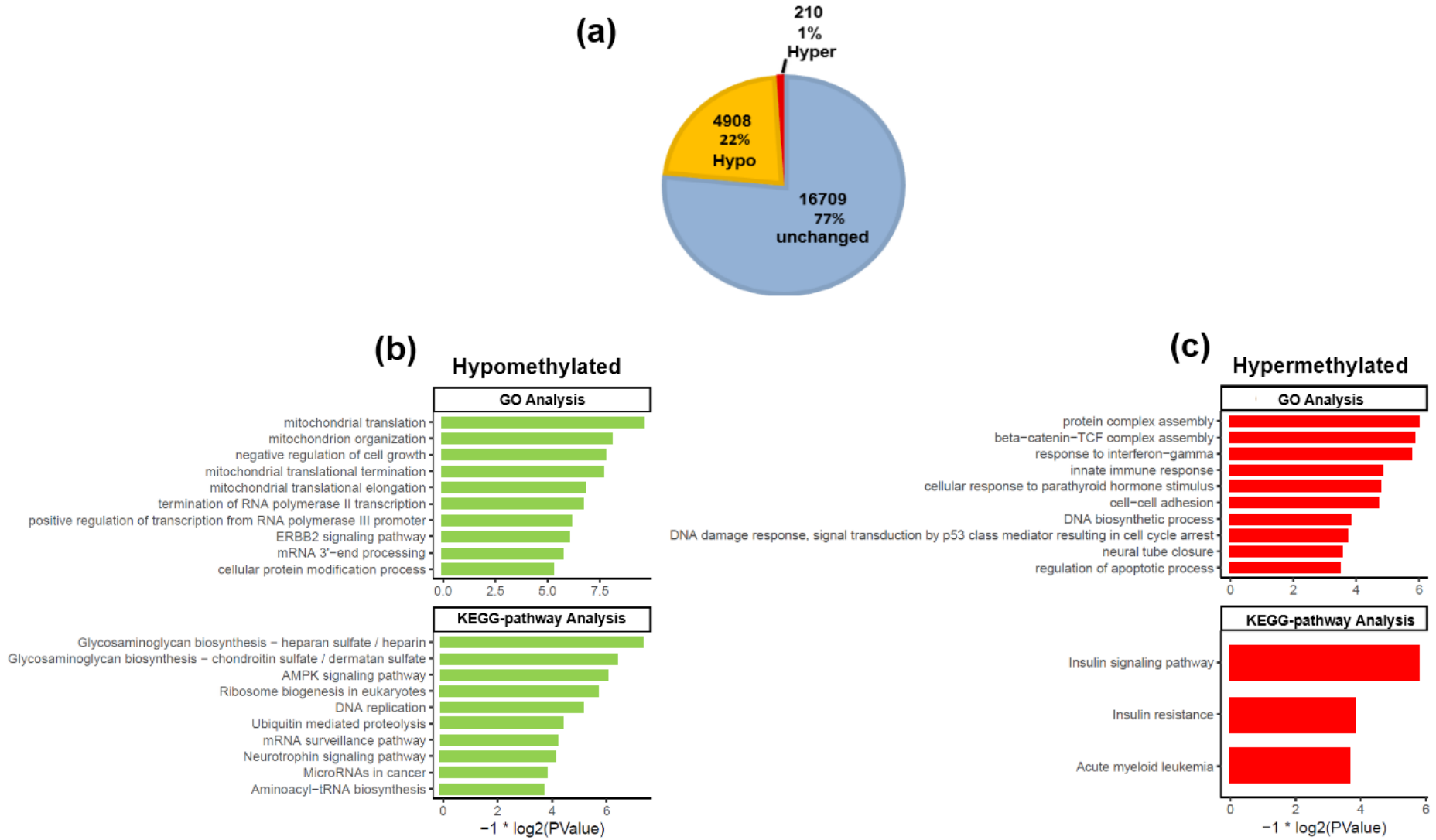

Figure 5.6 SRV-8 infection could affect the m6A epitranscriptome in Jurkat cells. On day 10 postinfection, m6A-containing mRNA fragments of uninfected and SRV-8-infected Jurkat cells were selected and sequenced using MeRIP-seq. The differential m6A methylation in the uninfected and SRV-8-infected Jurkat cells was analyzed by using the exomePeak package (version 1.9.1) in R, the false discovery rate [FDR] < 0.05 was used. (a) Numbers and percentages of the unchanged, hypomethylated and hypermethylated m6A sites in SRV-8-infected Jurkat cells. (b&c) GO enrichment analysis and Kyoto Encyclopedia of Genes and Genomes (KEGG)-pathway enrichment analysis of the (b) hypomethylated genes and (c) hypermethylated genes in SRV-8-infected Jurkat cells. The top ten enriched categories of each analysis are shown.

Jurkat cells when compared with other m6A “writers” and “erasers” (Section 5.3.1). A doxycycline-inducible shRNA that targets ALKBH5 was constructed and introduced into Jurkat cells by using lentiviral transduction system, generating the doxycycline-inducible shALKBH5 stable Jurkat cell line. When the shALKBH5 cells were treated with 1 μg/mL doxycycline for 3 days, the results showed that the ALKBH5 protein level was significantly decreased to 56% when compared with that in the untreated control samples (Fig. 5.7), while the doxycycline treatment did not change the protein expression level of ALKBH5 in the scramble Jurkat cells. In addition, the results of MTT colorimetric assay showed that the doxycycline-induced ALKBH5 knockdown did not change the cell viability in shALKBH5 Jurkat cells (Fig. 5.7c).

To further examine the effect of ALKBH5 knockdown on SRV replication in Jurkat cells, scramble and shALKBH5 Jurkat cells were infected with SRV-8 for 6 days, followed by 1 μg/mL doxycycline induction for 3 days. The viral RNA genome in the culture medium of SRV-8-infected cells with or without doxycycline induction was harvested and quantified using realtime PCR. The results showed that SRV-8 genome copy number was significantly decreased by ~30% in the infected doxycycline-induced shALKBH5 Jurkat cells when compared to that in the uninduced cells; whereas the viral genome copy number did not show any change in the infected scramble Jurkat cells that were induced by doxycycline (Fig. 5.8). The results suggest that ALKBH5 might be involved in SRV replication in Jurkat cells. As discussed earlier, ALKBH5 catalyzes the demethylation of m6A and the knockdown of ALKBH5 in the current study might have

(a)

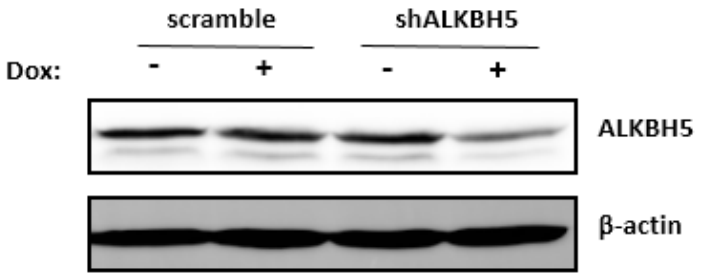

(b)

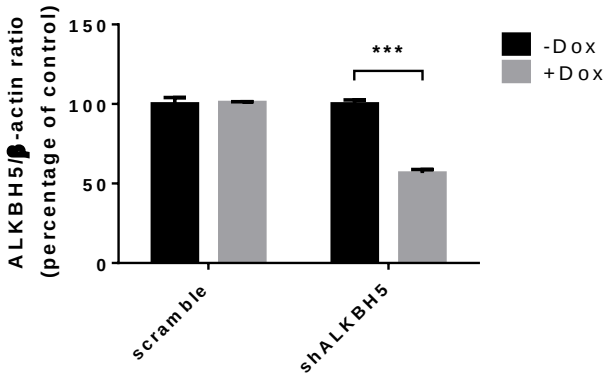

(c)

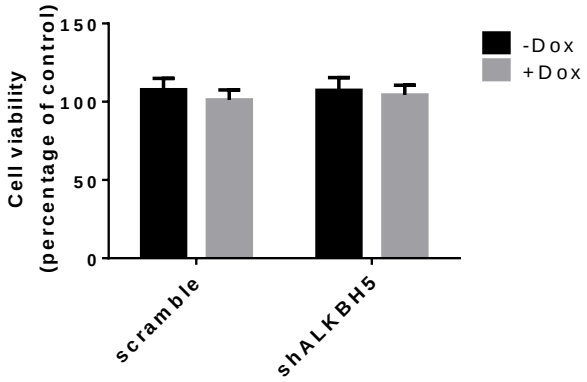

Figure 5.7 The ALKBH5 protein level was reduced in Jurkat cells by induced shALKBH5 expression. Scramble and shALKBH5 Jurkat cells were induced with 1 μg/mL doxycycline for 3 days. (a&b) The protein level of ALKBH5 was checked by western blot assay. (a) Representative blots are shown. (b) Data from three independent experiments were quantified and presented as the mean percentage relative to the uninduced control. (c) Cell viability was examined by MTT colorimetric assay. Data from three independent experiments were quantified and presented as the mean percentage relative to the uninduced control. Error bars represent the standard deviation. The data was statistically analyzed using the unpaired Student's *t*-test. *p<0.001 (***)* represents a significant difference compared with the uninduced control.

led to the increase of cellular or/and viral m6A modification; therefore, the results might also suggest that alterations of m6A modification might have a potential effect on the regulation of SRV replication in Jurkat cells.

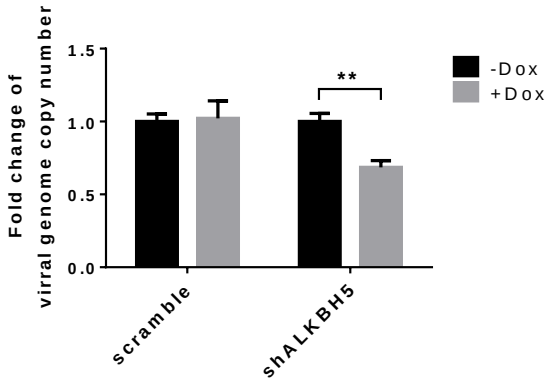

Figure 5.8 Knockdown of ALKBH5 suppressed SRV-8 replication in Jurkat cells. Scramble and shALKBH5 Jurkat cells were infected with SRV-8 for 6 days followed by 1 μg/mL doxycycline induction for 3 days. Viral genome in 140 μL culture medium was extracted and the copy number was measured using realtime PCR assay. Data from five independent experiments were quantified and the mean fold relative to the uninduced control is presented. Error bars represent the standard deviation. The data was statistically analyzed using the unpaired Student's *t*-test. *p<0.001 (***)* represents a significant difference compared with the uninduced control.

Since the m6A "readers", such as YTHDF1-3 and YTHDC1-2, could directly bind to m6A-methylated RNA and play a key role to execute the functions of m6A modification, it was then decided to investigate the roles of m6A "readers" on SRV-8 replication in Jurkat cells. Due to the time and technical limitations, only the doxycycline-inducible shYTHDF1 and shYTHDF3 stable Jurkat cell lines were successfully generated using lentiviral transduction system. The results showed that the protein levels of YTHDF1 and YTHDF3 were significantly reduced by ~44% in shYTHDF1 and shYTHDF3 Jurkat

cells treated with 1 μg/mL doxycycline for 3 days when compared to those of the untreated control samples (Fig. 5.9 and Fig. 5.10). However, doxycycline induction did not affect the protein levels of YTHDF1 and YTHDF3 in scramble Jurkat cells. Moreover, the results of MTT colorimetric assay showed that the doxycycline-induced YTHDF1 or YTHDF3 knockdown did not change the cell viability in shYTHDF1 and shYTHDF3 Jurkat cells respectively (Fig. 5.9c and Fig. 5.10c).

To investigate the effect of YTHDF1 and YTHDF3 knockdown on SRV replication, the shYTHDF1, shYTHDF3 and scramble Jurkat cells were infected with SRV-8 for 6 days followed by 1 μg/mL doxycycline induction for 3 days. The viral RNA genome in the culture medium of SRV-8-infected cells with or without doxycycline induction was harvested and quantified by realtime PCR. The results indicated that SRV-8 genome copy number was significantly decreased by 30% in the doxycycline-induced shYTHDF1 Jurkat cells, though no significant change in viral genome copy number was observed in the scramble Jurkat cells (Fig. 5.11). However, in the case of YTHDF3 knockdown, the viral genome copy number did not show any obvious change in the shYTHDF3 Jurkat cells (Fig. 5.11). These findings suggest that the YTHDF1 might promote SRV-8 replication in the infected Jurkat cells, while YTHDF3 might not participate in the regulation of SRV-8 replication in Jurkat cells.

(a)

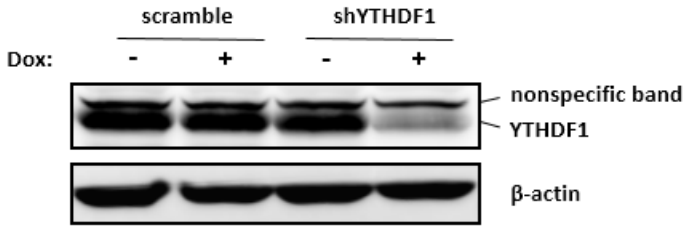

(b)

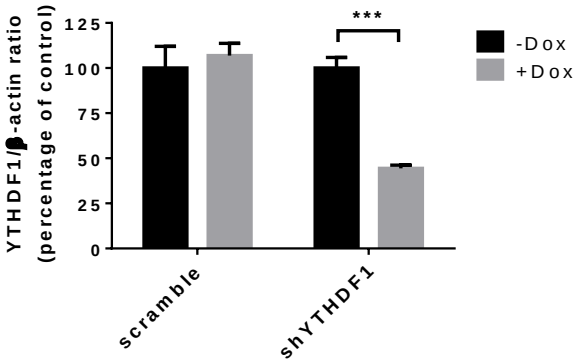

(c)

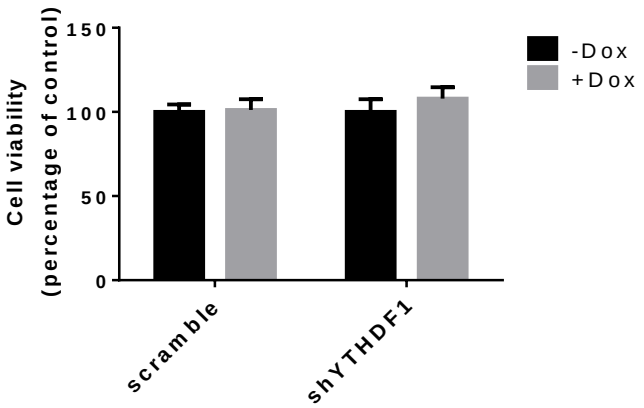

Figure 5.9 The YTHDF1 protein level was reduced in Jurkat cells by induced shYTHDF1 expression. Scramble and shYTHDF1 Jurkat cells were induced with 1 μg/mL doxycycline for 3 days. (a&b) The protein level of YTHDF1 was examined by western blot assay. (a) Representative blots are shown. (b) Data from three independent experiments were quantified and expressed as the mean percentage relative to the uninduced control. (c) Cell viability was examined by MTT colorimetric assay. Data from three independent experiments were quantified and expressed as the mean percentage relative to the uninduced control. Error bars represent the standard deviation. The data was statistically analyzed using the unpaired Student's *t*-test. *p<0.001 (***)* represents a significant difference compared with the uninduced control.

(a)

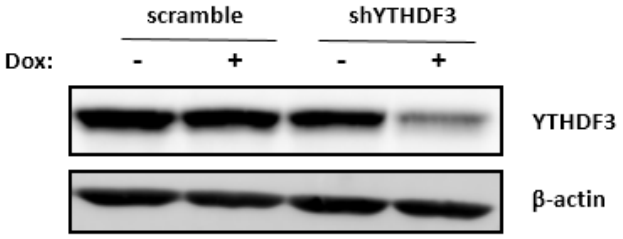

(b)

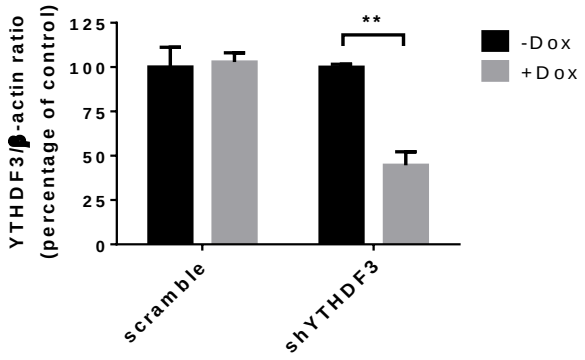

(c)

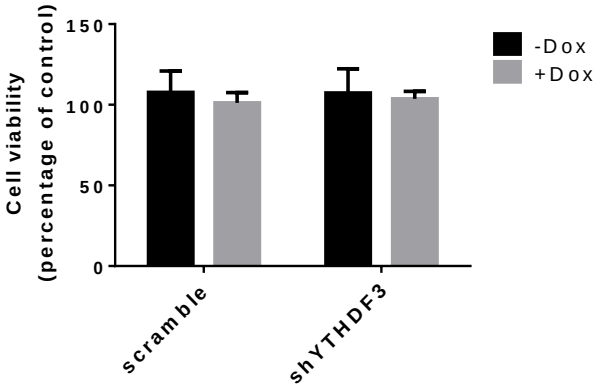

Figure 5.10 The YTHDF3 protein level was reduced in Jurkat cells by induced shYTHDF3 expression. Scramble and shYTHDF3 Jurkat cells were induced with 1 μg/mL doxycycline for 3 days. (a&b) The protein level of YTHDF3 was examined by western blot assay. (a) Representative blots are shown. (b) Data from three independent experiments were quantified and expressed as the mean percentage relative to the uninduced control. (c) Cell viability was examined by MTT colorimetric assay. Data from three independent experiments were quantified and expressed as the mean percentage relative to the uninduced control. Error bars represent the standard deviation. The data was statistically analyzed using the unpaired Student's *t*-test. *p<0.01 (**)* represents a significant difference compared with the uninduced control.

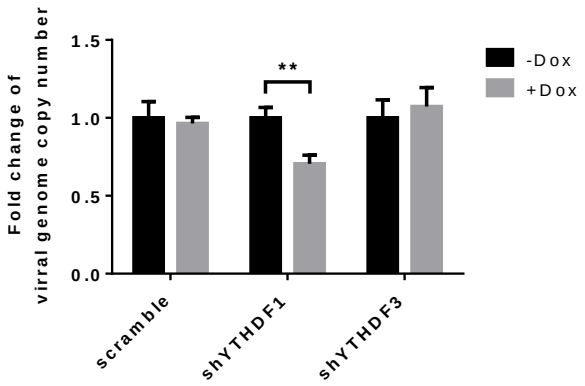

Figure 5.11 Knockdown of YTHDF1, but not YTHDF3, suppressed SRV-8 replication in Jurkat cells. Scramble, shYTHDF1 and shYTHDF3 Jurkat cells were infected with SRV-8 for 6 days followed by 1 μg/mL doxycycline induction for 3 days. Viral genome in 140 μL culture medium was extracted, and the copy number was measured using realtime PCR assay. Data from five independent experiments were quantified and the mean folds relative to the uninduced control are presented. Error bars represent the standard deviation. The data was statistically analyzed using the unpaired Student's *t*-test. *p<0.001 (***)* represents a significant difference compared with the uninduced control.

5.4 Discussion

In this chapter, the overall level of m6A RNA methylation was examined in the Jurkat cells with SRV-8 infection. The result has been shown that SRV-8 infection was able to decrease the global m6A level in Jurkat cells (Fig. 5.2), even though the protein levels of the major m6A regulators did not change in the infected cells (Fig. 5.1). Since the m6A modification is regulated by the cellular m6A machinery, which could be affected not only by the protein levels of m6A regulators but also by their locations and activities; therefore, the mechanisms behind the SRV-8 infection-induced m6A level reduction in Jurkat cells needed to be clarified in further studies. A recent study has demonstrated that the global m6A level was increased in HIV-1-infected MT4 cells (a

human T cell line), however, the underlying mechanism was still unknown [370]. The possible reason for the different effects of viral infection on host cellular m6A level might be due to the different virus and host cell types, which suggest the diverse roles of m6A in regulating the interactions between virus and host cell.

With the development of MeRIP-seq technique, the transcriptome-wide mapping of m6A sites at the nucleotide level has become feasible [41, 294]. In this chapter, the MeRIP-seq technique was used to map the m6A sites on SRV-8 viral RNAs as well as to investigate the effects of SRV-8 infection on the Jurkat cellular m6A epitranscriptome. The results have shown that SRV-8 viral RNAs contain six distinct m6A peaks distributed in the *gag*, *prt* and *env* genes (Fig. 5.4). The abundance of m6A peaks on SRV-8 viral RNAs implies the potential roles of m6A modification in regulating SRV replication. Notably, two of the most prominent m6A peaks were identified in the *env* gene, suggesting that the further studies to investigate whether these m6A peaks are able to affect the metabolism of *env* transcripts and the replication of SRV will be of interest. However, there is no m6A peak identified in the *pol* gene, 5'UTR and 3'UTR regions of SRV-8 viral RNAs. On the contrary, previous studies on HIV have demonstrated the enrichment of m6A peaks at the 3'UTR region of HIV viral RNAs [361, 370, 371]. In addition, as the functions of m6A are executed by binding to the m6A "readers" and previous studies have identified the YTHDF1-3 protein binding sites on HIV viral RNAs by using the PAR-CLIP method [361, 371]; therefore, further study is necessary to explore the binding sites of m6A "readers" on the SRV-8 viral RNAs, which could help

us to better understand the role of m6A sites in modulating the SRV-8 viral RNAs' metabolism.

Previous studies have demonstrated that viral infection was able to induce profound changes in the host cellular m6A epitranscriptome, which might affect a range of cellular pathways and regulate the interactions between virus and host cell [56, 313, 367, 370]. In this chapter, the SRV-8 infection has been shown to decrease the m6A peak abundance in the 5'UTR region but slightly increase it in the CDS region on the Jurkat cellular transcripts (Fig. 5.5). This finding suggests that SRV-8 infection was able to change the Jurkat cellular m6A epitranscriptome. Since the m6A modification in the 5'UTR region has been demonstrated to enhance mRNA stability and promote mRNA translation [320, 342], it is possible that the reduced m6A abundance in the 5'UTR region of some cellular transcripts might affect their stability and translation in SRV-8-infected Jurkat cells. Different from SRV-8, it has been reported that ZIKV and HIV-1 infection could increase the m6A abundance in the 5'UTR region of the host cellular transcripts whereas slightly decrease the m6A abundance in the 3'UTR region [313, 370]. The different effects of viral infection on the host cellular m6A epitranscriptome might result from different virus and host cell types, while the underlying mechanisms are still unclear and needed to be investigated in the future. In addition, the differential m6A peaks in SRV-8-infected Jurkat cells have been identified by comparing the levels of each m6A peak in the uninfected and SRV-8-infected Jurkat cells using the bioinformatics approaches (Fig. 5.6a). Interestingly, the results have shown that

among the differential m6A peaks, there were 4908 hypomethylated m6A peaks while only 210 hypermethylated m6A peaks. Although the accurate level of each differential m6A peak with hypomethylation or hypermethylation could not be quantified by bioinformatics analysis in detail, the more hypomethylated peaks than the hypermethylated peaks implies the down-regulation effect of SRV-8 infection on the global m6A level in Jurkat cells, which is consistent with the result of immune-northern blot analysis (Fig. 5.2). Additionally, GO enrichment analysis and KEGG-pathway enrichment analysis on the hypomethylated or hypermethylated genes have further proposed some enriched biological processes and pathways were affected in SRV-8-infected Jurkat cells (Fig. 5.6b and Fig. 5.6c). Interestingly, the functions of the top enriched processes are correlated to gene transcription and translation, such as RNA polymerase functions, mRNA 3'-end procession and ribosome biogenesis, suggesting the potential roles of m6A on gene expression in SRV-8-infected Jurkat cells. Indeed, previous studies have demonstrated that m6A modification could regulate gene expressions by mediating the m6A methylated-mRNA metabolism, such as mRNA stability and translation [48, 288, 311, 326, 473]. Therefore, further studies are needed to investigate how SRV infection-induced change of Jurkat cellular m6A epitranscriptome could affect the host cellular gene expression. Furthermore, our results have shown that the hypomethylated genes are also related to mitochondrial functions (Fig. 5.6b). Since one of the major functions of mitochondria is to produce energy, which is essential for the highly efficient viral replication in the infected cells, it is likely that the SRV-8 infection-induced change of m6A modification in the

mitochondrial-related genes might play a role to mediate the functions of mitochondria and thus regulate SRV replication. Interestingly, our data has also shown that the hypermethylated genes might relate to immune responses, such as interferon-gamma response, innate immune response and the insulin resistance response (Fig. 5.6c). A recent study has proposed that viral infection is able to promote insulin resistance in skeletal muscle through interferon-gamma [474]. Consistent with SRV-8, previous studies have also demonstrated that both ZIKV and HIV infection were able to affect the m6A modification of some host cellular transcripts that relate to immune responses and viral replication [313, 370]. These findings suggest the potential involvement of m6A in the host cellular immune responses during viral invasion. Collectively, the above results in this chapter suggest that SRV-8 infection was able to reprogramme Jurkat cellular m6A epitranscriptome and change the m6A levels of some functional genes involved in viral replication and immune-related pathways in Jurkat cells, suggesting the potential roles of m6A in mediating SRV replication and in the interactions between SRV and Jurkat cells. The viral infection-induced rearrangement of host cellular m6A epitranscriptome could be utilized by the virus to promote their replication and against host cellular defense responses, and/or be employed by the host cells to restrict viral infection. Thus, further studies might be necessary to investigate the functions of specific m6A modifications on SRV infection and the underlying mechanisms.

m6A RNA methylation is a dynamic reversible process regulated by the cellular m6A

machinery that contains the m6A “writers”, “erasers” and “readers”. The result in this chapter has shown that the knockdown of ALKBH5, an m6A “eraser”, was able to significantly decrease SRV-8 replication in the infected Jurkat cells, suggesting that m6A modification might negatively regulate SRV-8 replication in Jurkat cells (Fig. 5.8). Although ALKBH5 is recognized as the m6A-specific “eraser”, further study is necessary to confirm that ALKBH5 knockdown in the Jurkat cells was able to increase the m6A level, and the reduction of SRV-8 replication induced by ALKBH5 knockdown in Jurkat cells was correlated to the increased m6A level. Besides, the effects of other m6A “writers” and “erasers” on SRV-8 replication need to be further investigated to better understand the functions of m6A modification on SRV replication.

Interestingly, our results also showed that the decreased expression of YTHDF1, an m6A “reader”, was able to significantly reduce SRV-8 replication in the infected Jurkat cells, whereas knockdown of YTHDF3 has no effect on SRV-8 replication (Fig. 5.11). This finding further suggests the role of m6A modification in regulating SRV replication in Jurkat cells. A recent study has demonstrated that YTHDF1 could promote the translation of m6A-methylated mRNA [326]; therefore, it is possible that YTHDF1 in the SRV-8-infected Jurkat cells might promote the translation of specific m6A-methylated transcripts, leading to the increase of SRV replication. However, since both viral and cellular transcripts contain multiple m6A sites, it was still unclear that the YTHDF1-mediated increase of SRV-8 replication was due to its direct binding and effects on the SRV-8 viral RNAs or the indirect effects on the host cellular transcripts.

Previous studies on HIV have proposed that YTHDF1-3 could bind to the m6A-methylated HIV genomes and thus inhibit the reverse transcription of the viral genome; meanwhile, YTHDF1-3 was shown to enhance HIV viral protein translation in the infected cells [361, 370, 371, 378]. Moreover, a growing number of studies have also reported the important roles of m6A "readers" in regulating viral replication, such as IAV, KSHV, ZIKV and HCV [312, 313, 364, 367, 475]. YTHDF1-3 have been shown to inhibit HCV and ZIKV replication, and YTHDF2 but not YTHDF1 and YTHDF3 has been shown to enhance IAV replication but inhibit KSHV replication. The previous findings together with our results in this chapter strongly suggest that for different virus and host cell types, the m6A "readers" might have different effects on viral replication. Moreover, for the same virus and host cell, the "readers" might also play diverse roles at the different stages of viral replication cycle. However, the underlying mechanisms by which the m6A "readers" affect viral replication were still largely unclear. Moreover, it will be necessary to explore whether and how other m6A "readers" regulate SRV viral life cycle.

Taken together, the results in this chapter have highlighted the importance of m6A modification in the SRV-8 infection of Jurkat cells. It has been firstly reported that SRV-8 viral RNAs contain six distinct m6A peaks. Moreover, the SRV-8 infection has been shown to not only decrease the global m6A level in the infected Jurkat cells but also reprogramme the Jurkat cellular m6A epitranscriptome. Interestingly, the decreased protein expression level of ALKBH5 in the infected Jurkat cells has been shown to

significantly suppress SRV-8 replication, implying the negative regulatory role of m6A in modulating SRV-8 replication. Our previous result has demonstrated that SRV-8 infection was able to decrease the global levels of m6A in Jurkat cells, therefore, the findings proposed a potential feedback loop suggesting that SRV might reduce the m6A levels in host cells to enhance viral replication. In addition, YTHDF1 but not YTHDF3 has been shown to promote SRV-8 replication in Jurkat cells. Although the underlying mechanisms behind the rearrangement of Jurkat cellular m6A epitranscriptome during SRV-8 infection and the modulation of SRV-8 replication by ALKBH5 and YTHDF1 were still unclear, the results of our study firstly suggest the roles of m6A modification and the components of the m6A machinery in SRV infection, which could help us to better understand the biological roles of m6A modification under different physiological conditions. Indeed, delineating the viral and host cellular m6A RNA methylomes, as well as understanding how the viral and host cellular m6A modifications affect viral life cycle and host gene regulation will provide a novel insight for the development of new antiviral therapies.

Chapter 6

Summary

6.1 Summary

Summary of Chapter 3

In order to understand the pathogenicity of SRV in Jurkat cells *in vitro*, in chapter three, the infectivity and replication capacity of SRV-4 and SRV-8 in Jurkat cells were investigated. The successful infection was demonstrated by the formation of syncytia (Fig. 3.1) as well as the synthesis of viral LTR (Fig. 3.4) in the SRV-4/SRV-8-inoculated Jurkat cells. The results are the first time to demonstrate that SRV-4/SRV-8 was able to infect Jurkat cells *in vitro* and the infection reached a maximum level on day 10 postinfection. Although the specific mechanisms that led to the reduction of SRV-LTR on day 12 and day 14 postinfection have not been identified, one of the possible reasons might be the occurrence of apoptotic cell death in the infected cells, which has been shown in chapter four (Fig. 4.4 and Fig. 4.5). Additionally, the increased SRV genome copy number in the culture medium of the infected cells from day 2 to day 14 postinfection has demonstrated the replication capacity of SRV-4 and SRV-8 in Jurkat cells (Fig. 3.6). By comparing the SRV-4- and SRV-8-infected cells, the results showed that the SRV-8-infected cells displayed a relatively lower level of SRV-LTR but released a larger amount of SRV virions in the culture medium within 14 days infection period. However, the underlying mechanisms that led to these differences remain to be elucidated in the future.

Summary of Chapter 4

Exploring the interactions among viral infection, apoptosis and autophagy have been

the subject of intense study in the past decades. Depending on the types of viruses and host cells, the apoptotic pathway and autophagic pathway could be either induced or inhibited in the host cells by viral infection; and interestingly, the modulated autophagic pathway has been widely demonstrated to in turn regulate viral replication and pathogenesis [20, 24, 257, 258, 412, 425, 427]. In chapter four of this thesis, the results have shown that SRV-4/SRV-8 infection was able to enhance the formation of autophagosome as well as increase the conversion of LC3-I to LC3-II in Jurkat cells (Fig. 4.1 and Fig. 4.2). Moreover, the enhanced degradation of autophagosome has been identified in the infected cells by challenging the cells with CQ (Fig. 4.3). These findings reveal the increase of the entire autophagic flux in Jurkat cells with SRV-4/SRV-8 infection, suggesting the activation of the autophagic pathway by SRV infection of T lymphocytes. Moreover, the results have shown that both SRV-4 and SRV-8 were able to induce apoptosis in the infected Jurkat cells. The percentage of Annexin V^+ Jurkat cells was significantly increased by SRV-4/SRV-8 infection (Fig. 4.4). Consistently, the level of cleaved caspase-3/-8 were both significantly increased in the infected cells (Fig. 4.5 and Fig. 4.6). However, our results have further indicated that the mRNA expression levels of Fas/FasL and DR5/TRAIL were not increased in the infected Jurkat cells, suggesting that the activation of caspase-8 might be death receptors/ligands independent (Fig. 4.8).

A growing number of studies have demonstrated the anti-viral or pro-viral functions of autophagy in viral replication and viral pathogenesis [254, 257, 476, 477]. The result

in chapter four has shown that SRV replication was significantly increased in the Jurkat cells when autophagy was inhibited by knockdown of Beclin1, suggesting that autophagy might act as an anti-viral process to restrict SRV replication in the infected Jurkat cells (Fig. 4.10). However, other studies on RNA viruses, such as HIV and HTLV, have shown that the virus-induced autophagy was able to enhance viral replication [254, 415, 453]. In contrast to SRV infection that might enhance the entire autophagic flux in the infected Jurkat cells, those RNA viruses promoted the formation of autophagosome whereas blocked the degradation of autophagosome in the host cells. Accordingly, it is possible that the increased entire autophagic flux in SRV-infected Jurkat cells could directly recruit and degrade the intracellular SRV particles thus inhibit SRV replication. However, the specific mechanism of the autophagy-mediated reduction of SRV replication remains unclear and needs to be further clarified.

It has been widely shown that the virus-induced autophagy could affect the apoptotic pathway in the infected host cells [38, 40, 416, 431]. The results in chapter four are the first time demonstrating that the SRV-8-induced autophagy was able to enhance caspase-3/-8 activation and apoptosis in the infected Jurkat cells through the recruitment of procaspase-8 on autophagosome. Beclin1 knockdown and CQ treatment have been shown to significantly suppress and enhanced the SRV-induced apoptosis in Jurkat cells, respectively (Fig. 4.11 and Fig. 4.12). These findings suggest the important role of autophagosome in the SRV infection-induced apoptosis in Jurkat cells. Interestingly, the results have further indicated the co-localization of procaspase-

8 with LC3 and p62/SQSTM1, as well as the increased interaction between procaspase-8 and LC3 in the infected cells (Fig. 4.15, Fig. 4.16 and Fig. 4.17). These findings suggest that SRV infection might be able to induce the interaction of procaspase-8 with LC3 and p62/SQSTM1 and promote the accumulation of procaspase-8 on the autophagosomes, leading to apoptosis in Jurkat cells. However, whether and how the autophagosome-mediated caspase-8 activation was attributed to the formation of iDISC is still unclear and needs to be explored in the further studies. Since our results have shown that SRV-4/SRV-8 infection did not change the level of cleaved caspase-9 in Jurkat cells, the autophagy-induced caspase-8 activation might be the main pathway that leads to the SRV infection-induced apoptosis in Jurkat cells.

Summary of Chapter 5

The exciting and rapid progress has been made in recent years in understanding the interactions between m6A modification and viral infection, and some studies have revealed the novel effects of m6A modification and the cellular m6A machinery on viral replication and pathogenesis [45, 46, 56, 57, 362, 368]. In chapter five, the result has shown that SRV-8 infection could decrease the global m6A level of Jurkat cells, suggesting the potential involvement of m6A in regulating SRV infection (Fig. 5.2). Subsequently, six distinct m6A peaks have been identified in SRV-8 viral RNAs in the infected Jurkat cells (Fig. 5.4 and Table 5.1) and SRV-8 infection has been shown to reprogramme the Jurkat cellular m6A epitranscriptome (Fig. 5.5 and Fig. 5.6). Moreover, much more hypomethylated m6A peaks were identified than the

hypermethylated m6A peaks (Fig. 5.6), and the hypo/hypermethylated genes have been shown to be related to immune responses and viral replication. The findings suggest the involvement of m6A in regulating viral replication and mediating the host cellular immune responses during SRV infection on T lymphocytes. Consistently, previous studies have also shown that viral infection could change the host cellular m6A epitranscriptome, including some host cellular transcripts related to viral replication and immune responses [56, 313, 367, 370]. In future studies, the mechanisms by which SRV infection manipulates the host cellular m6A epitranscriptome, as well as the functions of the specific m6A modifications and m6A related factors on SRV infection will be of interest.

Interestingly, the results in chapter five have also shown that the depletion of ALKBH5 or YTHDF1 was able to significantly decrease SRV-8 replication in Jurkat cells (Fig. 5.8 and Fig. 5.11). The results are the first time implying that SRV-8 replication might be regulated by the Jurkat cellular m6A machinery, and the m6A modification might play a role in affecting SRV-8 replication in T lymphocytes. Indeed, previous studies have also demonstrated that the manipulation of the host cellular m6A machinery was able to affect viral replication in the infected cells [312, 313, 364, 367, 378, 475]. However, the underlying mechanisms of the m6A-mediated viral replication are still unclear. Due to the diverse distribution of m6A sites on different viral RNA genomes and transcripts as well as the various effects of the different viruses on the host cellular m6A epitranscriptomes, it is likely that there are various mechanisms of the m6A-mediated

viral infection for different viruses. Therefore, further studies might be needed to clarify the underlying mechanisms of the ALKBH5-/YTHDF1-mediated increase of SRV-8 replication in the infected Jurkat cells, which might provide a novel insight on the roles of m6A in viral infection.

Summary of the Thesis

In summary, the results presented in this thesis have provided new insight on the interactions among SRV infection, autophagy and apoptosis as well as the interactions between SRV infection and m6A RNA methylation in Jurkat cells. SRV-4/SRV-8 have been identified for the first time to be able to infect and replicate in Jurkat cells in *vitro*. Moreover, SRV-4/SRV-8 infection has been shown to increase autophagosome formation and enhance the entire autophagic flux, as well as induce the activation of caspase-3/-8 and apoptosis in Jurkat cells. The results are the first time showing that SRV infection is able to induce both autophagy and apoptosis in Jurkat cells. The results have further suggested that the SRV-8-induced autophay was able to inhibit viral replication in Jurkat cells. Moreover, the induced-autophagy has been shown to promote the activation of caspase-3/-8 and apoptosis in Jurkat cells. Since procaspase-8 has been shown to co-localized with p62/SQSTM1 and LC3 in the infected cells, and the SRV-8 infection has been shown to enhance the interaction between procaspase-8 and LC3; it is possible that procaspase-8 might be recruited to the autophagosomal membrane with the help of p62/SQSTM1 and LC3, which might lead to the activation of caspase-8 and apoptosis in the infected cells. Collectively, the results in this thesis

suggest that the SRV-induced autophagy might function as the pathogen defense response by inhibiting SRV replication and inducing the apoptotic cell death of the infected Jurkat cells, and the induced apoptosis might result from the enhanced formation of autophagosomes that congregate procaspase-8 for its activation.

In addition, the results in this thesis has also suggested that SRV-8 infection could decrease the global m6A level in Jurkat cells. Moreover, six m6A peaks were identified in SRV-8 viral RNAs, and SRV-8 infection was shown to reprogramme the Jurkat cellular m6A epitranscriptome, which might in turn affect the pathways that relate to immune responses and viral replication. Although the underlying mechanisms of the m6A level reduction and the m6A epitranscriptome reprogramming in Jurkat cells upon SRV-8 infection are still unknown, our results have provided the evidences suggesting that SRV infection could affect m6A modification in Jurkat cells, which might in turn affect the virus-host cells interactions. The resuts have also shown that knockdown of ALKBH5 or YTHDF1 in the infected Jurkat cells could significantly decrease SRV-8 replication, suggesting the regulatory role of the cellular m6A machinery in SRV replication. Knockdown of ALKBH5 could increase the global m6A levels, thus the result also imply that m6A modification in Jurkat cells might inhibit SRV replication. Therefore, the results in this thesis reveal a potential feedback loop indicating that SRV-8 infection could reduce the global levels of m6A in Jurkat cells which might enhance viral replication. And the reducing of m6A modification might be a novel strategy to inhibit the replicaition of SRV in T lymphocytes.

Due to the important roles of autophagy, apoptosis and m6A RNA methylation in viral infection, the results in this thesis might provide an insight for the understanding of SRV infection and pathogenesis, as well as provide possible targets for the development of new therapies and vaccines to against SRV infection.

References

1. Buchen-Osmond, C., *The universal virus database ICTVdB.* Computing in Science & Engineering, 2003. **5**(3): p. 16-25.

2. Daniel, M.D., et al., *A new type D retrovirus isolated from macaques with an immunodeficiency syndrome.* Science, 1984. **223**(4636): p. 602-5.

3. Lerche, N.W. and K.G. Osborn, *Simian retrovirus infections: potential confounding variables in primate toxicology studies.* Toxicol Pathol, 2003. **31**: p. 103-10.

4. Chopra, H.C. and M.M. Mason, *A new virus in a spontaneous mammary tumor of a rhesus monkey.* Cancer Res, 1970. **30**(8): p. 2081-6.

5. Jensen, E.M., et al., *Isolation and propagation of a virus from a spontaneous mammary carcinoma of a rhesus monkey.* Cancer Res, 1970. **30**(9): p. 2388-93.

6. Montiel, N.A., *An updated review of simian betaretrovirus (SRV) in macaque hosts.* J Med Primatol, 2010. **39**(5): p. 303-14.

7. Zao, C.L., et al., *A novel simian retrovirus subtype discovered in cynomolgus monkeys (Macaca fascicularis).* J Gen Virol, 2016. **97**(11): p. 3017-3023.

8. Tsai, C.C., et al., *Retroperitoneal fibromatosis and acquired immunodeficiency syndrome in macaques: clinical and immunologic studies.* Lab Anim Sci, 1986. **36**(2): p. 119-25.

9. Maul, D.H., et al., *Pathogenesis of simian AIDS in rhesus macaques inoculated with the SRV-1 strain of type D retrovirus.* Am J Vet Res, 1986. **47**(4): p. 863-8.

10. Gardner, M.B., et al., *Nonhuman primate retrovirus isolates and AIDS.* Adv Vet Sci Comp Med, 1988. **32**: p. 171-226.

11. Weiss, R.A., *The discovery of endogenous retroviruses.* Retrovirology, 2006. **3**: p. 67.

12. Heidecker, G., et al., *Induction of simian acquired immune deficiency syndrome (SAIDS) with a molecular clone of a type D SAIDS retrovirus.* J Virol, 1987. **61**(10): p. 3066-71.

13. Lerche, N.W., et al., *Inapparent carriers of simian acquired immune deficiency syndrome type D retrovirus and disease transmission with saliva.* J Natl Cancer Inst, 1986. **77**(2): p. 489-96.

14. Cheung, A.T. and M.B. Gardner, *Functional deficiency of polymorphonuclear leukocytes in simian acquired immunodeficiency syndrome.* Am J Vet Res, 1991. **52**(9): p. 1523-6.

15. van Kuyk, R.W., et al., *Characterization of rhesus macaque B-lymphoblastoid cell lines infected with simian type D retrovirus.* AIDS Res Hum Retroviruses, 1991. **7**(11): p. 899-909.

16. Maul, D.H., et al., *Simian retrovirus D serogroup 1 has a broad cellular tropism for lymphoid and nonlymphoid cells.* J Virol, 1988. **62**(5): p. 1768-73.

17. Schmid, D. and C. Munz, *Innate and adaptive immunity through autophagy.* Immunity, 2007. **27**(1): p. 11-21.

18. Rey-Jurado, E., et al., *Contribution of autophagy to antiviral immunity.* FEBS Lett, 2015. **589**(22): p. 3461-70.

19. Everett, H. and G. McFadden, *Apoptosis: an innate immune response to virus infection.* Trends Microbiol, 1999. **7**(4): p. 160-5.

20. Barber, G.N., *Host defense, viruses and apoptosis.* Cell Death Differ, 2001. **8**(2): p. 113-26.

21. Kim, K.H. and M.S. Lee, *Autophagy--a key player in cellular and body metabolism.* Nat Rev Endocrinol, 2014. **10**(6): p. 322-37.

22. Boya, P., F. Reggiori, and P. Codogno, *Emerging regulation and functions of autophagy.* Nat Cell Biol, 2013. **15**(7): p. 713-20.

23. Elmore, S., *Apoptosis: a review of programmed cell death.* Toxicol Pathol, 2007. **35**(4): p. 495-

516.

24. Dreux, M. and F.V. Chisari, *Viruses and the autophagy machinery.* Cell Cycle, 2010. **9**(7): p. 1295-1307.

25. Gannage, M., et al., *Matrix protein 2 of influenza A virus blocks autophagosome fusion with lysosomes.* Cell Host Microbe, 2009. **6**(4): p. 367-80.

26. Jackson, W.T., et al., *Subversion of cellular autophagosomal machinery by RNA viruses.* PLoS Biol, 2005. **3**(5): p. e156.

27. Huang, S.C., et al., *Enterovirus 71-induced autophagy detected in vitro and in vivo promotes viral replication.* J Med Virol, 2009. **81**(7): p. 1241-52.

28. Tanida, I., et al., *Knockdown of autophagy-related gene decreases the production of infectious hepatitis C virus particles.* Autophagy, 2009. **5**(7): p. 937-45.

29. Wang, X., et al., *HIV-1 and HIV-2 infections induce autophagy in Jurkat and CD4+ T cells.* Cellular Signalling, 2012. **24**(7): p. 1414-1419.

30. Fevrier, M., K. Dorgham, and A. Rebollo, *CD4+ T cell depletion in human immunodeficiency virus (HIV) infection: role of apoptosis.* Viruses, 2011. **3**(5): p. 586-612.

31. Zhou, X., et al., *Virus Infection and Death Receptor-Mediated Apoptosis.* Viruses, 2017. **9**(11).

32. Orvedahl, A. and B. Levine, *Viral evasion of autophagy.* Autophagy, 2008. **4**(3): p. 280-5.

33. Wileman, T., *Aggresomes and autophagy generate sites for virus replication.* Science, 2006. **312**(5775): p. 875-8.

34. Richards, A.L. and W.T. Jackson, *How positive-strand RNA viruses benefit from autophagosome maturation.* J Virol, 2013. **87**(18): p. 9966-72.

35. Wang, X., et al., *Novel pandemic influenza A (H1N1) virus infection modulates apoptotic*

pathways that impact its replication in A549 cells. Microbes Infect, 2014. **16**(3): p. 178-86.

36. Galluzzi, L., et al., *Viral control of mitochondrial apoptosis.* PLoS Pathog, 2008. **4**(5): p. e1000018.

37. Cuconati, A. and E. White, *Viral homologs of BCL-2: role of apoptosis in the regulation of virus infection.* Genes & Development, 2002. **16**(19): p. 2465-78.

38. Espert, L., et al., *Autophagy is involved in T cell death after binding of HIV-1 envelope proteins to CXCR4.* J Clin Invest, 2006. **116**(8): p. 2161-72.

39. Jiang, H., et al., *Human adenovirus type 5 induces cell lysis through autophagy and autophagy-triggered caspase activity.* J Virol, 2011. **85**(10): p. 4720-9.

40. Li, M., et al., *Respiratory Syncytial Virus Replication Is Promoted by Autophagy-Mediated Inhibition of Apoptosis.* J Virol, 2018. **92**(8).

41. Dominissini, D., et al., *Topology of the human and mouse m6A RNA methylomes revealed by m6A-seq.* Nature, 2012. **485**(7397): p. 201-6.

42. Schwartz, S., et al., *High-resolution mapping reveals a conserved, widespread, dynamic mRNA methylation program in yeast meiosis.* Cell, 2013. **155**(6): p. 1409-21.

43. Clancy, M.J., et al., *Induction of sporulation in Saccharomyces cerevisiae leads to the formation of N6-methyladenosine in mRNA: a potential mechanism for the activity of the IME4 gene.* Nucleic Acids Res, 2002. **30**(20): p. 4509-18.

44. Bodi, Z., et al., *Yeast targets for mRNA methylation.* Nucleic Acids Res, 2010. **38**(16): p. 5327-35.

45. Tan, B. and S.J. Gao, *RNA epitranscriptomics: Regulation of infection of RNA and DNA viruses by N(6) -methyladenosine (m(6) A).* 2018. **28**(4): p. e1983.

46. Kennedy, E.M., et al., *Viral Epitranscriptomics.* J Virol, 2017. **91**(9).

47. Li, Y., et al., *Transcriptome-wide N(6)-methyladenosine profiling of rice callus and leaf reveals the presence of tissue-specific competitors involved in selective mRNA modification.* RNA Biol, 2014. **11**(9): p. 1180-8.

48. Wang, X., et al., *N6-methyladenosine-dependent regulation of messenger RNA stability.* Nature, 2014. **505**(7481): p. 117-20.

49. Adhikari, S., et al., *m(6)A: Signaling for mRNA splicing.* RNA Biol, 2016. **13**(9): p. 756-9.

50. Slobodin, B., et al., *Transcription Impacts the Efficiency of mRNA Translation via Co-transcriptional N6-adenosine Methylation.* Cell, 2017. **169**(2): p. 326-337.e12.

51. Liu, N., et al., *N(6)-methyladenosine-dependent RNA structural switches regulate RNA-protein interactions.* Nature, 2015. **518**(7540): p. 560-4.

52. Wang, S., et al., *Novel insights on m(6)A RNA methylation in tumorigenesis: a double-edged sword.* Mol Cancer, 2018. **17**(1): p. 101.

53. Wang, S., et al., *Roles of RNA methylation by means of N(6)-methyladenosine (m(6)A) in human cancers.* Cancer Lett, 2017. **408**: p. 112-120.

54. Geula, S., et al., *Stem cells. m6A mRNA methylation facilitates resolution of naive pluripotency toward differentiation.* Science, 2015. **347**(6225): p. 1002-6.

55. Wang, Y., et al., *N6-methyladenosine modification destabilizes developmental regulators in embryonic stem cells.* Nat Cell Biol, 2014. **16**(2): p. 191-8.

56. Gokhale, N.S. and S.M. Horner, *RNA modifications go viral.* 2017. **13**(3): p. e1006188.

57. Brocard, M., A. Ruggieri, and N. Locker, *m6A RNA methylation, a new hallmark in virus-host interactions.* J Gen Virol, 2017. **98**(9): p. 2207-2214.

58. Power, M.D., et al., *Nucleotide sequence of SRV-1, a type D simian acquired immune deficiency syndrome retrovirus.* Science, 1986. **231**(4745): p. 1567-72.

59. Sonigo, P., et al., *Nucleotide sequence of Mason-Pfizer monkey virus: an immunosuppressive D-type retrovirus.* Cell, 1986. **45**(3): p. 375-85.

60. Henderson, L.E., et al., *Purification and N-terminal amino acid sequence comparisons of structural proteins from retrovirus-D/Washington and Mason-Pfizer monkey virus.* J Virol, 1985. **55**(3): p. 778-87.

61. Bradac, J. and E. Hunter, *Polypeptides of Mason-Pfizer monkey virus. I. Synthesis and processing of the gag-gene products.* Virology, 1984. **138**(2): p. 260-75.

62. Rasko, J.E., et al., *The RD114/simian type D retrovirus receptor is a neutral amino acid transporter.* Proc Natl Acad Sci U S A, 1999. **96**(5): p. 2129-34.

63. Yoshikawa, R., et al., *Simian retrovirus 4 induces lethal acute thrombocytopenia in Japanese macaques.* J Virol, 2015. **89**(7): p. 3965-75.

64. Torres, J.V., et al., *Neutralization epitope in the envelope glycoprotein of simian retrovirus-1 (SRV-1) and identification of the virus receptor.* J Med Primatol, 1991. **20**(4): p. 218-21.

65. Marin, M., et al., *N-linked glycosylation and sequence changes in a critical negative control region of the ASCT1 and ASCT2 neutral amino acid transporters determine their retroviral receptor functions.* J Virol, 2003. **77**(5): p. 2936-45.

66. Temin, H.M., *Function of the retrovirus long terminal repeat.* Cell, 1982. **28**(1): p. 3-5.

67. Zao, C.L., et al., *The complete genome and genetic characteristics of SRV-4 isolated from cynomolgus monkeys (Macaca fascicularis).* Virology, 2010. **405**(2): p. 390-6.

68. Marracci, G.H., et al., *Molecular cloning and cell-specific growth characterization of*

polymorphic variants of type D serogroup 2 simian retroviruses. Virology, 1999. **261**(1): p. 43-58.

69. Thayer, R.M., et al., *Sequence relationships of type D retroviruses which cause simian acquired immunodeficiency syndrome.* Virology, 1987. **157**(2): p. 317-29.

70. Li, B., M.K. Axthelm, and C.A. Machida, *Simian retrovirus serogroup 5: partial gag-prt sequence and viral RNA distribution in an infected rhesus macaque.* Virus Genes, 2000. **21**(3): p. 241-8.

71. Takano, J., et al., *Isolation and DNA characterization of a simian retrovirus 5 from a Japanese monkey (Macaca fuscata).* J Gen Virol, 2013. **94**(Pt 5): p. 955-9.

72. Nandi, J.S., et al., *New simian beta retroviruses from rhesus monkeys (Macaca mulatta) and langurs (Semnopithecus entellus) from Rajasthan, India.* Virus Genes, 2006. **33**(1): p. 107-16.

73. Hara, M., et al., *Isolation and characterization of a new simian retrovirus type D subtype from monkeys at the Tsukuba Primate Center, Japan.* Microbes Infect, 2005. **7**(1): p. 126-31.

74. Nandi, J.S., et al., *Natural infection by simian retrovirus-6 (SRV-6) in Hanuman langurs (Semnopithecus entellus) from two different geographical regions of India.* Virology, 2003. **311**(1): p. 192-201.

75. Giddens, W.E., Jr., et al., *Retroperitoneal fibromatosis and acquired immunodeficiency syndrome in macaques. Pathologic observations and transmission studies.* Am J Pathol, 1985. **119**(2): p. 253-63.

76. Henrickson, R.V., et al., *Epidemic of acquired immunodeficiency in rhesus monkeys.* Lancet, 1983. **1**(8321): p. 388-90.

77. Voevodin, A.F. and P.A. Marx, *Simian virology*. 2009: John Wiley & Sons.

78. Axthelm, M., et al. *Characterization of type D simian retroviruses*. in *Program and Abstracts of*

the 5th Annual Symposium on Nonhuman Primate Models for AIDS. 1987.

79. Nandi, J.S., et al., *A novel type D simian retrovirus naturally infecting the Indian Hanuman langur (Semnopithecus entellus).* Virology, 2000. **277**(1): p. 6-13.

80. Osborn, K.G., et al., *The pathology of an epizootic of acquired immunodeficiency in rhesus macaques.* Am J Pathol, 1984. **114**(1): p. 94-103.

81. MacKenzie, M., et al., *Hematologic abnormalities in simian acquired immune deficiency syndrome.* Lab Anim Sci, 1986. **36**(1): p. 14-9.

82. Guzman, R.E., R.L. Kerlin, and T.E. Zimmerman, *Histologic lesions in cynomolgus monkeys (Macaca fascicularis) naturally infected with simian retrovirus type D: comparison of seropositive, virus-positive, and uninfected animals.* Toxicol Pathol, 1999. **27**(6): p. 672-7.

83. Lerche, N.W., et al., *Natural history of endemic type D retrovirus infection and acquired immune deficiency syndrome in group-housed rhesus monkeys.* J Natl Cancer Inst, 1987. **79**(4): p. 847-54.

84. Lackner, A.A., et al., *Immunohistochemical localization of type D retrovirus serotype 1 in the digestive tract of rhesus monkeys with simian AIDS.* J Med Primatol, 1990. **19**(3-4): p. 339-49.

85. Marx, P.A. and L.J. Lowenstine, *Mesenchymal neoplasms associated with type D retroviruses in macaques.* Cancer Surv, 1987. **6**(1): p. 101-15.

86. Marx, P.A., et al., *Isolation of a new serotype of simian acquired immune deficiency syndrome type D retrovirus from Celebes black macaques (Macaca nigra) with immune deficiency and retroperitoneal fibromatosis.* J Virol, 1985. **56**(2): p. 571-8.

87. Paramastri, Y.A., et al., *Intracranial lymphomas in simian retrovirus-positive Macaca fascicularis.* Vet Pathol, 2002. **39**(3): p. 399-402.

88. Tsai, C.C., et al., *Subcutaneous fibromatosis associated with an acquired immune deficiency syndrome in pig-tailed macaques.* Am J Pathol, 1985. **120**(1): p. 30-7.

89. Rose, T.M., et al., *Identification of two homologs of the Kaposi's sarcoma-associated herpesvirus (human herpesvirus 8) in retroperitoneal fibromatosis of different macaque species.* J Virol, 1997. **71**(5): p. 4138-44.

90. Meyer, P.R., et al., *An immunopathologic evaluation of lymph nodes from monkey and man with acquired immune deficiency syndrome and related conditions.* Hematol Oncol, 1985. **3**(3): p. 199-210.

91. Kwang, H.S., et al., *Viremia, antigenemia, and serum antibodies in rhesus macaques infected with simian retrovirus type 1 and their relationship to disease course.* Lab Invest, 1987. **56**(6): p. 591-7.

92. Lackner, A.A., et al., *Distribution of a macaque immunosuppressive type D retrovirus in neural, lymphoid, and salivary tissues.* J Virol, 1988. **62**(6): p. 2134-42.

93. Lackner, A.A., et al., *Asymptomatic infection of the central nervous system by the macaque immunosuppressive type D retrovirus, SRV-1.* J Gen Virol, 1989. **70 (Pt 7)**: p. 1641-51.

94. Mitchell, J.L., et al., *Early immunopathology events in simian retrovirus, type 2 infections prior to the onset of disease.* Virology, 2011. **413**(2): p. 161-8.

95. Lackner, A.A., et al., *Mucosal epithelial cells and Langerhans cells are targets for infection by the immunosuppressive type D retrovirus simian AIDS retrovirus serotype 1.* J Med Primatol, 1989. **18**(3-4): p. 195-207.

96. Legrand, E.K., et al., *Monocyte function in rhesus monkeys with simian acquired immune deficiency syndrome.* Vet Immunol Immunopathol, 1985. **10**(2-3): p. 131-46.

97. Lerche, N.W., et al., *Evidence of infection with simian type D retrovirus in persons occupationally exposed to nonhuman primates.* J Virol, 2001. **75**(4): p. 1783-9.

98. Gravell, M., et al., *Transmission of simian acquired immunodeficiency syndrome (SAIDS) with type D retrovirus isolated from saliva or urine.* Proc Soc Exp Biol Med, 1984. **177**(3): p. 491-4.

99. Tsai, C.C., et al., *Maternal transmission of type D simian retrovirus (SRV-2) in pigtailed macaques.* J Med Primatol, 1990. **19**(3-4): p. 203-16.

100. Moazed, T.C. and M.E. Thouless, *Viral persistence of simian type D retrovirus (SRV-2/W) in naturally infected pigtailed macaques (Macaca nemestrina).* J Med Primatol, 1993. **22**(7-8): p. 382-9.

101. Daniel, M.D., et al., *Prevalence of antibodies to 3 retroviruses in a captive colony of macaque monkeys.* Int J Cancer, 1988. **41**(4): p. 601-8.

102. Lowenstine, L.J., et al., *Seroepidemiologic survey of captive Old-World primates for antibodies to human and simian retroviruses, and isolation of a lentivirus from sooty mangabeys (Cercocebus atys).* Int J Cancer, 1986. **38**(4): p. 563-74.

103. Kerr, J.F., A.H. Wyllie, and A.R. Currie, *Apoptosis: a basic biological phenomenon with wide-ranging implications in tissue kinetics.* Br J Cancer, 1972. **26**(4): p. 239-57.

104. Thompson, C.B., *Apoptosis in the pathogenesis and treatment of disease.* Science, 1995. **267**(5203): p. 1456-62.

105. Oberhammer, F.A., et al., *Chromatin condensation during apoptosis is accompanied by degradation of lamin A+B, without enhanced activation of cdc2 kinase.* J Cell Biol, 1994. **126**(4): p. 827-37.

106. Wyllie, A.H., J.F. Kerr, and A.R. Currie, *Cell death: the significance of apoptosis.* Int Rev Cytol,

1980. **68**: p. 251-306.

107. Fullard, J.F., A. Kale, and N.E. Baker, *Clearance of apoptotic corpses.* Apoptosis, 2009. **14**(8): p. 1029-37.

108. Hail, N., Jr., et al., *Apoptosis effector mechanisms: a requiem performed in different keys.* Apoptosis, 2006. **11**(6): p. 889-904.

109. Thornberry, N.A. and Y. Lazebnik, *Caspases: enemies within.* Science, 1998. **281**(5381): p. 1312-6.

110. Riedl, S.J. and Y. Shi, *Molecular mechanisms of caspase regulation during apoptosis.* Nat Rev Mol Cell Biol, 2004. **5**(11): p. 897-907.

111. Li, J. and J. Yuan, *Caspases in apoptosis and beyond.* Oncogene, 2008. **27**(48): p. 6194-206.

112. Salvesen, G.S. and V.M. Dixit, *Caspase activation: the induced-proximity model.* Proc Natl Acad Sci U S A, 1999. **96**(20): p. 10964-7.

113. Fesik, S.W., *Insights into programmed cell death through structural biology.* Cell, 2000. **103**(2): p. 273-82.

114. Galluzzi, L., O. Kepp, and G. Kroemer, *Mitochondria: master regulators of danger signalling.* Nat Rev Mol Cell Biol, 2012. **13**(12): p. 780-8.

115. Jiang, X. and X. Wang, *Cytochrome C-mediated apoptosis.* Annu Rev Biochem, 2004. **73**: p. 87-106.

116. Salvesen, G.S. and M. Renatus, *Apoptosome: the seven-spoked death machine.* Dev Cell, 2002. **2**(3): p. 256-7.

117. Li, P., et al., *Cytochrome c and dATP-dependent formation of Apaf-1/caspase-9 complex initiates an apoptotic protease cascade.* Cell, 1997. **91**(4): p. 479-89.

118. Srinivasula, S.M., et al., *Autoactivation of procaspase-9 by Apaf-1-mediated oligomerization.* Mol Cell, 1998. **1**(7): p. 949-57.

119. Tait, S.W. and D.R. Green, *Mitochondria and cell death: outer membrane permeabilization and beyond.* Nat Rev Mol Cell Biol, 2010. **11**(9): p. 621-32.

120. Cory, S. and J.M. Adams, *The Bcl2 family: regulators of the cellular life-or-death switch.* Nat Rev Cancer, 2002. **2**(9): p. 647-56.

121. Shimizu, S., M. Narita, and Y. Tsujimoto, *Bcl-2 family proteins regulate the release of apoptogenic cytochrome c by the mitochondrial channel VDAC.* Nature, 1999. **399**(6735): p. 483-7.

122. Adams, J.M. and S. Cory, *Bcl-2-regulated apoptosis: mechanism and therapeutic potential.* Curr Opin Immunol, 2007. **19**(5): p. 488-96.

123. Youle, R.J. and A. Strasser, *The BCL-2 protein family: opposing activities that mediate cell death.* Nat Rev Mol Cell Biol, 2008. **9**(1): p. 47-59.

124. MacFarlane, M. and A.C. Williams, *Apoptosis and disease: a life or death decision.* Conference and Workshop on Apoptosis and Disease, 2004. **5**(7): p. 674-678.

125. Locksley, R.M., N. Killeen, and M.J. Lenardo, *The TNF and TNF receptor superfamilies: integrating mammalian biology.* Cell, 2001. **104**(4): p. 487-501.

126. Tartaglia, L.A., et al., *A novel domain within the 55 kd TNF receptor signals cell death.* Cell, 1993. **74**(5): p. 845-53.

127. Ashkenazi, A. and V.M. Dixit, *Death receptors: signaling and modulation.* Science, 1998. **281**(5381): p. 1305-8.

128. Chicheportiche, Y., et al., *TWEAK, a new secreted ligand in the tumor necrosis factor family that*

weakly induces apoptosis. J Biol Chem, 1997. **272**(51): p. 32401-10.

129. Rubio-Moscardo, F., et al., *Characterization of 8p21.3 chromosomal deletions in B-cell lymphoma: TRAIL-R1 and TRAIL-R2 as candidate dosage-dependent tumor suppressor genes.* Blood, 2005. **106**(9): p. 3214-22.

130. Suliman, A., et al., *Intracellular mechanisms of TRAIL: apoptosis through mitochondrial-dependent and -independent pathways.* Oncogene, 2001. **20**(17): p. 2122-33.

131. Peter, M.E. and P.H. Krammer, *Mechanisms of CD95 (APO-1/Fas)-mediated apoptosis.* Curr Opin Immunol, 1998. **10**(5): p. 545-51.

132. Wajant, H., *The Fas signaling pathway: more than a paradigm.* Science, 2002. **296**(5573): p. 1635-6.

133. Peter, M.E., et al., *The CD95 receptor: apoptosis revisited.* Cell, 2007. **129**(3): p. 447-50.

134. Kischkel, F.C., et al., *Cytotoxicity-dependent APO-1 (Fas/CD95)-associated proteins form a death-inducing signaling complex (DISC) with the receptor.* Embo Journal, 1995. **14**(22): p. 5579-5588.

135. Luo, X., et al., *Bid, a Bcl2 interacting protein, mediates cytochrome c release from mitochondria in response to activation of cell surface death receptors.* Cell, 1998. **94**(4): p. 481-90.

136. Korsmeyer, S.J., et al., *Pro-apoptotic cascade activates BID, which oligomerizes BAK or BAX into pores that result in the release of cytochrome c.* Cell Death Differ, 2000. **7**(12): p. 1166-73.

137. Mizushima, N., *Autophagy: process and function.* Genes Dev, 2007. **21**(22): p. 2861-73.

138. Yang, Y.P., et al., *Molecular mechanism and regulation of autophagy.* Acta Pharmacol Sin, 2005. **26**(12): p. 1421-34.

139. Mizushima, N., Y. Ohsumi, and T. Yoshimori, *Autophagosome formation in mammalian cells.*

Cell Struct Funct, 2002. **27**(6): p. 421-9.

140. Li, W.W., J. Li, and J.K. Bao, *Microautophagy: lesser-known self-eating.* Cell Mol Life Sci, 2012. **69**(7): p. 1125-36.

141. Dice, J.F., *Chaperone-mediated autophagy.* Autophagy, 2007. **3**(4): p. 295-9.

142. Tsukada, M. and Y. Ohsumi, *Isolation and characterization of autophagy-defective mutants of Saccharomyces cerevisiae.* FEBS Lett, 1993. **333**(1-2): p. 169-74.

143. Xie, Z. and D.J. Klionsky, *Autophagosome formation: core machinery and adaptations.* Nat Cell Biol, 2007. **9**(10): p. 1102-9.

144. Nakatogawa, H., et al., *Dynamics and diversity in autophagy mechanisms: lessons from yeast.* Nat Rev Mol Cell Biol, 2009. **10**(7): p. 458-67.

145. Ohsumi, Y., *Molecular dissection of autophagy: two ubiquitin-like systems.* Nat Rev Mol Cell Biol, 2001. **2**(3): p. 211-6.

146. Yang, Z. and D.J. Klionsky, *Eaten alive: a history of macroautophagy.* Nat Cell Biol, 2010. **12**(9): p. 814-22.

147. Hosokawa, N., et al., *Nutrient-dependent mTORC1 Association with the ULK1â"Atg13â"FIP200 Complex Required for Autophagy.* Molecular Biology of the Cell, 2009. **20**(7): p. 1981.

148. Chang, H.J., et al., *ULK-Atg13-FIP200 complexes mediate mTOR signaling to the autophagy machinery.* Molecular Biology of the Cell, 2009. **20**(7): p. 1992-2003.

149. Mizushima, N., T. Yoshimori, and Y. Ohsumi, *The role of Atg proteins in autophagosome formation.* Annu Rev Cell Dev Biol, 2011. **27**: p. 107-32.

150. Kihara, A., et al., *Kihara A, Kabeya Y, Ohsumi Y, Yoshimori T.. Beclin-phosphatidylinositol 3-kinase complex functions at the trans-Golgi network. EMBO Rep 2: 330-335.* Embo Reports,

2001. **2**(4): p. 330.

151. He, C. and B. Levine, *The Beclin 1 interactome.* Current Opinion in Cell Biology, 2010. **22**(2): p. 140-149.

152. Funderburk, S.F., Q.J. Wang, and Z. Yue, *The Beclin 1-VPS34 complex--at the crossroads of autophagy and beyond.* Trends Cell Biol, 2010. **20**(6): p. 355-62.

153. Mizushima, N., T. Noda, and Y. Ohsumi, *Apg16p is required for the function of the Apg12p-Apg5p conjugate in the yeast autophagy pathway.* Embo j, 1999. **18**(14): p. 3888-96.

154. Suzuki, K., et al., *The pre-autophagosomal structure organized by concerted functions of APG genes is essential for autophagosome formation.* Embo j, 2001. **20**(21): p. 5971-81.

155. Hemelaar, J., et al., *A single protease, Apg4B, is specific for the autophagy-related ubiquitin-like proteins GATE-16, MAP1-LC3, GABARAP, and Apg8L.* Journal of Biological Chemistry, 2003. **278**(51): p. 51841-51850.

156. Ichimura, Y., et al., *A ubiquitin-like system mediates protein lipidation.* Nature, 2000. **408**(6811): p. 488-92.

157. Tanida, I., et al., *Human Apg3p/Aut1p homologue is an authentic E2 enzyme for multiple substrates, GATE-16, GABARAP, and MAP-LC3, and facilitates the conjugation of hApg12p to hApg5p.* J.biol.chem, 2002. **277**(16): p. 13739-13744.

158. Kabeya, Y., et al., *LC3, a mammalian homologue of yeast Apg8p, is localized in autophagosome membranes after processing.* Embo j, 2000. **19**(21): p. 5720-8.

159. Kirisako, T., et al., *Formation process of autophagosome is traced with Apg8/Aut7p in yeast.* J Cell Biol, 1999. **147**(2): p. 435-46.

160. Kabeya, Y., et al., *LC3, GABARAP and GATE16 localize to autophagosomal membrane depending*

on form-II formation. J Cell Sci, 2004. **117**(Pt 13): p. 2805-12.

161. Klionsky, D.J., et al., *Guidelines for the use and interpretation of assays for monitoring autophagy (3rd edition).* Autophagy, 2016. **12**(1): p. 1-222.

162. Mizushima, N. and T. Yoshimori, *How to interpret LC3 immunoblotting.* Autophagy, 2007. **3**(6): p. 542-5.

163. Mizushima, N., et al., *Mouse Apg16L, a novel WD-repeat protein, targets to the autophagic isolation membrane with the Apg12-Apg5 conjugate.* Journal of Cell Science, 2003. **116**(Pt 9): p. 1679-1688.

164. Mizushima, N., et al., *Dissection of autophagosome formation using Apg5-deficient mouse embryonic stem cells.* Journal of Cell Biology, 2001. **152**(4): p. 657-668.

165. Kirisako, T., et al., *The reversible modification regulates the membrane-binding state of Apg8/Aut7 essential for autophagy and the cytoplasm to vacuole targeting pathway.* J Cell Biol, 2000. **151**(2): p. 263-76.

166. Nakatogawa, H., Y. Ichimura, and Y. Ohsumi, *Atg8, a ubiquitin-like protein required for autophagosome formation, mediates membrane tethering and hemifusion.* Cell, 2007. **130**(1): p. 165-78.

167. Noda, N.N., et al., *Structural basis of target recognition by Atg8/LC3 during selective autophagy.* Genes Cells, 2008. **13**(12): p. 1211-8.

168. Noda, N.N., Y. Ohsumi, and F. Inagaki, *Atg8-family interacting motif crucial for selective autophagy.* FEBS Lett, 2010. **584**(7): p. 1379-85.

169. Shvets, E., et al., *The N-terminus and Phe52 residue of LC3 recruit p62/SQSTM1 into autophagosomes.* J Cell Sci, 2008. **121**(Pt 16): p. 2685-95.

170. Tung, Y.T., et al., *The evolutionarily conserved interaction between LC3 and p62 selectively mediates autophagy-dependent degradation of mutant huntingtin.* Cell Mol Neurobiol, 2010. **30**(5): p. 795-806.

171. Birgisdottir, A.B., T. Lamark, and T. Johansen, *The LIR motif - crucial for selective autophagy.* J Cell Sci, 2013. **126**(Pt 15): p. 3237-47.

172. Pankiv, S., et al., *p62/SQSTM1 binds directly to Atg8/LC3 to facilitate degradation of ubiquitinated protein aggregates by autophagy.* J Biol Chem, 2007. **282**(33): p. 24131-45.

173. Lamark, T., et al., *NBR1 and p62 as cargo receptors for selective autophagy of ubiquitinated targets.* Cell Cycle, 2009. **8**(13): p. 1986-90.

174. Shaid, S., et al., *Ubiquitination and selective autophagy.* Cell Death Differ, 2013. **20**(1): p. 21-30.

175. Kim, H.J., S. Lee, and J.U. Jung, *When autophagy meets viruses: a double-edged sword with functions in defense and offense.* Semin Immunopathol, 2010. **32**(4): p. 323-41.

176. Reggiori, F., et al., *Atg9 cycles between mitochondria and the pre-autophagosomal structure in yeasts.* Autophagy, 2005. **1**(2): p. 101-9.

177. Juhasz, G. and T.P. Neufeld, *Autophagy: a forty-year search for a missing membrane source.* PLoS Biol, 2006. **4**(2): p. e36.

178. Geng, J. and D.J. Klionsky, *The Golgi as a potential membrane source for autophagy.* Autophagy, 2010. **6**(7): p. 950-1.

179. He, C., et al., *Self-interaction is critical for Atg9 transport and function at the phagophore assembly site during autophagy.* Mol Biol Cell, 2008. **19**(12): p. 5506-16.

180. Yen, W.L., et al., *Atg27 is required for autophagy-dependent cycling of Atg9.* Mol Biol Cell, 2007.

18(2): p. 581-93.

181. Legakis, J.E., W.L. Yen, and D.J. Klionsky, *A cycling protein complex required for selective autophagy.* Autophagy, 2007. **3**(5): p. 422-32.

182. Chang, C.Y. and W.P. Huang, *Atg19 mediates a dual interaction cargo sorting mechanism in selective autophagy.* Mol Biol Cell, 2007. **18**(3): p. 919-29.

183. Jager, S., et al., *Role for Rab7 in maturation of late autophagic vacuoles.* J Cell Sci, 2004. **117**(Pt 20): p. 4837-48.

184. Tanaka, Y., et al., *Accumulation of autophagic vacuoles and cardiomyopathy in LAMP-2-deficient mice.* Nature, 2000. **406**(6798): p. 902-6.

185. Tanida, I., et al., *Lysosomal turnover, but not a cellular level, of endogenous LC3 is a marker for autophagy.* Autophagy, 2005. **1**(2): p. 84-91.

186. Bohley, P. and P.O. Seglen, *Proteases and proteolysis in the lysosome.* Experientia, 1992. **48**(2): p. 151-7.

187. Maiuri, M.C., et al., *Self-eating and self-killing: crosstalk between autophagy and apoptosis.* Nat Rev Mol Cell Biol, 2007. **8**(9): p. 741-52.

188. Marino, G., et al., *Self-consumption: the interplay of autophagy and apoptosis.* Nat Rev Mol Cell Biol, 2014. **15**(2): p. 81-94.

189. Booth, L.A., et al., *The role of cell signalling in the crosstalk between autophagy and apoptosis.* Cell Signal, 2014. **26**(3): p. 549-55.

190. Eisenberg-Lerner, A., et al., *Life and death partners: apoptosis, autophagy and the cross-talk between them.* Cell Death Differ, 2009. **16**(7): p. 966-75.

191. Youle, R.J. and D.P. Narendra, *Mechanisms of mitophagy.* Nat Rev Mol Cell Biol, 2011. **12**(1): p.

9-14.

192. Geisler, S., et al., *PINK1/Parkin-mediated mitophagy is dependent on VDAC1 and p62/SQSTM1.* Nat Cell Biol, 2010. **12**(2): p. 119-31.

193. Pyo, J.O., et al., *Essential roles of Atg5 and FADD in autophagic cell death: dissection of autophagic cell death into vacuole formation and cell death.* Journal of Biological Chemistry, 2015. **280**(21): p. 20722-20729.

194. Hou, W., et al., *Autophagic degradation of active caspase-8: A crosstalk mechanism between autophagy and apoptosis.* Autophagy, 2010. **6**(7): p. 891.

195. Amir, M., et al., *Inhibition of hepatocyte autophagy increases tumor necrosis factor-dependent liver injury by promoting caspase-8 activation.* Cell Death & Differentiation, 2013. **20**(7): p. 878-887.

196. Zhang, Y.B., W. Zhao, and R.X. Zeng, *Autophagic degradation of caspase-8 protects U87MG cells against H2O2-induced oxidative stress.* Asian Pac J Cancer Prev, 2013. **14**(7): p. 4095-9.

197. Rubinstein, A., et al., *The Autophagy Protein Atg12 Associates with Antiapoptotic Bcl-2 Family Members to Promote Mitochondrial Apoptosis.* Molecular Cell, 2011. **44**(5): p. 698-709.

198. Yousefi, S., et al., *Calpain-mediated cleavage of Atg5 switches autophagy to apoptosis.* Nat Cell Biol, 2006. **8**(10): p. 1124-32.

199. Betin, V.M. and J.D. Lane, *Caspase cleavage of Atg4D stimulates GABARAP-L1 processing and triggers mitochondrial targeting and apoptosis.* J Cell Sci, 2009. **122**(Pt 14): p. 2554-66.

200. Betin, V.M., et al., *A cryptic mitochondrial targeting motif in Atg4D links caspase cleavage with mitochondrial import and oxidative stress.* Autophagy, 2012. **8**(4): p. 664-76.

201. Young, M.M., et al., *Autophagosomal membrane serves as platform for intracellular death-*

inducing signaling complex (iDISC)-mediated caspase-8 activation and apoptosis. J Biol Chem, 2012. **287**(15): p. 12455-68.

202. Iurlaro, R. and C. Munoz-Pinedo, *Cell death induced by endoplasmic reticulum stress.* Febs j, 2016. **283**(14): p. 2640-52.

203. Pan, J.A., et al., *Inhibition of protein degradation induces apoptosis through a microtubule-associated protein 1 light chain 3-mediated activation of caspase-8 at intracellular membranes.* Mol Cell Biol, 2011. **31**(15): p. 3158-70.

204. Laussmann, M.A., et al., *Proteasome inhibition can induce an autophagy-dependent apical activation of caspase-8.* Cell Death Differ, 2011. **18**(10): p. 1584-97.

205. Zhang, Y.B., et al., *Autophagy protein p62/SQSTM1 is involved in HAMLET-induced cell death by modulating apotosis in U87MG cells.* Cell Death Dis, 2013. **4**: p. e550.

206. Tomar, D., et al., *TRIM13 regulates caspase-8 ubiquitination, translocation to autophagosomes and activation during ER stress induced cell death.* Biochim Biophys Acta, 2013. **1833**(12): p. 3134-3144.

207. Pyo, J.O., et al., *Essential roles of Atg5 and FADD in autophagic cell death: dissection of autophagic cell death into vacuole formation and cell death.* J Biol Chem, 2005. **280**(21): p. 20722-9.

208. Huang, S., et al., *p62/sequestosome-1 up-regulation promotes ABT-263-induced caspase-8 aggregation/activation on the autophagosome.* J Biol Chem, 2013. **288**(47): p. 33654-66.

209. Kang, R., et al., *The Beclin 1 network regulates autophagy and apoptosis.* Cell Death Differ, 2011. **18**(4): p. 571-80.

210. Pattingre, S., et al., *Bcl-2 Antiapoptotic Proteins Inhibit Beclin 1-Dependent Autophagy.* Cell,

2005. **122**(6): p. 927-939.

211. Maiuri, M.C., et al., *Maiuri, M. C. et al. Functional and physical interaction between Bcl-X(L) and a BH3-like domain in Beclin-1. EMBO J. 26, 2527-2539.* Embo Journal, 2007. **26**(10): p. 2527-2539.

212. Wei, Y., et al., *JNK1-Mediated Phosphorylation of Bcl-2 Regulates Starvation-Induced Autophagy.* Molecular Cell, 2008. **30**(6): p. 678-688.

213. Wirawan, E., et al., *Caspase-mediated cleavage of Beclin-1 inactivates Beclin-1-induced autophagy and enhances apoptosis by promoting the release of proapoptotic factors from mitochondria.* Cell Death & Disease, 2010. **1**(1): p. e18.

214. Luo, S. and D.C. Rubinsztein, *Apoptosis blocks Beclin 1-dependent autophagosome synthesis: an effect rescued by Bcl-xL.* Cell Death & Differentiation, 2010. **17**(2): p. 268-277.

215. Oral, O., et al., *Cleavage of Atg3 protein by caspase-8 regulates autophagy during receptor-activated cell death.* Apoptosis, 2012. **17**(8): p. 810-820.

216. Pagliarini, V., et al., *Proteolysis of Ambra1 during apoptosis has a role in the inhibition of the autophagic pro-survival response.* Cell Death & Differentiation, 2012. **8**(8): p. 1255-1257.

217. Ren, T., et al., *HTLV-2 Tax immortalizes human CD4+ memory T lymphocytes by oncogenic activation and dysregulation of autophagy.* J Biol Chem, 2012. **287**(41): p. 34683-93.

218. Rossman, J.S. and R.A. Lamb, *Autophagy, apoptosis, and the influenza virus M2 protein.* Cell Host Microbe, 2009. **6**(4): p. 299-300.

219. Kim, S.J., et al., *Hepatitis C virus triggers mitochondrial fission and attenuates apoptosis to promote viral persistence.* Proc Natl Acad Sci U S A, 2014. **111**(17): p. 6413-8.

220. Denizot, M., et al., *HIV-1 gp41 fusogenic function triggers autophagy in uninfected cells.*

Autophagy, 2008. **4**(8): p. 998-1008.

221. Borel, S., L. Espert, and M. Biard-Piechaczyk, *Macroautophagy Regulation during HIV-1 Infection of CD4+ T Cells and Macrophages.* Front Immunol, 2012. **3**: p. 97.

222. Espert, L., et al., *Differential role of autophagy in CD4 T cells and macrophages during X4 and R5 HIV-1 infection.* PLoS One, 2009. **4**(6): p. e5787.

223. Ouyang, L., et al., *Programmed cell death pathways in cancer: a review of apoptosis, autophagy and programmed necrosis.* Cell Prolif, 2012. **45**(6): p. 487-98.

224. Rohn, T.T., et al., *Depletion of Beclin-1 Due to Proteolytic Cleavage by Caspases in the Alzheimer's Disease Brain*. 2011. 68-78.

225. Espert, L., et al., *Autophagy is involved in T cell death after binding of HIV-1 envelope proteins to CXCR4.* Journal of Clinical Investigation, 2006. **116**(8): p. 2161.

226. Corcelle, E.A., P. Puustinen, and M. Jäättelä, *Apoptosis and autophagy: Targeting autophagy signalling in cancer cells -'trick or treats'?* Febs Journal, 2010. **276**(21): p. 6084-6096.

227. Mao, K. and D.J. Klionsky, *Xenophagy: A battlefield between host and microbe, and a possible avenue for cancer treatment.* Autophagy, 2017. **13**(2): p. 223-224.

228. Bauckman, K.A., N. Owusu-Boaitey, and I.U. Mysorekar, *Selective autophagy: xenophagy.* Methods, 2015. **75**: p. 120-7.

229. Talloczy, Z., H.W.t. Virgin, and B. Levine, *PKR-dependent autophagic degradation of herpes simplex virus type 1.* Autophagy, 2006. **2**(1): p. 24-9.

230. Alexander, D.E. and D.A. Leib, *Xenophagy in herpes simplex virus replication and pathogenesis.* Autophagy, 2008. **4**(1): p. 101-3.

231. Orvedahl, A., et al., *HSV-1 ICP34.5 confers neurovirulence by targeting the Beclin 1 autophagy*

protein. Cell Host Microbe, 2007. **1**(1): p. 23-35.

232. Deretic, V., *Autophagy: an emerging immunological paradigm.* J Immunol, 2012. **189**(1): p. 15-20.

233. Orvedahl, A., et al., *Autophagy protects against Sindbis virus infection of the central nervous system.* Cell Host Microbe, 2010. **7**(2): p. 115-27.

234. Sagnier, S., et al., *Autophagy Restricts HIV-1 Infection by Selectively Degrading Tat in CD4+ T Lymphocytes.* Journal of Virology, 2015. **89**(1): p. 615-25.

235. Brennan, K. and A.G. Bowie, *Activation of host pattern recognition receptors by viruses.* Current Opinion in Microbiology, 2010. **13**(4): p. 503-507.

236. Brubaker, S.W., et al., *Innate immune pattern recognition: a cell biological perspective.* Annual review of immunology, 2015. **33**: p. 257-290.

237. Lester, S.N. and K. Li, *Toll-like receptors in antiviral innate immunity.* J Mol Biol, 2014. **426**(6): p. 1246-64.

238. Lee, M.S. and Y.J. Kim, *Signaling pathways downstream of pattern-recognition receptors and their cross talk.* Annu Rev Biochem, 2007. **76**: p. 447-80.

239. Iwasaki, A., *Role of autophagy in innate viral recognition.* Autophagy, 2007. **3**(4): p. 354-6.

240. Lee, H.K., et al., *Autophagy-dependent viral recognition by plasmacytoid dendritic cells.* Science, 2007. **315**(5817): p. 1398-401.

241. Henault, J., et al., *Noncanonical autophagy is required for type I interferon secretion in response to DNA-immune complexes.* Immunity, 2012. **37**(6): p. 986-997.

242. Manuse, M.J., C.M. Briggs, and G.D. Parks, *Replication-independent activation of human plasmacytoid dendritic cells by the paramyxovirus SV5 Requires TLR7 and autophagy pathways.*

Virology, 2010. **405**(2): p. 383-9.

243. Munz, C., *Autophagy proteins in antigen processing for presentation on MHC molecules.* Immunol Rev, 2016. **272**(1): p. 17-27.

244. Munz, C., *Antigen processing by macroautophagy for MHC presentation.* Front Immunol, 2011. **2**: p. 42.

245. Paludan, C., et al., *Endogenous MHC class II processing of a viral nuclear antigen after autophagy.* Science, 2005. **307**(5709): p. 593-6.

246. Rock, K.L., E. Reits, and J. Neefjes, *Present Yourself! By MHC Class I and MHC Class II Molecules.* Trends Immunol, 2016. **37**(11): p. 724-737.

247. Leung, C.S. and G.S. Taylor, *Nuclear shelter: the influence of subcellular location on the processing of antigens by macroautophagy.* Autophagy, 2010. **6**(4): p. 560-1.

248. English, L., et al., *Autophagy enhances the presentation of endogenous viral antigens on MHC class I molecules during HSV-1 infection.* Autophagy, 2009. **10**(7): p. 480-487.

249. Schmid, D., M. Pypaert, and C. Munz, *Antigen-loading compartments for major histocompatibility complex class II molecules continuously receive input from autophagosomes.* Immunity, 2007. **26**(1): p. 79-92.

250. Liang, X.H., et al., *Protection against Fatal Sindbis Virus Encephalitis by Beclin, a Novel Bcl-2-Interacting Protein.* Journal of Virology, 1998. **72**(11): p. 8586.

251. Shelly, S., et al., *Autophagy is an essential component of Drosophila immunity against vesicular stomatitis virus.* Immunity, 2009. **30**(4): p. 588-98.

252. Liu, Y., et al., *Autophagy regulates programmed cell death during the plant innate immune response.* Cell, 2005. **121**(4): p. 567-577.

253. Sharma, M., et al., *Japanese encephalitis virus replication is negatively regulated by autophagy and occurs on LC3-I- and EDEM1-containing membranes.* Autophagy, 2014. **10**(9): p. 1637-1651.

254. Sir, D. and J.H. Ou, *Autophagy in viral replication and pathogenesis.* Mol Cells, 2010. **29**(1): p. 1-7.

255. Kirkegaard, K., *Subversion of the cellular autophagy pathway by viruses.* Curr Top Microbiol Immunol, 2009. **335**: p. 323-33.

256. Paul, P. and C. Münz, *Autophagy and Mammalian Viruses: Roles in Immune Response, Viral Replication, and Beyond.* Advances in Virus Research, 2016. **95**: p. 149.

257. Chiramel, A.I., N.R. Brady, and R. Bartenschlager, *Divergent Roles of Autophagy in Virus Infection.* Cells, 2013. **2**(1): p. 83-104.

258. Jackson, W.T., *Viruses and the autophagy pathway.* Virology, 2015. **480**: p. 450-6.

259. Liang, C., E. X, and J.U. Jung, *Downregulation of autophagy by herpesvirus Bcl-2 homologs.* Autophagy, 2008. **4**(3): p. 268-272.

260. Ku, B., et al., *Structural and Biochemical Bases for the Inhibition of Autophagy and Apoptosis by Viral BCL-2 of Murine γ-Herpesvirus 68.* Plos Pathogens, 2008. **4**(2): p. 239-242.

261. Lee, J.S., et al., *FLIP-mediated autophagy regulation in cell death control.* Nat Cell Biol, 2009. **11**(11): p. 1355-62.

262. Miller, S. and J. Krijnse-Locker, *Modification of intracellular membrane structures for virus replication.* Nat Rev Microbiol, 2008. **6**(5): p. 363-74.

263. Dales, S., et al., *ELECTRON MICROSCOPIC STUDY OF THE FORMATION OF POLIOVIRUS.* Virology, 1965. **26**: p. 379-89.

264. Schlegel, A., et al., *Cellular origin and ultrastructure of membranes induced during poliovirus*

infection. J Virol, 1996. **70**(10): p. 6576-88.

265. O'Donnell, V., et al., *Foot-and-mouth disease virus utilizes an autophagic pathway during viral replication.* Virology, 2011. **410**(1): p. 142-50.

266. Wong, J., et al., *Autophagosome supports coxsackievirus B3 replication in host cells.* J Virol, 2008. **82**(18): p. 9143-53.

267. Klein, K.A. and W.T. Jackson, *Picornavirus subversion of the autophagy pathway.* Viruses, 2011. **3**(9): p. 1549-61.

268. Sir, D., et al., *Replication of hepatitis C virus RNA on autophagosomal membranes.* J Biol Chem, 2012. **287**(22): p. 18036-43.

269. Wang, L., Y. Tian, and J.H. Ou, *HCV induces the expression of Rubicon and UVRAG to temporally regulate the maturation of autophagosomes and viral replication.* PLoS Pathog, 2015. **11**(3): p. e1004764.

270. Dreux, M., et al., *The Autophagy Machinery Is Required to Initiate Hepatitis C Virus Replication.* Proceedings of the National Academy of Sciences of the United States of America, 2009. **106**(33): p. 14046-14051.

271. Metz, P., et al., *Dengue Virus Inhibition of Autophagic Flux and Dependency of Viral Replication on Proteasomal Degradation of the Autophagy Receptor p62.* J Virol, 2015. **89**(15): p. 8026-41.

272. Beale, R., et al., *A LC3-interacting motif in the influenza A virus M2 protein is required to subvert autophagy and maintain virion stability.* Cell Host Microbe, 2014. **15**(2): p. 239-47.

273. Ren, Y., et al., *Proton Channel Activity of Influenza A Virus Matrix Protein 2 Contributes to Autophagy Arrest.* J Virol, 2016. **90**(1): p. 591-8.

274. Dinkins, C., M. Pilli, and J.H. Kehrl, *Roles of autophagy in HIV infection.* Immunol Cell Biol, 2015.

93(1): p. 11-7.

275. Nardacci, R., et al., *Role of autophagy in HIV infection and pathogenesis.* J Intern Med, 2017. **281**(5): p. 422-432.

276. Killian, M.S., *Dual role of autophagy in HIV-1 replication and pathogenesis.* AIDS Res Ther, 2012. **9**(1): p. 16.

277. Van Grol, J., et al., *HIV-1 inhibits autophagy in bystander macrophage/monocytic cells through Src-Akt and STAT3.* PLoS One, 2010. **5**(7): p. e11733.

278. Campbell, G.R., et al., *Human Immunodeficiency Virus Type 1 Nef Inhibits Autophagy through Transcription Factor EB Sequestration.* PLoS Pathog, 2015. **11**(6): p. e1005018.

279. Shoji-Kawata, S., et al., *Identification of a candidate therapeutic autophagy-inducing peptide.* Nature, 2013. **494**(7436): p. 201-6.

280. Kyei, G.B., et al., *Autophagy pathway intersects with HIV-1 biosynthesis and regulates viral yields in macrophages.* Journal of Cell Biology, 2009. **186**(2): p. 255-68.

281. Zhou, D. and S.A. Spector, *Human immunodeficiency virus type-1 infection inhibits autophagy.* Aids, 2008. **22**(6): p. 695-9.

282. Boccaletto, P., et al., *MODOMICS: a database of RNA modification pathways. 2017 update.* Nucleic Acids Res, 2018. **46**(D1): p. D303-d307.

283. Helm, M. and Y. Motorin, *Detecting RNA modifications in the epitranscriptome: predict and validate.* Nat Rev Genet, 2017. **18**(5): p. 275-291.

284. Karijolich, J. and Y.T. Yu, *The new era of RNA modification.* Rna, 2015. **21**(4): p. 659-60.

285. Li, S. and C.E. Mason, *The pivotal regulatory landscape of RNA modifications.* Annu Rev Genomics Hum Genet, 2014. **15**: p. 127-50.

286. Squires, J.E., et al., *Widespread occurrence of 5-methylcytosine in human coding and non-coding RNA.* Nucleic Acids Res, 2012. **40**(11): p. 5023-33.

287. Li, X., et al., *Transcriptome-wide mapping reveals reversible and dynamic N(1)-methyladenosine methylome.* Nat Chem Biol, 2016. **12**(5): p. 311-6.

288. Meyer, K.D. and S.R. Jaffrey, *The dynamic epitranscriptome: N6-methyladenosine and gene expression control.* Nat Rev Mol Cell Biol, 2014. **15**(5): p. 313-26.

289. Iwanami, Y. and G.M. Brown, *Methylated bases of transfer ribonucleic acid from HeLa and L cells.* Arch Biochem Biophys, 1968. **124**(1): p. 472-82.

290. Iwanami, Y. and G.M. Brown, *Methylated bases of ribosomal ribonucleic acid from HeLa cells.* Arch Biochem Biophys, 1968. **126**(1): p. 8-15.

291. Adams, J.M. and S. Cory, *Modified nucleosides and bizarre 5'-termini in mouse myeloma mRNA.* Nature, 1975. **255**(5503): p. 28-33.

292. Desrosiers, R., K. Friderici, and F. Rottman, *Identification of methylated nucleosides in messenger RNA from Novikoff hepatoma cells.* Proc Natl Acad Sci U S A, 1974. **71**(10): p. 3971-5.

293. Desrosiers, R.C., K.H. Friderici, and F.M. Rottman, *Characterization of Novikoff hepatoma mRNA methylation and heterogeneity in the methylated 5' terminus.* Biochemistry, 1975. **14**(20): p. 4367-74.

294. Meyer, K.D., et al., *Comprehensive analysis of mRNA methylation reveals enrichment in 3' UTRs and near stop codons.* Cell, 2012. **149**(7): p. 1635-46.

295. Wan, Y., et al., *Transcriptome-wide high-throughput deep m(6)A-seq reveals unique differential m(6)A methylation patterns between three organs in Arabidopsis thaliana.* Genome Biol, 2015.

16: p. 272.

296. Krug, R.M., M.A. Morgan, and A.J. Shatkin, *Influenza viral mRNA contains internal N6-methyladenosine and 5'-terminal 7-methylguanosine in cap structures.* J Virol, 1976. **20**(1): p. 45-53.

297. Zhao, B.S., I.A. Roundtree, and C. He, *Post-transcriptional gene regulation by mRNA modifications.* Nat Rev Mol Cell Biol, 2017. **18**(1): p. 31-42.

298. Batista, P.J., *The RNA Modification N(6)-methyladenosine and Its Implications in Human Disease.* Genomics Proteomics Bioinformatics, 2017. **15**(3): p. 154-163.

299. Maity, A. and B. Das, *N6-methyladenosine modification in mRNA: machinery, function and implications for health and diseases.* 2016. **283**(9): p. 1607-30.

300. Linder, B., et al., *Single-nucleotide-resolution mapping of m6A and m6Am throughout the transcriptome.* Nat Methods, 2015. **12**(8): p. 767-72.

301. Horowitz, S., et al., *Mapping of N6-methyladenosine residues in bovine prolactin mRNA.* Proc Natl Acad Sci U S A, 1984. **81**(18): p. 5667-71.

302. Bokar, J.A., et al., *Characterization and partial purification of mRNA N6-adenosine methyltransferase from HeLa cell nuclei. Internal mRNA methylation requires a multisubunit complex.* J Biol Chem, 1994. **269**(26): p. 17697-704.

303. Bokar, J.A., et al., *Purification and cDNA cloning of the AdoMet-binding subunit of the human mRNA (N6-adenosine)-methyltransferase.* Rna, 1997. **3**(11): p. 1233-47.

304. Liu, J., et al., *A METTL3-METTL14 complex mediates mammalian nuclear RNA N6-adenosine methylation.* Nat Chem Biol, 2014. **10**(2): p. 93-5.

305. Patil, D.P., et al., *m(6)A RNA methylation promotes XIST-mediated transcriptional repression.*

Nature, 2016. **537**(7620): p. 369-373.

306. Ping, X.L., et al., *Mammalian WTAP is a regulatory subunit of the RNA N6-methyladenosine methyltransferase.* Cell Res, 2014. **24**(2): p. 177-89.

307. Schwartz, S., et al., *Perturbation of m6A writers reveals two distinct classes of mRNA methylation at internal and 5' sites.* Cell Rep, 2014. **8**(1): p. 284-96.

308. Scholler, E., et al., *Interactions, localization, and phosphorylation of the m(6)A generating METTL3-METTL14-WTAP complex.* Rna, 2018. **24**(4): p. 499-512.

309. Wang, X., et al., *Structural basis of N(6)-adenosine methylation by the METTL3-METTL14 complex.* Nature, 2016. **534**(7608): p. 575-8.

310. Wang, P., K.A. Doxtader, and Y. Nam, *Structural Basis for Cooperative Function of Mettl3 and Mettl14 Methyltransferases.* Mol Cell, 2016. **63**(2): p. 306-317.

311. Yue, Y., J. Liu, and C. He, *RNA N6-methyladenosine methylation in post-transcriptional gene expression regulation.* Genes Dev, 2015. **29**(13): p. 1343-55.

312. Gokhale, N.S., et al., *N6-Methyladenosine in Flaviviridae Viral RNA Genomes Regulates Infection.* Cell Host Microbe, 2016. **20**(5): p. 654-665.

313. Lichinchi, G., et al., *Dynamics of Human and Viral RNA Methylation during Zika Virus Infection.* Cell Host Microbe, 2016. **20**(5): p. 666-673.

314. Lin, S., et al., *The m(6)A Methyltransferase METTL3 Promotes Translation in Human Cancer Cells.* Mol Cell, 2016. **62**(3): p. 335-345.

315. Zheng, G., et al., *Sprouts of RNA epigenetics: the discovery of mammalian RNA demethylases.* RNA Biol, 2013. **10**(6): p. 915-8.

316. Jia, G., et al., *N6-methyladenosine in nuclear RNA is a major substrate of the obesity-associated*

FTO. Nat Chem Biol, 2011. **7**(12): p. 885-7.

317. Loos, R.J. and G.S. Yeo, *The bigger picture of FTO: the first GWAS-identified obesity gene.* Nat Rev Endocrinol, 2014. **10**(1): p. 51-61.

318. Fu, Y., et al., *FTO-mediated formation of N6-hydroxymethyladenosine and N6-formyladenosine in mammalian RNA.* Nat Commun, 2013. **4**: p. 1798.

319. Hess, M.E., et al., *The fat mass and obesity associated gene (Fto) regulates activity of the dopaminergic midbrain circuitry.* Nat Neurosci, 2013. **16**(8): p. 1042-8.

320. Mauer, J., et al., *Reversible methylation of m(6)Am in the 5' cap controls mRNA stability.* Nature, 2017. **541**(7637): p. 371-375.

321. Wei, C., A. Gershowitz, and B. Moss, *N6, O2'-dimethyladenosine a novel methylated ribonucleoside next to the 5' terminal of animal cell and virus mRNAs.* Nature, 1975. **257**(5523): p. 251-3.

322. Keith, J.M., M.J. Ensinger, and B. Mose, *HeLa cell RNA (2'-O-methyladenosine-N6-)-methyltransferase specific for the capped 5'-end of messenger RNA.* J Biol Chem, 1978. **253**(14): p. 5033-9.

323. Zheng, G., et al., *ALKBH5 is a mammalian RNA demethylase that impacts RNA metabolism and mouse fertility.* Mol Cell, 2013. **49**(1): p. 18-29.

324. Tang, C., et al., *ALKBH5-dependent m6A demethylation controls splicing and stability of long 3'-UTR mRNAs in male germ cells.* Proc Natl Acad Sci U S A, 2018. **115**(2): p. E325-e333.

325. Xu, C., et al., *Structural basis for selective binding of m6A RNA by the YTHDC1 YTH domain.* Nat Chem Biol, 2014. **10**(11): p. 927-9.

326. Wang, X., et al., *N(6)-methyladenosine Modulates Messenger RNA Translation Efficiency.* Cell,

2015. **161**(6): p. 1388-99.

327. Theler, D., et al., *Solution structure of the YTH domain in complex with N6-methyladenosine RNA: a reader of methylated RNA.* Nucleic Acids Res, 2014. **42**(22): p. 13911-9.

328. Luo, S. and L. Tong, *Molecular basis for the recognition of methylated adenines in RNA by the eukaryotic YTH domain.* Proc Natl Acad Sci U S A, 2014. **111**(38): p. 13834-9.

329. Li, M., et al., *Ythdf2-mediated m(6)A mRNA clearance modulates neural development in mice.* 2018. **19**(1): p. 69.

330. Zhao, B.S., et al., *m(6)A-dependent maternal mRNA clearance facilitates zebrafish maternal-to-zygotic transition.* Nature, 2017. **542**(7642): p. 475-478.

331. Du, H., et al., *YTHDF2 destabilizes m(6)A-containing RNA through direct recruitment of the CCR4-NOT deadenylase complex.* Nat Commun, 2016. **7**: p. 12626.

332. Li, A., et al., *Cytoplasmic m(6)A reader YTHDF3 promotes mRNA translation.* Cell Res, 2017. **27**(3): p. 444-447.

333. Hsu, P.J., et al., *Ythdc2 is an N(6)-methyladenosine binding protein that regulates mammalian spermatogenesis.* Cell Res, 2017. **27**(9): p. 1115-1127.

334. Roundtree, I.A., et al., *YTHDC1 mediates nuclear export of N(6)-methyladenosine methylated mRNAs.* 2017. **6**.

335. Kasowitz, S.D., J. Ma, and S.J. Anderson, *Nuclear m6A reader YTHDC1 regulates alternative polyadenylation and splicing during mouse oocyte development.* 2018. **14**(5): p. e1007412.

336. Wojtas, M.N., et al., *Regulation of m(6)A Transcripts by the 3'-->5' RNA Helicase YTHDC2 Is Essential for a Successful Meiotic Program in the Mammalian Germline.* Mol Cell, 2017. **68**(2): p. 374-387.e12.

337. Bailey, A.S. and P.J. Batista, *The conserved RNA helicase YTHDC2 regulates the transition from proliferation to differentiation in the germline.* 2017. **6**.

338. Haussmann, I.U., et al., *m(6)A potentiates Sxl alternative pre-mRNA splicing for robust Drosophila sex determination.* Nature, 2016. **540**(7632): p. 301-304.

339. Lence, T., et al., *m(6)A modulates neuronal functions and sex determination in Drosophila.* Nature, 2016. **540**(7632): p. 242-247.

340. Zhou, K.I., et al., *N(6)-Methyladenosine Modification in a Long Noncoding RNA Hairpin Predisposes Its Conformation to Protein Binding.* J Mol Biol, 2016. **428**(5 Pt A): p. 822-833.

341. Zhou, J., et al., *Dynamic m(6)A mRNA methylation directs translational control of heat shock response.* Nature, 2015. **526**(7574): p. 591-4.

342. Meyer, K.D., et al., *5' UTR m(6)A Promotes Cap-Independent Translation.* Cell, 2015. **163**(4): p. 999-1010.

343. Fry, N.J., et al., *N(6)-methyladenosine is required for the hypoxic stabilization of specific mRNAs.* 2017. **23**(9): p. 1444-1455.

344. Dai, D., et al., *N6-methyladenosine links RNA metabolism to cancer progression.* Cell Death Dis, 2018. **9**(2): p. 124.

345. Batista, P.J., et al., *m(6)A RNA modification controls cell fate transition in mammalian embryonic stem cells.* Cell Stem Cell, 2014. **15**(6): p. 707-19.

346. Yoon, K.J., et al., *Temporal Control of Mammalian Cortical Neurogenesis by m(6)A Methylation.* Cell, 2017. **171**(4): p. 877-889.e17.

347. Hastings, M.H., *m(6)A mRNA methylation: a new circadian pacesetter.* Cell, 2013. **155**(4): p. 740-1.

348. Fustin, J.M., et al., *RNA-methylation-dependent RNA processing controls the speed of the circadian clock.* Cell, 2013. **155**(4): p. 793-806.

349. Luo, G.Z., et al., *Unique features of the m6A methylome in Arabidopsis thaliana.* Nat Commun, 2014. **5**: p. 5630.

350. Arribas-Hernandez, L. and S. Bressendorff, *An m(6)A-YTH Module Controls Developmental Timing and Morphogenesis in Arabidopsis.* 2018. **30**(5): p. 952-967.

351. Qi, S.T., et al., *N6-Methyladenosine Sequencing Highlights the Involvement of mRNA Methylation in Oocyte Meiotic Maturation and Embryo Development by Regulating Translation in Xenopus laevis.* J Biol Chem, 2016. **291**(44): p. 23020-23026.

352. Ivanova, I., et al., *The RNA m(6)A Reader YTHDF2 Is Essential for the Post-transcriptional Regulation of the Maternal Transcriptome and Oocyte Competence.* Mol Cell, 2017. **67**(6): p. 1059-1067.e4.

353. Xu, K., et al., *Mettl3-mediated m(6)A regulates spermatogonial differentiation and meiosis initiation.* Cell Res, 2017. **27**(9): p. 1100-1114.

354. Xiang, Y., et al., *RNA m(6)A methylation regulates the ultraviolet-induced DNA damage response.* Nature, 2017. **543**(7646): p. 573-576.

355. Zhang, C., et al., *Hypoxia induces the breast cancer stem cell phenotype by HIF-dependent and ALKBH5-mediated m(6)A-demethylation of NANOG mRNA.* Proc Natl Acad Sci U S A, 2016. **113**(14): p. E2047-56.

356. Cui, Q., et al., *m(6)A RNA Methylation Regulates the Self-Renewal and Tumorigenesis of Glioblastoma Stem Cells.* Cell Rep, 2017. **18**(11): p. 2622-2634.

357. Zhang, S., et al., *m(6)A Demethylase ALKBH5 Maintains Tumorigenicity of Glioblastoma Stem-*

like Cells by Sustaining FOXM1 Expression and Cell Proliferation Program. Cancer Cell, 2017. **31**(4): p. 591-606.e6.

358. Deng, X., et al., *RNA N(6)-methyladenosine modification in cancers: current status and perspectives.* 2018. **28**(5): p. 507-517.

359. Li, Z., et al., *FTO Plays an Oncogenic Role in Acute Myeloid Leukemia as a N(6)-Methyladenosine RNA Demethylase.* Cancer Cell, 2017. **31**(1): p. 127-141.

360. Riquelme-Barrios, S., et al., *Emerging Roles of N(6)-Methyladenosine on HIV-1 RNA Metabolism and Viral Replication.* Front Microbiol, 2018. **9**: p. 576.

361. Kennedy, E.M., et al., *Posttranscriptional m(6)A Editing of HIV-1 mRNAs Enhances Viral Gene Expression.* Cell Host Microbe, 2016. **19**(5): p. 675-85.

362. Gonzales-van Horn, S.R. and P. Sarnow, *Making the Mark: The Role of Adenosine Modifications in the Life Cycle of RNA Viruses.* Cell Host Microbe, 2017. **21**(6): p. 661-669.

363. Narayan, P., et al., *Unequal distribution of N6-methyladenosine in influenza virus mRNAs.* Mol Cell Biol, 1987. **7**(4): p. 1572-5.

364. Courtney, D.G., et al., *Epitranscriptomic Enhancement of Influenza A Virus Gene Expression and Replication.* Cell Host Microbe, 2017. **22**(3): p. 377-386.e5.

365. Ye, F., *RNA N(6)-adenosine methylation (m(6)A) steers epitranscriptomic control of herpesvirus replication.* Inflamm Cell Signal, 2017. **4**(3).

366. Hesser, C.R. and J. Karijolich, *N6-methyladenosine modification and the YTHDF2 reader protein play cell type specific roles in lytic viral gene expression during Kaposi's sarcoma-associated herpesvirus infection.* 2018. **14**(4): p. e1006995.

367. Tan, B., et al., *Viral and cellular N(6)-methyladenosine and N(6),2'-O-dimethyladenosine*

epitranscriptomes in the KSHV life cycle. 2018. **3**(1): p. 108-120.

368. Canaani, D., et al., *Identification and mapping of N6-methyladenosine containing sequences in simian virus 40 RNA.* Nucleic Acids Res, 1979. **6**(8): p. 2879-99.

369. Tsai, K., D.G. Courtney, and B.R. Cullen, *Addition of m6A to SV40 late mRNAs enhances viral structural gene expression and replication.* 2018. **14**(2): p. e1006919.

370. Lichinchi, G., et al., *Dynamics of the human and viral m(6)A RNA methylomes during HIV-1 infection of T cells.* 2016. **1**: p. 16011.

371. Tirumuru, N., et al., *N(6)-methyladenosine of HIV-1 RNA regulates viral infection and HIV-1 Gag protein expression.* 2016. **5**.

372. Thomason, A.R., et al., *Methylation of high-molecular-weight subunit RNA of feline leukemia virus.* J Virol, 1976. **20**(1): p. 123-32.

373. Kane, S.E. and K. Beemon, *Precise localization of m6A in Rous sarcoma virus RNA reveals clustering of methylation sites: implications for RNA processing.* Mol Cell Biol, 1985. **5**(9): p. 2298-306.

374. Beemon, K. and J. Keith, *Localization of N6-methyladenosine in the Rous sarcoma virus genome.* J Mol Biol, 1977. **113**(1): p. 165-79.

375. Stoltzfus, C.M. and R.W. Dane, *Accumulation of spliced avian retrovirus mRNA is inhibited in S-adenosylmethionine-depleted chicken embryo fibroblasts.* J Virol, 1982. **42**(3): p. 918-31.

376. Finkel, D. and Y. Groner, *Methylations of adenosine residues (m6A) in pre-mRNA are important for formation of late simian virus 40 mRNAs.* Virology, 1983. **131**(2): p. 409-25.

377. Chen-Kiang, S., J.R. Nevins, and J.E. Darnell, Jr., *N-6-methyl-adenosine in adenovirus type 2 nuclear RNA is conserved in the formation of messenger RNA.* J Mol Biol, 1979. **135**(3): p. 733-

52.

378. Lu, W., et al., *N(6)-methyladenosine-binding proteins suppress HIV-1 infectivity and viral production.* 2018.

379. Toro-Ascuy, D., et al., *Interactions between the HIV-1 Unspliced mRNA and Host mRNA Decay Machineries.* Viruses, 2016. **8**(11).

380. Rosenblum, L.L., R.A. Weiss, and M.O. McClure, *Virus load and sequence variation in simian retrovirus type 2 infection.* J Virol, 2000. **74**(8): p. 3449-54.

381. Zao, C.L., et al., *Virological and serological characterization of SRV-4 infection in cynomolgus macaques.* Arch Virol, 2011. **156**(11): p. 2053-6.

382. Boden, D., et al., *Enhanced gene silencing of HIV-1 specific siRNA using microRNA designed hairpins.* Nucleic Acids Res, 2004. **32**(3): p. 1154-8.

383. Chang, K., et al., *Creating an miR30-based shRNA vector.* Cold Spring Harb Protoc, 2013. **2013**(7): p. 631-5.

384. Silva, J.M., et al., *Second-generation shRNA libraries covering the mouse and human genomes.* Nat Genet, 2005. **37**(11): p. 1281-8.

385. Guo, J., et al., *Spinoculation triggers dynamic actin and cofilin activity that facilitates HIV-1 infection of transformed and resting CD4 T cells.* J Virol, 2011. **85**(19): p. 9824-33.

386. O'Doherty, U., W.J. Swiggard, and M.H. Malim, *Human immunodeficiency virus type 1 spinoculation enhances infection through virus binding.* J Virol, 2000. **74**(21): p. 10074-80.

387. Weber, K., et al., *RGB marking with lentiviral vectors for multicolor clonal cell tracking.* Nat Protoc, 2012. **7**(5): p. 839-49.

388. Dominissini, D., et al., *Transcriptome-wide mapping of N(6)-methyladenosine by m(6)A-seq*

based on immunocapturing and massively parallel sequencing. Nat Protoc, 2013. **8**(1): p. 176-89.

389. Meng, J., et al., *Exome-based analysis for RNA epigenome sequencing data.* Bioinformatics, 2013. **29**(12): p. 1565-7.

390. Meng, J., et al., *A protocol for RNA methylation differential analysis with MeRIP-Seq data and exomePeak R/Bioconductor package.* Methods, 2014. **69**(3): p. 274-81.

391. Montiel, N.A., et al., *Effects of simian betaretrovirus serotype 1 (SRV1) infection on the differentiation of hematopoietic progenitor cells (CD34+) derived from bone marrow of rhesus macaques (Macaca mulatta).* Comp Med, 2012. **62**(1): p. 61-8.

392. Yeung, M.L., et al., *A genome-wide short hairpin RNA screening of jurkat T-cells for human proteins contributing to productive HIV-1 replication.* J Biol Chem, 2009. **284**(29): p. 19463-73.

393. Purvis, S.F., et al., *HIV type 1 Tat protein induces apoptosis and death in Jurkat cells.* AIDS Res Hum Retroviruses, 1995. **11**(4): p. 443-50.

394. Zao, C., et al. *An Unusual SRV/DT, SRV-4-Like Outbreak in Cynomolgus Monkeys in the United States*. in *JOURNAL OF THE AMERICAN ASSOCIATION FOR LABORATORY ANIMAL SCIENCE*. 2009. AMER ASSOC LABORATORY ANIMAL SCIENCE 9190 CRESTWYN HILLS DR, MEMPHIS, TN 38125 USA.

395. Okamoto, M., et al., *Emergence of infectious malignant thrombocytopenia in Japanese macaques (Macaca fuscata) by SRV-4 after transmission to a novel host.* Sci Rep, 2015. **5**: p. 8850.

396. Lerche, N.W., J. Yee, and M.B. Jennings, *Establishing specific retrovirus-free breeding colonies of macaques: an approach to primary screening and surveillance.* Laboratory animal science,

1994. **44**(3): p. 217-221.

397. Gautam, R., et al., *Vesicular stomatitis virus-simian retrovirus type 2 vaccine protects macaques from detectable infection and B-cell destruction.* J Virol, 2011. **85**(12): p. 5889-96.

398. Iskandriati, D., et al., *Isolation and characterization of simian retrovirus type D from Macaca fascicularis and M. nemestrina in Indonesia.* Microbiology Indonesia, 2010. **4**(3).

399. Lerche, N.W., J.L. Yee, and M.B. Jennings, *Establishing specific retrovirus-free breeding colonies of macaques: an approach to primary screening and surveillance.* Lab Anim Sci, 1994. **44**(3): p. 217-21.

400. Hara, M., et al., *Survey of captive cynomolgus macaque colonies for SRV/D infection using polymerase chain reaction assays.* Comparative medicine, 2005. **55**(2): p. 145-149.

401. Hara, M., et al., *Detection of SRV/D shedding in body fluids of cynomolgus macaques and comparison of partial gp70 sequences in SRV/D-T isolates.* Virus Genes, 2007. **35**(2): p. 281-8.

402. Sato, K., et al., *Experimental evaluation of the zoonotic infection potency of simian retrovirus type 4 using humanized mouse model.* Sci Rep, 2015. **5**: p. 14040.

403. Chung, H.K., et al., *Development of real-time PCR assays for quantitation of simian betaretrovirus serotype-1, -2, -3, and -5 viral DNA in Asian monkeys.* J Virol Methods, 2008. **152**(1-2): p. 91-7.

404. White, J.A., et al., *Development of a generic real-time PCR assay for simultaneous detection of proviral DNA of simian Betaretrovirus serotypes 1, 2, 3, 4 and 5 and secondary uniplex assays for specific serotype identification.* J Virol Methods, 2009. **162**(1-2): p. 148-54.

405. Toohey, K., et al., *Human immunodeficiency virus envelope V1 and V2 regions influence replication efficiency in macrophages by affecting virus spread.* Virology, 1995. **213**(1): p. 70-9.

406. York-Higgins, D., et al., *Human immunodeficiency virus type 1 cellular host range, replication, and cytopathicity are linked to the envelope region of the viral genome.* J Virol, 1990. **64**(8): p. 4016-20.

407. Mori, K., et al., *Complex determinants of macrophage tropism in env of simian immunodeficiency virus.* J Virol, 1992. **66**(4): p. 2067-75.

408. Rudensey, L.M., et al., *Progression to AIDS in macaques is associated with changes in the replication, tropism, and cytopathic properties of the simian immunodeficiency virus variant population.* Virology, 1995. **207**(2): p. 528-42.

409. Philipp-Staheli, J., et al., *Genetic variability of the envelope gene of Type D simian retrovirus-2 (SRV-2) subtypes associated with SAIDS-related retroperitoneal fibromatosis in different macaque species.* Virol J, 2006. **3**: p. 11.

410. Cianciolo, G.J., et al., *Inhibition of lymphocyte proliferation by a synthetic peptide homologous to retroviral envelope proteins.* Science, 1985. **230**(4724): p. 453-455.

411. Cianciolo, G.J., R.J. Kipnis, and R. Snyderman, *Similarity between p15E of murine and feline leukaemia viruses and p21 of HTLV.* Nature, 1984. **311**(5986): p. 515-515.

412. Deretic, V., T. Saitoh, and S. Akira, *Autophagy in infection, inflammation and immunity.* Nat Rev Immunol, 2013. **13**(10): p. 722-37.

413. Levine, B., N. Mizushima, and H.W. Virgin, *Autophagy in immunity and inflammation.* Nature, 2011. **469**(7330): p. 323-35.

414. Lussignol, M., et al., *The herpes simplex virus 1 Us11 protein inhibits autophagy through its interaction with the protein kinase PKR.* J Virol, 2013. **87**(2): p. 859-71.

415. Kyei, G.B., et al., *Autophagy pathway intersects with HIV-1 biosynthesis and regulates viral*

yields in macrophages. J Cell Biol, 2009. **186**(2): p. 255-68.

416. Wang, X., et al., *HIV-1 and HIV-2 infections induce autophagy in Jurkat and CD4+ T cells.* Cell Signal, 2012. **24**(7): p. 1414-9.

417. O'Brien, V., *Viruses and apoptosis.* J Gen Virol, 1998. **79 (Pt 8)**: p. 1833-45.

418. Mbita, Z., R. Hull, and Z. Dlamini, *Human immunodeficiency virus-1 (HIV-1)-mediated apoptosis: new therapeutic targets.* Viruses, 2014. **6**(8): p. 3181-227.

419. Hui, K.P., et al., *Highly pathogenic avian influenza H5N1 virus delays apoptotic responses via activation of STAT3.* Sci Rep, 2016. **6**: p. 28593.

420. Sharma, M., et al., *Japanese encephalitis virus replication is negatively regulated by autophagy and occurs on LC3-I- and EDEM1-containing membranes.* Autophagy, 2014. **10**(9): p. 1637-51.

421. Roulston, A., R.C. Marcellus, and P.E. Branton, *Viruses and apoptosis.* Annu Rev Microbiol, 1999. **53**: p. 577-628.

422. Wang, X., et al., *Molecules from apoptotic pathways modulate HIV-1 replication in Jurkat cells.* Biochem Biophys Res Commun, 2011. **414**(1): p. 20-4.

423. Teodoro, J.G. and P.E. Branton, *Regulation of apoptosis by viral gene products.* J Virol, 1997. **71**(3): p. 1739-46.

424. Benedict, C.A., P.S. Norris, and C.F. Ware, *To kill or be killed: viral evasion of apoptosis.* Nat Immunol, 2002. **3**(11): p. 1013-8.

425. Koyama, A.H., et al., *Physiological significance of apoptosis in animal virus infection.* Microbes Infect, 2000. **2**(9): p. 1111-7.

426. Cuconati, A. and E. White, *Viral homologs of BCL-2: role of apoptosis in the regulation of virus infection.* Genes Dev, 2002. **16**(19): p. 2465-78.

427. Okamoto, T., et al., *Regulation of Apoptosis during Flavivirus Infection.* Viruses, 2017. **9**(9).

428. Tsapras, P. and I.P. Nezis, *Caspase involvement in autophagy.* Cell Death Differ, 2017. **24**(8): p. 1369-1379.

429. Gump, J.M. and A. Thorburn, *Autophagy and apoptosis: what is the connection?* Trends Cell Biol, 2011. **21**(7): p. 387-92.

430. Yeganeh, B., et al., *Hepatitis B and C virus-induced hepatitis: Apoptosis, autophagy, and unfolded protein response.* World J Gastroenterol, 2015. **21**(47): p. 13225-39.

431. Gou, H., et al., *Autophagy induces apoptosis and death of T lymphocytes in the spleen of pigs infected with CSFV.* Sci Rep, 2017. **7**(1): p. 13577.

432. Baehrecke, E.H., *Autophagy: dual roles in life and death?* Nat Rev Mol Cell Biol, 2005. **6**(6): p. 505-10.

433. Kroemer, G. and M. Jaattela, *Lysosomes and autophagy in cell death control.* Nat Rev Cancer, 2005. **5**(11): p. 886-97.

434. Thorburn, A., *Apoptosis and autophagy: regulatory connections between two supposedly different processes.* Apoptosis, 2008. **13**(1): p. 1-9.

435. Maiuri, M.C., et al., *Functional and physical interaction between Bcl-X(L) and a BH3-like domain in Beclin-1.* Embo j, 2007. **26**(10): p. 2527-39.

436. Luo, S., et al., *Bim inhibits autophagy by recruiting Beclin 1 to microtubules.* Mol Cell, 2012. **47**(3): p. 359-70.

437. Zhou, F., Y. Yang, and D. Xing, *Bcl-2 and Bcl-xL play important roles in the crosstalk between autophagy and apoptosis.* Febs j, 2011. **278**(3): p. 403-13.

438. Yee, K.S., et al., *PUMA- and Bax-induced autophagy contributes to apoptosis.* Cell Death Differ,

2009. **16**(8): p. 1135-45.

439. Bell, B.D., et al., *FADD and caspase-8 control the outcome of autophagic signaling in proliferating T cells.* Proc Natl Acad Sci U S A, 2008. **105**(43): p. 16677-82.

440. Yu, L., et al., *Regulation of an ATG7-beclin 1 program of autophagic cell death by caspase-8.* Science, 2004. **304**(5676): p. 1500-2.

441. Wang, J., *Beclin 1 bridges autophagy, apoptosis and differentiation.* Autophagy, 2008. **4**(7): p. 947-948.

442. Kang, R., et al., *The Beclin 1 network regulates autophagy and apoptosis.* Cell Death And Differentiation, 2011. **18**: p. 571.

443. Tanida, I., T. Ueno, and E. Kominami, *LC3 and Autophagy*, in *Autophagosome and Phagosome*, V. Deretic, Editor. 2008, Humana Press: Totowa, NJ. p. 77-88.

444. Pugsley, H.R., *Quantifying autophagy: Measuring LC3 puncta and autolysosome formation in cells using multispectral imaging flow cytometry.* Methods, 2017. **112**: p. 147-156.

445. Vermes, I., et al., *A novel assay for apoptosis. Flow cytometric detection of phosphatidylserine expression on early apoptotic cells using fluorescein labelled Annexin V.* J Immunol Methods, 1995. **184**(1): p. 39-51.

446. Zembruski, N.C., et al., *7-Aminoactinomycin D for apoptosis staining in flow cytometry.* Anal Biochem, 2012. **429**(1): p. 79-81.

447. Hande, K.R., *Etoposide: four decades of development of a topoisomerase II inhibitor.* Eur J Cancer, 1998. **34**(10): p. 1514-21.

448. Rodriguez-Enfedaque, A., et al., *zVAD-fmk upregulates caspase-9 cleavage and activity in etoposide-induced cell death of mouse embryonic fibroblasts.* Biochim Biophys Acta, 2012.

1823(8): p. 1343-52.

449. Taguwa, S., et al., *Dysfunction of autophagy participates in vacuole formation and cell death in cells replicating hepatitis C virus.* J Virol, 2011. **85**(24): p. 13185-94.

450. Joubert, P.E., et al., *Chikungunya virus-induced autophagy delays caspase-dependent cell death.* J Exp Med, 2012. **209**(5): p. 1029-47.

451. Wileman, T., *Autophagy as a defence against intracellular pathogens.* Essays Biochem, 2013. **55**: p. 153-63.

452. Gregoire, I.P., et al., *IRGM is a common target of RNA viruses that subvert the autophagy network.* PLoS Pathog, 2011. **7**(12): p. e1002422.

453. Tang, S.W., et al., *The cellular autophagy pathway modulates human T-cell leukemia virus type 1 replication.* J Virol, 2013. **87**(3): p. 1699-707.

454. 伍治平, et al., *猴 D 型逆转录病毒(SRV)感染恒河猴诱导脑细胞凋亡.* 西南国防医药, 2001(04): p. 242-244.

455. Perfettini, J.L., et al., *Mechanisms of apoptosis induction by the HIV-1 envelope.* Cell Death Differ, 2005. **12 Suppl 1**: p. 916-23.

456. Gougeon, M.L., *Apoptosis as an HIV strategy to escape immune attack.* Nat Rev Immunol, 2003. **3**(5): p. 392-404.

457. Matarrese, P. and W. Malorni, *Human immunodeficiency virus (HIV)-1 proteins and cytoskeleton: partners in viral life and host cell death.* Cell Death Differ, 2005. **12 Suppl 1**: p. 932-41.

458. Shedlock, D.J., et al., *HIV-1 viral genes and mitochondrial apoptosis.* Apoptosis, 2008. **13**(9): p. 1088-99.

459. Li, Q., et al., *Microarray analysis of lymphatic tissue reveals stage-specific, gene expression signatures in HIV-1 infection.* J Immunol, 2009. **183**(3): p. 1975-82.

460. Boudet, F., H. Lecoeur, and M.L. Gougeon, *Apoptosis associated with ex vivo down-regulation of Bcl-2 and up-regulation of Fas in potential cytotoxic CD8+ T lymphocytes during HIV infection.* J Immunol, 1996. **156**(6): p. 2282-93.

461. Badley, A.D., et al., *Upregulation of Fas ligand expression by human immunodeficiency virus in human macrophages mediates apoptosis of uninfected T lymphocytes.* J Virol, 1996. **70**(1): p. 199-206.

462. Herbeuval, J.P., et al., *CD4+ T-cell death induced by infectious and noninfectious HIV-1: role of type 1 interferon-dependent, TRAIL/DR5-mediated apoptosis.* Blood, 2005. **106**(10): p. 3524-31.

463. Herbeuval, J.P., et al., *Regulation of TNF-related apoptosis-inducing ligand on primary CD4+ T cells by HIV-1: role of type I IFN-producing plasmacytoid dendritic cells.* Proc Natl Acad Sci U S A, 2005. **102**(39): p. 13974-9.

464. Jin, Z., et al., *Cullin3-based polyubiquitination and p62-dependent aggregation of caspase-8 mediate extrinsic apoptosis signaling.* Cell, 2009. **137**(4): p. 721-35.

465. Deegan, S., et al., *Deficiency in the mitochondrial apoptotic pathway reveals the toxic potential of autophagy under ER stress conditions.* Autophagy, 2014. **10**(11): p. 1921-36.

466. Wei, W., et al., *Regulatory Role of N(6) -methyladenosine (m(6) A) Methylation in RNA Processing and Human Diseases.* 2017. **118**(9): p. 2534-2543.

467. Xiang, Y., et al., *m(6)A RNA methylation regulates the UV-induced DNA damage response.* Nature, 2017. **543**(7646): p. 573-576.

468. Lavi, S. and A.J. Shatkin, *Methylated simian virus 40-specific RNA from nuclei and cytoplasm of infected BSC-1 cells.* Proc Natl Acad Sci U S A, 1975. **72**(6): p. 2012-6.

469. Sommer, S., et al., *The methylation of adenovirus-specific nuclear and cytoplasmic RNA.* Nucleic Acids Res, 1976. **3**(3): p. 749-65.

470. Woodhouse, S.D., et al., *Transcriptome sequencing, microarray, and proteomic analyses reveal cellular and metabolic impact of hepatitis C virus infection in vitro.* Hepatology, 2010. **52**(2): p. 443-53.

471. Pastorino, B., et al., *Identification of cellular proteome modifications in response to West Nile virus infection.* Mol Cell Proteomics, 2009. **8**(7): p. 1623-37.

472. Jern, P. and J.M. Coffin, *Effects of retroviruses on host genome function.* Annu Rev Genet, 2008. **42**: p. 709-32.

473. Fu, Y., et al., *Gene expression regulation mediated through reversible m(6)A RNA methylation.* Nat Rev Genet, 2014. **15**(5): p. 293-306.

474. Sestan, M., et al., *Virus-Induced Interferon-gamma Causes Insulin Resistance in Skeletal Muscle and Derails Glycemic Control in Obesity.* Immunity, 2018. **49**(1): p. 164-177.e6.

475. Ye, F., E.R. Chen, and T.W. Nilsen, *Kaposi's Sarcoma-Associated Herpesvirus Utilizes and Manipulates RNA N(6)-Adenosine Methylation To Promote Lytic Replication.* J Virol, 2017. **91**(16).

476. Paul, P. and C. Munz, *Autophagy and Mammalian Viruses: Roles in Immune Response, Viral Replication, and Beyond.* Adv Virus Res, 2016. **95**: p. 149-95.

477. Levine, B. and G. Kroemer, *Autophagy in the pathogenesis of disease.* Cell, 2008. **132**(1): p. 27-42.